University of Southampton

Faculty of Engineering and Physical Sciences
School of Chemistry

Organic Semiconductor Design for Light-Emitting Electrochemical Cell Technology

by

Oliver James Ward

A thesis for the degree of
Doctor of Philosophy

April 2024

University of Southampton

Abstract

Faculty of Engineering and Physical Sciences
School of Chemistry

Doctor of Philosophy

Organic Semiconductor Design for Light-Emitting Electrochemical Cell Technology

by Oliver James Ward

Organic light-emitting electrochemical cells (OLECs) that comprise an active layer, an optional hole-injection layer, and a pair of electrodes, are promising alternatives to currently prevalent technologies. Small-molecule OLECs with active layers based on functionalised fluorene fragments tethered, by hydrocarbon chains, to alkylimidazolium pendants have a number of properties that make them especially viable targets in the design of next-generation OLEC devices.

Fluorene's ease of functionalisation allows a systematically varied group of arylfluorene salts to be generated, and a structure-activity relationship to be investigated. Cross-coupling of alkylated bromofluorenes with substituted bromobenzenes, by way of the corresponding dioxaborolanes, gives a set of neutral smart ink precursors that can be quaternised with alkylimidazoles. Inductive (both +I and -I) and mesomeric effects (both +M and -M) at the 3 and 4 positions of the aryl substituents are examined. Head-to-head comparison of matched pairs reveals the effects of substituent type and substitution pattern. 2,7-diarylfluorene smart inks and their 2-arylfluorene cousins are compared in order to establish the effect of, and extent of the π-system, independently of aryl group substitution pattern. The practical viability of smart inks bearing methylimidazolium pendants is compared with those bearing octylimidazolium pendants.

These arylfluorene smart inks form the training set used to establish an efficient, predictive computational modelling procedure. The substrate scope is probed by computational and spectroscopic analysis of a group of polyarenes based on phenanthrene, and the generation of a functioning OLEC device from a smart ink in this chemical family is demonstrated. The predictive model, in combination with a genetic algorithm, is used to further extend the substrate scope and generate a UV-emitting arylpyridine and a blue-emitting arylpyridinium analogue.

Contents

Declaration of Authorship **xi**

Acknowledgements **xiii**

Definitions and Abbreviations **xvii**

1 Introduction **1**
1.1 Light-emitting technology . . . 1
1.1.1 Light-emitting diodes . . . 1
1.1.2 Light-emitting electrochemical cells. . . . 2
1.1.3 Mechanism of action . . . 4
1.2 The state of the art . . . 6
1.2.1 OLEC materials . . . 6
1.2.2 Ionic transition-metal complexes . . . 7
1.2.3 Conjugated polymers . . . 8
1.2.4 Ionic small molecules . . . 8
1.2.5 Mixed systems . . . 10
1.2.6 Aggregation-induced effects . . . 12
1.2.7 Theoretical chemistry . . . 13
1.3 Scientific and technological aims . . . 16
1.3.1 Research programme . . . 16
1.3.2 Research priorities . . . 16
1.3.3 Fluorene-based UV and blue emitters . . . 17

2 Fluorene-based light-emitters **23**
2.1 Library synthesis . . . 23
2.1.1 Overview . . . 23
2.1.2 Establishment of a structure-activity relationship . . . 24
2.1.3 Synthetic route . . . 27
2.1.4 Synthesis of dialkylfluorenes . . . 28
2.1.5 Cross-coupling to form arylfluorenes and diarylfluorenes . . . 29
2.1.6 Quaternisation . . . 31
2.2 Experimental analysis . . . 33
2.2.1 Overview . . . 33
2.2.2 Calculation of the HOMO energy from a cyclic voltammogram . . . 33
2.2.3 Calculation of the optical bandgap from the UV-vis spectrum . . . 35
2.2.4 Electroluminescent devices . . . 36
2.2.5 Methylimidazolium *vs* octylimidazolium . . . 38

2.2.6 Arylfluorenes *vs* diarylfluorenes . . . 40
2.2.7 Functional group effects . . . 42
2.2.8 Functionalisation at position 3 *vs* position 4 . . . 42
2.2.9 HOMO energies and band gaps . . . 44
2.2.10 Solvatochromism . . . 45
2.3 Conclusions . . . 48

3 A predictive computational model 51
3.1 Introduction . . . 51
3.1.1 Benchmarking . . . 51
3.1.2 Phenanthrene-based systems . . . 52
3.2 Research and development . . . 55
3.2.1 Overview . . . 55
3.2.2 Directly functionalised fluorenes . . . 55
3.2.3 Comparing DFT to experimental data sets . . . 58
3.2.4 Comparing TD-DFT to experimental data sets . . . 61
3.2.5 Expanding the scope of the theoretical model . . . 62
3.2.6 A flow-photochemical synthetic method . . . 65
3.2.7 Extension of the computational model . . . 70
3.3 Conclusion . . . 71

4 Algorithmic structure determination 73
4.1 Introduction . . . 73
4.1.1 Background . . . 73
4.1.2 Finding smart inks algorithmically . . . 75
4.2 Research and Development . . . 76
4.2.1 Reducing the compute time of theoretical calculations . . . 76
4.2.2 Definition of the chemical space . . . 78
4.2.3 Generation of new chemical structures . . . 78
4.2.4 Identification of promising targets for UV-emission . . . 82
4.2.5 Realisation of a computationally generated structure . . . 83
4.3 Conclusion . . . 85

5 Conclusions 87
5.1 Project outcomes . . . 87
5.2 Future work . . . 89

6 Experimental details 91
6.1 General experimental techniques . . . 91
6.2 Synthetic procedure . . . 93
6.3 Fluorene-based smart inks . . . 94
6.3.1 1-Octyl-1*H*-imidazole . . . 94
6.3.2 2-Bromo-*bis*-9,9-(6'-bromohexyl)fluorene . . . 95
6.3.3 *Bis*-2,7-dibromo-*bis*-9,9-(6'-bromohexyl)fluorene . . . 96
6.3.4 2-(9,9-*Bis*(6-bromohexyl)-9*H*-fluoren-2-yl)-4,4,5,5-tetramethyl-1,3,2-dioxaborolane . . . 97
6.3.5 2,2'-(9,9-*Bis*(6-bromohexyl)-9*H*-fluorene-2,7-diyl)*bis*(4,4,5,5-tetramethyl-1,3,2-dioxaborolane) . . . 98

6.3.6 9,9-*Bis*(6-bromohexyl)-2,7-*bis*(3-methoxyphenyl)-9*H*-fluorene . . . 99
6.3.7 9,9-*Bis*(6-bromohexyl)-2,7-*bis*(4-methoxyphenyl)-9*H*-fluorene . . . 100
6.3.8 9,9-*Bis*(6-bromohexyl)-2,7-*bis*(2-methoxyphenyl)-9*H*-fluorene . . . 101
6.3.9 9,9-*Bis*(6-bromohexyl)-2,7-di-*m*-tolyl-9*H*-fluorene 102
6.3.10 9,9-*Bis*(6-bromohexyl)-2,7-di-*p*-tolyl-9*H*-fluorene 103
6.3.11 2,7-Di([1,1'-biphenyl]-3-yl)-9,9-*bis*(6-bromohexyl)-9*H*-fluorene . . . 104
6.3.12 2,7-Di([1,1'-biphenyl]-4-yl)-9,9-*bis*(6-bromohexyl)-9*H*-fluorene . . . 105
6.3.13 9,9-*Bis*(6-bromohexyl)-2-(3-methoxyphenyl)-9*H*-fluorene 106
6.3.14 9,9-*Bis*(6-bromohexyl)-2-(4-methoxyphenyl)-9*H*-fluorene 107
6.3.15 9,9-*Bis*(6-bromohexyl)-2-(*m*-tolyl)-9*H*-fluorene 108
6.3.16 9,9-*Bis*(6-bromohexyl)-2-(*p*-tolyl)-9*H*-fluorene 109
6.3.17 2-([1,1'-Biphenyl]-3-yl)-9,9-*bis*(6-bromohexyl)-9*H*-fluorene 110
6.3.18 2-([1,1'-Biphenyl]-4-yl)-9,9-*bis*(6-bromohexyl)-9*H*-fluorene 111
6.3.19 9,9-*Bis*(6-bromohexyl)-2-phenyl-9*H*-fluorene 112
6.3.20 9,9-*Bis*(6-bromohexyl)-2,7-diphenyl-9*H*-fluorene 113
6.3.21 9-(9,9-*Bis*(6-bromohexyl)-9*H*-fluoren-2-yl)phenanthrene 114
6.3.22 3,3'-((2,7-*Bis*(4-methoxyphenyl)-9*H*-fluorene-9,9-diyl)*bis*(hexane-6,1-diyl))*bis*(1-methyl-1*H*-imidazol-3-ium) trifluoromethanesulfonate . 115
6.3.23 3,3'-((2,7-*Bis*(3-methoxyphenyl)-9*H*-fluorene-9,9-diyl)*bis*(hexane-6,1-diyl))*bis*(1-octyl-1*H*-imidazol-3-ium) trifluoromethanesulfonate . . 116
6.3.24 3,3'-((2-(*m*-Tolyl)-9*H*-fluorene-9,9-diyl)*bis*(hexane-6,1-diyl))*bis*(1-octyl-1*H*-imidazol-3-ium) trifluoromethanesulfonate 117
6.3.25 3,3'-((2-Phenyl-9*H*-fluorene-9,9-diyl)*bis*(hexane-6,1-diyl))*bis*(1-methyl-1*H*-imidazol-3-ium) trifluoromethanesulfonate 118
6.3.26 3,3'-((2,7-Diphenyl-9*H*-fluorene-9,9-diyl)*bis*(hexane-6,1-diyl))*bis*(1-methyl-1*H*-imidazol-3-ium) trifluoromethanesulfonate 119
6.3.27 3,3'-((2,7-*Bis*(3-methoxyphenyl)-9*H*-fluorene-9,9-diyl)*bis*(hexane-6,1-diyl))*bis*(1-methyl-1*H*-imidazol-3-ium) trifluoromethanesulfonate . 120
6.3.28 3,3'-((2-(*m*-Tolyl)-9*H*-fluorene-9,9-diyl)*bis*(hexane-6,1-diyl))*bis*(1-methyl-1*H*-imidazol-3-ium) trifluoromethanesulfonate 121
6.3.29 3,3'-((2,7-*Bis*(4-methoxyphenyl)-9*H*-fluorene-9,9-diyl)*bis*(hexane-6,1-diyl))*bis*(1-octyl-1*H*-imidazol-3-ium) trifluoromethanesulfonate . . 122
6.3.30 3,3'-((2,7-Di-*m*-tolyl-9*H*-fluorene-9,9-diyl)*bis*(hexane-6,1-diyl))*bis*(1-methyl-1*H*-imidazol-3-ium) trifluoromethanesulfonate 123
6.3.31 3,3'-((2,7-Di-*m*-tolyl-9*H*-fluorene-9,9-diyl)*bis*(hexane-6,1-diyl))*bis*(1-octyl-1*H*-imidazol-3-ium) trifluoromethanesulfonate 124
6.3.32 3,3'-((2,7-Di-*p*-tolyl-9*H*-fluorene-9,9-diyl)*bis*(hexane-6,1-diyl))*bis*(1-methyl-1*H*-imidazol-3-ium) trifluoromethanesulfonate 125
6.3.33 3,3'-((2,7-Di-*p*-tolyl-9*H*-fluorene-9,9-diyl)*bis*(hexane-6,1-diyl))*bis*(1-octyl-1*H*-imidazol-3-ium) trifluoromethanesulfonate 126
6.3.34 3,3'-((2,7-Di([1,1'-biphenyl]-3-yl)-9*H*-fluorene-9,9-diyl)*bis*(hexane-6,1-diyl))*bis*(1-methyl-1*H*-imidazol-3-ium) trifluoromethanesulfonate 127
6.3.35 3,3'-((2,7-Di([1,1'-biphenyl]-3-yl)-9*H*-fluorene-9,9-diyl)*bis*(hexane-6,1-diyl))*bis*(1-octyl-1*H*-imidazol-3-ium) trifluoromethanesulfonate 128
6.3.36 3,3'-((2,7-Di([1,1'-biphenyl]-4-yl)-9*H*-fluorene-9,9-diyl)*bis*(hexane-6,1-diyl))*bis*(1-methyl-1*H*-imidazol-3-ium) trifluoromethanesulfonate 129

6.3.37 3,3'-((2,7-Di([1,1'-biphenyl]-4-yl)-9*H*-fluorene-9,9-diyl)*bis*(hexane-6,1-diyl))*bis*(1-octyl-1*H*-imidazol-3-ium) trifluoromethanesulfonate 130
6.3.38 3,3'-((2-(3-Methoxyphenyl)-9*H*-fluorene-9,9-diyl)*bis*(hexane-6,1-diyl))*bis*(1-methyl-1*H*-imidazol-3-ium) trifluoromethanesulfonate 131
6.3.39 3,3'-((2-(3-Methoxyphenyl)-9*H*-fluorene-9,9-diyl)*bis*(hexane-6,1-diyl))*bis*(1-octyl-1*H*-imidazol-3-ium) trifluoromethanesulfonate 132
6.3.40 3,3'-((2-(4-Methoxyphenyl)-9*H*-fluorene-9,9-diyl)*bis*(hexane-6,1-diyl))*bis*(1-methyl-1*H*-imidazol-3-ium) trifluoromethanesulfonate 133
6.3.41 3,3'-((2-(4-Methoxyphenyl)-9*H*-fluorene-9,9-diyl)*bis*(hexane-6,1-diyl))*bis*(1-octyl-1*H*-imidazol-3-ium) trifluoromethanesulfonate 134
6.3.42 3,3'-((2-(*p*-Tolyl)-9*H*-fluorene-9,9-diyl)*bis*(hexane-6,1-diyl)) *bis*(1-me-thyl-1*H*-imidazol-3-ium) trifluoromethanesulfonate 135
6.3.43 3,3'-((2-(*p*-Tolyl)-9*H*-fluorene-9,9-diyl)*bis*(hexane-6,1-diyl))*bis*(1-octyl-1*H*-imidazol-3-ium) trifluoromethanesulfonate 136
6.3.44 3,3'-((2-([1,1'-Biphenyl]-3-yl)-9*H*-fluorene-9,9-diyl)*bis*(hexane-6,1-diyl))*bis*(1-methyl-1*H*-imidazol-3-ium) trifluoromethanesulfonate . 137
6.3.45 3,3'-((2-([1,1'-Biphenyl]-3-yl)-9*H*-fluorene-9,9-diyl)*bis*(hexane-6,1-diyl))*bis*(1-octyl-1*H*-imidazol-3-ium) trifluoromethanesulfonate . . 138
6.3.46 3,3'-((2-([1,1'-Biphenyl]-4-yl)-9*H*-fluorene-9,9-diyl)*bis*(hexane-6,1-diyl))*bis*(1-methyl-1*H*-imidazol-3-ium) trifluoromethanesulfonate . 139
6.3.47 3,3'-((2-([1,1'-Biphenyl]-4-yl)-9*H*-fluorene-9,9-diyl)*bis*(hexane-6,1-diyl))*bis*(1-octyl-1*H*-imidazol-3-ium) trifluoromethanesulfonate . . 140
6.3.48 3,3'-((2-Phenyl-9*H*-fluorene-9,9-diyl)*bis*(hexane-6,1-diyl))*bis*(1-octyl-1*H*-imidazol-3-ium) trifluoromethanesulfonate 141
6.3.49 3,3'-((2,7-Diphenyl-9*H*-fluorene-9,9-diyl)*bis*(hexane-6,1-diyl))*bis*(1-octyl-1*H*-imidazol-3-ium) trifluoromethanesulfonate 142
6.3.50 3,3'-((2-(Phenanthren-9-yl)-9*H*-fluorene-9,9-diyl)*bis*(hexane-6,1-diyl))*bis*(1-methyl-1*H*-imidazol-3-ium) trifluoromethanesulfonate 143
6.3.51 3,3'-((2-(Phenanthren-9-yl)-9*H*-fluorene-9,9-diyl)*bis*(hexane-6,1-diyl))*bis*(1-octyl-1*H*-imidazol-3-ium) trifluoromethanesulfonate 144
6.4 Substituted fluorenes 145
6.4.1 2,4,6-*Tris*(2-fluorophenyl)-1,3,5,2,4,6-trioxatriborinane 145
6.4.2 2'-Fluoro-[1,1'-biphenyl]-2-amine 146
6.4.3 3'-Fluoro-[1,1'-biphenyl]-2-amine 147
6.4.4 2-Fluoro-2'-iodo-1,1'-biphenyl 148
6.4.5 3'-Fluoro-2-iodo-1,1'-biphenyl 149
6.4.6 4-Fluorofluorene 150
6.4.7 3-Fluorofluorene 151
6.5 Phenanthrenes 152
6.5.1 2-(6-Bromohexyl)isoindoline-1,3-dione 152
6.5.2 2-(6-(1*H*-Imidazol-1-yl)hexyl)isoindoline-1,3-dione 153
6.5.3 6-(1*H*-Imidazol-1-yl)hexan-1-amine 154
6.5.4 3,4-Dimethoxycyclobut-3-ene-1,2-dione 155
6.5.5 4-Hydroxy-2,3-dimethoxy-4-phenylcyclobut-2-en-1-one 156
6.5.6 3,4,4-Trimethoxy-2-phenylcyclobut-2-en-1-one 157
6.5.7 3,4-Diphenylcyclobut-3-ene-1,2-dione 158
6.5.8 Phenanthro[9,10-*c*]furan-1,3-dione 159
6.5.9 4-Hydroxy-2,3-dimethoxy-4-(4-methoxyphenyl)cyclobut-2-en-1-one 160

6.5.10 3-(4-Methoxyphenyl)-4-phenylcyclobut-3-ene-1,2-dione 161
6.5.11 6-Methoxyphenanthro[9,10-*c*]furan-1,3-dione 162
6.5.12 3-(Benzo[*d*][1,3]dioxol-5-yl)-4-phenylcyclobut-3-ene-1,2-dione . . . 163
6.5.13 2-(6-(1*H*-Imidazol-1-yl)hexyl)-1*H*-dibenzo[*e*,*g*]isoindole-1,3(2*H*)-dione 164
6.5.14 1-(6-(1,3-Dioxo-1,3-dihydro-2*H*-dibenzo[*e*,*g*]isoindol-2-yl)hexyl)-3-methyl-1*H*-imidazol-3-ium trifluoromethanesulfonate 165
6.6 Pyridine systems 166
6.6.1 4-(4-Methoxyphenyl)pyridine 166
6.6.2 4-(4-Methoxyphenyl)-1-methylpyridin-1-ium trifluoromethanesulfonate 167

Appendices **169**

Appendix A Absorbance spectra **169**

Appendix B Photoluminescence spectra **175**
Appendix B.1 Film state 175
Appendix B.2 Solution state 178

Appendix C Electroluminescence spectra **183**

Appendix D Cyclic voltammograms **187**

Appendix E Scanning electron microscope images **191**

Appendix F Computational data **193**

Appendix G Tabulated data **197**

References **199**

Declaration of Authorship

I declare that this thesis and the work presented in it is my own and has been generated by me as the result of my own original research.

I confirm that:

1. This work was done wholly or mainly while in candidature for a research degree at this University;
2. Where any part of this thesis has previously been submitted for a degree or any other qualification at this University or any other institution, this has been clearly stated;
3. Where I have consulted the published work of others, this is always clearly attributed;
4. Where I have quoted from the work of others, the source is always given. With the exception of such quotations, this thesis is entirely my own work;
5. I have acknowledged all main sources of help;
6. Where the thesis is based on work done by myself jointly with others, I have made clear exactly what was done by others and what I have contributed myself;
7. None of this work has been published before submission

Signed:..... Date:.....

Acknowledgements

First, effusive thanks go to my supervisor, Professor David Harrowven whose knowledge, patience, and sense of humour made working in the Harrowven lab a real pleasure.

Thanks also to my secondary supervisor, Professor Richard Whitby, who supported my foray into computational chemistry. Early versions of this thesis were improved by the invaluable advice of Dr Lynda Brown, Dr Matthias Baud, and Dr James Pearce.

Every part of my research was a collaborative effort. Chapter 2 would be little without the work of the engineers of Beeby group, most especially Dr Katie Court whose impact on this research cannot be overstated. Thanks to Dr Yi Li for providing much of the solid-state data that informed many important decisions. Chapter 3 owes a great deal to Dr Matthieu Hédouin whose computational contributions were always excellent. Chapter 4 could not have come about but for the persistence and vision of Jay Johal, to whom I am especially grateful for help automating DFT calculations.

It was great to work on the SmartT project, and thanks go to all who were part of it. Ed Jackman, who contributed significantly to Chapter 2, was my closest colleague throughout my PhD, and I could fill several pages with anecdotes and gratitude. Working with Dr Ella Bavinton, on the compounds that appear in Chapters 2 and 3, was a great pleasure. Michail Skoulikas and Ashley Shiels also deserve credit for many useful discussions.

Others who contributed indirectly to this work include Dr Dawid Drelinkiewicz (the solvatochromism investigation), Dr Ana Folgueiras (the black art of cyclic voltammetry), Dr Will Raimbach (flow-photochemistry), Rob Carroll (crystallography), Dr Sun Wei (many practical techniques), Dr Ryan Bennett (cyclobutenediones), and Dr Luke Wilding-Steele (cyclobutenediones). Katherine Marris and Johan Hadfield Chacha were excellent students whose project work set the stage for Chapter 3.

Lab 3007 and the rest of floor 3 were a great crowd to be part of. Thank you to all.

Thanks also go to the departmental staff, especially Dr Neil Wells, Professor John Langley, and Dr Julie Herniman who managed to ionise some very challenging structures. Also, to Keith and Mark in stores.

Finally, Dr Jordann Wells and Dr Rachel Wynn provided much needed advice at critical points, and Anthony Ashton's help with LaTeXwas a gift that keeps on giving.

To Dad, and the limitless imagination you bring to bear on all things... in the kitchen... until 4 AM.

Definitions and Abbreviations

Ac	Acyl
ACQ	Aggregation-caused quenching
APPI	Atmospheric pressure photoionization
$B_2(pin)_2$	*Bis*-pinacolatodiboron
C-PCM	Continuous polarisable continuum model
CV	Cyclic voltammetry
DBH	1,6-Dibromohexane
DCM	Dichloromethane
DFT	Density functional theory
DMA	Dimethylacetamide
DMF	N,N-Dimethylformamide
DMSO	Dimethylsulfoxide
EI	Electron ionization
ESI	Electrospray ionization
Et	Ethyl
FREA	Fused-ring electron acceptor
FT	Fourier-transform
GCMS	Gas chromatography coupled to mass spectrometry
HOMO	Highest occupied molecular orbital
HRMS	High-resolution mass spectrometry
ISC	Intersystem crossing
IPA	Isopropylalcohol
IR	Infrared
iTMC	Ionic transition metal complex
ITO	Indium tin oxide
LEC	Light-emitting electrochemical cell
LED	Light-emitting diode
lm	Lumen
LRMS	Low-resolution mass spectrometry
LUMO	Lowest unoccupied molecular orbital
Me	Methyl
MP	Melting point

NMR	Nuclear magnetic resonance
Oct	Octyl
OLEC	Organic light-emitting electrochemical cell
OLED	Organic light-emitting diode
PEDOT:PSS	Poly(3,4-ethylenedioxythiophene) polystyrene sulfonate
PES	Potential-energy surface
Ph	Phenyl
R_F	Retardation factor
SEM	Scanning electron microscope
SM	Small molecule
TADF	Thermally activated delayed fluorescence
TBAB	Tetrabutylammonium bromide
TD-DFT	Time-dependent density functional theory
Tf	Trifluoromethane sulfonyl
THF	Tetrahydrofuran
UV	Ultraviolet

Chapter 1

Introduction

1.1 Light-emitting technology

1.1.1 Light-emitting diodes

The light-emitting diode (LED) provides a source of bright light that is both cost-effective and efficient. Haitz's law, illustrated in Figure 1.1, describes cost per lumen falling, and light output per LED rising exponentially with time,[(1)] so the technology seems set to continue to provide ever-better access to light-emitting devices. In particular, the OLED (organic light-emitting diode) can be constructed on a tiny scale, and in vast quantities, with emissive properties that permit the manufacture of high-resolution, handheld displays. The purpose of this work isn't to challenge its utility, but to point to certain application-specific limitations of LED technology, and advance the development of a viable alternative - the organic light-emitting electrochemical cell (OLEC).

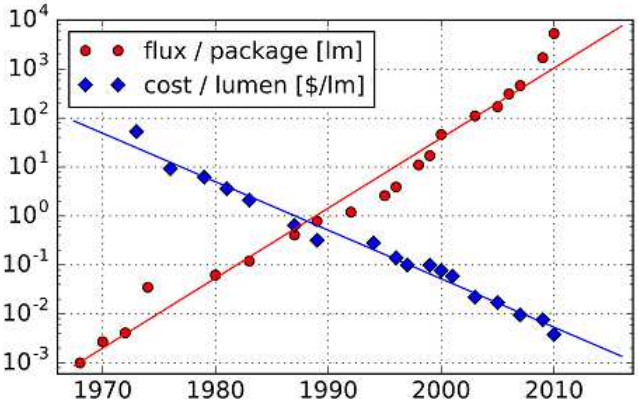

FIGURE 1.1: Haitz's law with a logarithmic $y-$axis.

The simplest LED consists of a semiconductor sandwiched between a pair of electrodes (Figure 1.2, layers 1 and 7). As an electrical current is passed through the semiconducting layer (layers 2 - 6), light is emitted at an intensity that scales with the thickness of the active layer (layer 4).[2] For an LED to function properly, the active layer must be very thin (around 100 nm), and the thickness must be highly uniform. This limits LEDs in the types of substrates on which they can be fabricated (layer 8). A suitable substrate is rigid, and flat, and will remain so throughout the lifetime of the device. In practice, LEDs have a more complicated structure, including layers optimised for the injection and transport of electrons and 'holes', as shown in Figure 1.2.[3]

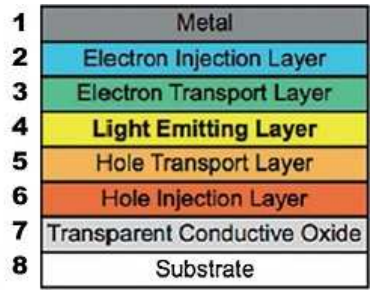

FIGURE 1.2: The complex structure of a typical OLED.

High-work-function metals are chosen as the anodes (layer 7 in Figure 1.2) for LED devices. This is so that the barrier to hole-injection into the highest occupied molecular orbital (HOMO) is minimized. The cathode (layer 1), on the other hand, must have a low work function. Electron-injection and hole-injection must be balanced for an LED to function efficiently, and too high a work function in the cathode metal prevents efficient electron-injection. Calcium is an example of a low-work-function metal that has desirable electronic properties, but is easily oxidised. The gap between the work functions of the electrodes, and the need to balance hole- and electron-injection means that the system is never in electrochemical equilibrium.[2]

1.1.2 Light-emitting electrochemical cells.

The simplest light-emitting electrochemical cell (LEC) has the same basic construction as an LED, but with an electrolyte added to the semiconducting layer. The electrolyte provides mobile ions which, when a voltage bias is applied, can redistribute within the active layer, preventing bi-layer formation at the electrodes, and leading to efficient charge-injection. This removes the limitation on cathode material that is a problem in LED-design. One benefit of this is that both electrodes, and ultimately the entire device, can be made of air-stable materials - a great advantage.[4] This modification also allows LECs to function efficiently without the need for many layers optimised for charge-transport.

Figure 1.3 shows a device which uses a silver cathode and an indium tin oxide (ITO) anode, with a layer of PEDOT:PSS for the injection and transport of holes. The active layer is made of a smart ink, commonly the polymer Super Yellow (*vide infra* 1.2.3) combined with an electrolyte. Much of the science of LEC devices is conducted using test devices such as this.

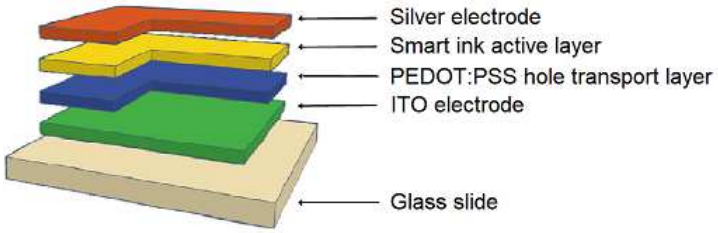

FIGURE 1.3: An OLEC device with a silver cathode, smart ink active layer, PEDOT:PSS hole transport layer, and ITO anode, printed onto glass.

In an LEC device with a pair of high-work-function electrodes, a *p-i-n* junction can form,[5] and a steady state is reached in which ion motion becomes insignificant. This means that electroluminescence is highly efficient. The benefit of the presence of mobile ions in the solid layer comes at the cost of long turn-on times, due to the slow reorganisation of ions as the bias is applied.[2]

In order for an LEC to function, a voltage must be applied that is larger than the energy gap of the semiconductor (3 - 5 V is typical), and this energy gap determines the colour of the emitted light. The active layer in an LEC device is typically around 100 nm thick, as in an LED, but the uniformity of the layer-thickness is not as tightly restricted. This opens up the possibility of printing light-emitting devices onto flexible substrates. The structure of a flexible OLEC device is shown in Figure 1.4.

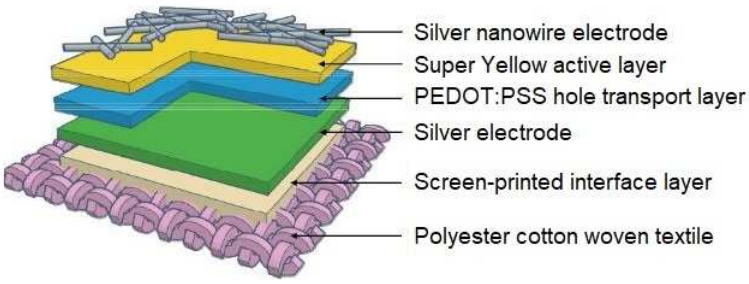

FIGURE 1.4: An OLEC device with a silver nanowire cathode, Super Yellow active layer, PEDOT:PSS hole transport layer, Ag anode, and polymer interface layer, printed onto a woven textile.

LEC devices continue to show poor performance compared to LED devices. The realisation of bright blue- and red-emitters, for visual displays, is a particular hurdle, as the human eye is less sensitive to wavelengths at either end of the visible light spectrum, and so the *perceived* brightness is lower for these emitters.[4]

The recent proliferation of new materials with which to build OLECs,[6] and their combination with a range of printing techniques, including spray coating,[7;8] inkjet printing,[9] spin-coating,[10] and slot-die coating,[11] permit the realisation of light-emission on flexible substrates. The device shown in Figure 1.4 emits light through the semi-transparent silver nanowire cathode. The interface layer is electrochemically inert, and establishes a flat surface onto which a very thin layer of silver can be deposited. The subsequent layers are intrinsically flexible.

There is considerable focus on developing the colour-tunability, efficiency, brightness, and stability of these devices, and this work takes aim at an unresolved problem in the field - the precise relationship between the chemical structure of the active layer and the colour of its emission.

1.1.3 Mechanism of action

Light is generated in electroluminescent devices by the generation of *carriers*, and their recombination in a semiconducting layer.[2] The valence band and the conduction band in a semiconductor are close enough in energy to allow the excitation of electrons from the former to the latter. The excitation of an electron into the conduction band leaves behind an electron hole - a quasiparticle defined as the absence of an electron where one would assume it to exist from the balancing of positive and negative charges in the substance. Both the electron in the conduction band, and the hole in the valence band can move throughout the substance.

When a voltage is applied across a diode, electrons in the conduction band move toward the anode and holes in the valence band move toward the cathode. Since electrons and holes are able to move through the electrodes and around the circuit (Figure 1.5), the regions near the electrodes remain electrically neutral while electrons and holes move across the device.

Further from the electrodes is an electrically charged region in which carrier recombination occurs. This type of interface is known as a p-n junction - the region near the anode is 'p-doped' and the region near the cathode is 'n-doped'. Electrons can flow readily from the cathode (or the n-doped part) to the anode (or the p-doped part), but not nearly as easily in reverse.

It should be understood that the n-doped and p-doped regions have no net charge, despite a relative abundance of electrons in the n-doped region and holes in the p-doped region. The doping is typically achieved by the addition of dopants - atoms or compounds whose function is to provide electrons or holes in an electrically neutral state. A well-known example of this is the addition of phosphorus to silicon to create an n-doped semiconductor. In an LEC, the doping occurs due to the oxidation of the

fluorophore near the anode, and reduction near the cathode, during device operation. Electric neutrality is maintained by the reorganisation of mobile ions.[12]

At the interface, as electrons move toward the anode and leave behind semiconductor cations, the region closer to the anode will accumulate net negative charge, and the region closer to the cathode will accumulate net positive charge. The surface across which these charged regions come into contact is known as the carrier recombination zone, and is the part of the device that emits light.

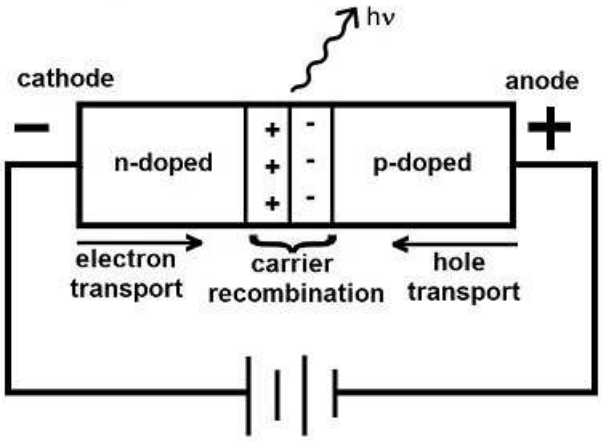

FIGURE 1.5: A circuit with a p-n junction diode.

The difference between an LED and an LEC, at the level of operational mechanism, is that the light-emitting layer in an LED consists of a neutral compound, or mixture of compounds, whereas an LEC utilises a charged active layer. The active layer in an LED must be thin (typically 100 nm) and highly uniform, as the neutral substance has limited ability to transport charges over long distances. This makes the formation of a p-doped region and an n-doped region less likely with greater separation of the neighbouring charged layers. An LEC does not face this problem, as the incorporation of charge into the active layer allows it to form a p-n junction across relatively large inter-electrode distances. The trade-off is that the requirement to be charged imposes additional limitations on the design of new active layers.

LECs based on ionic liquids, such as those with a host-guest architecture, have been shown to exhibit delayed electroluminescence due to differential carrier injection rates.[13] Where electron injection occurs more slowly than hole injection, the p-doped region grows, encompassing the majority of the active layer. The n-doped region then begins to grow, causing the p-doped region to recede, and the device to emit light.

1.2 The state of the art

1.2.1 OLEC materials

A wide array of different materials are available for the construction of OLECs. A variety of electrodes can be utilized, including graphene[14;15] and layers of carbon nanotubes,[16] which are interesting in that they open up the possibility of constructing completely metal-free LEC devices. The devices fabricated from the compounds synthesized in this study used, as electrodes, sputter-coated silver and indium tin oxide, which is transparent. Other electrodes that can be used include poly(3,4-ethylenedioxythiophene) mixed with poly(styrenesulfonate) (PEDOT-PSS), and semi-transparent, spray-coated silver nano-wires.[7]

LEC active-layers made from cadmium selenide quantum dots,[17] lead-containing perovskites,[18] and a variety of non-ionic compounds[19;20] have also been shown to produce light-emitting devices. Finding semiconductors that do not require heavy metals that are toxic, environmentally hazardous, or expensive is obviously desirable. The contrast between neutral and ionic light-emitters in OLEC devices is less clear. Non-ionic emitters must be accompanied by an electrolyte for the device to function, and when the electrolyte and light-emitting molecule are separable, phase separation may occur, reducing the activity of the device.[21]

Two chemical classes have received much of the attention in this field: conjugated polymers, one well-studied example of which is *Super Yellow* (**2**), and ionic transition-metal complexes (iTMC) that utilize a variety of metals and ligand systems.[22] Study of the latter is dominated by iridium(III) complexes such as **1**, in which iridium is chelated by aromatic, polydentate ligands[23].

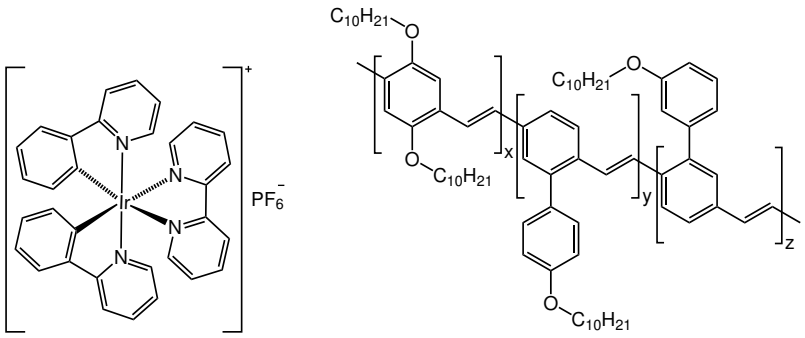

1

A high-performing iTMC

2

Super Yellow

FIGURE 1.6: Some of the best-performing active-layer chemicals yet made.

1.2.2 Ionic transition-metal complexes

iTMCs have an advantage over conjugated polymers in that, where only singlet excitons decay with emission of light in conjugated polymers, singlet and triplet excitons can both decay with light-emission in iTMCs, giving them a much higher theoretical efficiency ceiling.[4] LEC devices can be made with iTMC active layers that are highly efficient. Fast turn-on can also be achieved, although this is gained in a trade-off against electroluminescence degradation time, and quantum yield.[24] Many iridium complexes exhibiting bright emission in the orange and yellow-green regions of the electromagnetic spectrum have been synthesised.[25–27]

Much of the science of iTMC-based LEC devices has centred on device stability, and here, developments have been tremendous. Some very stable iridium complexes have been developed with extrapolated lifetimes of at least 2800 hours, with some lifetime estimates over 3000 hours.[28–30] A study by Kalyuzhny *et al.*[31] showed that the ruthenium-based iTMC-LECs that they studied (*e.g.* **3a**) were much more stable if fabricated and used under drybox conditions. They proposed a diaquoruthenium(II) complex (**3b**) as the *quencher* that gave rise to instability in the devices fabricated in ambient atmospheric conditions. Copper complexes have been synthesized that exhibit blue emission, but degradation in the common solvents used to fabricate LECs hampered their utility.[32]

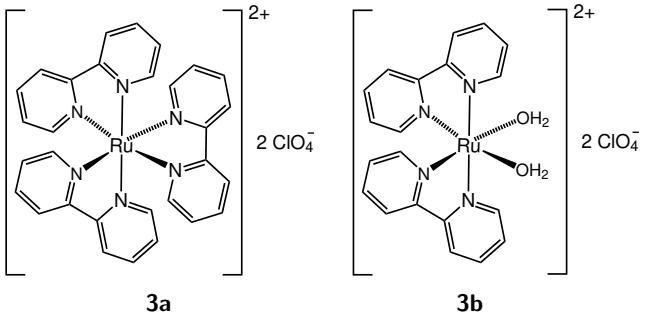

3a **3b**

FIGURE 1.7: A ruthenium comlpex studied by Kalyuzhny and a proposed *quencher*.

A number of hybrid systems with attractive emission properties have been created by the pairing of an organometallic component with an ionic small molecule.[6] These and other mixed systems are discussed separately (*vide infra* 1.2.5).

1.2.3 Conjugated polymers

The first OLECs with conjugated-polymer active layers were reported by Pei *et al.*[33] Orange-, green-, and blue-emitters based on blends of MEH-PPV (poly[2-methoxy-5-(2'-ethylhexyloxy)-1,4-phenylene vinylene], **4**), DOHO-PPP (poly[2-(3,6-dioxaheptyloxy-1,4-phenylene], **5**), and PEO (polyethylene oxide, **6**), with added electrolyte, were used to establish the operational mechanism of LEC devices. Notable advances in the conjugated polymer arena include the development of a multifluorophoric polymer that allows bright white-emitting devices to be constructed with only a single light-emitting compound.[34] Good charge transport properties, along with long lifetimes, good brightness, and high luminous efficiency have also been observed in conjugated polymer-based LECs.[35]

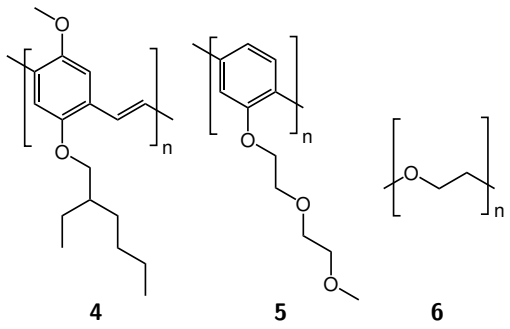

FIGURE 1.8: The polymers used as active-layer constituents in the first conjugated-polymer OLEC device.[33]

A study on the performance of polymer-based LEC devices showed that unencapsulated devices decay through interaction with water, whereas polymer-encapsulated devices decay due to spatial variation in the composition of the active layer.[36] The study also demonstrated arbitrarily high operation times for properly encapsulated devices.

1.2.4 Ionic small molecules

The final class of LEC to be discussed, and the focus of the rest of this work, is the ionic small-molecule OLEC, that is, a device that uses a single organic salt as the active layer. The advantages of this device construction, over the alternatives, can be summarised as follows:

- The use of an organic substance avoids metals that can be toxic, expensive, environmentally hazardous, or that lead to difficulties in synthesis, such as those found in perovskites, quantum dots, and iTMCs.
- The currently dominant Ir complexes have low HOMO-LUMO energy gaps, and therefore limited colour-tunability.[37] Organic polyaromatics with larger HOMO-LUMO gaps, and a great number of available structural modifications, show greater

promise, especially in the UV/blue, and deep red regions of the electromagnetic spectrum - areas in which iTMCs currently struggle to yield good results.[23]

- New polymers are more difficult to synthesize in great abundance due to the requirement that the polymerisation reaction yield be very close to quantitative. This is desirable but not essential in small-molecule synthesis - chemists are therefore much less restricted in the structures they can realise.
- Many polymers are tricky to manipulate, chemically or otherwise, whereas the solution-processability and solid-state properties of small molecules allow them to be handled easily in device-printing. The synthesis of polymers is also fraught with complications of gel-formation, which causes defects in the solid state.[38]
- Ionic small molecules, with a charged moiety tethered to a light-emitting moiety, do not face the problem of phase-separation.

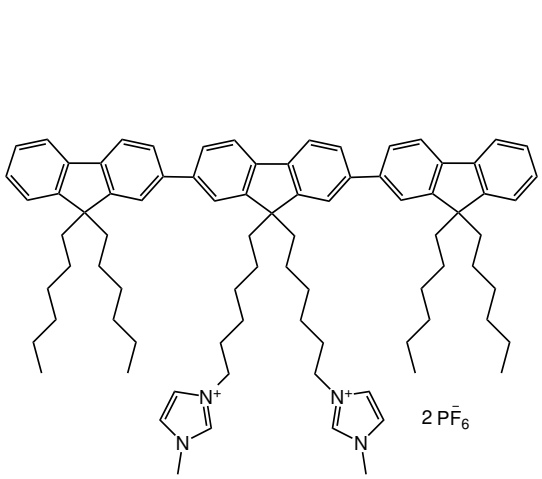

7

The first fluorene-based iSM used in an OLEC

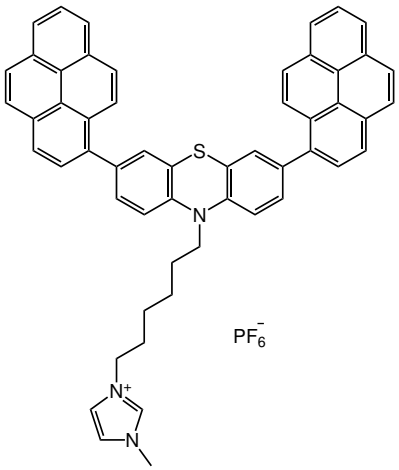

8

A green-emitting phenothiazine ink

FIGURE 1.9: Ionic small molecules for OLEC active layers.

The first breakthrough in the ionic small molecule arena was the synthesis of **7**, a blue-emitting terfluorene-based smart ink. Chen *et al.*[39] selected fluorene as the core of the fluorophore, in part, because of its reversible electrochemical properties (it can, in principle, transport both electrons and holes in the solid state). Cyanine molecules have also shown great promise as infra-red emitters. Pertegás *et al.* prepared LEC devices with luminescence quantum yields of up to 27% by using a pair of cyanine dyes as a host-guest system[40] (Figure 1.10).

Single-component, green-emitting OLECs, based on phenothiazine (*e.g.* **8**), were fabricated by Shanmugasundaram *et al.*[41] with good thermal stability, low turn-on voltages, and maximum luminescence of 499 cd/m^2. The straightforward synthetic procedure and

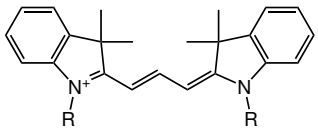

9a R = Et, **9b** R = *n*-Bu

FIGURE 1.10: A pair of dyes which act as host (**9a**) and guest (**9b**), with near-IR emission.

ease of functionalisation of the phenothiazine core make this a very attractive starting point from which to search for other visible light-emitters.

In summary, there has been a broad and, in places, successful effort to realise light-emitting devices that are unencumbered by some of the limitations of LED technology. A great variety of new smart inks has been generated as scientists have sought to understand the physics and physical chemistry at play, but there are still large gaps in our collective knowledge. The classes of compounds that have been under the most active investigation generally emit light within a narrow band of the electromagnetic spectrum, and much of the spectrum is represented poorly - the deep-blue and ultraviolet regions, in particular.

1.2.5 Mixed systems

Smart ink systems that incorporate multiple light-emitting components often display behaviour that is not simply the sum of the properties of the separate components. Interactions between fluorophores in mixed systems can include exciton quenching, which is usually undesirable. Exciton quenching is possible in single-component systems, but can be attenuated by mixture with a host, at very low concentration, as was observed for **10b**.

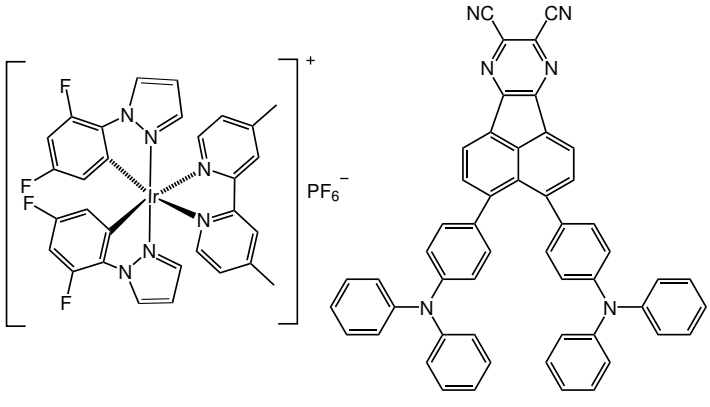

10a **10b**

FIGURE 1.11: An iridium(III) host and organic guest give efficient white emission.

White-emission was achieved by Chen *et al.*[42] with a host-guest system in which a blue-green-emitting, organometallic host (**10a**) was combined with an organic, red-emitting guest (**10b**). The red-emitter exhibited thermally activated delayed fluorescence (TADF), rendering it highly efficient due to the recycling of, ordinarily non-radiative, triplet excitons. Detailed discussion of TADF systems lies beyond the scope of this work.[43;44]

Green-emitting phosphonium salt **11** was shown by Adranno *et al.*[45] to form white-emitting electroluminescent devices when used as the guest in a blend with an ionic liquid host. The host was found to be the source of the blue emission, with green emission coming from the $MnBr_4^{2-}$ ions. The red emission was unexpected, and the authors proposed, on the basis of a drop in green emission during device operation, that some of the $MnBr_4^{2-}$ ions were temporarily converted into a red-emitting species. The phosphonium ion absorbs in the UV region (280 - 400 nm) then undergoes intersystem-crossing (IC) followed by energy transfer to the manganese complex. The emission of the manganese complex is thus enhanced.

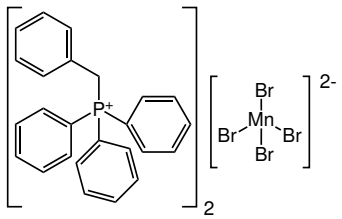

11

FIGURE 1.12: A mixed organic/inorganic system.

1.2.6 Aggregation-induced effects

The active layer of an OLEC, in practical use, is necessarily solid, and its condensed-state emission properties are therefore of primary interest. The emission characteristics of solutions are only of interest insofar as they enhance our understanding of the structure-activity relationship and guide us toward compounds highly emissive as aggregates.

Aggregation-induced emission was observed by Luo *et al.* in a propeller-shaped polyaromatic molecule, **12**.[46] Observation of increased UV-absorption on nanoaggregate formation indicated that the molecules in the nanoaggregate must be more conjugated than those in solution. It stands to reason that better conjugation stems from greater co-planarity in the molecule. Conversely, perfect co-planarity allows excimer formation, which is known to give rise to aggregation-caused quenching (ACQ) effects.

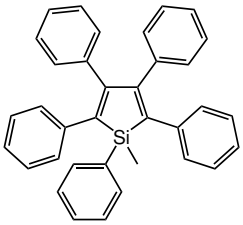

12

FIGURE 1.13: Luo's propeller-shaped molecule that exhibits AIE.

Luminogens based on fluorene and fluorenone have shown aggregation-induced emission enhancement by Chen *et al.*[47]. They also observed significant redshift, and significant enhancement of emission-intensity, on aggregate formation for a fluorene/fluorenone donor-acceptor compound.

A computational study by Gong *et al.*[48] examined the barriers to rotation between potential-energy-surface (PES) minima in the fluorene-thiophene compounds shown in Figure 1.14. They found PES minima for compounds with unsubstituted thiophenes (**13a**) at geometries with dihedral angles between the aromatic rings of around 40° and around 140°. The barrier to rotation between the minima was low, at around 1 kcal/mol. The barrier to planarity was slightly higher, at 1.25 kcal/mol. With the inclusion of methyl groups at the 3- and 4-positions of the thiophene (**13b**), the barrier to planarity greatly increased to 5.75 kcal/mol, but the barrier to rotation between PES minima (now located at around 60° and 120°) decreased to < 0.5 kcal/mol.

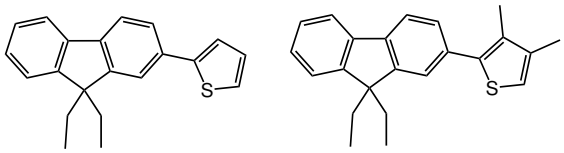

13a **13b**

FIGURE 1.14: Fluorene-thiophene molecules examined in the study by Gong *et al.*

1.2.7 Theoretical chemistry

Various groups have examined the predictive validity of different functionals and basis sets in, for the most part, TD-DFT (time-dependent density functional theory) studies, comparing calculated predictions to experimental data. A 2011 study by Fleming *et al.*[49] used TD-DFT to predict the UV/Vis spectra of oxazine dyes (**14**). They found that accounting for the presence of solvent significantly reduced the error in their predictions.

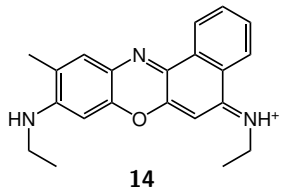

14

FIGURE 1.15: Oxazine dye studied by Fleming *et al.*

A study by Martynov *et al.*[50] found, for a group of phthalocyanine dyes (Figure 1.16), that starting geometry, solvation effects, and the basis set employed all affected the energy calculated, but not the trend across the group of compounds - a method that consistently predicts *relative* energies with high accuracy can be useful, even if the absolute values it gives are inaccurate.

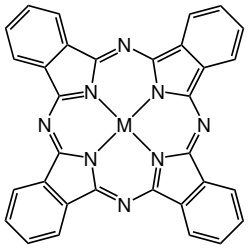

15a M = 2H; **15b** M = Zn

FIGURE 1.16: Phthalocyanine studied by Martynov *et al.*

Martynov *et al.* also found that, for vertical excitations, the best-performing computational methods used range-separated hybrid functionals.[50] Others have shown similar outcomes studying cyanines and various fluorophores:[51] conventional hybrid functionals (B3LYP and PBE0) perform well in prediction of the absorption and emission spectra of various dyes, and where they give inaccurate predictions for a group of compounds, the ranking within the group is preserved.

Fluorophores such as coumarins[52] and naphthalimides[53] have been studied with TD-DFT, and accounting for the presence of solvent has given better predictions. To decrease calculation time, time-independent DFT has been employed to predict UV-Vis spectra,[54] by making use of Kohn-Sham orbitals, but the predicted spectra differ visibly from the corresponding experimental spectra. This approach may be useful in very

high-throughput work, but the increased accuracy of TD-DFT is not generally considered costly, given the capabilities of modern hardware.

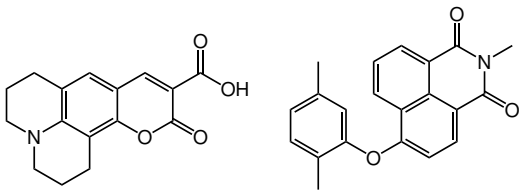

16 **17**

FIGURE 1.17: A coumarin solar cell fluorophore (**16**) and an electroluminiescent naphthalimide (**17**).

A study of bifluorene and substituted fluorenes used TD-DFT to examine the effect of polarity and extent-of-conjugation on excitation energy. It concluded that $CHCl_3$ decreased excitation energy, and did so most strongly for the most polar compounds that were examined. Compounds in which one aromatic ring is substituted with an electron-donating group, and the other with an electron-withdrawing group, such as **18**, displayed solvatochromic behaviour.[55] They concluded that, in general, excitation energy was lower in more conjugated systems. Other solvatochromic systems are discussed below (*vide infra* 2.2.10).

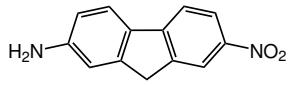

18

FIGURE 1.18: A polar push-pull system.

Ali *et al.*[56] found, for a diverse group of large, polyaromatic fused-ring electron acceptors (FREAs), based on fluorene, carbazole, and related scaffolds (Figure 1.19), that the conventional hybrid - PBE0, was the functional that gave the most accurate absolute predictions of λ_{max}, with an average error of 22 nm, and a maximum deviation from experimental data of 92 nm. Conversely, they found that the trend was best predicted by using a range-separated hybrid functional. Barboza *et al.*[57] looked at the excited states of unfunctionalised fluorene and found that range-corrected functionals were more effective at predicting electronic excitation energies than pure hybrids.

Adegoke *et al.*[58] showed that the HOMO - LUMO $\pi \rightarrow \pi*$ transition dominates electronic excitations in some polyaromatic fluorene-heterocycles, such as **22**. The HOMO - LUMO gap, whether calculated or extracted from spectral data, may not be predictive of emission wavelength for compounds with more exotic structures, however. Roohi *et al.*[59] predicted significant red-shift of the emission of some fluorene- and carbazole-based compounds (**23a**,**b**) that can undergo excited-state intramolecular proton-transfer.

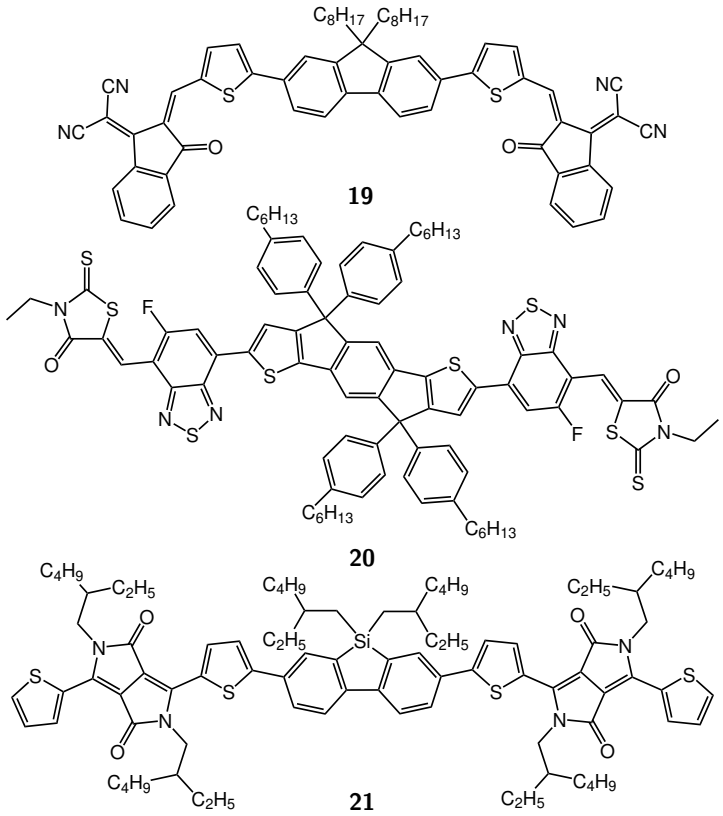

FIGURE 1.19: FREAs studied by Ali *et al.*

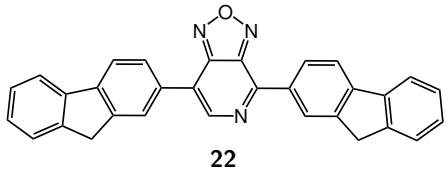

FIGURE 1.20: A representative example from the study by Adegoke *et al.*[58]

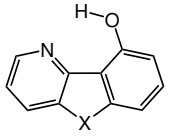

FIGURE 1.21: A system that undergoes excited-state intramolecular proton-transfer.

1.3 Scientific and technological aims

1.3.1 Research programme

This PhD thesis is part of a wider programme of research which aims to advance OLEC technology and its applications. The project is multidisciplinary, combining research from specialists in synthetic, physical, and theoretical chemistry, engineering and electronics, and biology. Naturally, individual contributions are not made in isolation. A major feature of the research has been the sharing of materials and data with other institutions and departments. A brief outline of the structure of the project will be beneficial to the reader's understanding of where this PhD sits in the broader research effort.

An engineering group, with a specialism in flexible electronics and smart materials, developed methods for printing OLECs onto flexible substrates, and polymer specialists developed self-healing device encapsulation. The synthetic chemistry group was tasked with providing new emissive materials for use in these devices. Working closely with the synthetic chemists, computational chemistry specialists sought ways of predicting the emissive properties of new chemical structures. A collaboration between electronics and biology groups studied the efficacy of antibacterial, UV-emitting OLEC devices in marine anti-fouling, and medical contexts, and prototyped a drug-free, anti-infective bandage.

The goal of the chemistry group, in general terms, was to make iterative improvements to our smart inks, using study of the photo-physics of new compounds, and relying on feedback from the engineers as to their practical viability. We were also concerned with aiding the development of a multitude of potential technological applications by enabling light-emission across a wide range of wavelengths. To this end, the group aimed to develop a smart-ink colour chart, spanning the visible electromagnetic spectrum, and if possible, extending into the UV and IR regions.

1.3.2 Research priorities

Ultimately, we would like to have the ability to rapidly converge on a high-performing smart ink structure, once an application has been identified, however the array of all feasible structures is too vast for even a modest experimental sampling of the overall chemical space to be practical. There are, however, structural elements that can be examined with some degree of isolation from one another, using, as a basis, a relatively small set of smart inks.

To date, there has not been a systematic effort to understand the relationship between the chemical structure of the light-emitters used in OLECs, and their emissive properties. While the predictive power of density functional theory is more-or-less universally recognised, and the applicability of the many functionals and basis sets is understood in general, a thorough benchmarking study, specific to the prediction of polyaromatic fragments' emissive properties, is required for us to accelerate the development of this field.

This work has two main intentions: first, to develop an understanding of the structure-activity relationship that determines the emission wavelength (and if possible, other properties) of an ionic small-molecule, and second, to apply the derived structure-activity relationship to the design of blue and ultraviolet light-emitters.

To this end, the first objective is to synthesise a systematically varied set of smart inks, and to observe any qualitative differences between the various subsets according to specific structural features. A computational procedure for predicting the absorbance and emission properties can then be established, using these smart inks as the training set. Testing of the model against experimental data, can then, by iterative refinement, improve the computational method.

Potential medical applications, such as an anti-infective bandage, are the proximate cause of interest in UV-emitting OLEC devices but, as with LEDs or any other type of light-emitter, the technology is general-purpose. The fact that blue and UV emission has proven difficult to realise is a sound reason to push the science beyond its existing limits in this area. It is safe to assume that applications will be found for UV-, visible-, and IR-emitting OLECs that have not yet been imagined.

1.3.3 Fluorene-based UV and blue emitters

Fluorene is incorporated into many organic fluorophores. Fluorene as the core of a luminogen has several advantages. It can be formed into oligomers and polymers with ease, as demonstrated by Yamaguchi *et al.*[60] (Scheme 1.1), and Liu *et al.*[61]; its electronics can be tuned by functionalisation of the arene; and the aliphatic carbon is easily alkylated, allowing a wide array of different substituents to be added to the molecule in a way that should minimally impact the electronics of the emissive part of the molecule.

In donor-acceptor systems, fluorene is very often used as the donor, in combination with an electron-deficient heterocyclic acceptor.[62–64] Figure 1.22 shows a UV/blue emitting bithiazole in which a fluorene fragment is the donor. It can also be used as a spacer, between a donor and an acceptor. A trio of red-emitters, in which fluorene is employed as a spacer, are shown in Figure 1.23.[65]

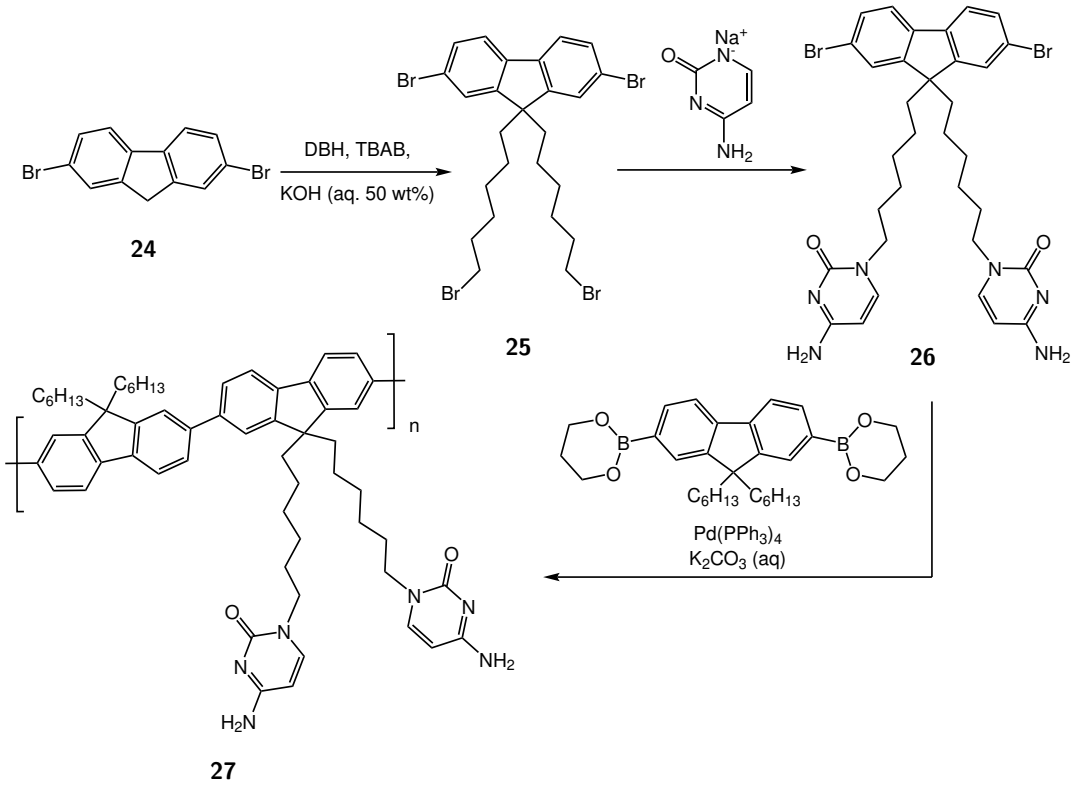

SCHEME 1.1: Synthesis of a fluorene-based AB copolymer.

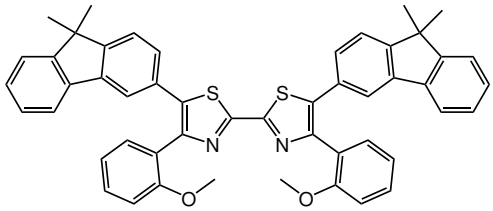

28

FIGURE 1.22: A compound in which fluorene acts as a donor.

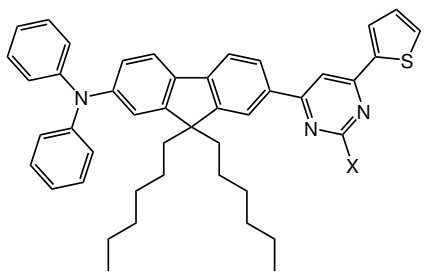

29a X = NH_2; **29b** X = OH; **29c** X = SH

FIGURE 1.23: Compounds in which fluorene acts as a spacer.

In a fluorene-ferrocene copolymer (Figure 1.24), a 9,9-dialkylfluorene acted as a donor, and the polymer's emission was substantially red shifted on oxidation of the ferrocene units.[66] A highly electron-withdrawing substituent at the 9-position enabled acceptor behaviour in the fluorene fragment. Charge transfer was so significant that the polymer resisted oxidation with $FeCl_3$.

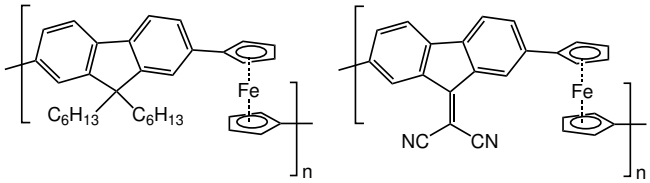

FIGURE 1.24: A pair of fluorene-ferrocene copolymers in which the role of fluorene depends on the functionality at the 9-position.

In 2012, Chen *et al.* reported the first UV-emitting LECs, with 2,2'-bifluorene derivative **31a**, (Figure 1.25).[67] This is a promising starting point for the design of UV emitting OLECs as the pi-system is not extensive, and the molecule is relatively small, allowing us to avoid difficulties such as the solution-processability of the compound.

Arumugam *et al.*[68] assessed bifluorene-based smart inks bearing a range of alkylimidazolium pendants and two different counterions. Octylimidazolium triflate salt, **31h**, was found to be the most viable smart ink in the set, with improved solution-processability in the device-fabrication process. Bathochromic shift was observed in both the absorption and PL emission of **31h**, going from solution to film state. Hypsochromic shift was observed in the spectra of **31a**. The thin film emission spectra contained additional bands at around 500 nm. These bands were stronger in compounds with smaller alkylimidazolium residues, suggesting that aggregation is the cause of the effect. The absorption of **31h**, in acetonitrile solution, was observed at 329 nm and at 340-343 nm in the film state. Its emission was observed at 383 nm in solution and at 385 nm in the film state.

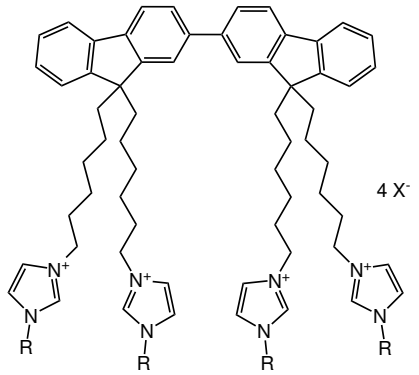

31a R = Me, X = PF_6; **31b** R = Me, X = CF_3SO_3
31c R = ^{n}Bu, X = PF_6; **31d** R = ^{n}Bu, X = CF_3SO_3
31e R = ^{n}Hex, X = PF_6; **31f** R = ^{n}Hex, X = CF_3SO_3
31g R = ^{n}Oct, X = PF_6; **31h** R = ^{n}Oct, X = CF_3SO_3

FIGURE 1.25: Bifluorene-based smart inks studied by Chen and Harrowven.

Shanmugasundaram *et al.* reported a pair of fluorene-based light-emitters with emission peaks at 389 (**32a**) and 390 nm (**32b**).[69] Emission wavelengths below 400 nm and a very straightforward method for modification of the structure, by known synthetic procedures, make this the ideal starting point for this study.

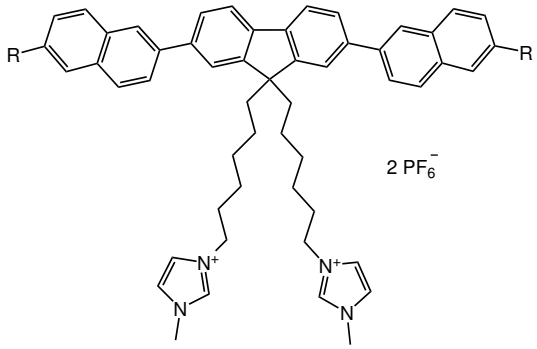

32a R = OMe; **32b** R = OEt

FIGURE 1.26: Deep blue emitters.

A generalisation of **32a**,**b** is shown in Figure 1.27. This is the starting point for the investigation of fluorenes in this thesis.

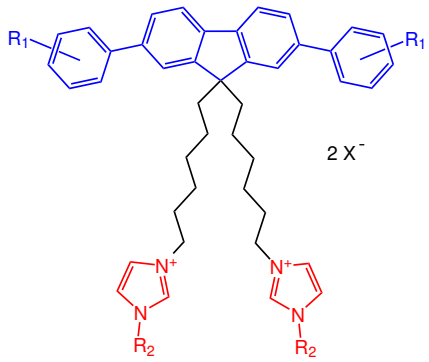

33

FIGURE 1.27: A generalisation of the structure of **32a**,**b**

The polyaromatic fragment, rendered in blue, has photo-physical and redox properties that enable electroluminescence. Polyaromatic compounds of this type are, generally, semiconductors. They are able to transport both electrons and holes by addition or removal of electrons from the frontier orbitals situated on the aromatic system. Systems based on substituted phenylfluorenes are slightly simpler than **32a** and **32b**, but are amenable to a great deal of structural modification, using readily available substituted benzenes.

The imidazolium fragments (in red) introduce charge. This enables the fabrication of OLEC systems with single-component active layers (as opposed to blends with electrolytes). Cations in small-molecule OLECs are often nitrogen-containing heterocycles or tetra-alkylammonium units. They are stable and are relatively passive in the redox processes at play in an electroluminescent device. These charged units are tethered to the core fluorophore by a hexylene linker chain, chosen for its simplicity and synthetic utility. A great variety of different terminal alkyl substituents can be incorporated into the imidazolium. They are usually kept simple (1-methylimidazolium is very common), but offer scope to tune the physical and aggregation properties of compounds of this kind.

The X^- anions are a potential source of variation in physical and electrochemical properties, but are usually chosen to be small (and, therefore mobile), non-nucleophilic, and redox-inactive under the conditions of device operation.

Keeping most of a structure constant, across a series of compounds, and varying certain moieties in a systematic way, allows us to attempt to isolate the effects of those parts of the structure. In this case, a general structure consisting of a fluorene core, hexylene linkers, imidazolium cations, and trifluoromethanesulfonate anions can be held constant. This allows us to focus on the influence of modifications to the chromophore (through introduction of aromatic substituents), and to the terminal substituents.

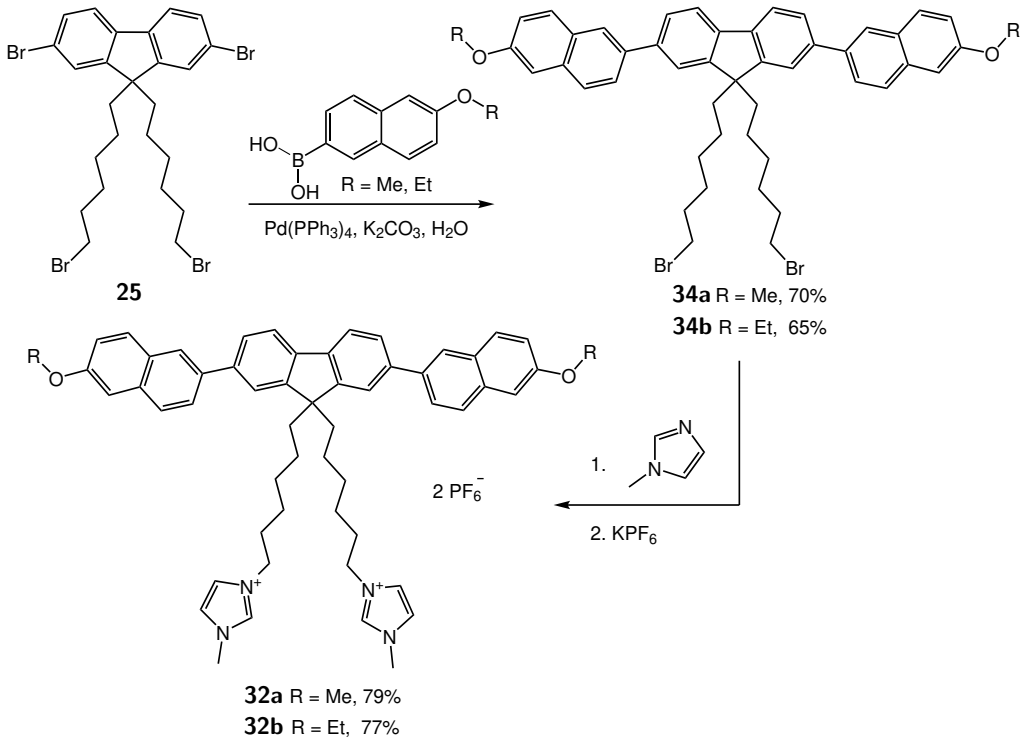

SCHEME 1.2: Synthesis of fluorene-naphthalenes employed by Shanmugasundaram.[69]

The synthetic approach used to generate these compounds was similar to that used by Yamaguchi *et al.*[60] Tetrabromide **25**, generated, as before, from 2,7-dibromofluorene and 1,6-dibromohexane, was cross-coupled, under Suzuki conditions, with a pair of naphthalene boronic acids (**34a**,**b**). These were quaternised, using 1-methylimidazole, then a final anion exchange gave the target smart inks. This procedure was identified as a useful means of accessing structures related to **33**.

Chapter 2

Fluorene-based light-emitters

2.1 Library synthesis

2.1.1 Overview

Herein are presented the synthesis and characterisation of a range of novel light-emitters; all close relatives of the fluorene-naphthalene system shown in Figure 1.26. A total of 36 fluorene-based smart inks formed the basis of this investigation.† 18 are arylfluorenes, shown in Figure 2.1, and another 18, shown in Figure 2.2, are diarylfluorene analogues.

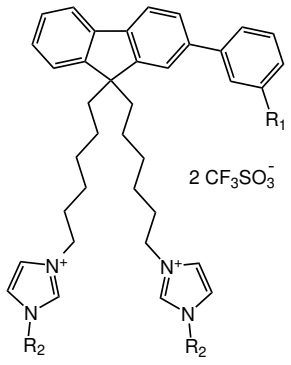

35a	$R_1 = R_2 = Me$	**35b**	$R_1 = Me, R_2 = n\text{-Oct}$
35c	$R_1 = OMe, R_2 = Me$	**35d**	$R_1 = OMe, R_2 = n\text{-Oct}$
35e	$R_1 = Ph, R_2 = Me$	**35f**	$R_1 = Ph, R_2 = n\text{-Oct}$
35g†	$R_1 = CF_3\ R_2 = Me$	**35h**†	$R_1 = CN, R_2 = Me$
35i	$R_1 = H, R_2 = Me$	**35j**	$R_1 = H, R_2 = n\text{-Oct}$

3-substituted arylfluorenes

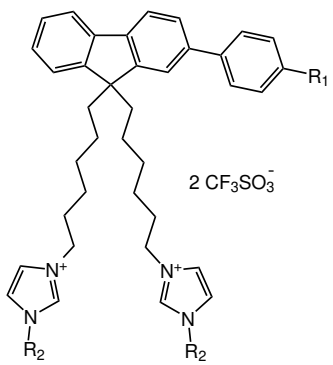

36a	$R_1 = R_2 = Me$	**36b**	$R_1 = Me, R_2 = n\text{-Oct}$
36c	$R_1 = OMe, R_2 = Me$	**36d**	$R_1 = OMe, R_2 = n\text{-Oct}$
36e	$R_1 = Ph, R_2 = Me$	**36f**	$R_1 = Ph, R_2 = n\text{-Oct}$
36g†	$R_1 = CF_3\ R_2 = Me$	**36h**†	$R_1 = CN, R_2 = Me$

4-substituted arylfluorenes

FIGURE 2.1: General structures of the arylfluorene compounds under investigation.

†Compounds synthesised and characterised by Dr Clementine E. Bavinton. UV-vis absorption spectra were collected by Edward H. Jackman

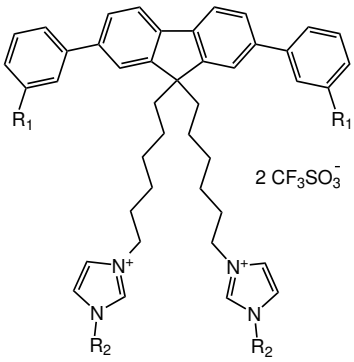

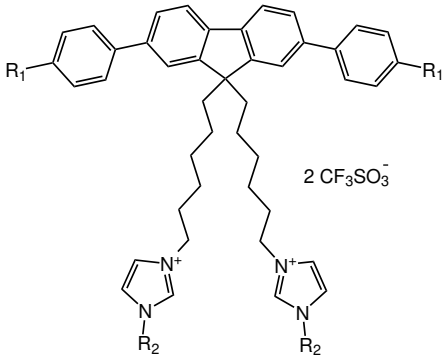

37a	$R_1 = R_2 = Me$	**37b**	$R_1 = Me, R_2 = n\text{-Oct}$	**38a**	$R_1 = R_2 = Me$	**38b**	$R_1 = Me, R_2 = n\text{-Oct}$
37c	$R_1 = OMe, R_2 = Me$	**37d**	$R_1 = OMe, R_2 = n\text{-Oct}$	**38c**	$R_1 = OMe, R_2 = Me$	**38d**	$R_1 = OMe, R_2 = n\text{-Oct}$
37e	$R_1 = Ph, R_2 = Me$	**37f**	$R_1 = Ph, R_2 = n\text{-Oct}$	**38e**	$R_1 = Ph, R_2 = Me$	**38f**	$R_1 = Ph, R_2 = n\text{-Oct}$
37g‡	$R_1 = CF_3\ R_2 = Me$	**37h**†	$R_1 = CN, R_2 = Me$	**38g**‡	$R_1 = CF_3\ R_2 = Me$	**38h**†	$R_1 = CN, R_2 = Me$
37i	$R_1 = H, R_2 = Me$	**37j**	$R_1 = H, R_2 = n\text{-Oct}$				

3-substituted diarylfluorenes 4-substituted diarylfluorenes

FIGURE 2.2: General structures of the diarylfluorene compounds under investigation.

The factors that determined the selection of functional groups were stability, synthetic viability, and simplicity. A systematically varied set of compounds was conceived with the goal of isolating the effects of individual structural features. Our work on bifluorene-based smart inks determined, to some extent, the features that would be varied in this study.

2.1.2 Establishment of a structure-activity relationship

Several hypotheses formed the basis of this investigation. The electronics of the fluorene moiety should have a significant impact on emission wavelength. The effect of substituents on the molecular orbitals could allow us to vary this independently. The extent of similarly conjugated π-systems would also be expected to have a major effect on emission wavelength. The nature of the counter-ion and length of the hydrocarbon tether would not be expected to alter the emission wavelength significantly, but could impact other physical properties. Likewise, the heterocyclic terminus on the carbon chain might affect physical properties and π-stacking interactions. The number of charged units could affect device efficiency without significantly changing emission wavelength.

Smart inks were investigated that incorporate phenyl and ten different substituted phenyl groups, chosen for the simplicity of their synthesis, stability, availability of requisite precursors, along with the systematic variation in electronic effect that they induce. It was predicted that both the presence of a functional group and its position on the phenyl ring would have an effect on emission wavelength and that this effect would be more pronounced for functional groups that induce a stronger mesomeric effect (+M or -M).

The substituted phenyl groups included in this investigation were 3-tolyl, 4-tolyl, 3-trifluoromethylphenyl, 4-trifluoromethylphenyl, 3-methoxyphenyl, 4-methoxyphenyl, 3-cyanophenyl, 4-cyanophenyl, 3-biphenyl, and 4-biphenyl. In order to examine +I, -I, +M, and -M effects independently of one another, a set of 4 functional groups with complementary Hammett substituent constants was required. Methoxy (+M, -I, σ_p = -0.27), cyano (-M, -I σ_p = 0.66), methyl (+I, σ_p = -0.17), and trifluoromethyl (-I, σ_p = 0.54) were chosen as exemplars from each of the 4 categories.

The effect of adding additional phenyl substituents was also studied by comparison of phenylfluorenes with biphenylfluorenes and *bis*(phenyl)fluorene with *bis*-(biphenyl)fluorene analogues (Figure 2.3). As these differ in respect of their symmetry, the conclusions drawn from these comparisons might not be straightforward. The initial hypothesis was that arylfluorenes would exhibit lower-wavelength emission than their diarylfluorenes analogues and that this would be due, principally, to their smaller conjugated π-systems.

The final comparison to be made was that between 1-methylimidazolium and 1-octylimidazolium smart inks (Figure 2.4). Our starting assumption was that the emission wavelength would not be significantly impacted by this difference, but that emission intensity in the solid state may be impacted for reasons stated in Section 1.2.6. The first set of compounds made were those incorporating phenyl, tolyl, methoxyphenyl, and biphenyl groups, and these were used as the initial training set for the computational analysis detailed in Chapter 3, and for much of the device-fabrication process. A colleague then synthesised those bearing cyanophenyl and trifluoromethylphenyl groups, by which time discoveries had been made about the inefficacy of the octylimidazolium smart inks, hence the absence of inks combining CN or CF_3 groups with octylimidazolium pendants.

The counter-ion was not varied in this investigation as a study by Arumugam *et al.* had concluded that, for the bifluorene systems, triflate salts tended to have better solubility profiles for device-printing than did the hexafluorophosphate salts. The length of the alkyl chain also has a significant effect on solubility, but fine-tuning of the solubility of promising molecules was not necessary at this stage. Given the difference in charge multiplicity between the bifluorene-based smart inks and those investigated herein, firm assumptions about the effect of alkyl chain length were deemed to be outside the scope of this study.

For each of the synthesised smart inks, once isolated and characterised, a UV-vis spectrum, a fluorescence spectrum, and a cyclic voltammogram were obtained. The voltammetric data were used to calculate the HOMO energy. The UV-vis spectrum gave the HOMO - LUMO gap. Details of these calculations are given in section 2.2.

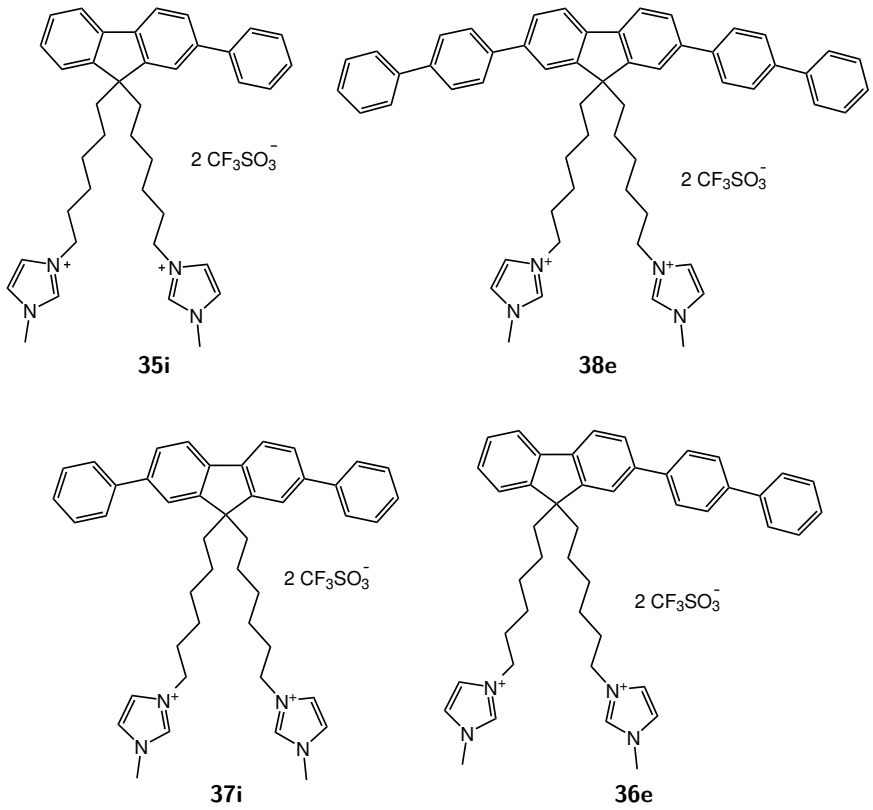

FIGURE 2.3: Compounds with π-systems consisting of phenyl and biphenyl groups bonded to fluorene.

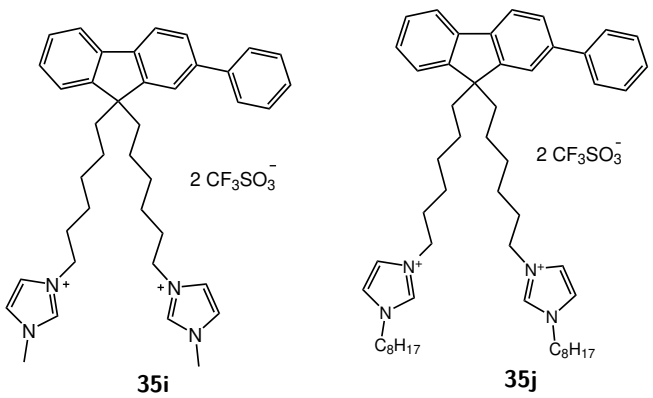

FIGURE 2.4: Compounds that differ in the size of their imidazolium pendants.

2.1.3 Synthetic route

A modification of the procedure used by Shanmugasundaram,[69] to synthesise the fluorene-naphthalene compounds (Scheme 1.2), was employed to prepare the aforementioned series of compounds (Figure 2.1 and Figure 2.2). Scheme 2.1 shows the synthesis of **35a**–**j** and **36a**–**h** by this route. First, bromofluorene **39** was alkylated at the benzylic position with 1,6-dibromohexane (DBH) to give **40**. Then dioxaborolane **41** was generated by Miyaura coupling. A range of arylbromides were then used in Suzuki coupling reactions to generate the corresponding arylfluorenes **42** and **43**. Quaternisation with alkylimidazoles, followed by ion exchange, gave the smart inks **35a**–**j** and **36a**–**h**.

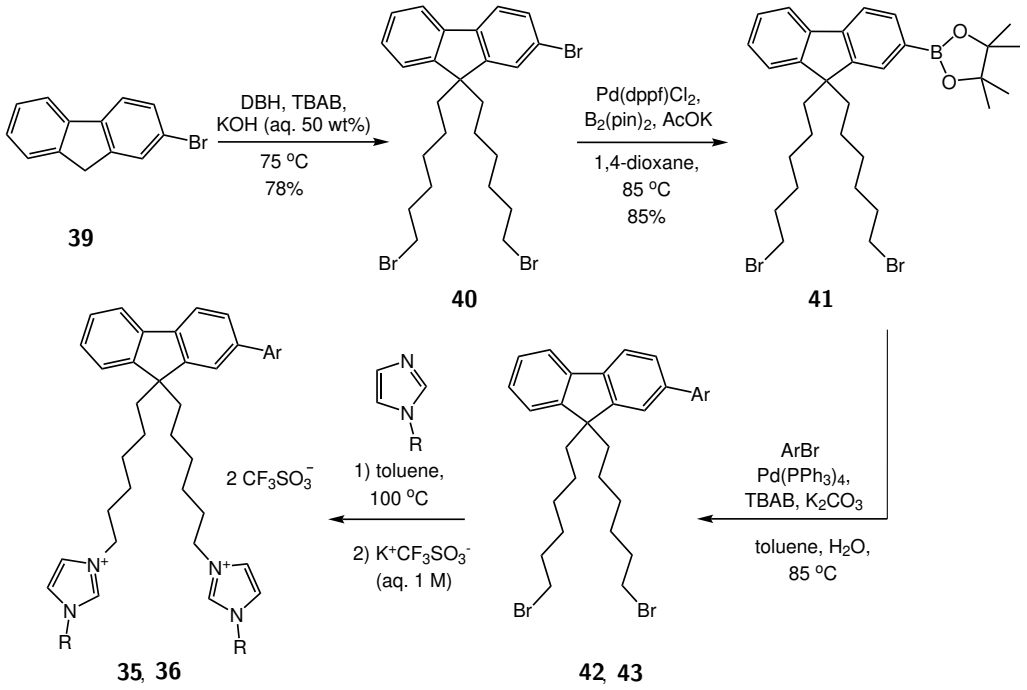

SCHEME 2.1: Synthetic route to **35a**–**j** and **36a**–**h**.

The adoption of a late-branching synthetic route allowed starting materials to be synthesised in bulk, then divided into aliquots for the following reaction steps. This minimised the number of reactions required to generate a wide array of unique materials. The number of reactions required to synthesise this set of smart inks could, in principle, have been reduced by performing the quaternisation before the Suzuki coupling, but the limited solubility of the imidazolium salts rendered this approach impractical.

The same strategy was subsequently applied to dibromofluorene **24**. The bis-alkylation step to **25** and the bis-borylation step to **44** each proceeded smoothly allowing the library of smart inks **37a**–**j** and **38a**–**h** to be prepared in good yields (Scheme 2.2, Table 2.2). In the following sections (2.1.4 - 2.1.6) each step of this sequence will be discussed in detail.

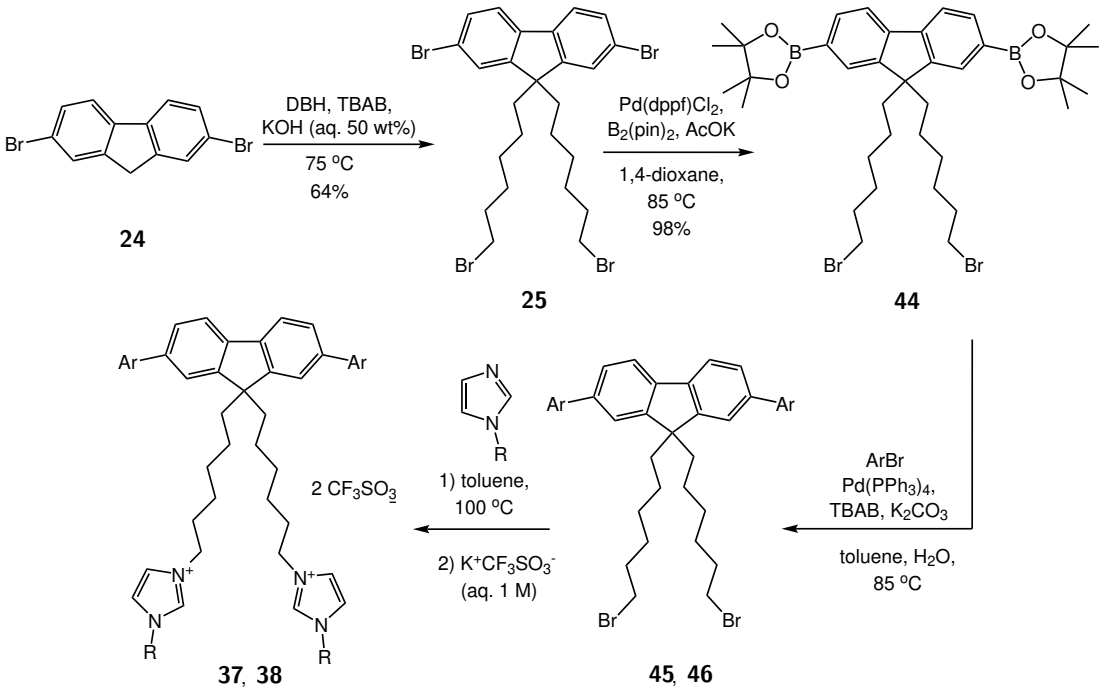

SCHEME 2.2: Synthetic route to **37a**–**j** and **38a**–**h**.

2.1.4 Synthesis of dialkylfluorenes

The alkylation of bromofluorenes **24** and **39** required a very high concentration of 1,6-dibromohexane for oligomerisaton (**47**), intramolecular cyclisation (**48**), or inexhaustive reaction (**49**) to be avoided. A colleague[70] found that using 7 equivalents of 1,6-dibromohexane resulted in a significantly lower yield of the target molecule than using 10 equivalents. His work also showed that significant amounts of **48** and **49** were formed, along with small amounts of numerous other compounds, when smaller excesses of 1,6-dibromohexane were used. Because the myriad by-products that were formed tended to have similar R_F values in column chromatography, their separation was difficult to achieve. The reaction was performed with an excess of 1,6-dibromohexane sufficient to avoid their formation altogether. As 1,6-dibromohexane is an oil, it was used neat.

Once the reaction was complete, dilution with DCM allowed a standard work-up to be performed, giving an oil that consisted, predominantly, of 1,6-dibromohexane. This and the target dialkylfluorene compound have very similar R_F values and are highly lipophilic, so extremely non-polar solvent systems were used to separate them. A reaction that started with 10 g of 2-bromofluorene (40.8 mmol) used approximately 65 mL of 1,6-dibromohexane, of which approximately 13 mL was consumed in the production of the target molecule. The remaining 52 mL of 1,6-dibromohexane, having a boiling point of 243 °C, could not be easily distilled from the mixture. The method of isolating the target molecule that was found to be most efficient was chromatography with petroleum ether or hexane. A silica gel slurry around 20 cm deep, in a 9 cm diameter column, with a very porous frit was used. The first 6 L of eluent was collected as quickly as possible

and discarded. Fractions were then collected as normal and, once the 1,6-dibromohexane had all eluted, 10% DCM in petroleum ether or hexane was used. Some of the target compound was inevitably lost to the earlier, mixed fractions, and in general, a fresh reaction was a much more fruitful means of isolating more of the target molecule than further chromatography.

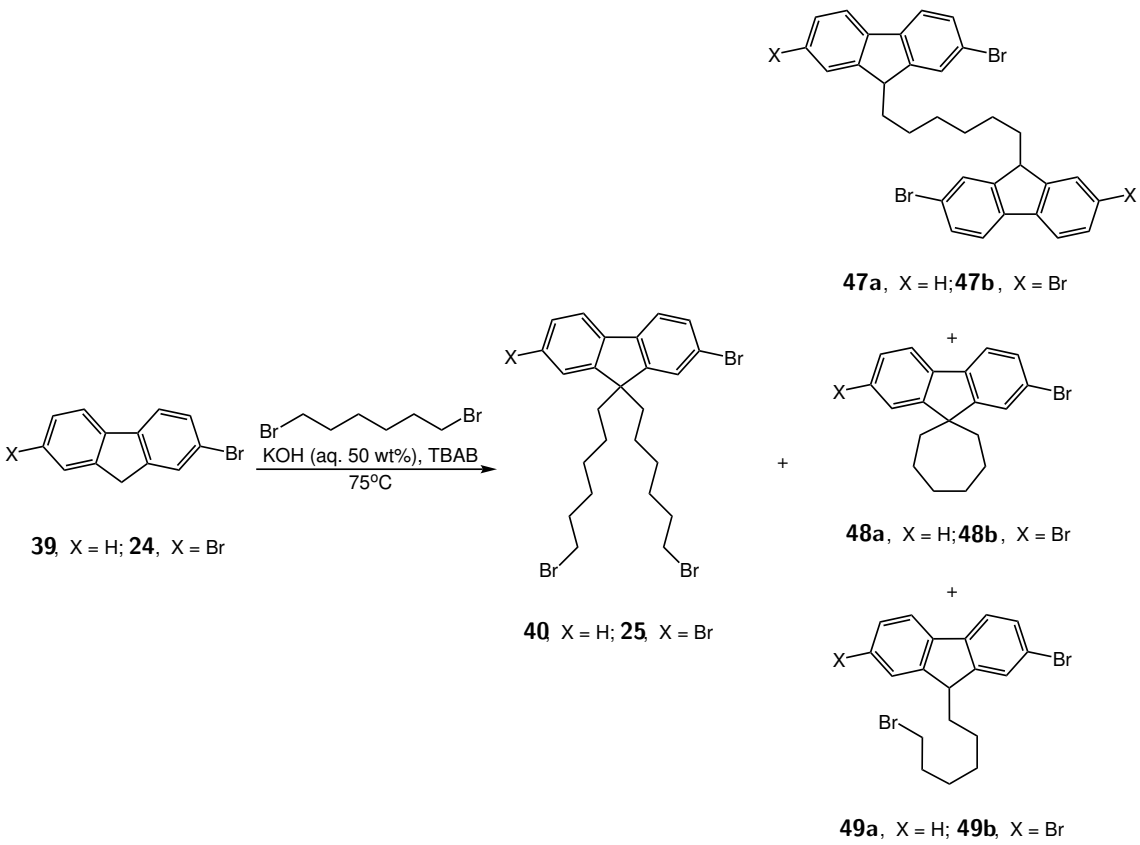

Scheme 2.3: By-products of 2-bromofluorene alkylation.

Production of alkylated fluorenes on a larger scale, using the same methods, would be problematic. A 40 mmol reaction produced a mixture of oils that was around 1 cm deep, when loaded into the large, 9 cm diameter column used throughout this PhD. A scale-up of this process would require more specialised equipment. Only a few instances of this reaction were required in order to give enough material to complete the work, so optimisation of the process was not prioritised.

2.1.5 Cross-coupling to form arylfluorenes and diarylfluorenes

The fluorene-naphthalene compounds reported by Shanmugasundaram *et al.* (**32a**,**b**) were synthesised without conversion of dibromofluorene **25** to dioxaborolane **44**. Instead, the dibromofluorene was reacted, under Suzuki coupling conditions, with an arylboronic acid (Scheme 1.2). If the desired arylboronic acid happened to be available, or cheap to acquire, this approach was the most economical. In this work, a single, large-scale

Miyaura coupling was employed (**25** → **44**, Scheme 2.2), so that a variety of cheap, readily available arylbromides could be used as Suzuki coupling partners. The Miyaura coupling proved straightforward and high-yielding, and the only difficulty encountered in the process emerged from the tendency of *bis*-pinacolatodiboron ($B_2(pin)_2$) to degrade over time. Once this had been identified as the cause of lower-than-expected yields, simply sieving the reagent, to separate the *bis*-pinacolatodiboron powder from crystalline impurities, gave much better results.

The Suzuki coupling of a dioxaborolane **41** and **44** and an arylbromide was not fraught with practical difficulties, but yields varied greatly, depending on the arylbromide substrate. Arylbromides in which the carbon bonded to bromine is electron-rich tended to give lower yields in this reaction. The most problematic arylbromide substrates included in this study were 4-bromoanisole and 2-bromoanisole. Reactions with 4-bromoanisole gave **46b** in 57% and **43a** in 27% yield (Table 2.1 and Table 2.2). This was not considered low enough to warrant further investigation.

The first set of inks to be synthesised were those based on *bis*-(methoxyphenyl)fluorenes. Scheme 2.4 shows the disparity in yields achieved under identical conditions for the 3 different bromoanisoles (**42a**, **43a** and **51a**). The reaction with *ortho*-bromoanisole was attempted a second time without improvement, so the study of 2-substituted arylfluorenes and diarylfluorenes was set aside. The need to provide a significant quantity of each smart ink to our collaborators[‡] made it prudent to focus efforts on those substances which gave moderate to high yields at every stage of their synthesis.

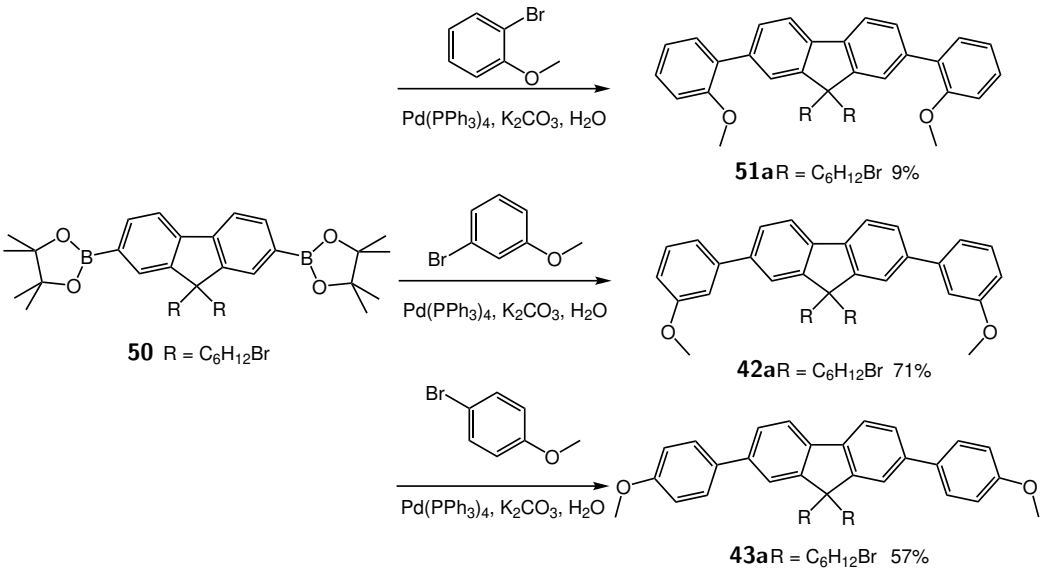

SCHEME 2.4: Formation of *bis*-(methoxyphenyl)fluorenes.

[‡]A standard batch of OLECs consisted of 9 devices, each requiring 0.15 mL of a 70 mg/mL solution. 190 mg of a smart ink permitted 2 batches to be fabricated, which was considered ideal.

2.1.6 Quaternisation

Quaternisation of the bromoalkane residues to form imidazolium salts (**41** → **35a**–**j**, **36a**–**h**, Scheme 2.1 & **44**→**37a**–**j**, **38a**–**h**, Scheme 2.2) proceeded well, provided a significant excess of the parent imidazole was used, and several days were allowed for complete reaction. Reaction in a non-polar solvent proved best as it allowed the imidazolium bromide salt (*e.g.* **52a**,**b**) to precipitate from solution as it formed (Scheme 2.5 is an illustrative example). Excess imidazole could then be decanted away with the solvent, once the reaction was complete. After washing the residue with toluene, anion exchange was performed (**52a**,**b** → **35i**,**j**). In this final step, washing with copious water was required to rid the mixture of excess KBr. Triflate salts were sonicated in water and collected by filtration repeatedly to ensure complete removal of KBr. As the solid residues were sonicated repeatedly in water, and the water discarded, the form of the residue changed visibly. In general, the residue began as a white or off-white solid, and became an off-white gum after several washes, indicating the removal of KBr.

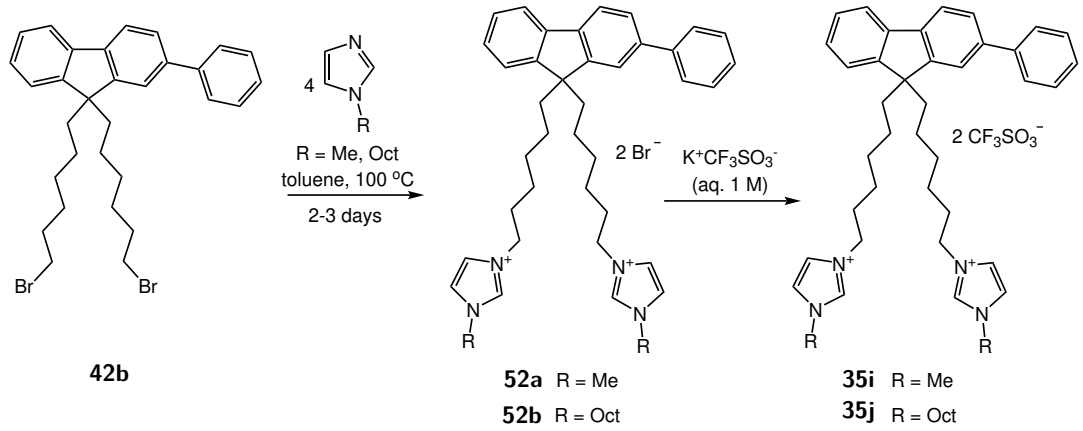

SCHEME 2.5: The quaternisation of **42b**.

If too little imidazole was used in the quaternisation reaction, or if the reaction was not given adequate time, some of the bromoalkane residues remained unreacted. Separation of a singly-substituted compound, such as **53**, from the desired dications, was not straightforward, so the mixture had to be subjected to the reaction conditions again in such instances. This process was unreliable and usually failed to give a completely quaternised smart ink. Reaction for 2 or 3 days with a twofold stoichiometric excess of an alkylimidazole was found to be sufficient, with replenishment of any lost toluene.

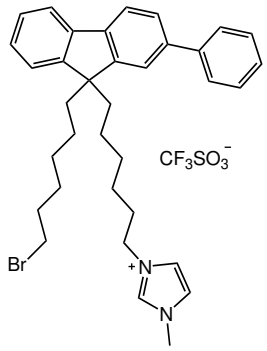

53

FIGURE 2.5: A singly-substituted smart ink.

TABLE 2.1: Synthesis of arylfluorene smart inks.

	Ar	R	Yield **42** and **43** (%)	Yield **35** and **36** (%)
42c, **35a**	3-MeC_6H_4	Me	44	65
42c, **35b**	3-MeC_6H_4	Oct	44	25
42a, **35c**	3-MeOC_6H_4	Me	60	94
42a, **35d**	3-MeOC_6H_4	Oct	60	72
42d, **35e**	3-PhC_6H_4	Me	42	35
42d, **35f**	3-PhC_6H_4	Oct	42	14
42b, **35i**	C_6H_5	Me	84	63
42b, **35j**	C_6H_5	Oct	84	77
43b, **36a**	4-MeC_6H_4	Me	24	70
43b, **36b**	4-MeC_6H_4	Oct	24	99
43a, **36c**	4-MeOC_6H_4	Me	27	64
43a, **36d**	4-MeOC_6H_4	Oct	27	67
43c, **36e**	4-PhC_6H_4	Me	96	34
43c, **36f**	4-PhC_6H_4	Oct	96	80

TABLE 2.2: Synthesis of diarylfluorene smart inks.

	Ar	R	Yield **45** and **46** (%)	Yield **37** and **38** (%)
45a, **37a**	3-MeC_6H_4	Me	72	52
45a, **37b**	3-MeC_6H_4	Oct	72	70
45b, **37c**	3-MeOC_6H_4	Me	71	58
45b, **37d**	3-MeOC_6H_4	Oct	71	41
45c, **37e**	3-PhC_6H_4	Me	57	33
45c, **37f**	3-PhC_6H_4	Oct	57	57
45d, **37i**	C_6H_5	Me	70	50
45d, **37j**	C_6H_5	Oct	70	87
46a, **38a**	4-MeC_6H_4	Me	61	91
46a, **38b**	4-MeC_6H_4	Oct	61	83
46b, **38c**	4-MeOC_6H_4	Me	57	33
46b, **38d**	4-MeOC_6H_4	Oct	57	58
46c, **38e**	4-PhC_6H_4	Me	75	14
46c, **38f**	4-PhC_6H_4	Oct	75	57

2.2 Experimental analysis

2.2.1 Overview

The oxidation and reduction potentials of a semiconductor can be used to determine its interfacial energy-level alignment with anode and cathode materials. This is important to know as a large energy-level mismatch with either the cathode or anode would result in inefficient transport of electrons or holes respectively. Both potentials can be obtained from cyclic voltammetry (CV) measurements, but accurate measures of the reduction potential are impossible in the presence of moisture. Given the impracticality of thorough drying of the imidazolium salts under investigation, the absolute energy of the LUMO can be calculated from the sum of the HOMO energy (from cyclic voltammetry) and the HOMO-LUMO gap (from UV-vis absorption).

The barrier to electron-injection is defined as the difference between the LUMO energy of the semiconductor and the Fermi energy of the cathode, which is defined for a given metal at a given temperature. The hole-injection barrier is similarly defined using the HOMO energy and the Fermi energy of the anode. Typical Fermi energy values for silver are around 5.5 eV and those for indium tin oxide (ITO) are around 3.0 eV. Temperature, surface topology, and the presence of impurities and adsorbed gasses can affect the electrochemical properties of the electrodes, but their examination lies outside the scope of this work.

2.2.2 Calculation of the HOMO energy from a cyclic voltammogram

The absolute energy of the HOMO of a species can be calculated from the potential at which it begins to oxidise in an electrochemical cell. A compound's oxidation peak onset can be extracted from its cyclic voltammogram, by a process detailed below. The oxidation peak onset must be compared to that of a standard, measured against a reference electrode. Ferrocene is the standard in common use[71]. The potential of the Fc^+/Fc redox couple, in eV, is taken as its half-wave potential, defined as,

$$E_{1/2} = \frac{1}{2}(E_{pc} + E_{pa}), \tag{2.1}$$

where E_{pa} is the *anodic* peak maximum and E_{pc} is the *cathodic* peak minimum. The anodic and cathodic peaks, measured against saturated calomel electrode (SCE), were found to be 0.36 eV and 0.44 eV respectively, giving a half-wave potential of 0.40 eV. The potential of ferrocene against vacuum is -4.8 eV,[72] so the energy of the HOMO in eV is given by:

$$E_{HOMO} = -(E_{onset} + 4.4). \tag{2.2}$$

The evaluation of E_{onset} involved a degree of judgement, but the process presented below was an attempt to generate the values in as objective a manner as possible. An example illustrates the process.

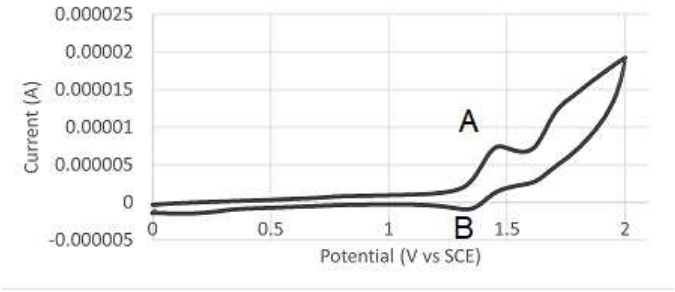

FIGURE 2.6: The cyclic voltammogram of **38e**.

The oxidation peak (**A**, Figure 2.6) is very clear, but its onset appears gradual, because the 'baseline' is non-zero and gradually increasing. It is difficult to determine exactly when the increase in current, and therefore oxidation, begins. Note that the reduction peak (**B**, Figure 2.6) is also visible, but without thorough drying and degassing of the sample, any calculations based on this peak would be meaningless.

A numerical approximation to the first derivative of a CV curve (Figure 2.7) can be obtained as follows: for a given data point on the voltammogram, take the difference between two measured current values that are 5 data points apart. Do the same for the corresponding potential values, and divide the former by the latter to give $\frac{\Delta A}{\Delta V}$ for that point. The same process was applied to the $\frac{\Delta A}{\Delta V}$ values to give an approximation to $\frac{d^2A}{dV^2}$. Values 5 data points apart were used to avoid the problem of adjacent identical values producing zeroes.

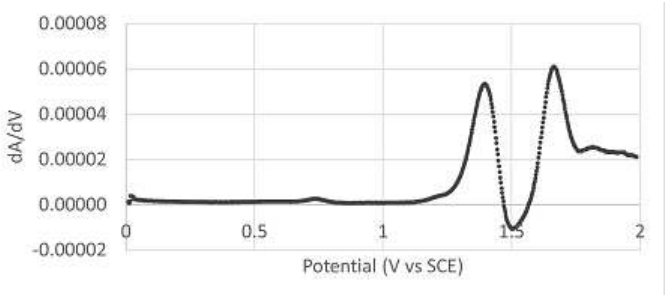

FIGURE 2.7: A numerical approximation of the first derivative of the voltammogram 'curve'.

The slope of the curve prior to the oxidation peak in the voltammogram is roughly constant, so the first derivative gives a nearly flat line until the onset of oxidation. It is, however, still unclear at which potential value the oxidation begins, partly due to the fact that $\frac{\Delta A}{\Delta V}$ sits slightly above the x-axis, and partly due to the smooth increase in gradient. The onset appears to occur somewhere around 1.2 - 1.3 V, in this case.

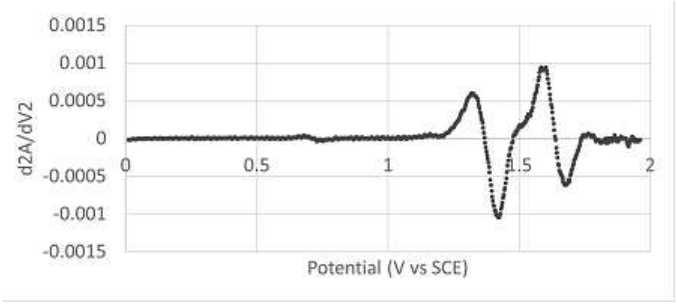

FIGURE 2.8: A numerical approximation of the second derivative of the voltammogram 'curve'.

In the 2nd derivative approximation (Figure 2.8), the values before the oxidation peak sit on the x-axis, and the rise in the gradient occurs more abruptly than in either of the other plots. Close examination of the data shows a sharp rise in the $\frac{d^2A}{dV^2}$ values beginning at 1.27 V.

The energy of the HOMO is simply:

$$E_{HOMO} = -(1.27 + 4.4) = -5.67\ eV. \tag{2.3}$$

2.2.3 Calculation of the optical bandgap from the UV-vis spectrum

The HOMO to LUMO $\pi \rightarrow \pi*$ transition was shown to be the dominant transition in a set of fluorene-based semiconductors,[58] so it was predicted that the HOMO - LUMO gap would be approximated by the optical band gap, which can be calculated by the Tauc method.[73]

The Tauc method, briefly summarised, involves finding the point of steepest increase in absorbance, running from low to high frequency, and plugging the corresponding wavelength into the formula:

$$E_{opt} = \frac{1239.95}{L_{onset}}, \tag{2.4}$$

where E_{opt} is the optical band-gap of the material, and L_{onset} is the wavelength at which absorbance is increasing most rapidly. Figure 2.9 is the absorbance spectrum of **38e**. The steepest part of the slope was assumed to be located at about the mid-point of the absorbance band and from the approximately sigmoid shape of the curve in that part of the spectrum, this was a safe assumption. The point on the curve at 50% of the absorbance maximum occurs at 361 nm and the band-gap was given by,

$$E_{opt} = \frac{1239.95}{361} = 3.43\ eV. \tag{2.5}$$

The final value to be calculated is the absolute energy of the LUMO:

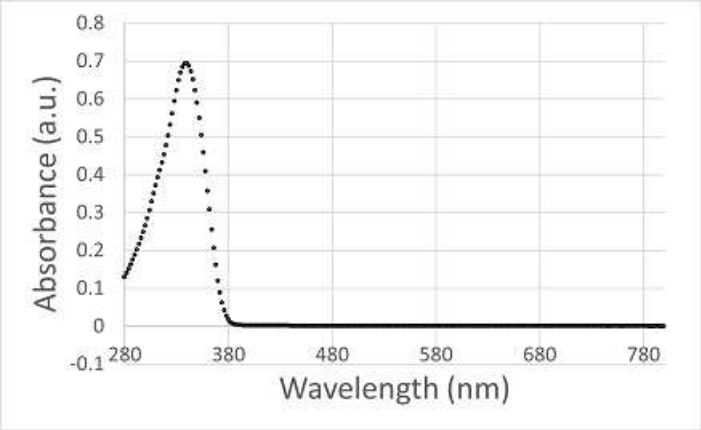

FIGURE 2.9: The UV-visible absorption spectrum of compound **38e**.

$$E_{HOMO} + E_{opt} = E_{LUMO}, \tag{2.6}$$

$$-5.67\ eV + 3.43\ eV = -2.24\ eV. \tag{2.7}$$

2.2.4 Electroluminescent devices

The smart inks described in this chapter and the OLEC device fabrication process were in simultaneous development throughout the research programme. OLECs fabricated early in the project used polymer/electrolyte blends based on Super Yellow and other well known polymers. Potassium trifluoromethanesulfonate (KOTf) was used as the supporting electrolyte.[††]

First, a PEDOT:PSS suspension in water was spray coated directly on to the ITO-coated glass substrate and dried. A solution of the electroluminescent polymer in toluene was then mixed with solutions of KOTf and the ion-dissolving polymer polyethylene oxide in cyclohexanone. The resulting solution was spray coated over the PEDOT:PSS layer and dried. A layer of silver nanowires was then spray coated and silver conductive paint was used to connect the device to a circuit.

When experimental smart inks were used, the active layer and PEDOT:PSS were applied by spin-coating due to persistent problems with nozzle-blockage when spray coating was attempted. When printing onto a glass/ITO slide, the top electrode was always a solid layer of silver applied by sputter coating. Many parameters (*e.g.* spin speeds, annealing times and temperatures, and solution amounts and concentrations) required adjustment as more devices were made. It became clear that no single set of parameters would result in optimal performance with every smart ink. A method was established which tended

[††]All data from electroluminescent devices, as well as all thin film photoluminescence data, and all images from scanning electron microscopy were collected by Dr Katie Court and Dr Yi Li and were reproduced with permission. This collaboration was time-limited so data for some compounds could not be collected.

to produce more working devices than failures, but the eradication of failures was not possible nor was optimisation of the process for each new ink practicable.

The data obtained from devices that use experimental smart inks could not be assumed to be perfectly reliable. There are several factors that could affect the electroluminescence of OLEC devices, including the thickness of the active layer, and the concentrations of fluorophores and electrolyte in the active layer. Figure 2.10 shows the electroluminescence spectra from a pair of OLEC devices that used **37b** and **38e**. **37b** exhibited electroluminescence with a peak at or just above 400 nm, but the precise value is not clear and no further structure is discernible. The latter has 50 times the intensity and a spectrum in which the λ_{max} value is easily extracted. The location and shape of a secondary peak are also very clear.

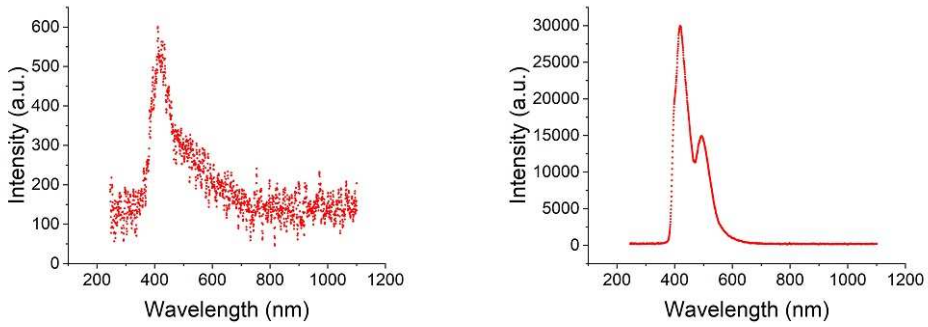

EL spectrum of **37b** EL spectrum of **38e**

FIGURE 2.10: Electroluminescence spectra from two OLEC device[74;75].

The inconsistency of the electroluminescence data limited their use in this investigation. High quality photoluminescence data, in solution and film states, were acquired for a wider range of compounds and provide a better description of true emission colour.[††] The first thing to note about the thin film photoluminescence spectra of **35a-38h** is that they tended to have a 2-band structure, with some spectra displaying two very distinct bands, and others, a major band with a shoulder peak. λ_{max} values taken from global maxima were used for all analysis, unless otherwise stated.

Solution photoluminescence spectra tend to have a 2-band structure with both bands very similar in intensity, and the global maximum can lie on either band. Photoluminescence spectra for **37b** and **38e** in the film state and in solution (Figure 2.11) are shown for comparison with the electroluminescence data shown above. In some cases, 2 λ_{max} values are used in discussion of a compound's emission, one for λ_{max} and another for a local maximum of very similar intensity.

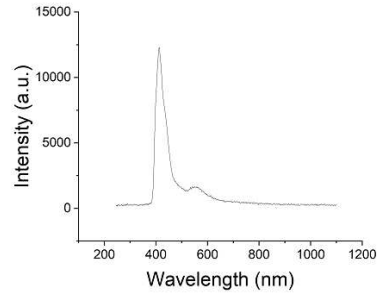

Film PL spectrum of **37b**[74;75]

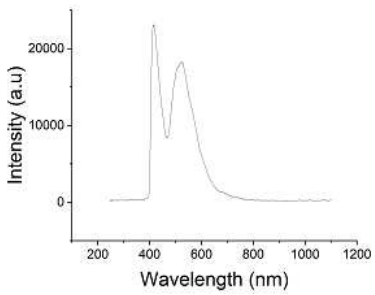

Film PL spectrum of **38e**[74;75]

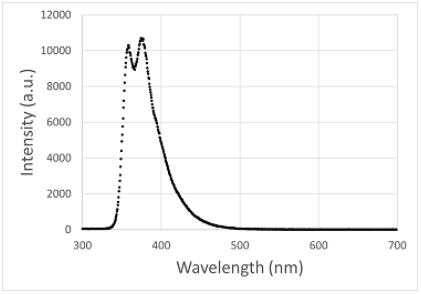

Solution PL spectrum of **37b**

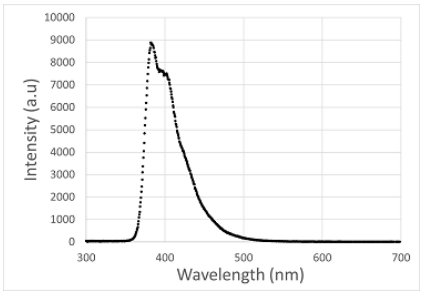

Solution PL spectrum of **38e**

FIGURE 2.11: Solution and thin film photoluminescence spectra of **37b** and **38e**.

2.2.5 Methylimidazolium *vs* octylimidazolium

Data tabulated in Appendix G show the wavelengths of the 2 peaks in the solution-state emission spectra of pairs of compounds. With an average difference in emission peak wavelength of < 1 nm for a 1-methylimidazolium/1-octylimidazolium pair, emission wavelength in acetonitrile solution appears to be barely affected by the length of the terminal alkyl chain.

Figure 2.12 shows images, from a scanning electron microscope (SEM), of OLEC devices fabricated using four smart inks (Figure 2.13). **35a** produced a very even film (the thin, dark band) on an ITO electrode (the bottom-most of the two bright lines). **35b** differs from **35a** only in that it bears an octylimidazolium pendant, and produced a highly uneven film. Likewise, an even layer of **35e** (which bears a methylimidazolium pendant) contrasts with an uneven layer for **35f** (its octylimidazolium analogue). These are representative examples that demonstrate the poor performance of octylimidazolium salts in the fabrication process. See Appendix E for SEM images of other OLEC devices.

It is possible that modifications to the fabrication process, such as the use of different solvent systems in the spin coating step, would improve the evenness of the layers formed from octylimidazolium inks. The fabrication method proved to be generally reliable across a fairly diverse range of smart inks, so pursuit of high performance from uncooperative inks such as these was deemed not to be a priority. The synthesis of new octylimidazolium smart inks was therefore discontinued.

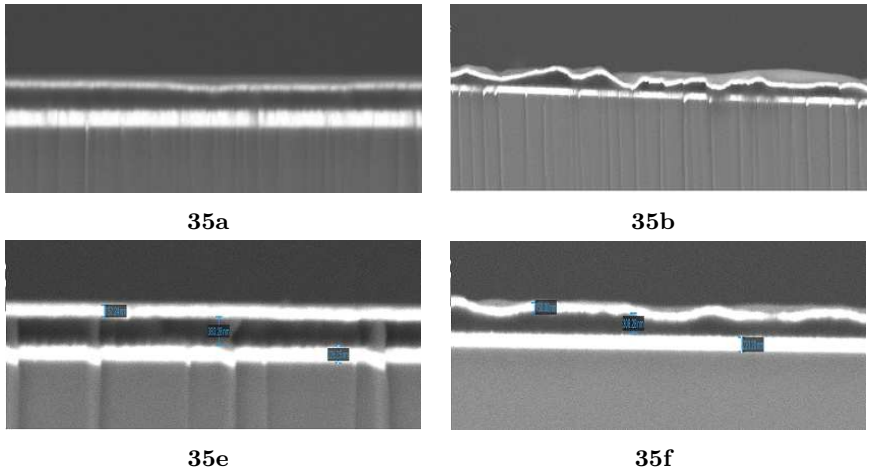

FIGURE 2.12: SEM images of OLEC devices using **35a**, **35b**, **35e** and **35f**[74;75].

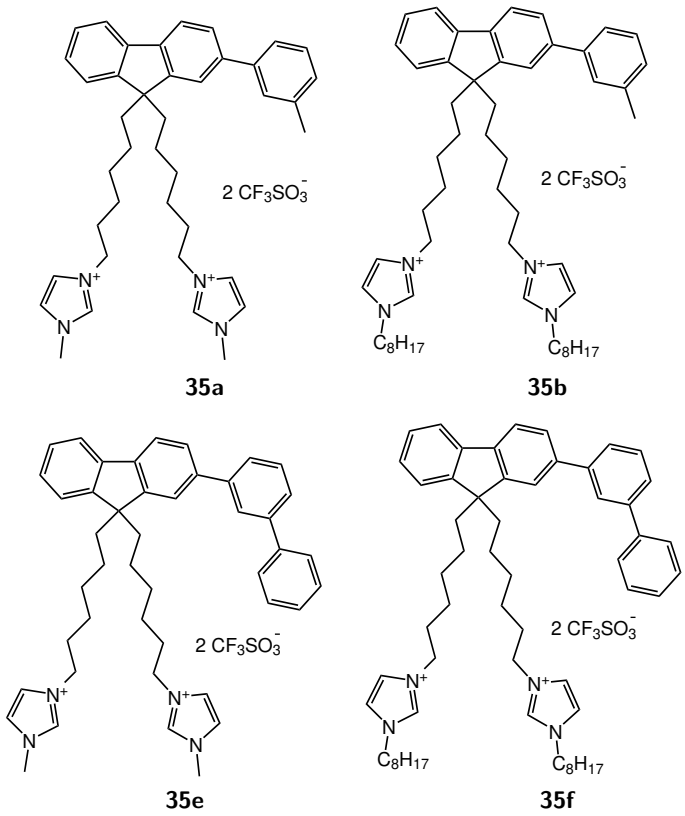

FIGURE 2.13: Two methyl/octylimidazolium pairs, compared in Figure 2.12.

Few octylimidazolium inks produced working devices, so solid-state data on this subclass was not complete enough for meaningful conclusions to be drawn. Analysis of the relationship between structure and activity in the fluorophore was therefore restricted to methylimidazolium variants.*

*__38d__ was among the few octylimidazolium inks to produce a fairly even film and a high quality electroluminescence spectrum. Due to the inadvertent loss of the only sample of 1-methylimidazolium analogue **38c**, **38d** was used for later analysis.

2.2.6 Arylfluorenes *vs* diarylfluorenes

No strict pattern emerged from the solution-state data (Table 2.3), when compounds were compared in arylfluorene/diarylfluorene pairs. Thin-film photoluminescence spectra, on the other hand, showed that a diarylfluorene analogue always emits longer-wavelength light than the corresponding arylfluorene. This result could be rationalised by the presence of more extensive π-systems leading to lower HOMO-LUMO gaps, and thus lower energy emissive transitions. Nonetheless, it is curious that the effect is only visible in the solid state. It is plausible that rotation of the aromatic substituents is more restricted in the solid state, resulting in greater co-planarity between fluorene and aryl substituents.

TABLE 2.3: Emission and absorption maxima of fluorene-based smart inks

Compound (R_1 substituent)	EL λ_{max} (nm)	Film PL λ_{max} (nm)	Solution PL λ_{max} (nm)	Abs λ_{max} (nm)
Arylfluorenes				
35a (3-Me)	412.5	388.5	382	292
35c (3-OMe)	417.5	392	378	314
35e (3-Ph)	407.5	371	380	290
35i (3-H)	415	414	347	313
36a (4-Me)	413	385.5	361	294
36c (4-OMe)	411.5	410.5	363	313
36e (4-Ph)	409.5	414	378	319
Diarylfluorenes				
37a (3-Me)	411	414	359	326
37c (3-OMe)	487.5[a]	414	360	328
37e (3-Ph)	410	392.5	360	327
37i (3-H)	409	410	373	327
38a (4-Me)	410	434.5	359	330
38d (4-OMe)	412.5	422	385	334
38e (4-Ph)	419.5	414	382	339

[a]This highly anomalous result was one of the first obtained, when the ink-purification method and the OLEC fabrication procedure were immature. It was excluded from the analyses presented in this thesis.

The phenylfluorenes were an exception. Their analysis was plagued with difficulties (very thin or uneven films/short circuits), so their thin-film photoluminescence data (Appendix B) was considered unreliable.

Another property that differs between these two groups is symmetry. It is possible that intermolecular interactions in the solid state are stronger for the more symmetrical compounds. This stands to reason if the effect of stronger intermolecular interactions is to induce a bathochromic shift in the photoluminescence of the fluorophore.

The case of the *bis*-4-tolyl derivative **38a** is also noteworthy. It was found to exhibit thin film photoluminescence at a significantly longer wavelength than any other smart ink in

this set (434.5 nm). This supports the hypothesis that the colour of emission in the solid state is strongly affected by intermolecular interaction. This diarylfluorene scaffold has the greatest symmetry of those studied, and the lowest degrees of freedom available, so it is plausible that intermolecular interactions, in the solid state, are significantly stronger for **38a** than for the other smart inks in the set.

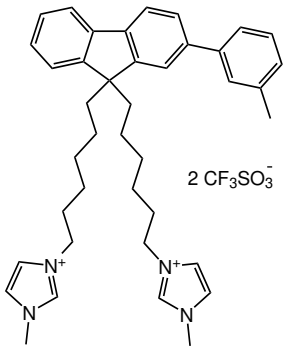

35a

($\lambda_{max} = 388.5$ nm)

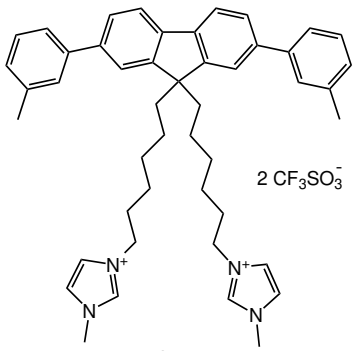

37a

($\lambda_{max} = 414$ nm)

FIGURE 2.14: An arylfluorene/diarylfluorene pair.

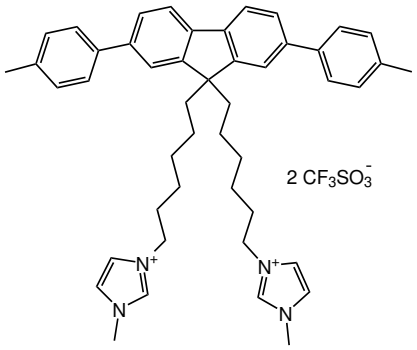

38a

FIGURE 2.15: The longest-wavelength emitter in the set ($\lambda_{max} = 434.5$ nm)

Returning to the solution photoluminescence data (Table 2.3), pairs of compounds with 4-biphenyl substituents showed, by far, the largest differences in emission-peak wavelength. These contrast starkly with otherwise identical 3-biphenyl group-bearing compounds, and the reason is not obvious. Stronger intermolecular interactions in the 4-substituted compounds are a possibility.

If there are long-range interactions between the fluorene core and the terminal phenyl groups, the ground state of a 4-biphenylfluorene (**36e**,**f** and **38e**,**f**) could contain terminal phenyl groups that sit in the plane of the fluorene core. This may lower the HOMO-LUMO gap, as is normally observed with an increase in conjugation (albeit, in this case, a long-range one), and thus raise the wavelength of emission. In order for the terminal phenyl group in a 3-biphenylfluorene (**35e**,**f** and **37e**,**f**) to sit in the plane of the fluorene core, the medial phenylene must also sit in that plane - a situation that is unlikely due to

steric barriers. This is speculation, and data on more compounds with similar structures would be needed for a firm conclusion to be drawn.

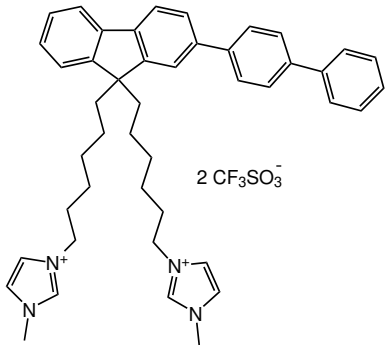

36e

An arylfluorene (λ_{max} = 357, 378 nm)

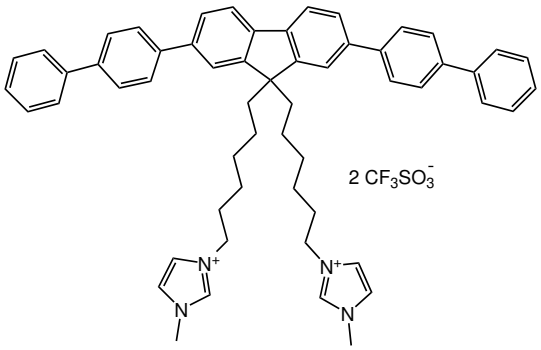

38e

A diarylfluorene ($\lambda_{max} = 382, 402$ nm)

FIGURE 2.16: Compounds with 4-biphenyl groups exhibit bathochromic shift relative to other compounds in the set, most acutely in the case of **38e**.

The fact that emission wavelength does not appear to be strongly linked to the extent of conjugation of the π-systems for these compounds, or the existence of non-zero barriers to planarity, indicates that the fluorene moiety and the other aromatic moieties may absorb and emit somewhat independently of one another.

2.2.7 Functional group effects

It was predicted at the outset that a clear pattern would reveal itself, with predictable relationships between similarly functionalised compounds. No strict pattern emerged from the solution-state emission data (Table 2.3). A tendency for compounds with functional groups that extend the π-system to exhibit longer wavelength photoluminescence emission in solution was discovered, which was unsurprising, but the pattern was neither strong, nor mirrored in the thin film data.

If the emission profile of a polyarene in this class is dominated by a single fragment, one should expect that modification of the less strongly emitting fragments would have a relatively small effect on emission colour. The weak trends observed for these arylfluorenes seem to indicate that the fluorene fragment is the dominant emitter. This hypothesis was tested by direct functionalisation of fluorene, and the results are presented below (*vide infra* 3.2.2).

2.2.8 Functionalisation at position 3 *vs* position 4

The comparison of 3- and 4-functionalised pairs was more complex than the others that were made. The solution-state emission spectra showed no discernible pattern, except in

the case of *bis*-biphenylfluorenes (Table 2.3), where the 4-substituted variants exhibited much longer wavelength emission than their 3-substituted counterparts.

UV-vis absorption spectra taken in acetonitrile solution revealed a general pattern in which compounds with groups at the 3 position had higher bandgaps than those substituted at the 4 position (Table 2.4). For tolylfluorenes (**35a**, **36a**, **37a** and **38a**), this trend was weak. The tolylfluorenes had very similar bandgaps to one another, which was an unsurprising finding, given the minimal effect a methyl group has on the electronics and steric environment of a benzene ring.

TABLE 2.4: Orbital energies and bandgaps of fluorene-based smart inks.

Compound (R_1 substituent)	Optical bandgap (eV)	E_{HOMO} (eV)	E_{LUMO} (eV)
Arylfluorenes			
35a (3-Me)	3.83	-5.81	-1.98
35c (3-OMe)	3.82	-5.88	-2.06
35e (3-Ph)	3.82	-5.87	-2.06
35i (3-H)	3.83	-5.81	-1.98
36a (4-Me)	3.80	-5.77	-1.96
36c (4-OMe)	3.76	-5.63	-1.88
36e (4-Ph)	3.67	-5.77	-2.10
Diarylfluorenes			
37a (3-Me)	3.59	-5.71	-2.12
37c (3-OMe)	3.59	-5.77	-2.16
37e (3-Ph)	3.59	-5.77	-2.17
37i (3-H)	3.62	-5.73	-2.11
38a (4-Me)	3.58	-5.67	-2.08
38d (4-OMe)	3.52	-5.51	-1.98
38e (4-Ph)	3.43	-5.67	-2.24

Thin-film photoluminescence spectra showed a strict pattern: wherever a methoxyphenyl or biphenyl group was present (**35c**,**e**, **36c**,**e**, **37c**,**e** and **38c**,**e**), the 3-substituted compound exhibited lower wavelength emission than the corresponding 4-substituted compound, with a mean difference of 22 nm. Where tolyl groups were present, the differences were much smaller (**38a**, already touched upon above, was a clear outlier). The fact that the position of a substituent appeared to have a larger effect on emission-wavelength than its type, and that this effect was only visible in the thin-film photoluminescence data, lent further support to the hypothesis that intermolecular interactions in the solid state are a very important factor.

The general trends in optical bandgap and thin film PL emission peak wavelength matched, so unsurprisingly, the correlation found between them was fairly strong (Figure 2.17, $R^2 = 0.866$). It is not clear how much of the variance in photoluminescence λ_{max} can be accounted for by intermolecular interaction in the thin film, but with 13.4% of the variance unaccounted for, a reasonably large effect is probable.

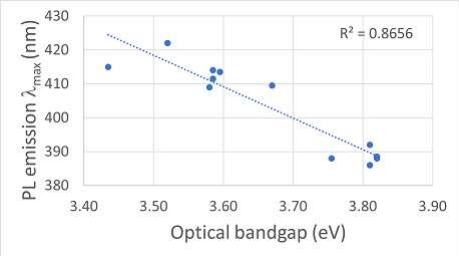

FIGURE 2.17: PL emission in the solid state vs optical bandgap.

2.2.9 HOMO energies and band gaps

HOMO energies (Table 2.4) ranged from -5.92 eV, in the case of *bis*-4-trifluorophenyl fluorene **38g**, to -5.51 eV, in the case of *bis*-4-methoxyphenyl fluorene **38c**. As a general rule, a methylimidazolium-pendant-bearing compound and the corresponding octylimidazolium-pendant-bearing compound had very close, or the same HOMO energy. Similar HOMO energies for these pairs were expected as their HOMO and LUMO are situated entirely on the aromatic fluorophore.[76]

Compounds with electron-donors at the 4 position generally had higher-energy HOMOs. Compounds with electron-withdrawing groups anywhere, and the arylfluorenes functionalised at the 3 position, had the lowest-energy HOMOs. The gap between the lowest and highest HOMO energies was relatively small, so all of the compounds in this set should be compatible with the same anode materials.

Optical band gaps ranged from 3.43 eV, in the case of *bis*-*p*-biphenyl fluorene **38e**, to 3.83 eV in the cases of *m*-tolyl **35a**, and phenylfluorene **35i**. These compounds represent opposite extremes in the structures of the fluorophores they carry. The higher bandgap materials have the least extensive π-systems in the set, and **38e**, the most. The trend held across the full set of molecules, and when considered as groups that have 3, 4, or 6 aromatic rings in their fluorophores, no overlap is observed between the 3-ring group and the 6-ring group. This unsurprising finding provided one simple heuristic with which to design light-emitters, or rather, confirmed one of the basic assumptions made at the outset.

2.2.10 Solvatochromism

Many fluorescent compounds exhibit significant solvatochromism or solvent-induced colour change in emission or absorption spectra. This occurs due to the differential stability of the excited and ground states in various solvents. If the excited state is more polar than the ground state, it is more stable in more polar solvents. Less energy is therefore required to excite the molecule from the ground state to the excited state, so a bathochromic shift, or *positive solvatochromism*, is observed. *Negative solvatochromism* is a hypsochromic shift in the absorption or emission spectrum of a compound due to its excited state being *less* polar than its ground state.[77]

Solvatochromic compounds tend to be multifluorophoric with a donor-acceptor structure in which the acceptor is a fragment with a strongly electron-withdrawing moiety. The donor may or may not contain a strongly electron-donating moiety, as in the case of **54**. Computational work on several solvatochromic compounds[78;79] (*e.g.* **55** and **56**) locates the HOMO predominantly on the donor fragment, and the LUMO predominantly on the acceptor fragment (Figure 2.20 and Figure 2.21). In **55**, the relatively electron-rich carbazole fragments contribute greatly to the HOMO and very little to the LUMO and as such, would be expected to act as donors. The terminal carboxylic acid in **56**, functionalised with two inductively electron-withdrawing chloride groups, contributes greatly to the LUMO and little to the HOMO, and acts as an electron acceptor.

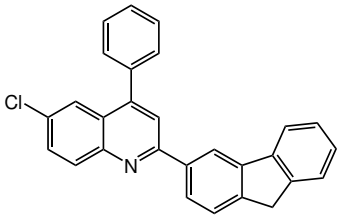

54

FIGURE 2.18: A compound in which unfunctionalised fluorene acts as an electron-donor.

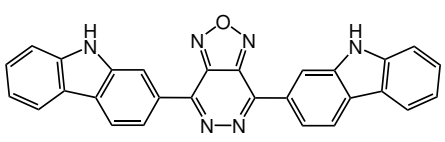

55

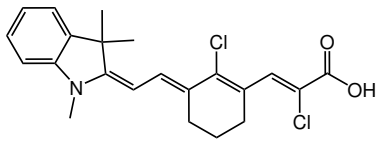

56

FIGURE 2.19: Solvatochromic compounds analysed by DFT.[78;79]

Among the fluorene-based systems studied, only those with cyanophenyl residues resemble these donor-acceptor systems. **36i**† is a simplified molecular fragment corresponding

†Compounds synthesised and characterised by Dr Clementine E. Bavinton. UV-vis absorption spectra were collected by Edward H. Jackman

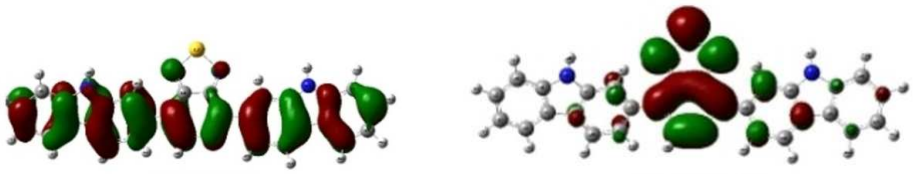

The HOMO of **55** The LUMO of **55**

FIGURE 2.20: Frontier orbitals of **55** calculated by DFT using B3LYP and 6-311G.[78]

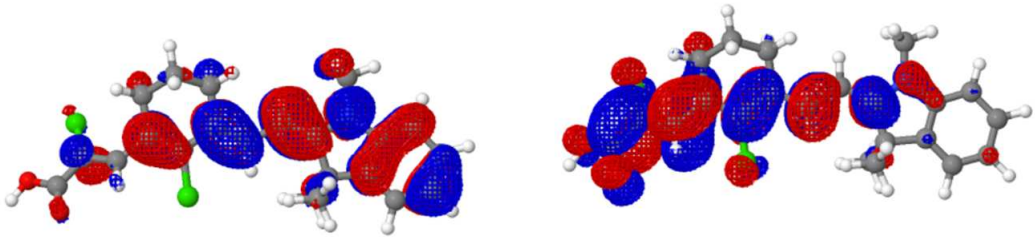

The HOMO of **56** The LUMO of **56**

FIGURE 2.21: Frontier orbitals of **56** calculated by DFT using B3LYP and 6-31G(d).[79]

to the smart ink **36h**, for use in computational calculations (Figure 2.22). For a rationalisation of this simplification, and details of the computational procedure used see Chapter 3. Figure 2.23 shows visualisations of the HOMO and LUMO of this fragment. The fluorene fragment appears to make a higher contribution to the HOMO than to the LUMO, and the inverse is true of the cyanophenyl fragment. Neither the HOMO nor the LUMO is located, in its entirety, on one fragment, however, which indicates that little if any solvatochromic shift should be observed for a compound with this fluorophore.

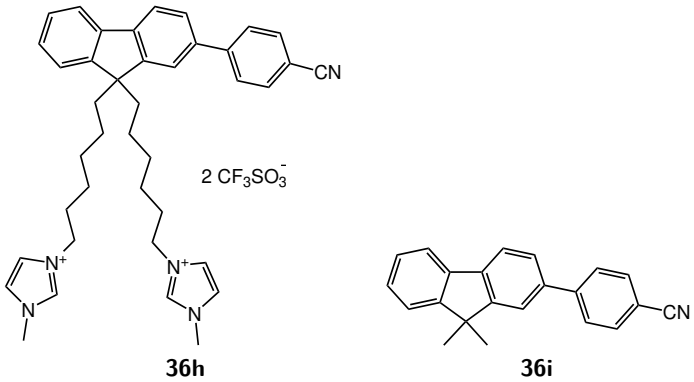

FIGURE 2.22: A smart ink and the simplification used in computational calculations.

A flow-UV-vis setup was used to measure the absorption of **36h** across a solvent gradient. Due to the insolubility of **36h** in solvents at the extremes of polarity, mixtures with acetonitrile were used. The least polar solvent system used was 1:1 MeCN:Et_2O.

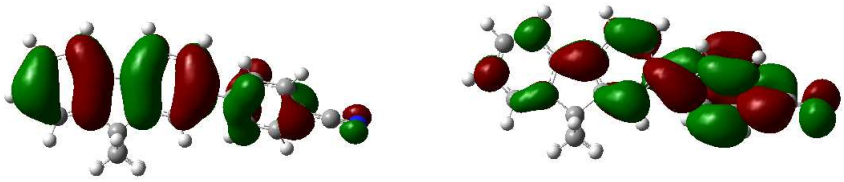

The HOMO of **36i** The LUMO of **36i**

FIGURE 2.23: Frontier orbitals of **36i** calculated by DFT using ωB97XD and 6-31G(d).

The percentage of acetonitrile was increased from 50% to 100% at constant solute concentration. The ratio of water was then increased from 0% to 50% at constant solute concentration. Figure 2.24 shows overlaid absorption spectra acquired at the extremes, and at 100% acetonitrile. The negligible change in λ_{max} demonstrates a lack of solvatochromic behaviour that can be extrapolated to the rest of the compounds in the series.

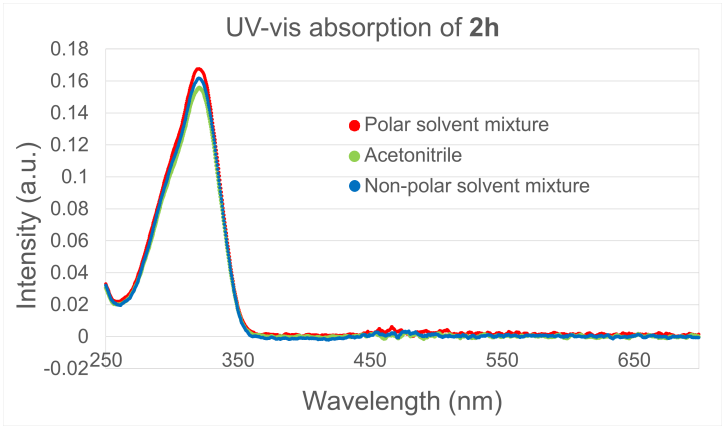

FIGURE 2.24: Overlayed UV-vis absorption spectra of **36h** in 1:1 MeCN:H_2O, in neat MeCN, and in 1:1 MeCN:Et_2O.

2.3 Conclusions

So far, it is not possible to give a straightforward plan for the design of a smart ink of a given colour, but it is possible to elucidate several key principles. These principles are general but may prove less relevant to the design of certain structures to the extent that they differ from those in this study.

Structural modifications to the fluorene fluorophore are likely to have a more substantial effect on emission colour than modifications to other components of the smart ink. Establishing the relative importance of each component part early on makes it likely that we can achieve significant blue- or red-shifting. Fine-tuning could then be achieved by modification elsewhere. The emission colour of the smart inks discussed herein appears to be dominated by the fluorene moiety, and controlled to a lesser extent by the rest of the aromatic fluorophore.

That the position of a substituent on a phenyl group appears to have a more substantial effect than the makeup of that substituent was a surprising finding. The analyses presented in this chapter used experimental measures of bulk properties. Given that there appears to be a complex and subtle relationship between molecular structure and function, a much closer look at the electronic differences between compounds will be needed in order to take this investigation further.

The terminal alkyl chain affects physical properties without having a substantial impact on emission colour. The octylimidazolium smart inks were failures, by-and-large. This was due to their tendency to form highly uneven layers when deposited as films. It could be that solvent is trapped by the octyl chains, and bubbles out slowly as the film dries. Without a targeted investigation of the film-deposition process, it is impossible to say, but for the purpose of this work, they were deemed too unruly to be worthy of further study.

Intermolecular interactions have a very significant effect on solid-state emission colour. Symmetrical compounds with relatively few degrees of freedom exhibit red-shifted emission in the solid state, relative to their close structural relatives. Although the close packing of complex compounds is very difficult to predict, once a small number of exemplars in a given family of smart inks have been made, it is simple in principle to shift the emission colour by changing the steric environment of the fluorophore.

While steric bulk may be desirable for colour-tuning, it can be a hindrance in the fabrication process. Careful design of the fluorophore may be needed in order to avoid excessively large side-chains that thwart the production of working devices.

There are two natural paths forward. The first involves close analysis of the electronics of fluorene-based systems, using computational methods to establish orbital energies and

geometries. Analysis of the effect of substituents on frontier orbital energies should, in principle, give a much more precise description of the structure-activity relationship.

The second is an expansion of the range of substrates included in the investigation. Thus far, structural variety has been minimal, so general conclusions about small-molecule smart inks are impossible to draw. The next part of this work attempts to make progress toward a more generally applicable predictive model, while building a deeper understanding of the structure-activity relationship at play.

Chapter 3

A predictive computational model

3.1 Introduction

3.1.1 Benchmarking

A sophisticated, multi-step computational procedure, developed in collaboration with Matthieu Hédouin,[80] allowed prediction of absorption and emission peak wavelengths with extremely high accuracy (R^2 = 0.991 and 0.994 respectively). Hédouin performed theoretical calculations on simplified structures that correspond to smart inks presented in Chapter 2. We provided the experimental data against which a variety of computational methods were benchmarked.

Density functional theory (DFT) was used for geometry optimisation and natural transition orbital (NTO) analysis, and time-dependent density functional theory (TD-DFT) was used for calculation of vertical excitations. The state-specific polarisable continuum model was used to simulate the solvation of the fluorophore. Potential energy surface minima were found by harmonic frequency calculations after every geometry optimisation. A natural transition orbital analysis of an excited state of **35a** revealed that the particle NTO (corresponding to the LUMO), and hole NTO (corresponding to the HOMO) were located entirely on the arylfluorene aromatic system (Figure 3.1). Simplified structures, substituting methyl groups for the alkylimidazolium pendants, were employed thereafter (Figure 3.2). As noted in Chapter 2, the first compounds synthesised were used as the initial training set, so the fluorene-based fluorophores that contain biphenyl, tolyl, or methoxyphenyl groups appear in the benchmarking study, along with a fluorene-phenanthrene structure discussed below (*vide infra* 3.1.2).

In the study by Hédouin, absorption spectra were calculated as follows. Ground state geometry optimisation was performed for all conformers of a molecule and the most stable conformer was selected. The solvent environment from this optimisation was stored and used in the calculation of excitations.

Emission energies were calculated by first, optimising the geometry of an excited state. The solvent environment established in this calculation was stored, and optimisation of the ground state geometry was then performed using the stored solvent environment. Emission energy was given by the difference in energy between the two structures.

The substrate scope of this procedure was tested using a range of polyaromatic structures including heterocycles, alkene-linked polyarenes, a thiourea, and others. **57** and **58** (Figure 3.3) are examples of compounds that were incorporated into the model using experimental data from collaborators, and **59** and **60**, among others, used literature data. The predictive accuracy of the model was unchanged on addition of a varied group of aromatic compounds but failed to predict the λ_{max} values for absorption or emission of β-carotene (**61**), which is highly conjugated but aliphatic.

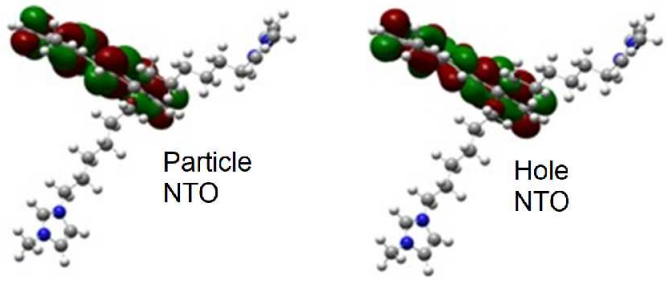

FIGURE 3.1: Natural transition orbitals for **35a**.

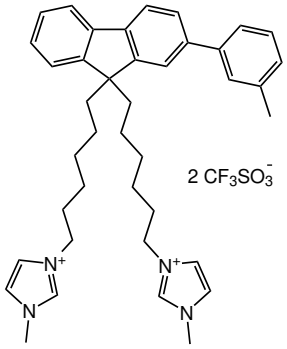

35a

The full structure of **35a**.

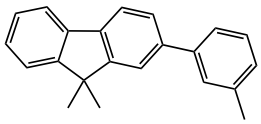

35k

The simplification of **35a**.

FIGURE 3.2: A full smart ink and the fragment containing the frontier orbitals.

3.1.2 Phenanthrene-based systems

Fluorene-phenanthrene systems **62a** and **62b** (Figure 3.4) were included in the benchmarking study. As the they do not fit the pattern of structural variation in the other fluorene-based smart inks, they were not included in the analysis presented in the previous chapter.

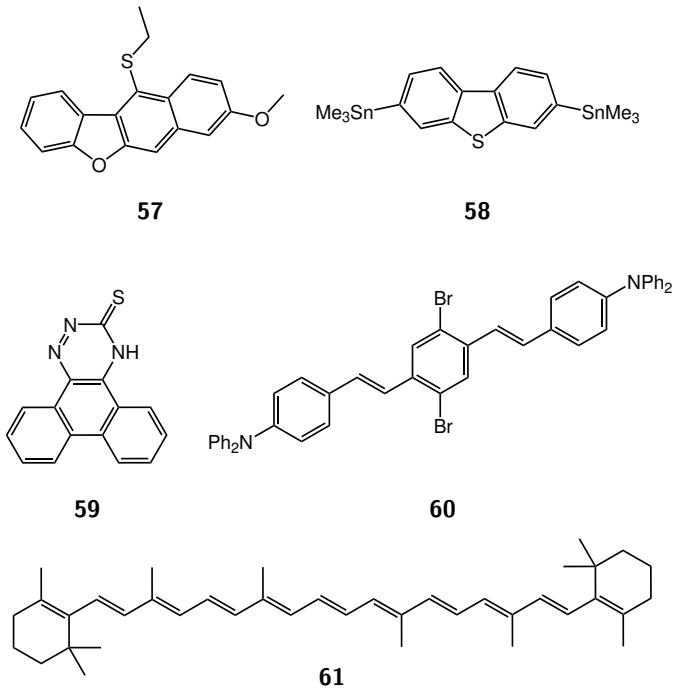

FIGURE 3.3: Some of the compounds analysed by Hédouin *et al.*

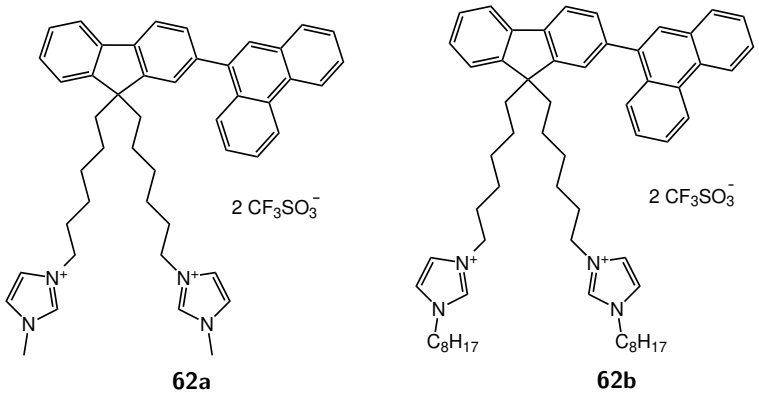

FIGURE 3.4: UV-emitting fluorene-phenanthrene systems.

The synthesis of the fluorene-phenanthrene smart inks (Scheme 3.1) was carried out according to the same procedure as was used for the other arylfluorene smart inks **35** and **36** (Scheme 2.1). The first 2 steps were identical, and the discussion laid out in 2.1.4 applies. The Suzuki coupling to form **64** was performed under the same conditions as for the arylfluorenes **35** and **36**, and gave an exceptional yield (91%). The 14-electron π-system is not fully aromatic, instead consisting of two discrete benzene rings, and a vinyl group, to which bromine is bonded. This structure undergoes cross-coupling far more readily than a typical bromoarene.

Our engineering collaborators found these compounds to be promising materials for use in UV-emitting OLECs, with photoluminescence emission peaks at 364 nm (**62a**) and 363

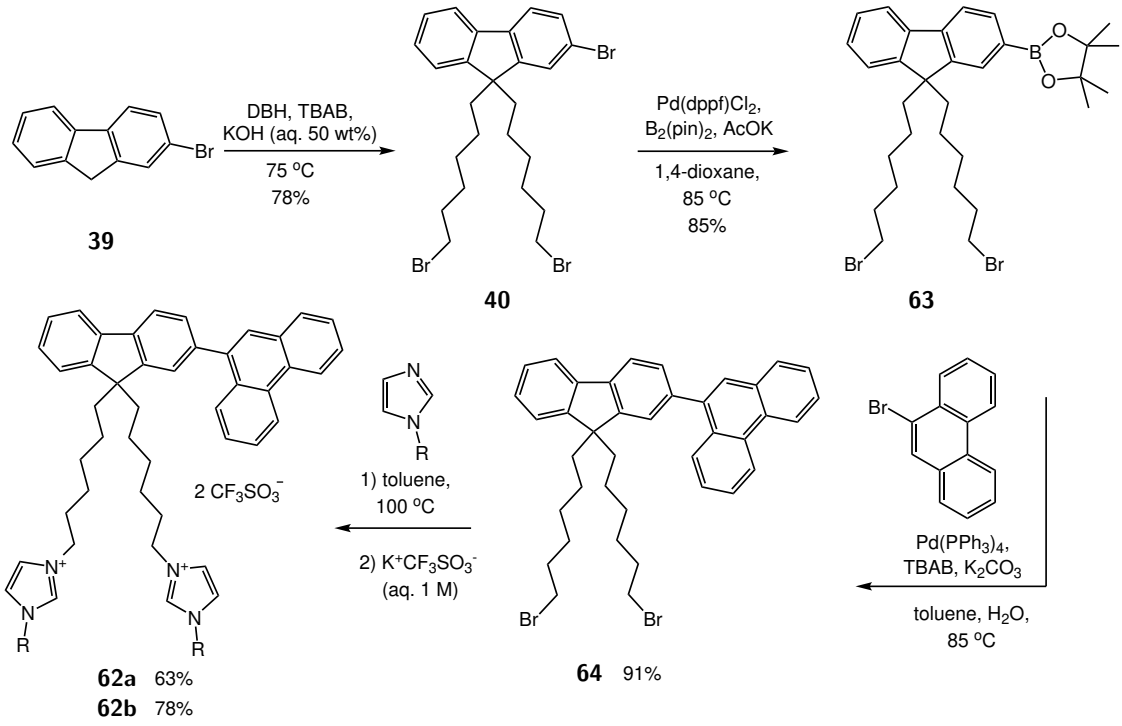

SCHEME 3.1: Synthesis of fluorene-phenanthrene smart inks.

nm (**62b**). These compounds were studied very early in the research programme, when the OLEC fabrication process was not well understood. As such, the electroluminescence data (Figure 3.5) for these compounds were of low-quality, but indicated that their emission peaks would be found at, or just below, 400 nm.

Phenanthrene, as the core of a fluorophore, was identified as a promising alternative to fluorene in the search for UV-emitting smart inks. Recent work in the Harrowven group,[81;82] on the development of practicable syntheses of phenanthrene-based systems made them an attractive object of study.

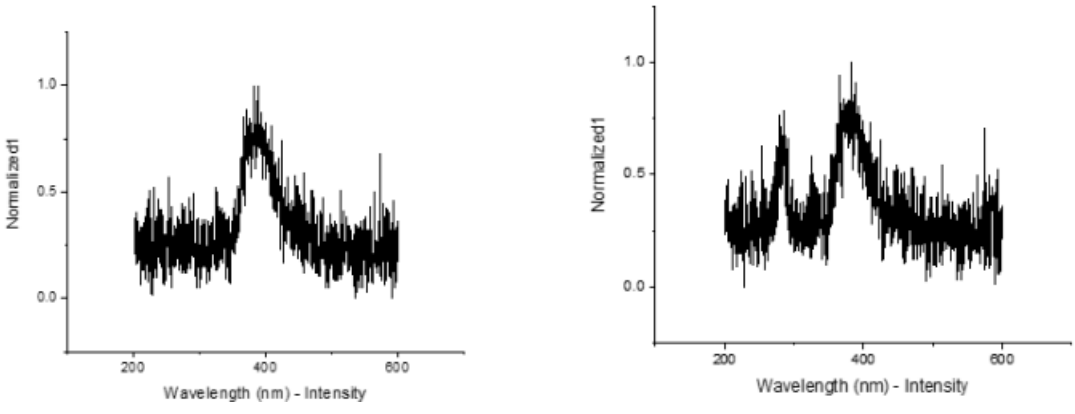

FIGURE 3.5: Electroluminescence of **62a**,**b**.

3.2 Research and development

3.2.1 Overview

Our collaboration with Hédouin *et al.* led them to examine an array of compounds using the range-separated hybrid functional ωB97XD along with the large 6-31+G(d,p) basis set. This set of parameters formed the basis for the computational analysis reported herein, but computational efficiency and expansion of the substrate scope were prioritised in our own work. The desired outcome was a simpler model which predicted absorption and emission with good accuracy, in very little time, on an ordinary desktop computer.

To that end, the ωB97XD functional with the smaller 6-31G(d) basis set, and the continuous polarisable-continuum model (C-PCM) were chosen for our work. ωB97XD was chosen as, being a long-range corrected functional, it is optimised for calculation of excitations. The choice of basis set was a balance of rigour and simplicity. The diffuse function in the 6-31+G(d,p) basis set helps the simulation to account for long-range bonding interactions and to describe anions, and was deemed unnecessary. Likewise, the p-polarisation function added to the hydrogen atoms improves calculations involving polarised bonds, such as hydrogen bonds, and was also deemed unnecessary. The state-specific polarisable continuum model used in the benchmarking study requires optimisation of the geometries of multiple structures. It was replaced with the continuous polarisable continuum model which can be applied to a single DFT or TD-DFT calculation.

The analysis of a structure consisted of a single ground-state geometry optimisation, followed by harmonic frequency calculation, and vertical excitation calculations for the 6 lowest-lying excited states. As with the more involved process detailed above, 9,9-dimethylfluorenes were analysed in lieu of full smart ink structures.

3.2.2 Directly functionalised fluorenes

Hédouin ran calculations on many substituted fluorenes (Figure 3.7) so that the synthetic chemistry team could identify alternative fluorophores. Fluorine, chlorine, and methoxy groups were selected as mesomeric electron-donating groups, and acyl groups were used as mesomeric electron-withdrawing groups.

The model predicted that electron donor substituents would shorten the wavelengths of absorption and emission, but not below those of unsubstituted fluorene (absorption λ_{max} = 264 nm, emission λ_{max} = 302 nm). The shortest absorption and emission wavelengths were predicted for fluorenes with an electron donor at the R_4 position. Substituents at the R_2 position were predicted to have the least effect. The model predicted that electron-withdrawing substituents would raise the wavelengths of absorption

and emission, and do so most strongly if attached at the R_4 position. Negligible difference was made to the predicted transitions by substituting fluorine for chlorine. **66a**–**g** span the full range of predicted emission wavelengths (Table 3.2).

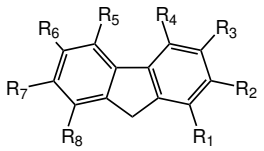

65

FIGURE 3.6: Numbering convention for fluorene.

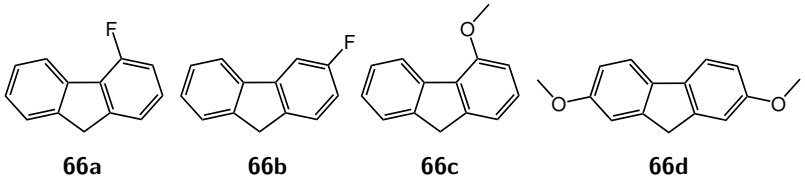

66a **66b** **66c** **66d**

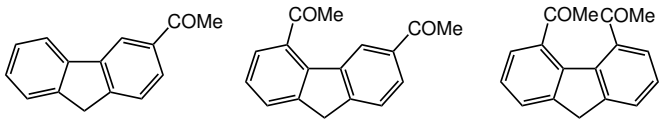

66e **66f** **66g**

FIGURE 3.7: A selection of the substituted fluorenes analysed by DFT.

Fluorofluorenes **66a** and **66b** were synthesised as detailed in Scheme 3.2 and Scheme 3.3 respectively.

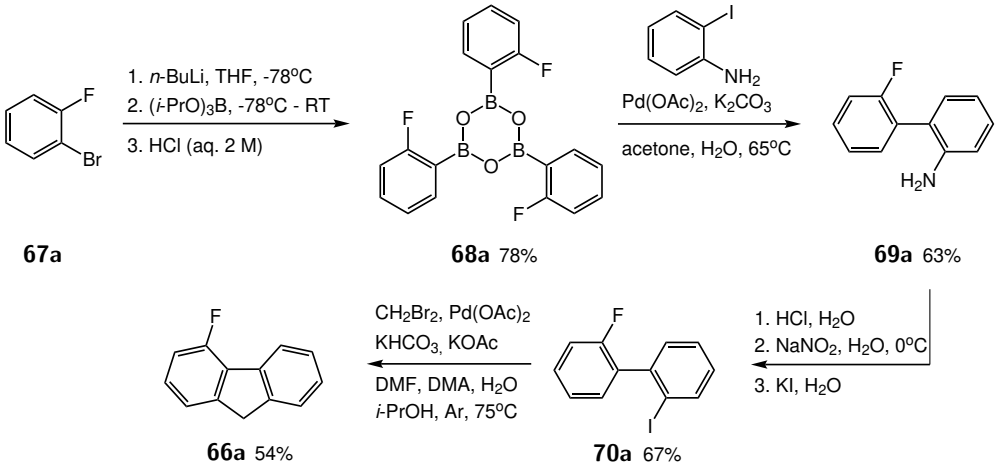

67a **68a** 78% **69a** 63%

66a 54% **70a** 67%

SCHEME 3.2: Synthesis of 4-fluorofluorene.

Conversion of a bromobenzene (**67a**,**b**) into an arylboronic acid (**68a**,**b**) came with 2 complications. The first was that the boronic acid product tended to condense to form polymers and oligomers, such as trimeric anhydride **68a**. Their isolation and characterisation was therefore not straightforward. In general, the complex mixture of arylboronic acid derivatives could be used without purification, as it was in Scheme 3.3.

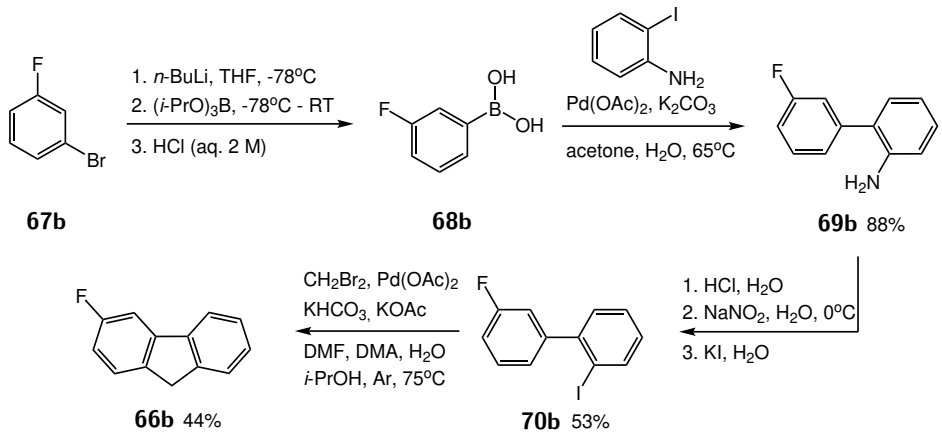

SCHEME 3.3: Synthesis of 3-fluorofluorene.

The second complication stemmed from the presence of inseparable impurities at several stages in the synthesis. Given the difficulties encountered characterising the arylboronic acids, it was not possible to identify or separate such impurities at this stage. At every subsequent stage in the synthesis, the compounds formed were so similar in their Rf values that they could not be fully separated from one another by chromatography. A very small amount ($\approx$ 20 mg) of each of the target fluorofluorenes was isolated, at high purity, for characterisation.

The emission of these compounds was predicted to span 84 nm, which is a much wider range than is covered by the arylfluorenes and diarylfluorenes discussed herein. This indicates that it is the fluorene core that controls emission wavelength much more strongly than the arene or arenes to which it is bonded. **66a** and **66b** were predicted to have the deepest UV-emission and were synthesised (Scheme 3.2 and Scheme 3.3). **66a** had absorbance and emission peaks at 260 and 301 nm respectively. **66b** had absorbance and emission peaks at 258 and 313 nm respectively[‡‡]. While these compounds exhibited deep UV-emission, and were therefore appealing, difficulties in the synthesis of significant quantities hampered their conversion into full smart inks.

TABLE 3.1: Predicted transitions of substituted fluorenes

	Absorption λ_{max} (nm)	Emission λ_{max} (nm)
66a	272	378
66b	283	379
66c	291	384
66d	311	386
66e	346	414
66f	346	419
66g	347	462

[‡‡]Note that the wavelength predictions by Hédouin are for specific electronic transitions. True λ_{max} values may differ substantially if a system can undergo several bright transitions. In these cases, high-energy transitions appear to contribute strongly to the emission spectra, hence lower-than-expected λ_{max} values.

3.2.3 Comparing DFT to experimental data sets

Time-independent DFT calculations gave predictions of HOMO energies that differed significantly from those determined by voltammetry (Table 3.2). They were not considered in isolation, however. It was the *goodness-of-fit* between the two sets of values that was deemed to be most important. Figure 3.8 shows a plot of DFT-calculated HOMO energies of the fluorene-based molecules described in Chapter 2 against those derived from cyclic voltammetry. The goodness-of-fit was high ($R^2 = 0.914$), representing fairly tight correlation between the sets of values, and therefore reasonably high predictive validity for the computational model, when used to predict HOMO energies.

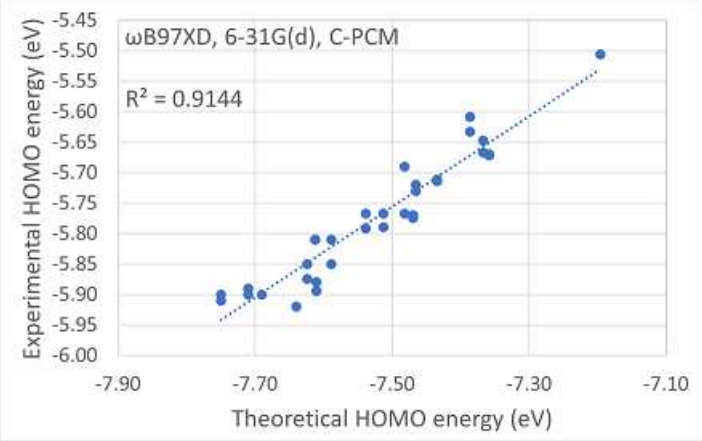

FIGURE 3.8: Values for HOMO energy from CV vs those from DFT.

An equation for the HOMO energy of a polyarene, given its DFT-calculated HOMO energy was determined from the best fit curve:

$$E_{exp} = 0.6834\ E_{DFT} - 0.6271 \tag{3.1}$$

2nd and higher-order polynomial best fit curves gave higher R^2 values (up to 0.94) at the cost of increasingly substantial deviations from linearity, outside the included range of values. It is possible that these data would be best explained using a polynomial fit, but data points across a much wider range of HOMO energies would be required to establish this. The 2nd order polynomial approximation accounted for 93% of the variance in the data set ($R^2 = 0.930$) and gave the following equation for experimental HOMO energy, which deviates slightly from linearity, and could provide a sensible approximation across a wider wavelength range:

$$E_{exp} = 0.64\ E_{calc}^2 + 10.29\ E_{calc} + 35.56 \tag{3.2}$$

Figure 3.9 shows the tight correlation ($R^2 = 0.945$) between the experimentally determined optical band gaps and computationally determined HOMO-LUMO gaps of the

TABLE 3.2: Calculated and experimental values for HOMO energy, bandgap (exp.)/HOMO-LUMO gap (calc.), and excitation wavelength.

Compound (R_1 substituent)	E_{HOMO} (eV) Calc.	Exp.	Bandgap (eV) Calc.	Exp.	Emission λ_{max} (nm) Calc.	Exp.
Arylfluorenes						
35a (3-Me)	-7.59	-5.81	8.15	3.83	267	386
35c (3-OMe)	-7.61	-5.88	8.16	3.82	268	392
35e (3-Ph)	-7.62	-5.87	8.13	3.82	267	388
35i (3-H)	-7.61	-5.81	8.16	3.83	267	-
35g (3-CF_3)	-7.71	-5.90	8.12	3.80	273	-
35h (3-CN)	-7.75	-5.86	8.00	3.80	273	-
36a (4-Me)	-7.54	-5.77	8.11	3.80	268	386
36c (4-OMe)	-7.39	-5.63	8.01	3.76	271	388
36e (4-Ph)	-7.51	-5.77	7.90	3.67	276	410
36g (4-CF_3)	-7.72	-5.86	8.05	3.79	275	-
36h (4-CN)	-7.75	-5.81	7.73	3.67	284	-
Diarylfluorenes						
37a (3-Me)	-7.43	-5.71	7.80	3.59	281	414
37c (3-OMe)	-7.47	-5.77	7.81	3.59	282	414
37e (3-Ph)	-7.48	-5.77	7.78	3.59	283	412
37i (3-H)	-7.47	-5.81	7.81	3.62	281	-
37g (3-CF_3)	-7.71	-5.89	7.83	3.62	288	-
37h (3-CN)	-7.69	-5.90	7.74	3.58	288	-
38a (4-Me)	-7.37	-5.67	7.75	3.58	284	409
38d (4-OMe)	-7.20	-5.51	7.65	3.52	271	422
38e (4-Ph)	-7.36	-5.67	7.54	3.43	292	415
38g (4-CF_3)	-7.64	-5.92	7.72	3.57	291	-
38h (4-CN)	-7.71	-5.89	7.47	3.44	301	-
Phenanthrenes						
76a	-8.14	-	7.19	3.25	360	-
76b	-8.00	-	7.08	3.15	367	-
76c	-8.63	-	7.26	3.32	335	-
76d	-7.92	-	6.93	3.05	368	-
76f	-7.95	-	7.04	3.05	365	-
76g	-8.03	-	7.09	3.12	364	-
77a	-7.80	-	6.83	3.90	368	-
77c	-7.74	-	6.72	3.50	383	-

fluorene-based molecules. The degree to which this is a usefully predictive result depends on the degree to which emission colour is determined by bandgap in smart inks. Adegoke *et al.*[58] demonstrated the dominance of the $\pi \rightarrow \pi*$ transition in the electronic excitations of fluorene-based light-emitters. On this basis, it was predicted that there would be fairly strong, positive correlation between theoretical HOMO-LUMO gap and emission colour.

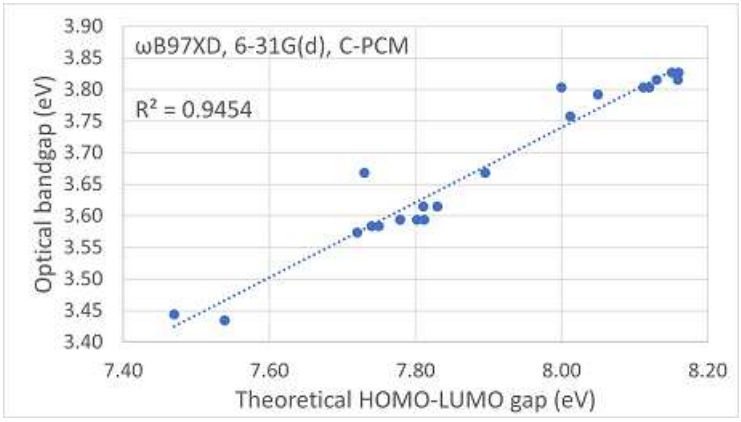

FIGURE 3.9: Bandgap values from absorption spectra vs those from DFT.

Figure 3.10 shows the correlation between theoretically determined HOMO-LUMO gap and thin-film photoluminescence λ_{max}. 83.7% of the variance ($R^2 = 0.837$) was accounted for by the theoretical model which gave a standard error of 8.09. This meant that a photoluminescence emission colour could be predicted with an error margin of approximately ±8 nm. As the visible part of the light spectrum spans a range of around 300 nm, for display applications, a difference of 8 nm is subtle.

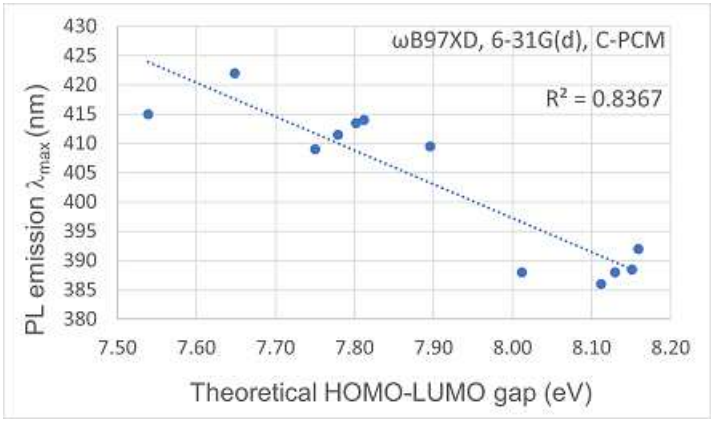

FIGURE 3.10: DFT-calculated HOMO-LUMO gap vs photoluminescence (PL) emission peak wavelength.

3.2.4 Comparing TD-DFT to experimental data sets

The correlation between optical bandgap and TD-DFT-calculated emission peak is shown in Figure 3.11. The correlation ($R^2 = 0.989$) was higher than that with time-independent DFT-calculated HOMO-LUMO gap. That this method had similar predictive validity to the time-independent method was an unsurprising result, given that the excitation calculations are performed on the output geometries from the DFT calculations.

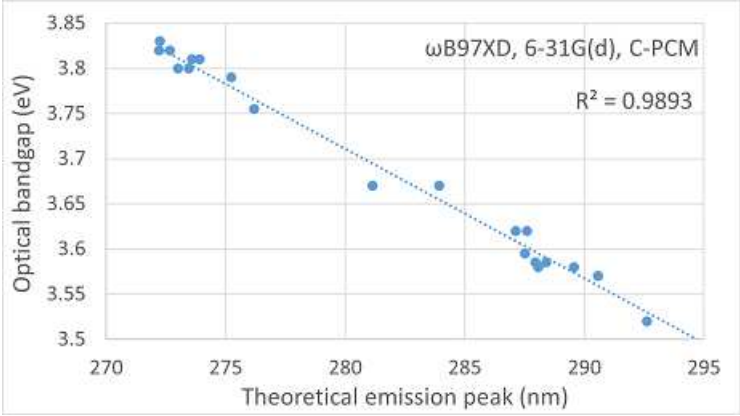

FIGURE 3.11: Optical bandgap plotted against TD-DFT-calculated emission peak.

Likewise, thin film photoluminescence emission peak wavelength correlates with TD-DFT-calculated emission peak only slightly more strongly than it does with DFT-calculated HOMO-LUMO gap (Figure 3.12). Emission peaks calculated by TD-DFT accounted for 85.0% ($R^2 = 0.850$) of the variance in the photoluminescence emission maxima of thin films.

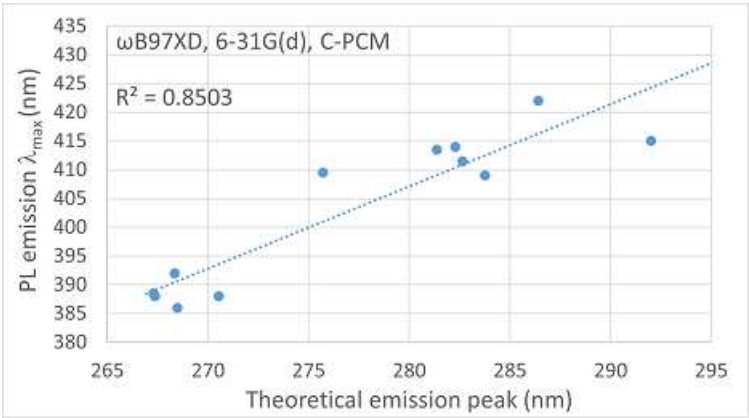

FIGURE 3.12: Thin film photoluminescence peak wavelengths plotted against TD-DFT-calculated emission peaks.

3.2.5 Expanding the scope of the theoretical model

Previous work in the Harrowven group resulted in the development of a flow-photochemical method for the synthesis of fused phenanthrene-maleic anhydride systems[82]. The promising results from phenanthrenes **62a** and **62b** suggested that good access to UV and visible light-emission could be achieved with this class of structures. The synthesis (Scheme 3.4) is fairly tolerant of common functional groups, and although it is multi-step, it does not require purification of every intermediate compound. A number of fluorophores (**76a**–**i**) are accessible via this route (Figure 3.13).[82]

Part of the appeal of phenanthrene-based systems is that the category includes helicenes (**77a**–**c**) with non-planar aromatic systems (Figure 3.14). Circularly polarised luminescence from chiral organic compounds[83] finds application in photonics and display technology, including circularly polarised electroluminescence from an OLED[84]. It has also been employed for the photocatalytic generation of chiral materials[85;86]. These exotic structures, compared with planar phenanthrenes, allow the limits of our predictive model to be probed further.

The modular construction of the fluorophore from separate aryl halides is an attractive feature as it allows the incorporation of heteroatoms into the polyarene ring system - something which is not nearly as straightforward with the fluorene-based systems discussed above. These acid anhydrides are stable intermediates and can be transformed into smart inks by the 2-step process detailed in Scheme 3.5.

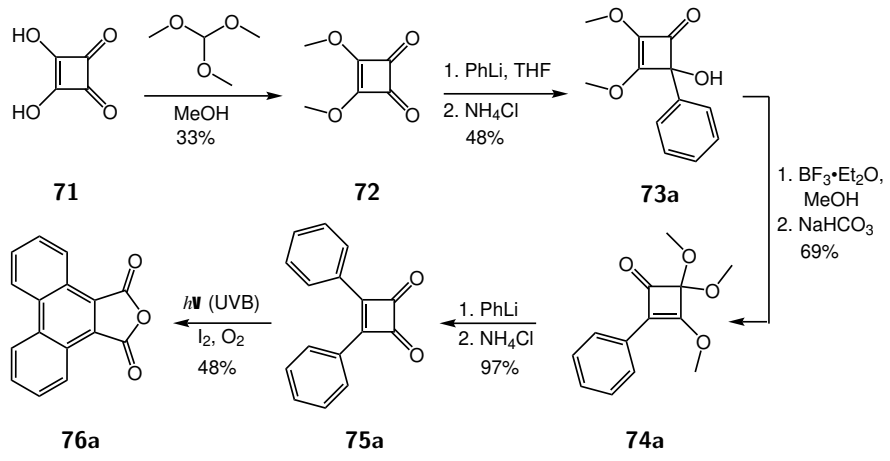

SCHEME 3.4: Synthesis of anhydride **76a**, devised in the Harrowven group.[81]

Heteroyclic fluorophores were examined in our benchmarking study and they were handled well by the rigorous computational method employed (Figure 3.15). Helicenes, with non-planar aromatic systems, had not yet been examined, however. UV-vis absorption spectra were acquired for **76a**–**d**,**f**,**g** and **77a**,**c**. Their optical bandgaps were compared with DFT-calculated values. Figure 3.16 shows the relationship between optical bandgap and calculated HOMO-LUMO gap for the fluorenes (blue dots) and maleic anhydrides

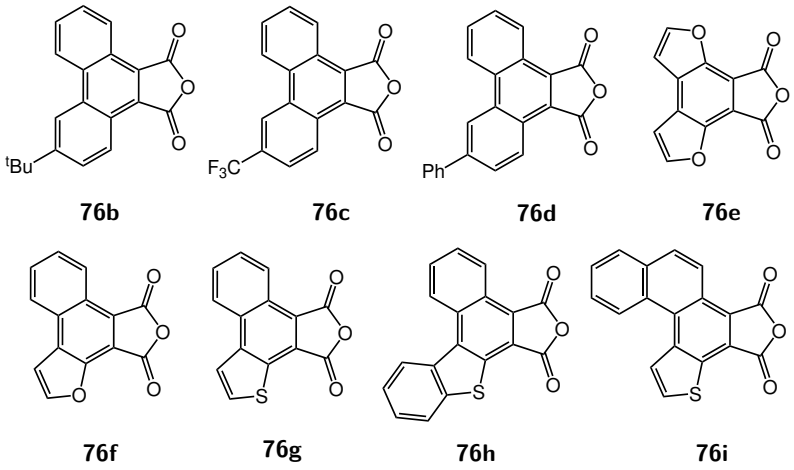

FIGURE 3.13: A range of maleic anhydrides accessed by the flow-photochemical method established in the Harrowven group.[81;82]

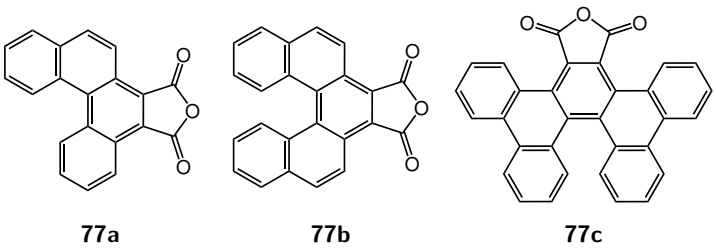

FIGURE 3.14: Helicenes accessible by the same photochemical route.

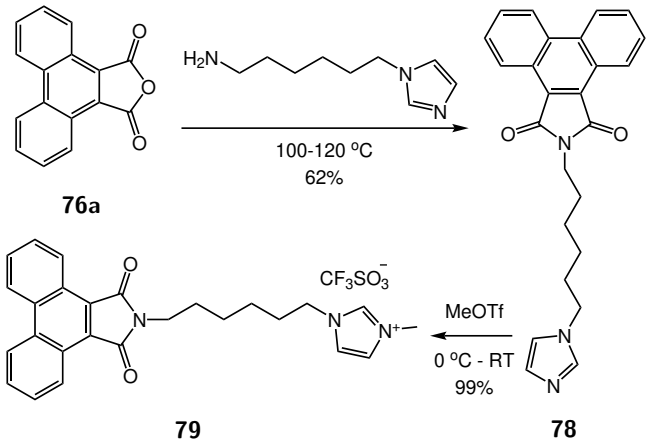

SCHEME 3.5: 2-step synthesis of a smart ink based on **76a**.

(red dots), with 2 very clear outliers corresponding to helicenes **77a** and **77c** (black dots). The omission of the two helicenes from the dataset brings the predictive validity of the model from weak ($R^2 = 0.658$) to very strong ($R^2 = 0.982$). Figure 3.17 is the same graph plotted without the 2 outliers. One explanation for this failure is that the non-planar ring systems in helicene structures are treated by the simulation as groups of discrete alkenes and polyenes.

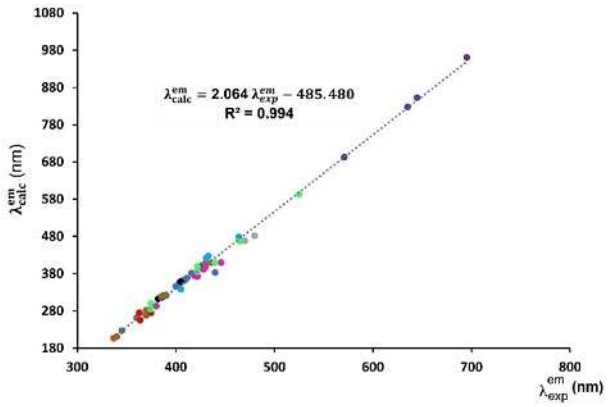

FIGURE 3.15: Predicted emission peak maxima, plotted against experimental values, for a range of aromatic compounds including organometallic and heterocyclic systems.

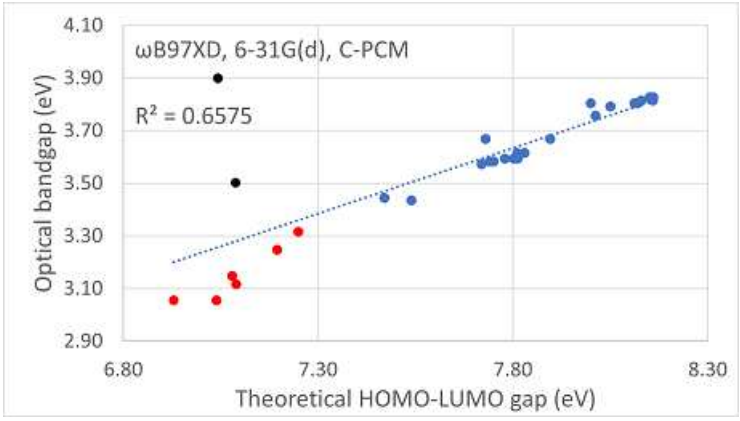

FIGURE 3.16: Relationship between optical bandgap and DFT-calculated HOMO-LUMO gap for a group of compounds that includes 2 helicenes.

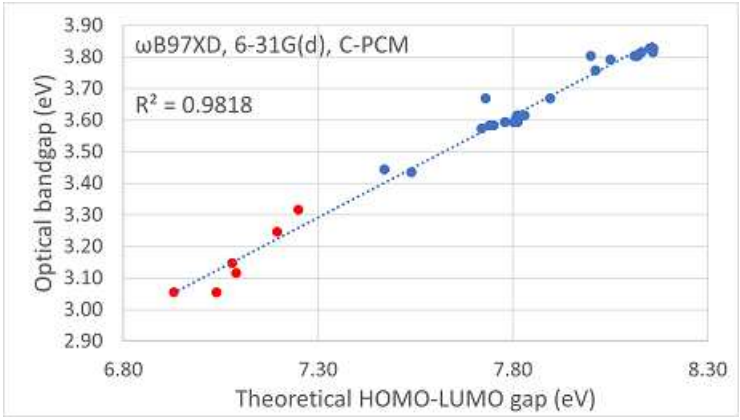

FIGURE 3.17: Relationship between optical bandgap and DFT-calculated HOMO-LUMO gap excluding helicenes.

These data were acquired using the same set of computational parameters as above (ωB97XD, 6-31G(d), C-PCM). Calculations were performed using the acid anhydrides, as shown (Figure 3.13, Figure 3.14, and **76a**), and the corresponding methylmaleimides (Figure 3.18). There was negligible difference between the two sets' calculated orbital energies, and the results did not differ whichever heteroatom was used. The data presented are from calculations using **80a**–**h**.

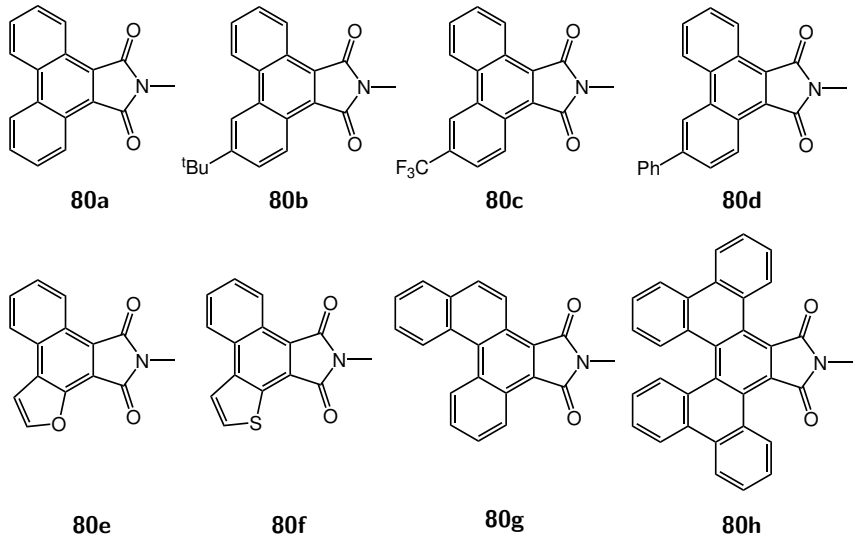

FIGURE 3.18: The methylmaleimides corresponding to **76a**–**d**,**f**,**g** and **77a**,**c**.

Smart ink **79** was synthesised (Scheme 3.5) and used to fabricate a green-emitting OLEC device ($\lambda_{max} = 510$ nm). The device generated dim light from a thin active layer, thereby providing a proof-of-concept for smart inks based on this set of fluorophores.

3.2.6 A flow-photochemical synthetic method

The study that discovered the synthetic route to the acid anhydrides shown above also found that the same conditions failed to cyclise certain diarylcyclobutenediones into fused polyarenes (Figure 3.19). Oxidative ring-expansion of the cyclobutenedione fragment was demonstrated in all cases, but arenes with strongly electron-donating groups at the 4-position resisted cyclisation. Some reactions gave very low yields of the fused product, some gave only the diarylmaleic anhydride (**82a**–**d**), and others gave intractable mixtures.

The proposed mechanism for this transformation, detailed in Scheme 3.6, contains two independent oxidations. The ring-expansion to form **83e** requires oxidising conditions (a combination of I_2 and O_2 was used in this study) and moisture. The second oxidation involves dearomatisation of 2 arenes, to form **83f**, followed by dehydrogenative rearomatisation to give phenanthrene derivative **76a**. The relative ease with which the diarylcyclobutenediones form maleic anhydrides, contrasted with their reluctance

to form fused polyarenes. It is possible that, in some cases, the wavelength needed for photoinduced cyclisation differs markedly from that needed for cyclobutene ring opening (**81** → **82**) or that the reaction was much slower under the conditions used. Alternatively, the ring-opening of **83f** back to **83e** may be more significant in some cases than in others. Importantly, steric constraints are unlikely to be the reason for these stopping at the intermediate stage as several helicenes formed in reasonable yields under these conditions.

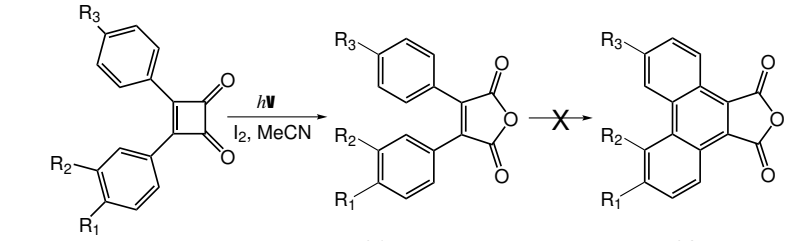

FIGURE 3.19: Photochemical reactions that failed to produce fused phenanthrenes.

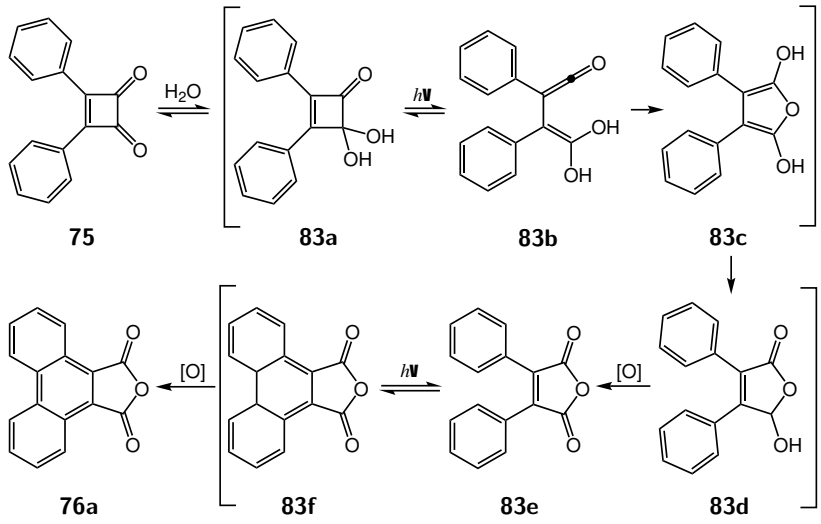

SCHEME 3.6: Proposed mechanism for formation of **76a**

To test if the reaction could be pushed toward phenanthrene formation, a new, highly flexible, photochemical method was employed in an attempt to access some products that had proven elusive. Figure 3.20 shows a schematic of the photo-flow reactor used in our group. A peristaltic pump, with two input lines, pumps the reaction mixture and a gas (O_2 in this case) into a photo-reactor simultaneously. This results in *segmented flow* - the reaction mixture is broken into many short segments, separated by bubbles of O_2. The reaction mixture has a high surface area, and as the catalytic iodine reacts with dihydrophenanthrene **83f**, HI is produced. In turn, this either disproportionates to H_2 and I_2 or it reacts with O_2 to regenerate I_2, with production of water. The flow

rate is calculated based on the known internal volume of the reactor and the desired residence time for the reaction. This time will be known only approximately in the case of reactions performed under segmented flow, as the introduction and aggregation of gas bubbles in the solution is a complication which is very difficult to take full account of.

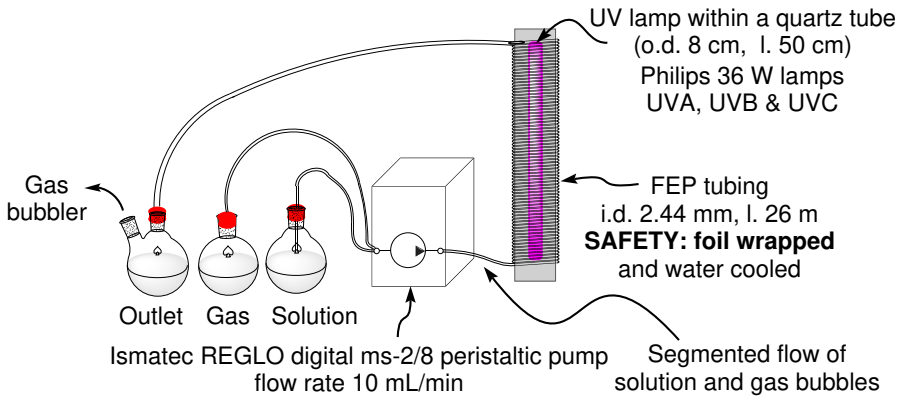

FIGURE 3.20: Flow set up 1

An alternative method (Figure 3.21), known as *circulating flow*, is simpler to set up and easy to monitor. Unlike the method described above, the reaction mixture is returned to its original flask, once it has passed through the reactor. With a high flow rate (around 20 mL/min with the equipment used in this study), a reaction mixture of around 100 mL or less can be passed through the reactor many times. If the optimal light exposure time is unknown, for a given reaction, it can be monitored periodically and stopped once complete.

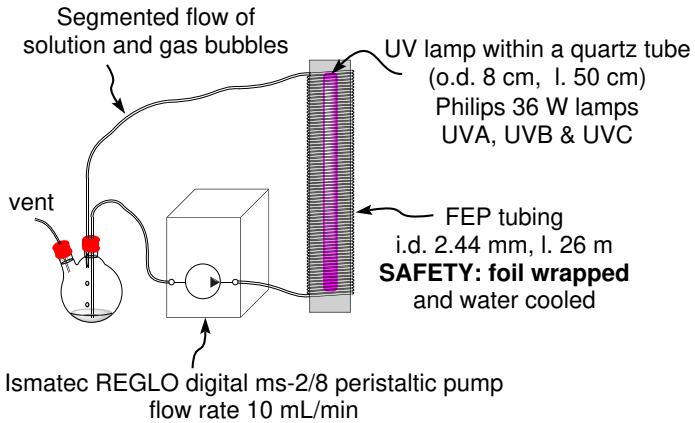

FIGURE 3.21: Flow set up 2 (circulating flow)

Two variants of this set up were used in this work: one with a single input line (Flow set up 2, Figure 3.21), and a dual-input variant with a second input line which was either attached to a gas inlet or left open to air (Flow set up 3, Figure 3.22). Flow set up 2 is suitable for reactions in which none of the reagents or products are gaseous. Flow set up 3 is suitable for segmented flow reactions.

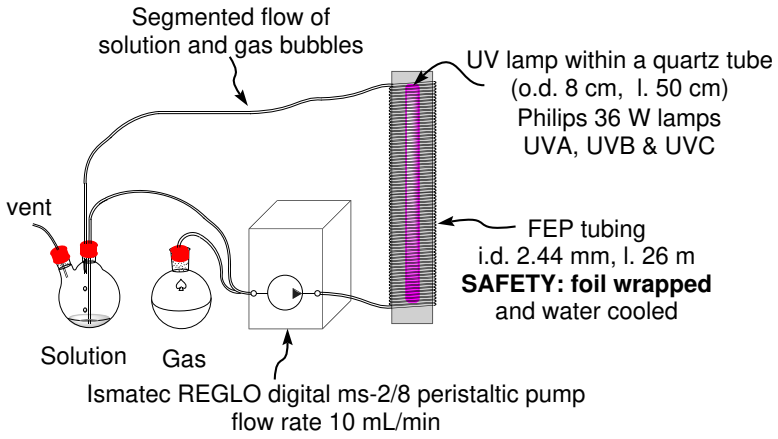

FIGURE 3.22: Flow set up 3 (circulating flow)

It was postulated that the photo-induced dearomatisation step would proceed optimally under different wavelengths of radiation for different substrates. The optimal conditions for generation of anhydride **76a** (using UV-A light) were used for all subsequent reactions in that investigation. UV-B and UV-C radiation were both able to effect the desired transformation, however, with UV-B being the more effective of the two. UV-B was employed in the photo-flow reactions in this work.

The dual-input method (flow set up 3) was used to generate **76a** in 48% yield, over 3 hours. This prompted an attempt to prepare and isolate methoxyphenanthrene anhydride **82a** (Scheme 3.7), which had not been isolated after exposure to UV-A, in the original study. The experiment was fraught with practical difficulties, however. Blockages formed in multiple parts of the apparatus, necessitating a high flow rate (>15 mL/min). When a high flow rate was used, the solution would be pushed into the connector which joins the input lines with some force, often leading to the solution being pumped into the gas inlet. This problem was especially difficult to prevent when air was used as the gas, and the gas inlet was left open to the ambient atmosphere. Leaks at the joins between tubes and connectors are more common in flow set up 3, due to its higher complexity.

The single-input method (flow set up 2) was adopted with much greater success. The removal of the gas inlet necessitated a switch from catalytic oxidant (I_2) to stoichiometric oxidant. Note that, in a circulating flow reaction, if the total volume of the reacting solution is lower than the internal volume of the flow reactor, the solution reservoir completely empties periodically. When the solution is then returned from the reactor to the reservoir, a small amount pools and is simultaneously pumped back into the reactor. Some amount of air is mixed in with the solution in this process, so there is an extent to which the system produces segmented flow after every cycle but the first.

This set up was found to be low-maintenance, and very user-friendly. Mass spectrometry was used to monitor the reaction, initially every half hour, and then every hour or two

once it became apparent that the relative concentration of the starting material was being reduced very slowly. **82a** was eventually isolated in 25% yield, after a total of 23 hours over 3 sessions.

An attempt to synthesise compound **82d** from cyclobutenedione **75e**, using flow set up 2, resulted in the production of none of the desired compound. After 21 hours over 4 sessions, a peak in the mass spectrum at $m/z = 295$ (M+H) provided evidence of the formation of **82d**, but this was not isolated.

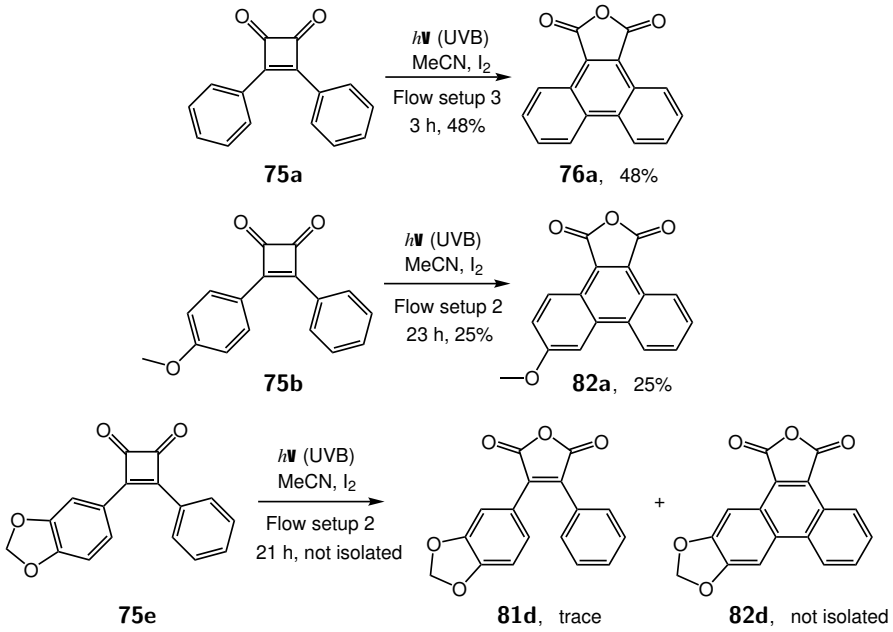

Scheme 3.7: Flow-photochemical reactions of cyclobutenediones.

Time constraints precluded further investigation of this synthetic method. Due to the discontinuation of a collaboration with engineers, whose task included the fabrication of OLECs, no further smart inks were synthesised from this set of fluorophores. The partial success of this alternative method sets a promising stage for the development of further smart inks in this highly varied family of structures.

3.2.7 Extension of the computational model

Fluorofluorenes **66a** and **66b** and maleimide smart ink **79** were incorporated reasonably well into the computational model. Their inclusion in the comparison of calculated HOMO-LUMO gap with optical bandgap causes a slight drop in the correlation between experiment and calculation ($R^2 = 0.956$). The computational model underestimated the bandgaps of the fluorofluorenes (green dots) and overestimated the bandgap of the maleimide smart ink (orange dot), but the overall predictive validity of the model remained high.

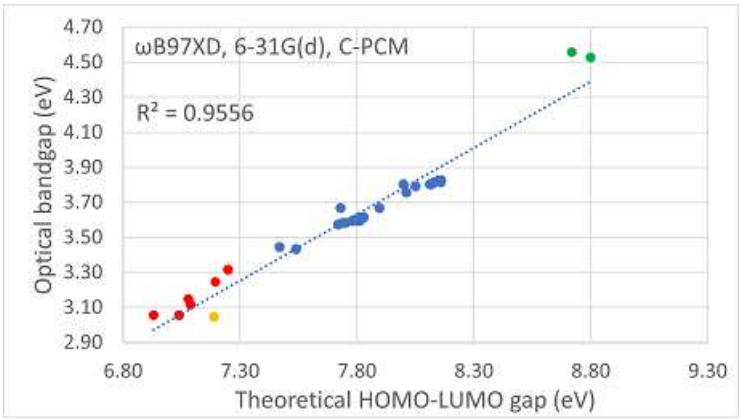

FIGURE 3.23: Optical bandgap vs theoretical HOMO-LUMO gap, **66a**,**b** and **79** included.

3.3 Conclusion

A theoretical model has been established for prediction of the optical bandgaps of smart ink fluorophores with very high accuracy ($R^2 = 0.956$). The film-state photoluminescence was predicted reasonably well by the model, with 85% of the variance accounted for ($R^2 = 0.850$). For this family of structures, therefore, theoretical calculations gave predictions of solid state emission peak wavelength with an error of about ±8 nm. This provides a useful tool in the search for new organic light-emitters.

A pair of fluorofluorene compounds (**66a** and **66b**) were determined to be very promising fluorophores for UV-emission applications. They were incorporated into the theoretical model without a significant reduction of predictive validity. A different synthetic approach would be required if they are to be used at scale.

This model failed in 2 cases. β-carotene and helicenes were not able to be incorporated into the model. Given the moderate success of the model for planar aromatic compounds, which are ubiquitous among smart inks, it did not seem appropriate to weaken the predictive validity of the model in order to incorporate exotic structure types. If non-aromatic or non-planar aromatic compounds are to be used as fluorophores in future work, benchmarking studies targeting those structure types will be required.

A set of aromatic compounds based on phenanthrene were identified as promising light-emitters for OLEC applications. They were incorporated into the theoretical model very well, and a brief exploration of a new flow-photochemical synthetic method proved fruitful in 2 cases. This opens up a promising avenue of exploration for the generation of new visible light-emitters.

At this stage, a solid foundation had been set down for the prediction of the emissive properties of a diverse class of aromatic compounds. Our ultimate goal - the ability to discover a viable chemical structure, with desirable emissive properties, without having to synthesise a large library, was still not met. Trial and error, and guesswork were still very much part of the equation. With the ability to quickly assess large numbers of structures *in silico*, all that was required to achieve our stated aim, was a means of automating the generation of structures to be analysed. The following chapter describes an attempt to generate, from first principles, and with minimal human bias, a chemical structure that has all of the properties we want from a smart ink.

Chapter 4

Algorithmic structure determination

4.1 Introduction

4.1.1 Background

At this stage in the research programme, we had the ability to analyse a non-helicene aromatic chemical structure using DFT and TD-DFT and predict, with good accuracy, the chemical's frontier orbital energies and the wavelength associated with the most dominant electronic transition between them. Once the computational procedure for establishing the emissive properties of a structure had been established, it was straightforward to input a long list of structures (which could belong to a diverse range of chemical families) and automate the generation and analysis of results. The problem of deciding *which* structures to input remained, however.

A colleague[87] had developed an algorithm which could automatically generate chemical structures according to a predefined set of rules governing which molecular fragments were permitted in which combinations. When used in conjunction with the methods of the previous chapter, the identification of promising candidates could, in principle, be fully automated. This allowed the identification of candidate structures in classes that had not yet been considered.

Analysis of various structural features had shown, for compounds based on fluorene and phenanthrene, how bathochromic and hypsochromic shift could be achieved. The magnitude of the shift that was achieved within a family of structures was fairly low. The fluorenes exhibited emission in the deep blue region with some emission in the UV-A region. The phenanthrenes exhibited emission in the blue and blue-green regions. With emission wavelength determined predominantly by the core aromatic fragment and

less so by substituents, it seemed that significant shift of emission wavelength in either direction would be most readily achieved using chemicals with different core aromatic fragments, *i.e.* ones not based on fluorene or phenanthrene.

Thus far, the approach of researchers has been to create chemicals based on molecular fragments already known to exhibit many of the desired properties. Fluorene and phenanthrene are in this category, and both can be found many times in the literature on the topic of OLECs. Other structural motifs that appear many times in the literature are simple arenes, conjugated systems based on thiophene and other heterocycles such as carbazole, and fused polyarenes based on napthalene, pyrene and others. In a recent review[6], 20 of the 27 ionic small molecules discussed were based on either fluorene, carbazole, phenanthroimidazole, or pyrene, or a combination thereof (Figure 4.1). 26 of those 27 used alkylimidazolium ions tethered to the fluorophore, and all 27 used hexafluorophosphate as the counterion. Success reported in the literature, and in our own work, with systems based on fluorene and phenanthrene set the direction of the bulk of this study.

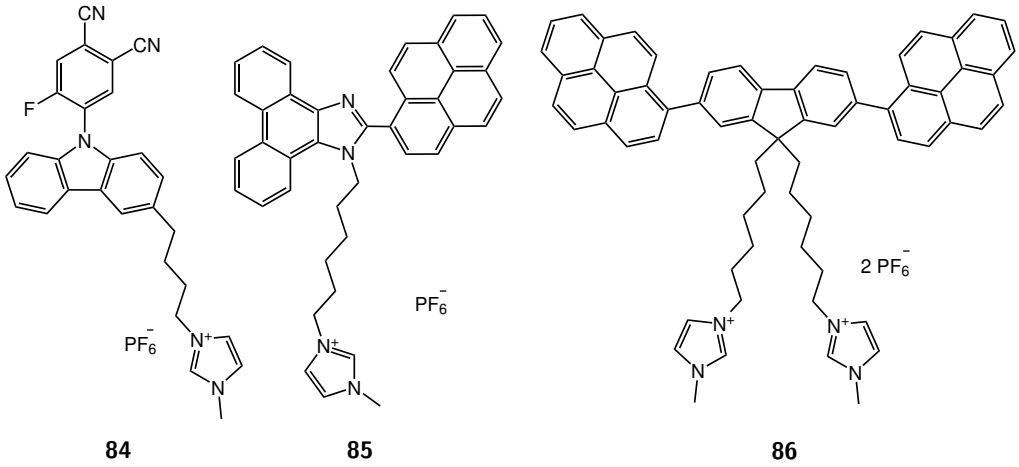

FIGURE 4.1: A representative sample of ionic small molecules that use combinations of common molecular fragments

There is an understandable temptation to stick to chemistry based on familiar molecular scaffolds. A greater likelihood of producing a high-functioning material, and the availability of well-studied synthetic methods, contribute to the wealth of research using these common fragments. Less commonly studied fragments present difficulties and opportunities that may prove worth an investment of effort, if there is an incentive to study them.

4.1.2 Finding smart inks algorithmically

Algorithmic structure-generation is an emerging field that removes, to some degree, guesswork and human bias from the problem of deciding which chemicals to study. The hope is that, with sufficient computational power, and the broadest feasible chemical space defined, very few stones will be left unturned in the search for new light-emitters.

The work of a collaborating computational chemistry specialist,[87] Jay Johal, produced an algorithm which generated chemical structures in a generational cycle, homing in on those with some predefined target property. In the work described below, Johal produced, amended, and ran the structure-generating algorithm. We provided descriptions of the molecular fragments to be used and wavelengths to be targeted, along with assessments of the viability of generated structures for synthesis in the laboratory. We also completed an assay of basis sets and all experimental work.

A structure-generating rule-set was defined by the atoms and fragments that the algorithm may use. The algorithm generated a specified number of structures according to these rules. The structures were then paired using 2-way tournament selection, detailed discussion of which lies outside the scope of this work[88]. For each *parent* pair, a *child* pair is generated by combination of structural motifs of each of the parents (Figure 4.2). Alterations are made to a small, randomly determined, subset of the child structures, at a predefined frequency, mimicking the process of genetic mutation in biological reproduction.

Since orbital energies and electronic transition energies are readily calculated by DFT and TD-DFT respectively, these were ideal targets for such an algorithm. These properties could be determined for new child structures, as they were generated, and the structures with absorption and emission maxima that more closely approximated the target value were then more likely to be selected as the parents of the next generation. A single run consisted of up to 30 generations, or cycles.

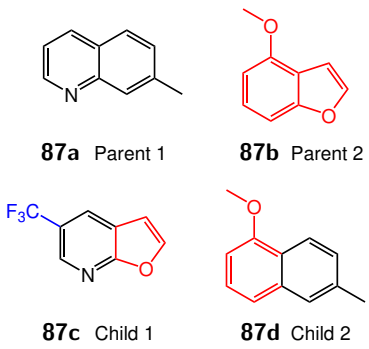

FIGURE 4.2: An example of the generation of 2 child structures from 2 parent structures with a random mutation applied to Child 1 (**87c**)

4.2 Research and Development

4.2.1 Reducing the compute time of theoretical calculations

The computational work presented in the previous chapter was suitable for the analysis of a relatively small number of substrates. A typical geometry optimisation took around 3 hours, and TD-DFT would then take around 30 minutes to 1 hour. To analyse 100 structures by this method would therefore take around a fortnight. For very high-throughput analysis, this method was, therefore, sub-optimal.

In order to have a genetic algorithm generate and analyse a large population of chemical structures in a reasonable time, while not compromising accuracy, an assay of basis sets was required. In the benchmarking study by Hédouin *et al.*,[80] the basis set was chosen as an industry standard which reliably produced high quality simulations. The accuracy of the model was prioritised and no emphasis was placed on calculation time. The computational work of the previous chapter used a basis set chosen based on the perceived advantages of diffuse and polarisation functions. While 6-31G(d) was an effective choice, no quantitative data was used to demonstrate that it was optimal.

The approach used in this work was to assay an array of chemical fragments by DFT and TD-DFT in order to find the most CPU time-efficient method for calculating energy values for their frontier orbitals and the corresponding electronic transitions. This method was then used with a far larger, algorithm-generated structure set to identify potential smart inks.[87] An overall reduction in compute time was sought, whether this came primarily from faster geometry optimisation (DFT), faster excitation calculations (TD-DFT), or a balanced reduction across both methods.

The functional was kept the same as in previous work as it had proven highly effective. The continuous polarisable continuum model was also used, as before, because interaction with the solvent sphere was deemed important. The basis sets assayed were 3-21G, 6-21G, 4-31G, 6-31G, 6-31+G, 6-31G(d), 6-31+G(d), and 6-31++G(d).

3-21G is known to predict unrealistic geometries in many cases. The addition of a polarisation function to the heavy atoms (3-21G(d)) improves calculations but some problems remain, such as the prediction of trigonal planar geometry for primary amines. 6-21G, 4-31G, and 6-31G represent intermediate levels of theory, which were predicted to perform significantly better than 3-21G, at some cost to calculation speed. The remaining basis sets represent higher levels of theory, known to perform well for molecules without highly exotic structures. These were predicted to be unnecessarily costly with regard to calculation time.

The fluorene-based fluorophores containing methoxyphenyl, biphenyl, and tolyl groups were used as input structures. Experimental data for the corresponding smart inks had

been acquired in full by the time this assay was performed. The predictive validity of the computational model was unchanged on addition of the acid anhydrides discussed in Chapter 3, so it was thought likely that extending this assay to include those structures would have very little effect.

Figure 4.3 shows total calculation times, across all of the included structures, for geometry optimisations and excitation calculations. The secondary axis shows the goodness-of-fit of calculated HOMO-LUMO gap and optical bandgap. While every basis set generated a high goodness-of-fit, there was a clear difference between 3-21G/6-21G, and the larger basis sets. All basis sets from 4-31G to 6-31++G(d) generated a goodness-of-fit, with experimental data, over 0.996, or very strong correlation.

Surprisingly, there was almost no difference in total calculation time between 3-21G, 6-21G, 4-31G, and 6-31G. As diffuse and polarisation functions were added thereafter (6-31G(d), 6-31+G, 6-31+G(d), and 6-31++G(d)), calculation times rose sharply. This assay confirmed that 6-31G(d) was a very good choice for low-throughput work, with high accuracy and relatively low calculation time. However, for very high-throughput work, 6-31G was identified as the most efficient basis set. 6-31G gave very similar accuracy to the larger basis sets, in around half the time taken by the method that used 6-31G(d).

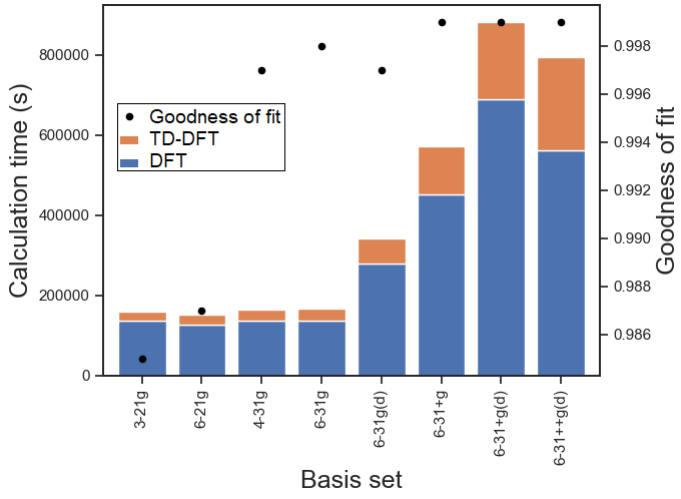

FIGURE 4.3: Total calculation time and goodness of fit for each basis set

Interestingly, geometry optimisations using 6-31+g(d) took longer than the strictly larger 6-31++G(d). It may be the case that diffuse functions on hydrogen atoms allow the ground state structures to be found with fewer calculation iterations, despite the higher complexity of the calculations. Given the lack of obvious long-range bonding interactions in the structures analysed, this is a surprising finding. It could indicate that long-range interactions between the fluorene core and adjacent arenes are more important than first anticipated.

4.2.2 Definition of the chemical space

Carefully defined rules govern the generation and mutation of structures. There was an amount of trial and error in the process of defining these rules as it was not obvious, at the outset, which structural motifs would be preferred by the algorithm. Initially, the rule-set was defined as broadly as possible, and the restrictions were modified after each run. This approach allowed certain types of structure to be eliminated, while searching the widest possible chemical space.

We defined the structure-generation instructions in terms of chemical fragments. The implementation of those instructions was completed by Johal[87]. As the synthetic partner in this collaboration, our role was to guide our collaborator's use of the algorithm to generate results that could be realised practically.

Several simple fragments were used as starting points - benzene, cyclopentadiene, furan, pyrrole, and thiophene. The initial structure generation rules were defined as follows. First, fuse up to 6 of these rings, excluding any phenalene-type structures. Then replace up to 1 aromatic CH group, not already adjacent to a heteroatom, with nitrogen. Finally, replace any hydrogen atom on an aromatic group with methyl, methoxy, dimethylamino, cyano, fluorine, or CF_3. This rule-set was intended to produce robust aromatic molecules with feasible synthetic pathways. The restriction on the number of aromatic CH groups to be replaced with nitrogen was intended to produce compounds that could be readily converted to cations via alkylation, without the production of polycations.

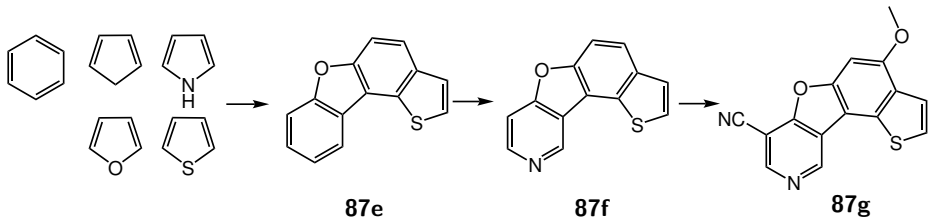

SCHEME 4.1: The initial generation of a structure by the genetic algorithm.

4.2.3 Generation of new chemical structures

The first run searched for green emitters and produced 70 structures with bright transitions predicted in or very close to the correct wavelength range (500-600 nm). Not a single thiophene was generated, but every other possible mutation was present in multiple structures. A representative sample of these is shown in Figure 4.4. Extensive, fused aromatic systems, often with large numbers of substituents, were common features and all of the structures in the set presented a significant synthetic challenge, far beyond that of the blue-emitting fluorene systems.

88b contains 2 nitrogen atoms introduced by the replacement of an aromatic CH group. This is due to a random mutation, not a failure of the algorithm to adhere to the

structure-generation rules set out above. In the interest of maintaining as wide a search-space as possible, this was permitted in future iterations.

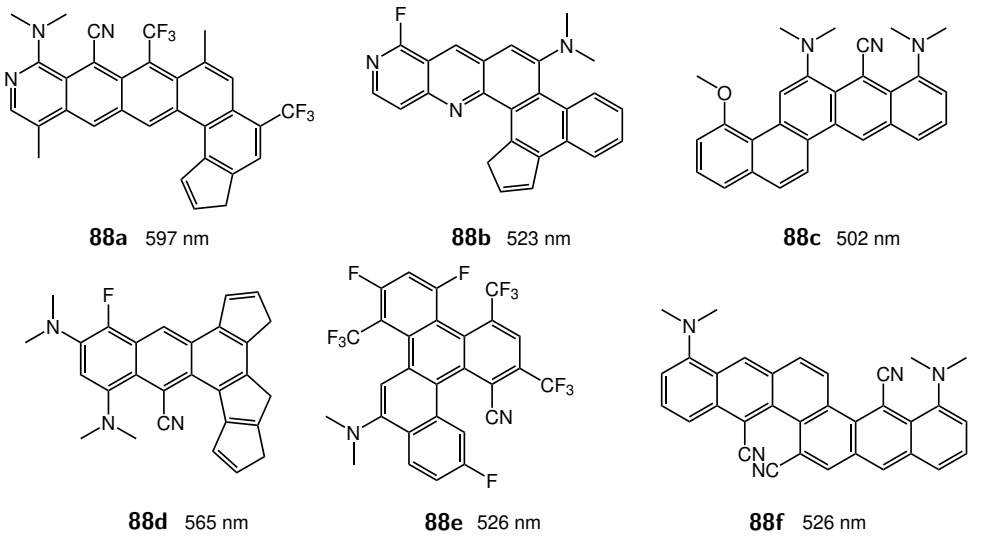

FIGURE 4.4: A selection of the structures generated in the first run of the genetic algorithm with predicted transition wavelengths.

The next run continued to employ the same mutation restrictions and allowed the bonding together (as opposed to fusing) of fragments in child-generation. Rules preventing the generation of helicene motifs and terminal cyclopentadiene units were introduced at this stage. A more targeted search for structures predicted to emit at 500 nm produced structures of similar description to those of the previous run (Figure 4.5).

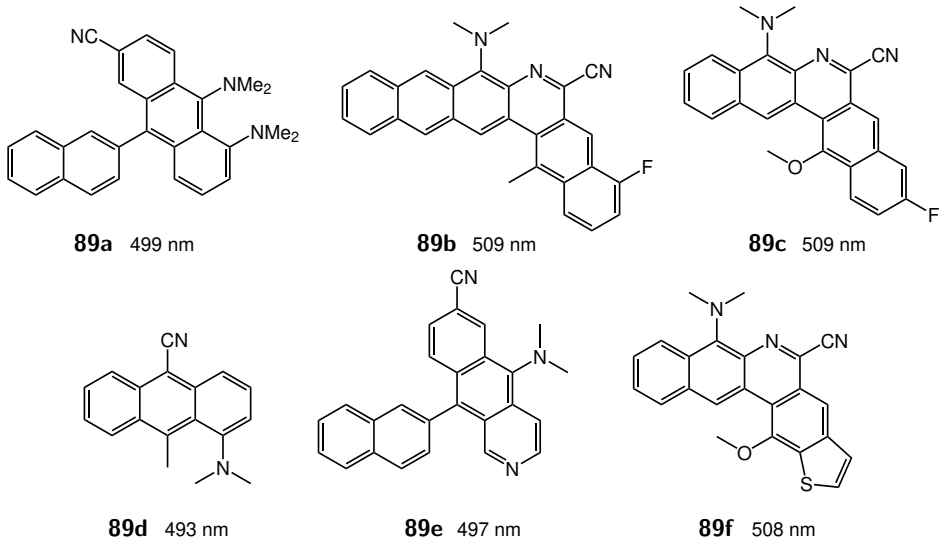

FIGURE 4.5: A selection of the structures generated in the second run of the genetic algorithm with predicted transition wavelengths.

The structures generated in the second run were, with a few exceptions such as **89d**, highly complex and therefore not sensible synthetic targets for OLEC applications. In the third run, 2 major changes were made. A group of new arenes was introduced for the initial structure-generation step (Figure 4.6), and fused systems of more than 4 rings were removed from consideration. A very large population of structures emerged with bright transitions in the target wavelength range, which was set at 500-600 nm in the interest of casting the widest possible net with the substantially altered structure-generation rule set. (Figure 4.7). Many structures were significantly simpler than those generated in previous runs but were still, generally, highly complex.

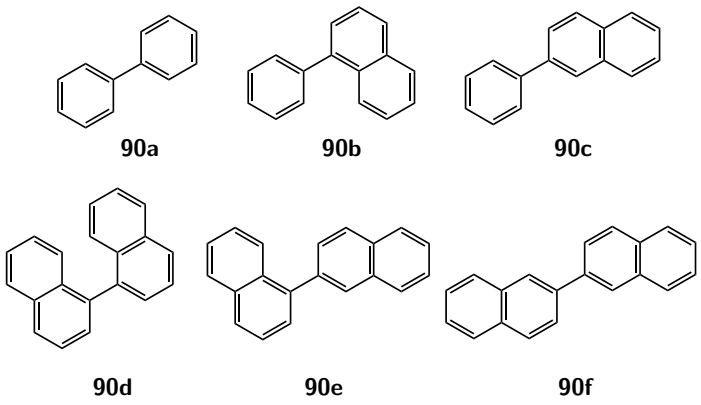

FIGURE 4.6: Core arenes introduced in the third run of the algorithm

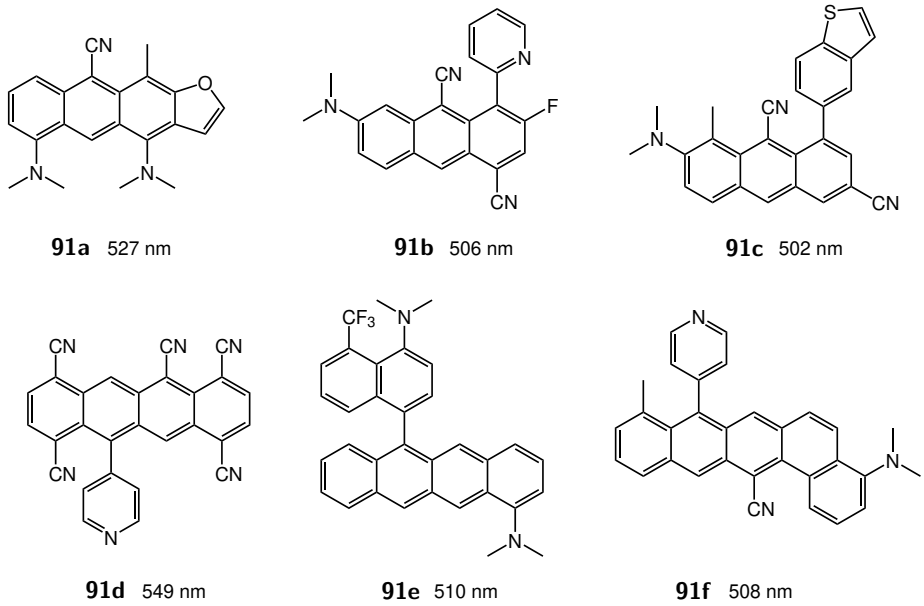

FIGURE 4.7: A selection of the structures generated in the third run of the genetic algorithm with predicted transition wavelengths.

A fourth run used the same restrictions on structure, with UV-A (315 - 400 nm) as the target range. Very few of the structures contained fused systems of more than 2 rings, and while some compounds contained large numbers of functional groups, many were considered to be synthetically viable. In this case, electronic transitions were predicted in the target wavelength range, but longer-wavelength emission peaks were predicted. These compounds, much like the fluorene smart inks discussed in previous chapters, would likely emit across the deep blue and UV-A regions.

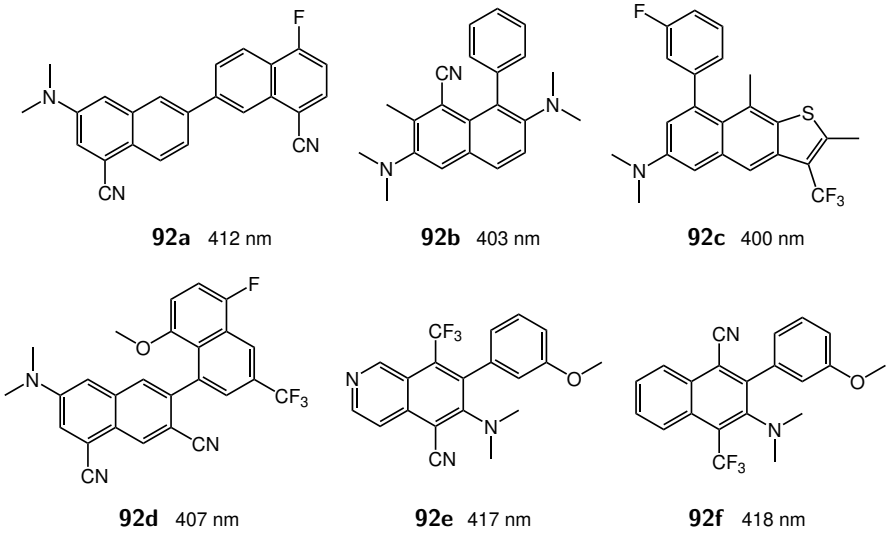

FIGURE 4.8: A selection of the structures generated in the fourth run of the genetic algorithm with predicted transition wavelengths.

A search for UV-B-emitters (280 - 315 nm), using the same parameters as the previous two runs, generated a large number of structures based on biphenyl, with bright, high-energy transitions. Many were functionalised in ways that permit straightforward synthesis. A representative sample is shown in Figure 4.9.

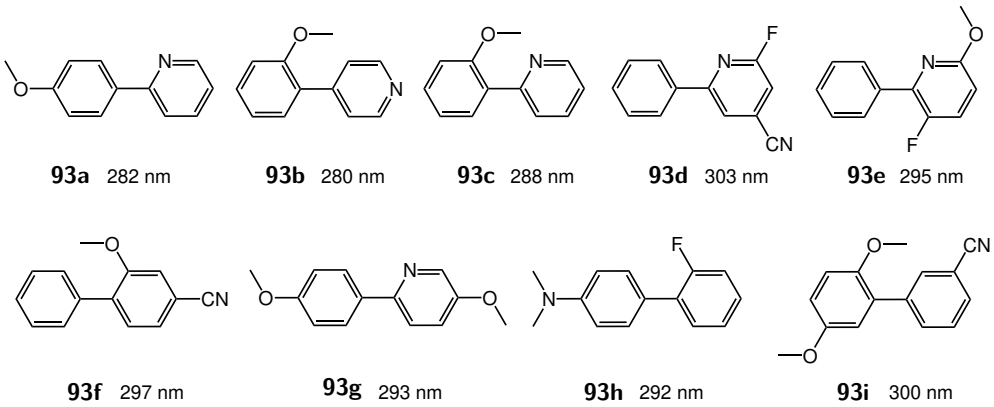

FIGURE 4.9: A selection of the structures generated in the fifth run of the genetic algorithm with predicted transition wavelengths.

4.2.4 Identification of promising targets for UV-emission

Several methoxyphenylpyridines (**93a**–**c**) were identified as promising (having short-wavelength emission and facile synthesis), and 9 such structures (**93a**–**c**,**j**–**o**) were analysed by DFT/TD-DFT using a larger basis set (6-31+G(d,p))[87]. **93k** was predicted to have the brightest transition in the target wavelength range.

This set of regioisomers was selected as the compounds can all be synthesised by Suzuki coupling of the appropriate methoxyphenylboronic acid with an iodopyridine (Scheme 4.2), all of which are readily available. A methoxyphenylpyridine could be modified or prepared for use in an OLEC in a number of ways. The neutral pyridine could be mixed with an electrolyte, or they could be methylated to form pyridinium salts. Alternatively, in place of the methoxy group, a tethered ionic group could be added to give a compound such as **94**. Introducing charge in this way should have relatively little impact on the electronics, and therefore emission colour, of the fluorophore.

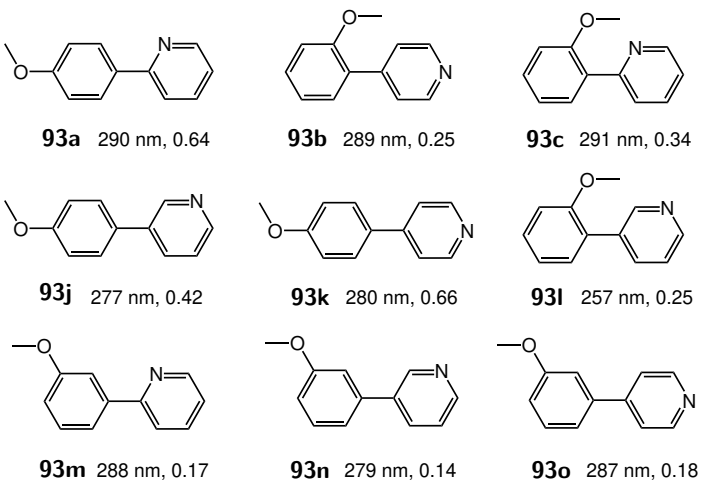

FIGURE 4.10: Promising biaryls selected for further analysis, with predicted transition wavelengths and oscillator strengths.

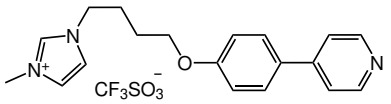

94

FIGURE 4.11: A smart ink based on **93k**

4.2.5 Realisation of a computationally generated structure

93k was synthesised by Suzuki coupling of 4-methoxyphenylboronic acid and 4-iodopyridine, and then methylated, with MeOTf, to form pyridinium salt **97**. **93k** was obtained in relatively good yield. In the methylation step, the reaction was cooled in an ice bath, and after addition of MeOTf and removal from the ice bath, the pyridinium salt precipitated from the reaction mixture instantly.

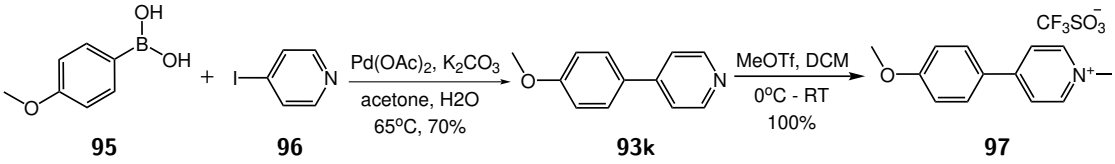

SCHEME 4.2: Synthesis of an algorithmically-generated structure and a pyridinium derivative.

93k and **97** differ substantially in their UV-vis absorption and emission. There is very little overlap in their absorption or fluorescence spectra (Figure 4.12). **93k** has UV-B absorption (λ_{max} = 274 nm) and UV-A emission (λ_{max} = 338 nm). The cationic fluorophore exhibits significant bathochromic shift in absorption (λ_{max} = 334 nm) and emission (λ_{max} = 424 nm), relative to its neutral precursor.

For chemicals in this family, introducing charge through the methoxy group is an effective way of generating short-wavelength emitters, and if longer-wavelength emission is desired, a pyridinium ion can be generated. **98**, synthesised by a colleague on the same research program,[89] is another example of a salt with charge introduced as part of the fluorophore, and was the longest-wavelength emitter generated in this work. A useful design heuristic is revealed by this observation; the introduction of positive charge into a fluorophore is a simple means of inducing substantial bathochromic shift in its absorption and emission.

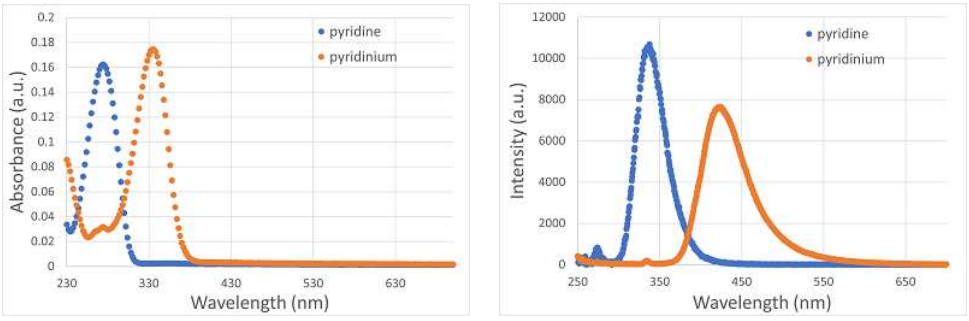

UV-vis absorbance spectra Fluorescence spectra

FIGURE 4.12: Absorbance and fluorescence emission of **93k** and **97**

93k was incorporated into the predictive model established in the previous chapter. Using ωB97XD, 6-31G(d), and C-PCM as before, its calculated HOMO-LUMO gap was

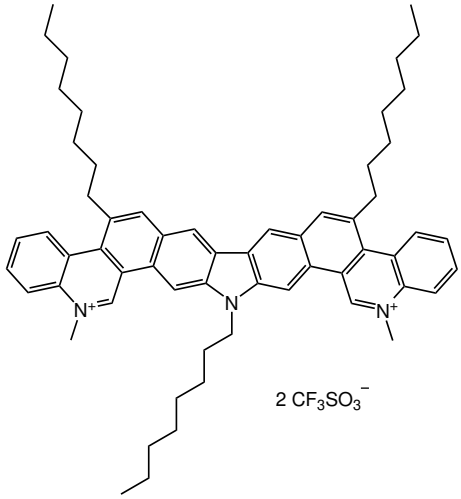

98

FIGURE 4.13: Long-wavelength emitter **98**

compared to its optical bandgap (Figure 4.14, purple dot) and the correlation remained very high ($R^2 = 0.959$).

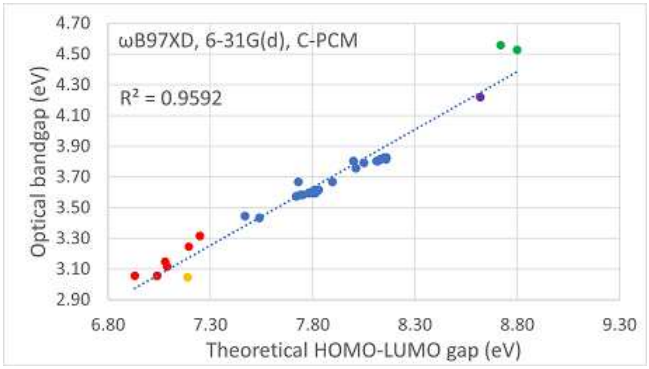

FIGURE 4.14: Optical bandgap vs theoretical HOMO-LUMO gap, **93k** included.

Pyridinium salt **97** could not be included in the model due to severe underestimation of the HOMO-LUMO gap by the computational model (Figure 4.15, black dot).

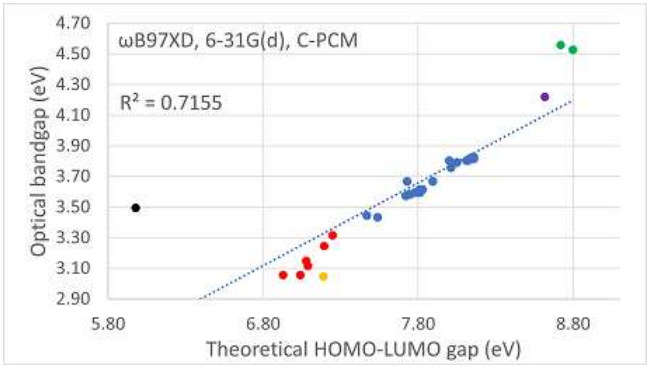

FIGURE 4.15: Optical bandgap vs theoretical HOMO-LUMO gap, **97** included.

4.3 Conclusion

Once an appropriate set of parameters had been established for the genetic algorithm, a promising fluorophore was quickly identified. The computational method used to predict absorption and emission was optimised for this purpose. This process required a far lower investment of time and resources than the synthesis of a large library of chemicals, followed by experimental analysis of their absorption and emission properties.

The algorithm generated very many structures with predicted transitions in the target ranges which were 85 - 100 nm wide. In the interest of searching the widest possible chemical space, as the algorithm's structure-generation rule set was being honed, large target wavelength ranges were used. Once a rule set to generate many synthetically viable structures has been established, more narrowly defined criteria can be used.

In the search for visible- or IR-emitters, tighter restrictions on the types of permitted fragments will likely be required. Synthetic routes to the larger fused aromatic systems that the algorithm generated were not obvious. The parallel use of structure-generating algorithms and AI models which assess the synthetic viability of those structures is an area of current interest. It is possible that advances in AI will allay, at least in part, the need to use human judgement to determine which chemical structures are viable. For the time being, iterative refinement of a genetic algorithm's parameters, followed by more in-depth analysis of the most promising structures, is an effective means of identifying compounds worthy of practical investigation.

Chapter 5

Conclusions

5.1 Project outcomes

Figure 5.1 shows the range of emission colours achieved in this PhD (**a** - **b**), and by the group as a whole (**a** - **c**). The structural variation across the spectrum is immediately apparent (Figure 5.2 and Figure 5.3). As each researcher tended to focus his or her efforts on a certain chemical class, their contributions tended to belong to a narrow range of the electromagnetic spectrum.

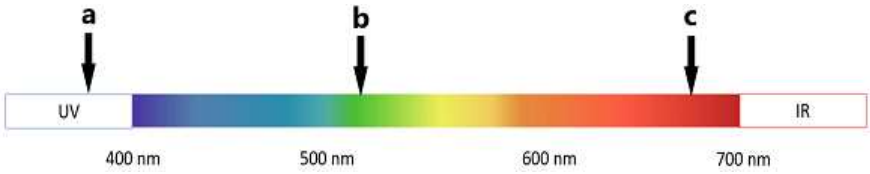

FIGURE 5.1: The part of the electromagnetic spectrum covered by compounds synthesised in this work, and in others associated with the programme of research.

The study of fluorene systems generated blue-emitting smart inks in abundance. This led, naturally, to an effort to generate UV-emitters, for applications in medical contexts. New UV-emitters were less readily forthcoming than anticipated. A systematic study, which used them as a training set, produced a model with which a great variety of structures could be analysed.

The success of the computational model, and a desire to extend it to include other structure classes, led to a study of phenanthrene-based systems and the fabrication of a green-emitting OLEC device. Helicenes were discovered to be in non-conformity with the other phenanthrene-based chromophores, and had to be set aside.

Finally, algorithmic structure-generation was employed, alongside the DFT method, in the design of a UV-B emitter. Introduction of charge to the chromophore revealed another limitation of the computational model.

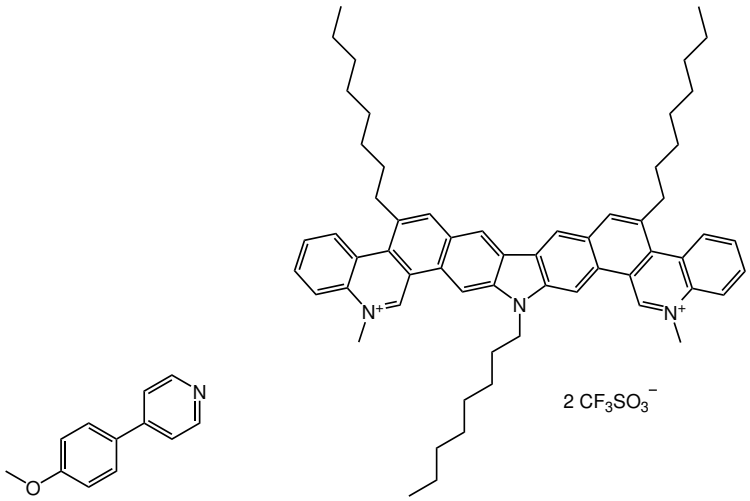

93k UV, 338 nm

98 red, 685 nm [89]

FIGURE 5.2: The compounds at the extremes of emission-wavelength.

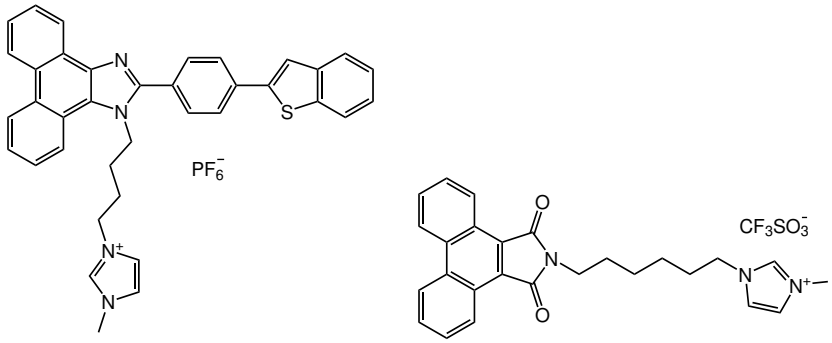

99 green, 494 nm, [90]

79 green, 510 nm

FIGURE 5.3: Green-emitters.

A better understanding of the relationship between the structure, and emissive and physical properties of polyaromatic smart inks has been gained, but simple heuristics have proven difficult to come by. The interactions between seemingly disparate structural features have shown themselves to be complex and subtle. It seems that those who make it their business to find better ways to predict chemical properties will have plenty to do for the foreseeable future.

This PhD can be summarised as an attempt to accelerate the development of light-emitting technology by bringing together modest advances in a collection of disciplines: synthetic and physical chemistry, computational modelling, engineering, and generative AI.

5.2 Future work

The OLEC, like its older sibling, the OLED, is a general-purpose technology. Attempting to count the number of uses that have been found for OLEDs and LEDs, or to calculate the sum of their economic worth would be a fool's errand. It is impossible to predict, with any certainty, the technological applications that will be imagined for light-emitters in future. OLECs are still in their infancy, so in the short-term, their fundamental chemistry and physics will need to see advances, if they are to become economically viable products.

Small-molecular fluorenes, phenanthrenes, and the other structures examined in this thesis, will likely serve as stepping-stones en route to far more effective light-emitters. Their structural features and syntheses are relatively simple to understand, so they serve the purposes of modern science well, but their emissive properties would need to improve by orders of magnitude before they could emerge from academia.

All of that said, there are areas that this thesis touched on, but did not explore in any depth, and which are clearly interesting. The most obvious of these is helicene chemistry. The computational model developed in Chapter 3 completely failed to predict their emissive properties, so the drawing board will have to be returned to by anyone wishing to design emitters that use them. The generation of plane-polarised light from helicenes is an exciting possibility.

Aggregation effects could be probed by more subtle modification of the non-emissive parts of the molecules than was used in this work. The fact that calculations using gas-phase structures produced a strongly predictive model indicates that the compounds studied in this project are not strongly influenced by effects that arise from close-packing. There were outliers in the data, however. Light-emitters that respond to pressure could be a technology to watch out for.

Recent years have seen huge advances in AI, which it is easy to imagine will enter the science of chemistry soon. This thesis contains a brief excursion into this territory, and the outcomes are promising. Systems which can analyse the chemical literature far more effectively than the most industrious human scientist will very likely be one of the targets for developers in this space. The proof-of-concept which comprises Chapter 4 is another stepping-stone, not intended to produce a workable product, but intended to show that a functional material can be realised rapidly, and with high accuracy in the prediction of its properties. This is the space to watch most attentively, not just for advances in OLEC science, but for step-changes in the approach taken to the entire science of chemistry.

Chapter 6

Experimental details

6.1 General experimental techniques

Melting points: Melting points were recorded on a Stuart SMP20 digital melting point apparatus or an Electrothermal IA9100 digital melting point apparatus and are uncorrected.

Infrared Spectra: Infrared spectra were recorded solid as thin films or as solid compressions using a Nicolet 380 Laboratory FT-IR spectrometer or a Nicolet iS5 Laboratory FT-IR spectrometer. Absorption maxima (ν_{max}) are expressed as very strong (vs), strong (s), medium (m), weak (w), very weak (vw), or broad (br) and are quoted in wavenumbers (ν, cm^{-1}).

UV-Vis Absorption Spectra: Spectra were recorded on a Horiba Scientific Duetta Fluorescence and Absorbance Spectrometer. A pair of identical quartz glass cuvettes (path length 1 cm) was used, and experiments were carried out in acetonitrile. An acetonitrile blank was recorded and subtracted from the raw data to give the spectra. The wavelength of maximum absorbance (λ_{max}) is given in nm with the molar extinction coefficient (ϵ) in parentheses ($dm^3mol^{-1}cm^{-1}$).

NMR Spectra: ^{1}H, ^{13}C, and ^{19}F spectra were recorded on a Bruker AVIIIHD 400 (400/101/376 MHz) spectrometer at 298 K unless stated otherwise. Experiments were carried out in deuterated chloroform ($CDCl_3$) unless otherwise stated, supplied by Sigma Aldrich and stored over dried K_2CO_3 to neutralise trace acidity. Chemical shifts were reported in parts per million (ppm) downfield of tetramethylsilane with residual solvent as the internal standard. Assignments were made on the basis of chemical shifts, coupling constants, DEPT-135, COSY, HSQC, HMBC (or NOAH sequences) and comparison with literature values where available. Resonances are depicted as s (singlet), d (doublet), t (triplet), q (quartet), sxt (sextet), sept (septet), m (multiplet), br (broad) and app

(apparent). Coupling constants (J) are given in Hz and are rounded to the nearest 0.1 Hz.

Low Resolution Mass Spectrometry (ESI+): Samples were analysed using a Waters (Manchester, UK) Acquity TQD mass tandem quadrupole mass spectrometer. Samples were introduced to the mass spectrometer via an Acquity H-Class quaternary solvent manager (with TUV detector at 254 nm, sample and column manager). Ultrahigh performance liquid chromatography was undertaken using Waters BEH C18 column (or equivalent) (50 mm x 2.1 mm 1.7 µm). Gradient elution from 20% acetonitrile (0.2% formic acid) to 100% acetonitrile (0.2% formic acid) was performed over five to ten minutes at a flow rate of 0.6 mL min^{-1}.

High Resolution Mass Spectrometry (ESI+): Samples were analysed using a MaXis (Bruker Daltonics, Bremen, Germany) time of flight (TOF) mass spectrometer. Samples were introduced to the mass spectrometer via a Dionex Ultimate 3000 autosampler and uHPLC pump. Ultrahigh performance liquid chromatography was performed using a Waters UPLC BEH C18 (50 mm x 2.1 mm 1.7 µm) column. Gradient elution from 20% acetonitrile (0.2% formic acid) to 100% acetonitrile (0.2% formic acid) was performed in five minutes at a flow rate of 0.6 mL min^{-1}. High resolution positive ion electrospray ionisation mass spectra were recorded. Alternatively, samples were analysed using a solariX (Bruker Daltonics, Bremen, Germany) FT-ICR mass spectrometer equipped with a 4.7 T superconducting magnet. Samples were infused via a syringe driver at a flow rate of 5 µL min^{-1}. Mass spectra were recorded using positive ion atmospheric pressure photoionisation. Isotopes ^{1}H, ^{13}C, ^{14}N, ^{16}O, ^{19}F, and ^{79}Br were used to calculate exact masses.

High Resolution Mass Spectrometry (APPI): Samples were analysed using a solariX (Bruker Daltonics, Bremen, Germany) FT-ICR mass spectrometer equipped with a 4.7 T superconducting magnet. Samples were infused via syringe driver at a flow rate of 5 μL min^{-1}. Mass spectra were recorded using positive ion atmospheric pressure photoionisation. Isotopes ^{1}H, ^{13}C, ^{14}N, ^{16}O, ^{19}F, and ^{79}Br were used to calculate exact masses.

Chromatography: Thin layer chromatography was carried out on Merck Silica Gel 60 Å F 254 0.2 mm plates, which were visualised under fluorescence UV (254 nm) followed by staining with aqueous 1% $KMnO_4$, or ethanolic polymolybdenic acid (PMA). Column chromatography was carried out under slight positive pressure using silica gel with the stated solvent system.

Solvents and Reagents: Reagents that were commercially available were purchased and used without further purification unless stated otherwise. Dry THF was obtained from Fisher in an AcroSeal bottle. All air sensitive reactions were carried out under argon using flame or oven dried apparatus.

6.2 Synthetic procedure

A four-step synthetic procedure afforded all of the arylfluorene and diarylfluorene smart inks that are presented in Chapter 2 and Chapter 3:

1. Alkylation of a bromofluorene
2. Miyaura borylation
3. Suzuki cross-coupling with a substituted bromobenzene
4. Quaternisation with an imidazole, followed by anion-exchange

In general, reaction conditions do not vary across the different examples of these reactions. Column chromatography conditions, especially in the case of the products of the Suzuki cross-coupling reactions, were established independently, for each new reaction.

Difficulty isolating the imidazolium salts, in the quaternisation step, led to experimentation with the reaction conditions and purification. Several procedures are presented.

6.3 Fluorene-based smart inks

6.3.1 1-Octyl-1*H*-imidazole

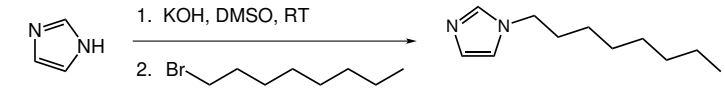

100
$C_3H_4N_2$
Mol Wt: 68.08

101
$C_{11}H_{20}N_2$
Mol Wt: 180.30

A mixture of imidazole (4.00 g, 58.8 mmol) and KOH (3.31 g, 59.0 mmol) in DMSO (20.0 mL) was stirred until all of the solids had dissolved (2.5 h). 1-Bromooctane (8.10 mL, 49.3 mmol) was added and followed after 20 h by water (60 mL). The resulting solution was extracted with $CHCl_3$ (6×20 mL), then the combined organic phases were washed with water (6×100 mL), dried over $MgSO_4$ and concentrated *in vacuo* yielding the title compound as a tan oil, (8.18 g, 45.4 mmol, 92%). Analytical data are consistent with literature values.[91]

LRMS (ESI+) m/z: 181 $[M+H]^+$, $C_{11}H_{20}N_2$, Relative intensity: 100%

^{1}H NMR (400 MHz, $CDCl_3$, 25 °C):
δ = 7.45 (1H, s, Ar-**H**), 7.03 (1H, s, Ar-**H**), 6.88 (1H, s, Ar-**H**), 3.90 (2H, t, J = 7.2 Hz, C**H**$_2$), 1.81-1.69 (2H, m, C**H**$_2$), 1.33-1.18 (10H, m, 5×C**H**$_2$), 0.87 (3H, t, J = 6.7 Hz, C**H**$_3$) ppm

^{13}C NMR (101 MHz, $CDCl_3$, 25 °C):
δ = 137.0 (**C**H), 129.2 (**C**H), 118.7 (**C**H), 47.0 (**C**H$_2$), 31.6 (**C**H$_2$), 31.0 (**C**H$_2$), 29.0 (**C**H$_2$), 29.0 (**C**H$_2$), 26.5 (**C**H$_2$), 22.5 (**C**H$_2$), 14.0 (**C**H$_3$) ppm

6.3.2 2-Bromo-*bis*-9,9-(6'-bromohexyl)fluorene

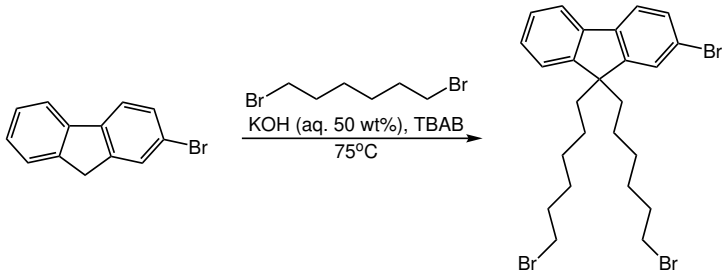

39
$C_{13}H_9Br$
Mol Wt: 245.12

40
$C_{25}H_{31}Br_3$
Mol Wt: 571.24

2-Bromofluorene **39** (10.0 g, 40.9 mmol), tetrabutylammonium bromide (1.59 g, 4.94 mmol), and 1,6-dibromohexane (65 mL, 420 mmol), were added to aqueous KOH (50 wt%, 50 mL) at room temperature. After 17 hours at 75 °C, the mixture was cooled to room temperature and diluted with DCM (20 mL). The organic layer was separated and washed sequentially with H_2O (2 x 15 mL), HCl (2M, 20 mL), and H_2O (2 x 15 mL), then dried over $MgSO_4$ and concentrated *in vacuo*. Purification by column chromatography (silica; 0-70% DCM in hexane) afforded the title compound as an colourless oil (18.3 g, 32.0 mmol, 78%). Analytical data are consistent with literature values.[92]

HRMS (APPI) Found: 567.9979 $[M]^+$, $C_{25}H_{31}Br_3$, Required: 567.9976

^{1}H NMR (400 MHz, $CDCl_3$, 25 °C):
δ = 7.68 (1H, m, Ar-**H**), 7.57 (1H, d, J = 8.6 Hz, Ar-**H**), 7.50 - 7.45 (2H, m, 2×Ar-**H**), 7.38 - 7.31 (3H, m, 3×Ar-**H**), 3.29 (4H, t, J = 6.8 Hz, 2×C**H**$_2$Br), 2.03 - 1.89 (4H, m, 2×C**H**$_2$), 1.67 (4H, app quin, J = 7.2 Hz, 2×C**H**$_2$), 1.26 - 1.16 (4H, m, 2×C**H**$_2$), 1.14 - 1.03 (4H, m, 2×C**H**$_2$), 0.68 - 0.55 (4H, m, 2×C**H**$_2$) ppm

^{13}C NMR (101 MHz, $CDCl_3$, 25 °C):
δ = 152.6 (**C**), 149.9 (**C**), 140.1 (**C**), 140.0 (**C**), 130.0 (**C**H), 127.6 (**C**H), 127.1 (**C**H), 126.0 (**C**H), 122.8 (**C**H), 121.1 (**C**H), 121.0 (**C**), 119.8 (**C**H), 55.2 (**C**), 40.1 (**C**H$_2$), 33.9 (**C**H$_2$), 32.6 (**C**H$_2$), 29.0 (**C**H$_2$), 27.7 (**C**H$_2$), 23.5 (**C**H$_2$) ppm

6.3.3 *Bis*-2,7-dibromo-*bis*-9,9-(6'-bromohexyl)fluorene

Synthesised following the procedure detailed in 6.3.2, using the following reagent amounts and column conditions:
2,7-dibromofluorene: 10.0 g, 30.9 mmol
1,6-dibromohexane: 48 mL, 464 mmol
TBAB: 2.15 g, 6.68 mmol
KOH (aq., 50 wt%): 200 mL
Yield: 12.9 g, 19.9 mmol, 64% (off-white solid)
Column chromatography: 0-50% DCM in hexane
Analytical data are consistent with literature values.[47]

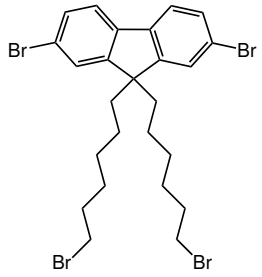

102
$C_{25}H_{30}Br_4$
Mol Wt: 650.13

MP 71.6 - 73.0 °C

HRMS (APPI) Found: 645.9079 $[M]^+$, $C_{25}H_{30}Br_4$, Required: 645.9081

^{1}H NMR (400 MHz, $CDCl_3$, 25 °C):
δ = 7.54 (2H, d, J = 8.2 Hz, 2×Ar–**H**), 7.47 (2H, dd, J = 8.3, 1.6 Hz, 2×Ar–**H**), 7.44 (2H, d, J = 1.5 Hz, 2×Ar–**H**), 3.31 (4H, t, J = 6.8 Hz, 2×C**H**$_2$Br), 1.98 - 1.90 (4H, m, 2×C**H**$_2$), 1.68 (4H, quin, J = 7.1 Hz, 2×C**H**$_2$), 1.26 - 1.17 (4H, m, 2×C**H**$_2$), 1.14 - 1.04 (4H, m, 2×C**H**$_2$), 0.66 - 0.54 (4H, m, 2×C**H**$_2$) ppm

^{13}C NMR (101 MHz, $CDCl_3$, 25 °C):
δ = 152.2 (2×**C**), 139.1 (2×**C**), 130.3 (2×**C**H), 126.1 (2×**C**H), 121.6 (2×**C**H), 121.2 (2×**C**), 55.5 (**C**), 40.0 (2×**C**H$_2$), 33.9 (2×**C**H$_2$), 32.6 (2×**C**H$_2$), 28.9 (2×**C**H$_2$), 27.7 (2×**C**H$_2$), 23.5 (2×**C**H$_2$) ppm

6.3.4 2-(9,9-*Bis*(6-bromohexyl)-9*H*-fluoren-2-yl)-4,4,5,5-tetramethyl-1,3,2-dioxaborolane

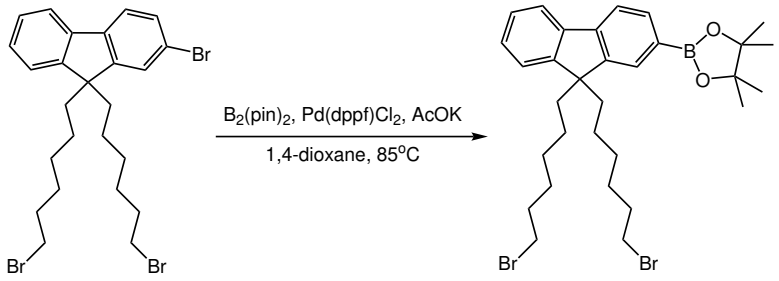

40

$C_{25}H_{31}Br_3$
Mol Wt: 571.24

41

$C_{31}H_{43}BBr_2O_2$
Mol Wt: 618.30

Tribromide **40** (2.23 g, 3.90 mmol), $B_2(pin)_2$ (1.15 g, 4.52 mmol), and AcOK (2.52 g, 25.7 mmol) were dissolved in 1,4-dioxane (38 mL). The mixture was sonicated under argon for 5 minutes, then Pd(dppf)Cl_2 (207 mg, 0.28 mmol) was added and the mixture was sonicated again, under argon, for a further 10 minutes. After 19 hours at 85 °C, the mixture was cooled to room temperature, filtered through celite, and concentrated *in vacuo*. $CHCl_3$ (30 mL) was added then the solution was washed sequentially with H_2O (2 x 20 mL), HCl (2M, 30 mL), and H_2O (2 x 20 mL), dried over $MgSO_4$, filtered, and concentrated *in vacuo*. Purification by column chromatography (silica; 40-60% DCM in petrol) yielded the title compound as a white solid (2.05 g, 3.31 mmol, 85%). Analytical data are consistent with literature values.[61]

MP 83.5 – 85.5 °C

HRMS (APPI) Found: 616.1718 $[M]^+$, $C_{31}H_{43}BBr_2O_2$, Required: 616.1723

^{1}H NMR (400 MHz, $CDCl_3$, 25 °C):
δ = 7.84-7.80 (1H, m, Ar-**H**), 7.75-7.69 (3H, m, 3×Ar-**H**), 7.37-7.31 (3H, m, 3×Ar-**H**), 3.27 (4H, t, J = 6.8 Hz, 2×C**H**$_2$Br), 2.07-1.91 (4H, m, 2×C**H**$_2$), 1.64 (4H, app quin, J = 7.2 Hz, 2×C**H**$_2$), 1.40 (12H, s, 4×C**H**$_3$), 1.22-1.13 (4H, m, 2×C**H**$_2$), 1.11-1.01 (4H, m, 2×C**H**$_2$), 0.67-0.50 (4H, m, 2×C**H**$_2$) ppm

^{13}C NMR (101 MHz, $CDCl_3$, 25 °C):
δ = 150.9 (**C**), 149.5 (**C**), 144.1 (**C**), 140.9 (**C**), 133.8 (**C**H), 128.7 (**C**H), 127.6 (**C**H), 126.8 (**C**H), 122.8 (**C**H), 120.2 (**C**H), 119.0 (**C**H), 83.7 (**C**), 54.9 (**C**), 40.1 (**C**H$_2$), 33.9 (**C**H$_2$), 32.6 (**C**H$_2$), 29.0 (**C**H$_2$), 27.7 (**C**H$_2$), 24.9 (**C**H$_3$), 23.4 (**C**H$_2$) ppm. 1x (**C**) not observed due to splitting by boron nucleus.

FT-IR (ν_{max} cm^{-1}, solid):
2976 (w), 2930 (m), 2857 (w), 1609 (w), 1352 (vs), 1143 (s), 1080 (m), 963 (m), 847 (m), 742 (s)

6.3.5 2,2'-(9,9-*Bis*(6-bromohexyl)-9*H*-fluorene-2,7-diyl)*bis*(4,4,5,5-tetramethyl-1,3,2-dioxaborolane)

Synthesised following the procedure detailed in 6.3.4, using the following reagent amounts, and column conditions:
Tetrabromide **102**: 2.00 g, 3.08 mmol
AcOK: 2.14 g, 21.8 mmol
1,4-dioxane: 40 mL
$B_2(pin)_2$: 1.78 g, 7.01 mmol
$Pd(dppf)Cl_2$: 210 mg, 0.28 mmol
Column chromatography:
silica; 10% ethyl acetate in hexane
Yield: 2.25 g, 3.02 mmol, 98% (white solid)
Analytical data are consistent with literature values.[61]

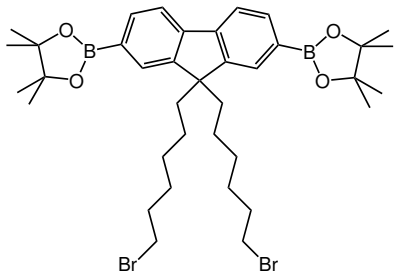

50
$C_{37}H_{54}B_2Br_2O_4$
Mol Wt: 744.26

MP 114.2 - 121.8 °C

HRMS (APPI) Found: 742.2572 $[M]^+$,$C_{37}H_{54}B_2Br_2O_4$, Required: 742.2575

^{1}H NMR (400 MHz, $CDCl_3$, 25 °C):
δ = 7.82 (2H, dd, J = 7.5, 1.1 Hz, 2×Ar-**H**), 7.76-7.71 (4H, m, 4×Ar-**H**), 3.26 (4H, t, J = 6.9 Hz, 2×C**H**$_2$Br), 2.06-1.98 (4H, m, 2×C**H**$_2$), 1.63 (4H, app quin, 2×C**H**$_2$), 1.45-1.36 (24H, m, 8×C**H**$_3$), 1.21-1.10 (4H, m, 2×C**H**$_2$), 1.10-0.99 (4H, m, 2×C**H**$_2$), 0.62-0.50 (4H, m, 2×C**H**$_2$) ppm

^{13}C NMR (101 MHz, $CDCl_3$, 25 °C):
δ 150.1 (2×**C**), 143.9 (2×**C**), 133.8 (2×**C**H), 128.7 (2×**C**H), 119.4 (2×**C**H), 83.8 (4×**C**), 55.0 (**C**), 39.9 (2×**C**H$_2$), 33.9 (2×**C**H$_2$), 32.6 (2×**C**H$_2$), 28.9 (2×**C**H$_2$), 27.7 (2×**C**H$_2$), 24.9 (8×**C**H$_3$), 23.4 (2×**C**H$_2$) ppm. 2×(**C**) not observed due to splitting by boron nucleus.

FT-IR (ν_{max} cm^{-1}, solid):
2977 (w), 2930 (m), 2857 (w), 1607 (w), 1348 (vs), 1143 (s), 1079 (m), 963 (m), 857 (m)

6.3.6 9,9-*Bis*(6-bromohexyl)-2,7-*bis*(3-methoxyphenyl)-9*H*-fluorene

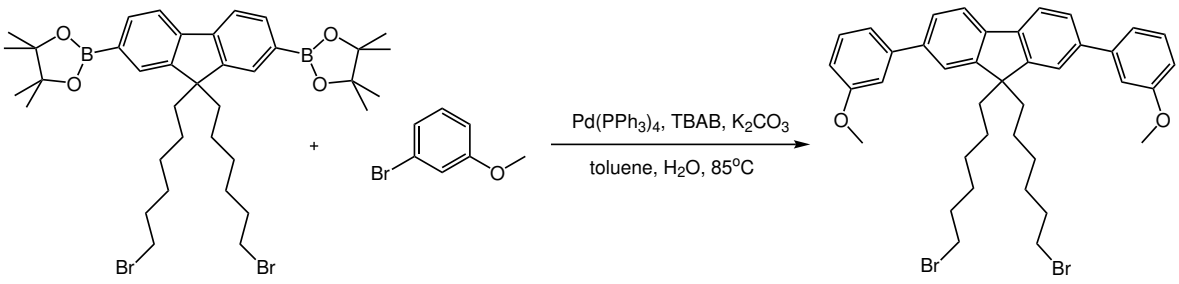

50 $C_{37}H_{54}B_2Br_2O_4$ Mol Wt: 744.26

103 C_7H_7BrO Mol Wt: 187.04

45b $C_{39}H_{44}Br_2O_2$ Mol Wt: 704.59

Dioxaborolane **50** (497 mg, 0.65 mmol), TBAB (40 mg, 0.10 mmol), 3-bromoanisole (0.20 mL, 1.46 mmol), and K_2CO_3 (670 mg, 5.00 mmol) were partitioned between toluene (4.0 mL) and H_2O (2.0 mL). The mixture was sonicated under argon for 15 minutes, then $Pd(PPh_3)_4$ (61 mg, 0.05 mmol) was added, and the mixture was sonicated again, under argon, for a further 10 minutes. After 13.5 hours at 85 °C the mixture was cooled to room temperature, filtered through celite, washed sequentially with H_2O (2 x 30 mL), brine (30 mL), and H_2O (2 x 30 mL), dried over $MgSO_4$, and concentrated *in vacuo*. Purification by column chromatography (silica; 2% to 5% ethyl acetate in hexane) gave the title compound as a colourless oil (327 mg, 0.46 mmol, 71%).

HRMS (ESI) Found: 703.1781 $[M + H]^+$, $C_{39}H_{44}Br_2O_2$, Required: 703.1786

^{1}H NMR (400 MHz, $CDCl_3$, 25 °C):
δ = 7.79 (2H, d, J = 7.8 Hz, 2×Ar-**H**), 7.62 (2H, dd, J = 7.8, 1.6 Hz, 2×Ar-**H**), 7.57 (2H, d, J = 1.3 Hz, 2×Ar-**H**), 7.45-7.39 (2H, m, 2×Ar-**H**), 7.31-7.28 (2H, m, 2×Ar-**H**), 7.25-7.22 (2H, m, Ar-**H**), 6.94 (2H, ddd, J = 8.2, 2.5, 0.8 Hz, 2×Ar-**H**), 3.92 (s, 6H, 2×OC**H**$_3$), 3.27 (4H, t, J = 6.8 Hz, 2×C**H**$_2$Br), 2.11-2.02 (4H, m, 2×C**H**$_2$), 1.72-1.62 (4H, m, 2×C**H**$_2$), 1.27-1.16 (4H, m, 2×C**H**$_2$), 1.15-1.05 (4H, m, 2×C**H**$_2$), 0.79-0.67 (4H, m, 2×C**H**$_2$) ppm

^{13}C NMR (101 MHz, $CDCl_3$, 25 °C):
δ = 160.0 (2×**C**), 151.3 (2×**C**), 143.1 (2×**C**), 140.2 (2×**C**), 140.0 (2×**C**), 129.8 (2×**C**H), 126.2 (2×**C**H), 121.4 (2×**C**H), 120.0 (2×**C**H), 119.7 (2×**C**H), 113.2 (2×**C**H), 112.2 (2×**C**H), 55.4 (2×**C**H$_3$), 55.1 (**C**), 40.3 (2×**C**H$_2$), 33.9 (2×**C**H$_2$), 32.6 (2×**C**H$_2$), 29.1 (2×**C**H$_2$), 27.8 (2×**C**H$_2$), 23.6 (2×**C**H$_2$) ppm

FT-IR (ν_{max} cm^{-1}, film):
2930 (s), 1599 (s), 1466 (vs), 1214 (vs), 1035 (s), 779 (s)

6.3.7 9,9-*Bis*(6-bromohexyl)-2,7-*bis*(4-methoxyphenyl)-9*H*-fluorene

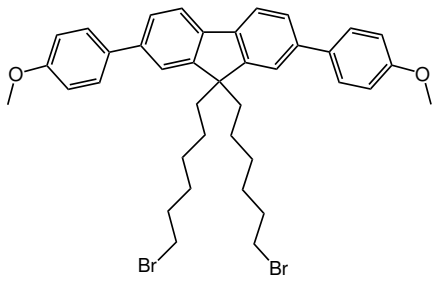

46b
$C_{39}H_{44}Br_2O_2$
Mol Wt: 704.59

Synthesised following the procedure detailed in 6.3.6, with the following reagent amounts, and column conditions:
Dioxaborolane **50**: 500 mg, 0.65 mmol
TBAB: 32 mg, 0.10 mmol
4-bromoanisole: 0.20 mL, 1.46 mmol
K_2CO_3: 683 mg, 5.00 mmol
toluene: 6.0 mL
H_2O: 3.0 mL
$Pd(PPh_3)_4$: 55 mg, 0.05 mmol
Reaction time: 45 h
Column chromatography: silica; 5% ethyl acetate in hexane.
Yield: 263.0 mg, 0.37 mmol, 57% (colourless oil)

HRMS (ESI) Found: 703.1781 $[M + H]^+$, $C_{39}H_{44}Br_2O_2$, Required: 703.1786

^{1}H NMR (400 MHz, $CDCl_3$, 25 °C):
δ = 7.76 (2H, d, J = 7.8 Hz, 2×Ar-**H**), 7.67-7.60 (4H, m, 4×Ar-**H**), 7.57 (2H, dd, J = 7.8, 1.6 Hz, 2×Ar-**H**), 7.53 (2H, d, J = 1.3 Hz, 2×Ar-**H**), 7.08-7.00 (4H, m, 4×Ar-**H**), 3.89 (6H, s, 2×C**H**$_3$), 3.28 (4H, t, J = 6.8 Hz, 2×C**H**$_2$Br), 2.10-2.01 (4H, m, 2×C**H**$_2$), 1.67 (4H, quin, J = 7.2 Hz, 2×C**H**$_2$), 1.28 – 1.18 (4H, m, 2×C**H**$_2$), 1.11 (4H, quin, J = 7.4 Hz, 2×C**H**$_2$), 0.80 – 0.68 (4H, m, 2×C**H**$_2$) ppm

^{13}C NMR (101 MHz, $CDCl_3$, 25 °C):
δ = 159.1 (2×**C**), 151.2 (2×**C**), 139.62 (2×**C**), 139.56 (2×**C**), 134.1 (2×**C**), 128.2 (4×**C**H), 125.7 (2×**C**H), 120.9 (2×**C**H), 119.9 (2×**C**H), 114.2 (4×**C**H), 55.4 (2×**C**H$_3$), 55.1 (**C**), 40.3 (2×**C**H$_2$), 33.9 (2×**C**H$_2$), 32.6 (2×**C**H$_2$), 29.1 (2×**C**H$_2$), 27.7 (2×**C**H$_2$), 23.6 (2×**C**H$_2$) ppm

FT-IR (ν_{max} cm^{-1}, film):
2931 (m) 1608 (m), 1516 (vs), 1465 (s), 1437 (m), 1247 (vs), 1179 (s), 1044 (m), 1028 (m), 818 (s)

6.3.8 9,9-*Bis*(6-bromohexyl)-2,7-*bis*(2-methoxyphenyl)-9*H*-fluorene

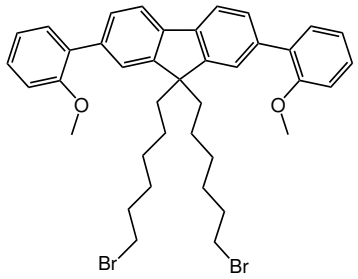

104a

$C_{39}H_{44}Br_2O_2$
Mol Wt: 704.59

Synthesised following the procedure detailed in 6.3.6, with the following reagent amounts, and column conditions:
Dioxaborolane **50**: 500 mg, 0.65 mmol
TBAB: 42 mg, 0.10 mmol
3-bromoanisole: 0.20 mL, 1.46 mmol
K_2CO_3: 674 mg, 5.00 mmol
toluene: 4.0 mL
H_2O: 2.0 mL
$Pd(PPh_3)_4$: 58 mg, 0.05 mmol
Reaction time: 3.5 days
Column chromatography: silica; 5 to 10% ethyl acetate in hexane.
Yield: 40.5 mg, 0.06 mmol, 9% (colourless oil)

HRMS (APPI) Found: 702.1717 $[M]^+$, $C_{39}H_{44}Br_2O_2$, Required: 702.1708

^{1}H NMR (400 MHz, $CDCl_3$, 25 °C):
δ = 7.76 (2H, d, J = 8.4 Hz, 2×Ar-**H**), 7.57 – 7.51 (4H, m, 4×Ar-**H**), 7.44 (2H, dd, J = 7.5, 1.8 Hz, 2×Ar-**H**), 7.39 – 7.32 (2H, m, 2×Ar-**H**), 7.09 (2H, td, J = 7.4, 1.0 Hz, 2×Ar-**H**), 7.04 (2H, dd, J = 8.3, 0.9 Hz, 2×Ar-**H**), 3.86 (6H, s, 2×C**H**$_3$), 3.29 (4H, t, J = 6.9 Hz, 2×C**H**$_2$Br), 2.06 – 1.98 (4H, m, 2×C**H**$_2$), 1.70 (4H, quin, J = 7.2 Hz, 2×C**H**$_2$), 1.28 – 1.21 (4H, m, 2×C**H**$_2$), 1.12 (4H, app quin, J = 7.3 Hz, 2×C**H**$_2$), 0.91 – 0.80 (4H, m, 2×C**H**$_2$) ppm

^{13}C NMR (101 MHz, $CDCl_3$, 25 °C):
δ = 156.6 (2×**C**), 150.3 (2×**C**), 139.7 (2×**C**), 137.1 (2×**C**), 131.2 (2×**C**), 130.9 (2×**C**H), 128.5 (2×**C**H), 128.2 (2×**C**H), 124.3 (2×**C**H), 121.0 (2×**C**H), 119.2 (2×**C**H), 111.6 (2×**C**H), 55.7 (2×**C**H$_3$), 54.8 (**C**), 40.1 (2×**C**H$_2$), 33.9 (2×**C**H$_2$), 32.7 (2×**C**H$_2$), 29.2 (2×**C**H$_2$), 27.8 (2×**C**H$_2$), 23.8 (2×**C**H$_2$) ppm

FT-IR (ν_{max} cm^{-1}, film):
1464 (s), 1239 (s), 1026 (s), 750 (vs)

6.3.9 9,9-*Bis*(6-bromohexyl)-2,7-di-*m*-tolyl-9*H*-fluorene

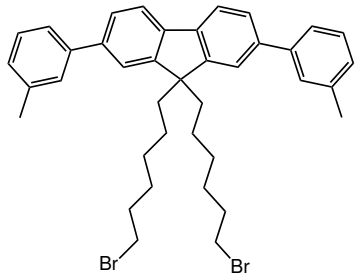

45a
$C_{39}H_{44}Br_2$
Mol Wt: 672.59

Synthesised following the procedure detailed in 6.3.6, with the following reagent amounts, and column conditions:
Dioxaborolane **50**: 510 mg, 0.68 mmol
3-bromotoluene: 0.17 mL, 1.40 mmol
K_2CO_3: 465 mg, 3.40 mmol
$Pd(PPh_3)_4$: 58 mg, 0.05 mmol
TBAB: 40 mg, 0.12 mmol
toluene: 4.0 mL
H_2O: 2.0 mL
Reaction time: 17.5 h
Column chromatography: silica; 20-50% DCM in petrol
Yield: 330 mg, 0.49 mmol, 72% (off-white oil)

HRMS (APPI) Found: 670.1804 $[M]^+$, $C_{39}H_{44}Br_2$, Required: 670.1810

^{1}H NMR (400 MHz, $CDCl_3$, 25 °C):
δ = 7.79 (2H, dd, J = 7.8, 0.5 Hz, 2×Ar-**H**), 7.62 (2H, dd, J = 7.8, 1.7 Hz, 2×Ar-**H**), 7.58 (2H, dd, J = 1.7, 0.5 Hz, 2×Ar-**H**), 7.54 – 7.48 (4H, m, 4×Ar-**H**), 7.44 – 7.37 (2H, m, 2×Ar-**H**), 7.24 – 7.19 (2H, m, 2×Ar-**H**), 3.29 (4H, t, J = 6.8 Hz, 2×C**H**$_2$Br), 2.49 (6H, s, 2×C**H**$_3$), 2.14 – 2.04 (4H, m, 2×C**H**$_2$), 1.68 (4H, quin, J = 7.2 Hz, 2×C**H**$_2$), 1.29 – 1.18 (4H, m, 2×C**H**$_2$), 1.12 (4H, quin, J = 7.4 Hz, 2×C**H**$_2$), 0.81 – 0.69 (4H, m, 2×C**H**$_2$) ppm

^{13}C NMR (101 MHz, $CDCl_3$, 25 °C):
δ = 151.2 (2×**C**), 141.6 (2×**C**), 140.3 (2×**C**), 140.1 (2×**C**), 138.4 (2×**C**), 128.7 (2×**C**H), 127.93 (2×**C**H), 127.90 (2×**C**H), 126.2 (2×**C**H), 124.3 (2×**C**H), 121.4 (2×**C**H), 120.0 (2×**C**H), 55.2 (**C**), 40.4 (2×**C**H$_2$), 34.0 (2×**C**H$_2$), 32.7 (2×**C**H$_2$), 29.1 (2×**C**H$_2$), 27.8 (2×**C**H$_2$), 23.6 (2×**C**H$_2$), 21.6 (2×**C**H$_3$) ppm

FT-IR (ν_{max} cm^{-1}, film):
2928 (m), 2855 (m), 2360 (m), 1464 (s), 907 (s), 826 (s), 782 (s), 731 (vs), 701 (s)

6.3.10 9,9-*Bis*(6-bromohexyl)-2,7-di-*p*-tolyl-9*H*-fluorene

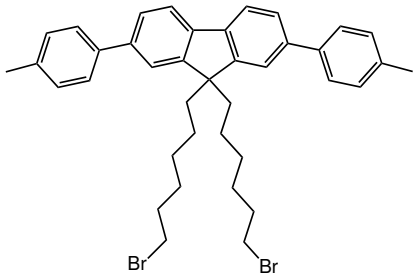

46a
$C_{39}H_{44}Br_2$
Mol Wt: 672.59

Synthesised following the procedure detailed in 6.3.6, with the following reagent amounts, and column conditions:
Dioxaborolane **50**: 512 mg, 0.69 mmol
4-bromotoluene: 237 mg, 1.36 mmol
K_2CO_3: 476 mg, 3.40 mmol
$Pd(PPh_3)_4$: 58 mg, 0.048 mmol
TBAB: 40 mg, 0.12 mmol
toluene: 4.0 mL
H_2O: 2.0 mL
Reaction time: 17.5 h
Column chromatography: silica; 20-50% $CHCl_3$ in hexane
Yield: 277 mg, 0.41 mmol, 61% (off-white oil)

HRMS (APPI) Found: 670.1804 $[M]^+$, $C_{39}H_{44}Br_2$, Required: 670.1810

^{1}H NMR (400 MHz, $CDCl_3$, 25 °C):
δ = 7.77 (2H, dd, J = 7.8, 0.5 Hz, 2×Ar-**H**), 7.63 – 7.57 (6H, m, 6×Ar-**H**), 7.55 (2H, dd, J = 1.6, 0.5 Hz, 2×Ar-**H**), 7.31 (4H, dd, J = 8.4, 0.6 Hz, 4×Ar-**H**), 3.28 (4H, t, J = 6.8 Hz, 2×C**H**$_2$Br), 2.44 (6H, s, 2×C**H**$_3$), 2.10 – 2.02 (4H, m, 2×C**H**$_2$), 1.67 (4H, quin, J = 7.2 Hz, 2×C**H**$_2$), 1.27 – 1.17 (4H, m, 2×C**H**$_2$), 1.10 (4H, quin, J = 7.4 Hz, 2×C**H**$_2$), 0.79 – 0.69 (4H, m, 2×C**H**$_2$) ppm

^{13}C NMR (101 MHz, $CDCl_3$, 25 °C):
δ = 151.2 (2×**C**), 140.0 (2×**C**), 139.9 (2×**C**), 138.7 (2×**C**), 137.0 (2×**C**), 129.5 (4×**C**H), 127.0 (4×**C**H), 125.9 (2×**C**H), 121.2 (2×**C**H), 120.0 (2×**C**H), 55.1 (**C**), 40.3 (2×**C**H$_2$), 33.9 (2×**C**H$_2$), 32.6 (2×**C**H$_2$), 29.1 (2×**C**H$_2$), 27.7 (2×**C**H$_2$), 23.6 (2×**C**H$_2$), 21.1 (2×**C**H$_3$) ppm

FT-IR (ν_{max} cm^{-1}, film):
2928 (m), 2855 (w), 1465 (m), 1247 (m), 1052 (m), 907 (m), 807 (vs), 730 (s)

6.3.11 2,7-Di([1,1'-biphenyl]-3-yl)-9,9-*bis*(6-bromohexyl)-9*H*-fluorene

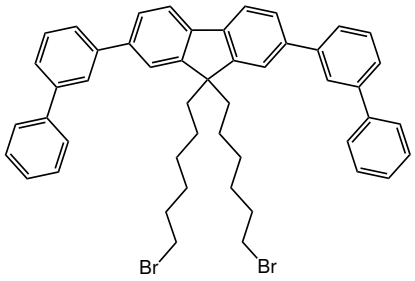

45c
$C_{49}H_{48}Br_2$
Mol Wt: 796.73

Synthesised following the procedure detailed in 6.3.6, with the following reagent amounts, and column conditions:
Dioxaborolane **50**: 1.01 g, 1.35 mmol
3-bromobiphenyl: 0.48 mL, 2.90 mmol
K_2CO_3: 941 mg, 6.81 mmol
$Pd(PPh_3)_4$: 126 mg, 0.11 mmol
TBAB: 89 mg, 0.28 mmol
toluene: 8.0 mL
H_2O: 4.0 mL
Reaction time: 16 h
Column chromatography: silica; 20 - 50% $CHCl_3$ in hexane
Yield: 608 mg, 0.76 mmol, 57% (off-white oil)

HRMS (APPI) Found: 794.2120 $[M]^+$, $C_{49}H_{48}Br_2$, Required: 794.2123

^{1}H NMR (400 MHz, $CDCl_3$, 25 °C):
δ = 7.90 (2H, td, J = 1.8, 0.4 Hz, 2×Ar-**H**), 7.84 (2H, dd, J = 7.9, 0.4 Hz, 2×Ar-**H**), 7.74 – 7.67 (8H, m, 8×Ar-**H**), 7.65 – 7.55 (6H, m, 6×Ar-**H**), 7.55 – 7.48 (4H, m, 4×Ar-**H**), 7.42 (2H, tt, J = 7.4, 1.2 Hz, 2×Ar-**H**), 3.28 (4H, t, J = 6.8 Hz, 2×C**H**$_2$Br), 2.14 – 2.05 (4H, m, 2×C**H**$_2$), 1.74 – 1.63 (4H, m, 2×C**H**$_2$), 1.29 – 1.19 (4H, m, 2×C**H**$_2$), 1.18 – 1.07 (4H, m, 2×C**H**$_2$), 0.83 – 0.72 (4H, m, 2×C**H**$_2$) ppm

^{13}C NMR (101 MHz, $CDCl_3$, 25 °C):
δ = 151.4 (2×**C**), 142.1 (2×**C**), 141.9 (2×**C**), 141.3 (2×**C**), 140.17 (2×**C**), 140.16 (2×**C**), 129.2 (2×**C**H), 128.8 (4×**C**H), 127.4 (2×**C**H), 127.3 (4×**C**H), 126.3 (2×**C**H), 126.17 (2×**C**H), 126.16 (2×**C**H), 126.1 (2×**C**H), 121.5 (2×**C**H), 120.2 (2×**C**H), 55.2 (**C**), 40.3 (2×**C**H$_2$), 33.9 (2×**C**H$_2$), 32.6 (2×**C**H$_2$), 29.1 (2×**C**H$_2$), 27.8 (2×**C**H$_2$), 23.6 (2×**C**H$_2$) ppm

FT-IR (ν_{max} cm^{-1}, film):
2929 (m), 2855 (w), 2359 (w), 1597 (m), 1463 (s), 906 (s), 756 (vs), 730 (vs), 700 (vs)

6.3.12 2,7-Di([1,1'-biphenyl]-4-yl)-9,9-*bis*(6-bromohexyl)-9*H*-fluorene

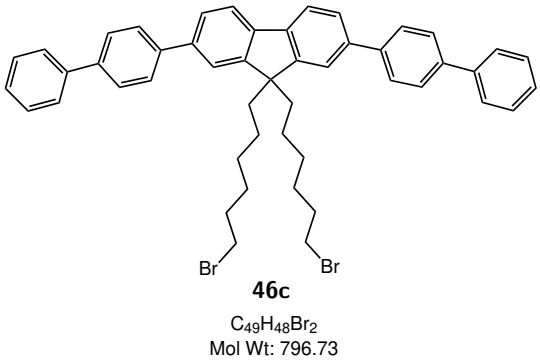

Synthesised following the procedure detailed in 6.3.6, with the following reagent amounts, and column conditions:
Dioxaborolane **50**: 1.00 g, 1.35 mmol
4-bromobiphenyl: 667 mg, 2.86 mmol
K_2CO_3: 943 mg, 6.83 mmol
$Pd(PPh_3)_4$: 121 mg, 0.11 mmol
TBAB: 92 mg, 0.28 mmol
toluene: 8.0 mL
H_2O: 4.0 mL
Reaction time: 16 h
Column chromatography: silica; 20 - 50% $CHCl_3$ in hexane
Yield: 801 mg, 1.01 mmol, 75% (off-white oil)

HRMS (APPI) Found: 794.2122 $[M]^+$, $C_{49}H_{48}Br_2$, Required: 794.2123

^{1}H NMR (400 MHz, $CDCl_3$, 25 °C):
δ = 7.83 (2H, dd, J = 7.8, 0.4 Hz, 2×Ar-**H**), 7.82 – 7.73 (8H, m, 8×Ar-**H**), 7.72 – 7.66 (6H, m, 6×Ar-**H**), 7.65 (2H, d, J = 1.2 Hz, 2×Ar-**H**), 7.54 – 7.47 (4H, m, 4×Ar-**H**), 7.43 – 7.37 (2H, m, 2×Ar-**H**), 3.29 (4H, t, J = 6.8 Hz, 2×C**H**$_2$Br), 2.16 – 2.04 (4H, m, 2×C**H**$_2$), 1.69 (4H, quin, J = 7.1 Hz, 2×C**H**$_2$), 1.31 – 1.19 (4H, m, 2×C**H**$_2$), 1.19 – 1.08 (4H, m, 2×C**H**$_2$), 0.84 – 0.71 (4H, m, 2×C**H**$_2$) ppm

^{13}C NMR (101 MHz, $CDCl_3$, 25 °C):
δ = 151.4 (2×**C**), 140.7 (2×**C**), 140.4 (2×**C**), 140.14 (2×**C**), 140.07 (2×**C**), 139.6 (2×**C**), 128.8 (4×**C**H), 127.54 (4×**C**H), 127.50 (4×**C**H), 127.4 (2×**C**H), 127.0 (4×**C**H), 126.1 (2×**C**H), 121.3 (2×**C**H), 120.2 (2×**C**H), 55.2 (**C**), 40.3 (2×**C**H$_2$), 33.9 (2×**C**H$_2$), 32.6 (2×**C**H$_2$), 29.1 (2×**C**H$_2$), 27.8 (2×**C**H$_2$), 23.6 (2×**C**H$_2$) ppm

FT-IR (ν_{max} cm^{-1}, film):
3028 (w), 2929 (m), 2855 (w), 2359 (w), 1464 (s), 906 (s), 818 (s), 764 (s), 728 (vs), 696 (s)

6.3.13 9,9-*Bis*(6-bromohexyl)-2-(3-methoxyphenyl)-9*H*-fluorene

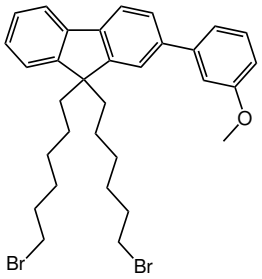

42a
$C_{32}H_{38}Br_2O$
Mol Wt: 598.46

Synthesised following the procedure detailed in 6.3.6, with the following reagent amounts, and column conditions:
Dioxaborolane **41**: 1.1 g, 1.8 mmol
3-bromoanisole: 0.23 mL, 1.8 mmol
K_2CO_3: 1.0 g, 7.4 mmol
$Pd(PPh_3)_4$: 62 mg, 0.050 mmol
TBAB: 78 mg, 0.24 mmol
toluene: 8.0 mL
H_2O: 4.0 mL
Reaction time: 15 h
Column chromatography: silica; 20 - 50% DCM in hexane
Yield: 640 mg, 1.07 mmol, 60% (off-white oil)

HRMS (APPI) Found: 596.1287 $[M]^+$, $C_{32}H_{38}Br_2O$, Required: 596.1289

^{1}H NMR (400 MHz, $CDCl_3$):
δ = 7.77 (1H, dd, J = 7.8, 0.5 Hz, Ar-**H**), 7.76 - 7.72 (1H, m, Ar-**H**), 7.61 (1H, dd, J = 7.8, 1.7 Hz, Ar-**H**), 7.56 (1H, dd, J = 1.6, 0.5 Hz, Ar-**H**), 7.42 (1H, app. t, J = 8.3 Hz, Ar-**H**), 7.40 - 7.31 (3H, m, Ar-**H**), 7.29 (1H, ddd, J = 7.6, 1.7, 1.0 Hz, Ar-**H**), 7.24 - 7.22 (1H, m, Ar-**H**), 6.94 (1H, ddd, J = 8.2, 2.6, 0.9 Hz, Ar-**H**), 3.92 (3H, s, OC**H**$_3$), 3.28 (4H, t, J = 6.8 Hz, C**H**$_2$Br), 2.07 - 1.99 (4H, m, C**H**$_2$), 1.72 - 1.63 (4H, m C**H**$_2$), 1.26 - 1.17 (4H, m, C**H**$_2$), 1.10 (4H, quin, J = 7.5 Hz, C**H**$_2$), 0.77 - 0.63 (4H, m, C**H**$_2$) ppm

^{13}C NMR (101 MHz, $CDCl_3$, 25 °C):
δ = 160.0 (**C**), 150.9 (**C**), 150.6 (**C**), 143.1(**C**), 140.7 (**C**), 140.5 (**C**), 139.9 (**C**), 129.8 (**C**H), 127.1 (**C**H), 126.9 (**C**H), 126.1 (**C**H), 122.8 (**C**H), 121.4 (**C**H), 119.9 (**C**H), 119.8 (**C**H), 119.7 (**C**H), 113.2 (**C**H), 112.2 (**C**H), 55.3 (**C**H$_3$), 55.0 (**C**), 40.2 (2×**C**H$_2$), 33.9 (2×**C**H$_2$), 32.6 (2×**C**H$_2$), 29.0 (2×**C**H$_2$), 27.7 (2×**C**H$_2$), 23.5 (2×**C**H$_2$) ppm

FT-IR (ν_{max} cm^{-1}, film):
3004 (w), 2929 (s), 2855 (m), 1599 (m), 1456 (s), 1215 (s), 1053 (m), 1036 (m), 777 (s), 741 (vs)

6.3.14 9,9-*Bis*(6-bromohexyl)-2-(4-methoxyphenyl)-9*H*-fluorene

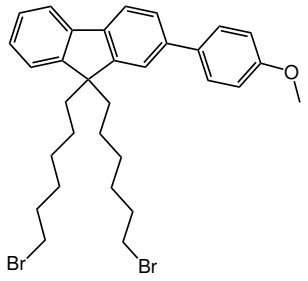

43a

$C_{32}H_{38}Br_2O$

Mol Wt: 598.46

Synthesised following the procedure detailed in 6.3.6, with the following reagent amounts, and column conditions:
Dioxaborolane **41**: 1160 mg, 1.88 mmol
4-bromoanisole: 0.24 mL, 1.8 mmol
K_2CO_3: 1.01 g, 7.30 mol
$Pd(PPh_3)_4$: 75 g, 0.06 mmol
TBAB: 60 mg, 0.19 mmol
toluene: 8.0 mL
H_2O: 4.0 mL
Reaction time: 15 h
Column chromatography: silica gel; 20 - 50% DCM in hexane
Yield: 304 mg, 0.51 mmol, 27% (off-white oil)

HRMS (APPI) Found: 596.1278 $[M]^+$, $C_{32}H_{38}Br_2O$, Required: 596.1289

^{1}H NMR (400 MHz, $CDCl_3$, 25 °C):
δ = 7.75 (1H, dd, J = 7.8, 0.6 Hz, Ar-**H**), 7.74 – 7.71 (1H, m, Ar-**H**), 7.65 – 7.60 (2H, m, 2×Ar-**H**), 7.55 (1H, dd, J = 7.8, 1.7 Hz, Ar-**H**), 7.51 (1H, dd, J = 1.7, 0.6 Hz, Ar-**H**), 7.39 – 7.29 (3H, m, 3×Ar-**H**), 7.06 – 7.00 (2H, m, 2×Ar-**H**), 3.89 (3H, s, C**H**$_3$), 3.28 (4H, t, J = 6.8 Hz, 2×C**H**$_2$Br), 2.02 (4H, dd, J = 9.7, 6.8 Hz, 2×C**H**$_2$), 1.71 – 1.62 (4H, m, 2×C**H**$_2$), 1.26 – 1.16 (4H, m, 2×C**H**$_2$), 1.14 – 1.04 (4H, m, 2×C**H**$_2$), 0.75 – 0.62 (4H, m, 2×C**H**$_2$) ppm

^{13}C NMR (101 MHz, $CDCl_3$, 25 °C):
δ = 159.1 (**C**), 151.0 (**C**), 150.5 (**C**), 140.8 (**C**), 139.8 (**C**), 139.7 (**C**), 134.1 (**C**), 128.2 (2×**C**H), 127.0 (**C**H), 126.9 (**C**H), 125.6 (**C**H), 122.7 (**C**H), 120.9 (**C**H), 119.9 (**C**H), 119.7 (**C**H), 114.2 (2×**C**H), 55.4 (**C**H$_3$), 55.0 (**C**), 40.3 (2×**C**H$_2$), 33.9 (2×**C**H$_2$), 32.6 (2×**C**H$_2$), 29.0 (2×**C**H$_2$), 27.7 (2×**C**H$_2$), 23.5 (2×**C**H$_2$) ppm

FT-IR (ν_{max} cm^{-1}, film):
3003 (w), 2929 (s), 2855 (m), 1606 (m), 1517 (s), 1451 (s), 1246 (vs), 1179 (s), 1043 (m), 823 (vs), 741 (vs)

6.3.15 9,9-*Bis*(6-bromohexyl)-2-(*m*-tolyl)-9*H*-fluorene

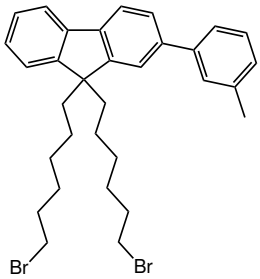

42c

$C_{32}H_{38}Br_2$

Mol Wt: 582.46

Synthesised following the procedure detailed in 6.3.6, with the following reagent amounts, and column conditions:
Dioxaborolane **41**: 1.11 g, 1.79 mmol
3-bromotoluene: 0.17 mL, 1.4 mmol
K_2CO_3: 1.04 g, 7.53 mmol
$Pd(PPh_3)_4$: 64 mg, 0.06 mmol
TBAB: 54 mg, 0.17 mmol
toluene: 8.0 mL
H_2O: 4.0 mL
Reaction time: 15.5 h
Column chromatography: silica; 5 - 30% DCM in hexane
Yield: 355 mg, 0.61 mmol, 44% (off-white oil)

HRMS (APPI) Found: 580.1340 $[M]^+$, $C_{32}H_{38}Br_2$, Required: 580.1340

^{1}H NMR (400 MHz, $CDCl_3$, 25 °C):
δ = 7.77 (1H, dd, J = 7.9, 0.6 Hz, Ar-**H**), 7.76 – 7.73 (1H, m, Ar-**H**), 7.60 (1H, dd, J = 7.8, 1.7 Hz, Ar-**H**), 7.56 (1H, dd, J = 1.7, 0.6 Hz, Ar-**H**), 7.52 – 7.48 (2H, m, 2×Ar-**H**), 7.42 – 7.31 (4H, m, 4×Ar-**H**), 7.23 – 7.19 (1H, m, Ar-**H**), 3.29 (4H, t, J = 6.8 Hz, 2×C**H**$_2$Br), 2.49 (3H, s, C**H**$_3$), 2.08 – 2.00 (4H, m, 2×C**H**$_2$), 1.72 – 1.63 (4H, m, 2×C**H**$_2$), 1.27 – 1.18 (4H, m, 2×C**H**$_2$), 1.15 – 1.05 (4H, m, 2×C**H**$_2$), 0.75 – 0.64 (4H, m, 2×C**H**$_2$) ppm

^{13}C NMR (101 MHz, $CDCl_3$, 25 °C):
δ = 150.9 (**C**), 150.5 (**C**), 141.5 (**C**), 140.8 (**C**), 140.3 (**C**), 140.2 (**C**), 138.4 (**C**), 128.7 (**C**H), 127.90 (**C**H), 127.89 (**C**H), 127.1 (**C**H), 126.9 (**C**H), 126.1 (**C**H), 124.3 (**C**H), 122.8 (**C**H), 121.4 (**C**H), 119.9 (**C**H), 119.8 (**C**H), 55.0 (**C**), 40.2 (2×**C**H$_2$), 33.9 (2×**C**H$_2$), 32.6 (2×**C**H$_2$), 29.0 (2×**C**H$_2$), 27.7 (2×**C**H$_2$), 23.5 (2×**C**H$_2$), 21.6 (2×**C**H$_3$) ppm

FT-IR (ν_{max} cm^{-1}, film):
3004 (w), 2929 (s), 2855 (m), 1599 (m), 1456 (s), 1215 (s), 1053 (m), 1036 (m), 777 (s), 741 (vs)

6.3.16 9,9-*Bis*(6-bromohexyl)-2-(*p*-tolyl)-9*H*-fluorene

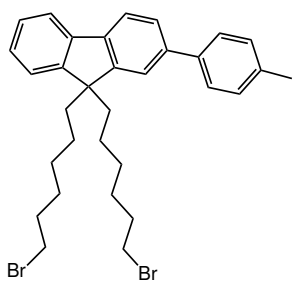

43b

$C_{32}H_{38}Br_2$

Mol Wt: 582.46

Synthesised following the procedure detailed in 6.3.6, with the following reagent amounts, and column conditions:
Dioxaborolane **41**: 1.10 g, 1.78 mmol
4-bromotoluene: 184 mg, 1.08 mmol
K_2CO_3: 1.00 g, 7.25 mmol
$Pd(PPh_3)_4$: 61 mg, 0.05 mmol
TBAB: 77 mg, 0.24 mmol
toluene: 8.0 mL
H_2O: 4.0 mL
Reaction time: 15.5 h
Column chromatography: silica, 5 - 20% DCM in hexane
Yield: 150 mg, 0.258 mmol, 24% (colourless oil)

HRMS (APPI) Found: 580.1345 $[M]^+$, $C_{32}H_{38}Br_2$, Required: 580.1340

^{1}H NMR (400 MHz, $CDCl_3$, 25 °C):
δ = 7.78-7.71 (2H, m, 2×Ar-**H**), 7.61-7.56 (3H, m, 3×Ar-**H**), 7.54 (1H, d, J = 1.7 Hz, Ar-**H**), 7.39-7.28 (5H, m, 5×Ar-**H**), 3.28 (4H, t, J = 6.8 Hz, 2×C**H**$_2$Br), 2.43 (3H, s, C**H**$_3$), 2.08-1.96 (4H, m, 2×C**H**$_2$), 1.66 (4H, dt, J = 14.5, 7.0 Hz, 2×C**H**$_2$), 1.26-1.16 (4H, m, 2×C**H**$_2$), 1.09 (4H, app quin, J = 7.5 Hz, 2×C**H**$_2$), 0.75-0.61 (4H, m, 2×C**H**$_2$) ppm

^{13}C NMR (101 MHz, $CDCl_3$, 25 °C):
δ = 150.9 (**C**), 150.5 (**C**), 140.8 (**C**), 140.11 (**C**), 140.06 (**C**), 138.7 (**C**), 137.0 (**C**), 129.5 (2 x **C**H), 127.01 (**C**H), 126.99 (2 x **C**H), 126.9 (**C**H), 125.8 (**C**H), 122.8 (**C**H), 121.2 (**C**H), 119.9 (**C**H), 119.7 (**C**H), 55.0 (**C**), 40.2 (**C**H$_2$), 33.9 (**C**H$_2$), 32.6 (**C**H$_2$), 29.0 (**C**H$_2$), 27.7 (**C**H$_2$), 23.5 (**C**H$_2$), 21.1 (**C**H$_3$) ppm

FT-IR (ν_{max} cm^{-1}, film):
3018 (w), 2928 (s), 2855 (m), 1451 (s), 813 (vs), 740 (vs)

6.3.17 2-([1,1'-Biphenyl]-3-yl)-9,9-*bis*(6-bromohexyl)-9*H*-fluorene

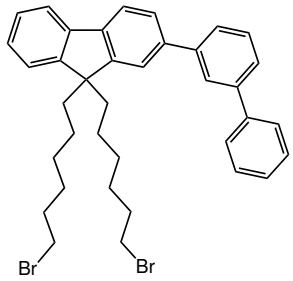

42d
$C_{37}H_{40}Br_2$
Mol Wt: 644.54

Synthesised following the procedure detailed in 6.3.6, with the following reagent amounts, and column conditions:
Dioxaborolane **41**: 1.05 g, 1.70 mmol
3-bromobiphenyl: 0.24 mL, 1.6 mmol
K_2CO_3: 1.06 g, 7.64 mmol
$Pd(PPh_3)_4$: 65 mg, 0.06 mmol
TBAB: 45 mg, 0.14 mmol
toluene: 8.0 mL
H_2O: 4.0 mL
Reaction time: 15 h
Column chromatography: silica; 20% $CHCl_3$ in hexane
Yield: 438 mg, 0.68 mmol, 42% (off-white oil)

HRMS (APPI) Found: 642.1491 $[M]^+$, $C_{37}H_{40}Br_2$, Required: 642.1497

^{1}H NMR (400 MHz, $CDCl_3$, 25 °C):
δ = 7.90 (1H, td, J = 1.8, 0.6 Hz, Ar-**H**), 7.81 (1H, dd, J = 7.8, 0.5 Hz, Ar-**H**), 7.79 – 7.75 (1H, m, Ar-**H**), 7.74 – 7.65 (4H, m, Ar-**H**), 7.64 – 7.49 (5H, m, 5×Ar-**H**), 7.45 – 7.32 (4H, m, 4×Ar-**H**), 3.29 (4H, t, J = 6.8 Hz, 2xC**H**$_2$Br), 2.10-2.01 (4H, m, 2×C**H**$_2$), 1.73-1.63 (4H, m, 2×C**H**$_2$), 1.28 – 1.18 (4H, m, C**H**$_2$), 1.11 (4H, quin, J = 7.5 Hz, 2×C**H**$_2$), 0.81 – 0.64 (4H, m, 2×C**H**$_2$) ppm

^{13}C NMR (101 MHz, $CDCl_3$, 25 °C):
δ = 151.1 (**C**), 150.6 (**C**), 142.2 (**C**), 142.0 (**C**), 141.3 (**C**), 140.8 (**C**), 140.6 (**C**), 140.1 (**C**), 129.3 (**C**H), 128.9 (2×**C**H), 127.5 (**C**H), 127.4 (2×**C**H), 127.2 (**C**H), 127.0 (**C**H), 126.23 (2 x **C**H), 126.20 (**C**H), 126.1 (**C**H), 122.9 (**C**H), 121.5 (**C**H), 120.1 (**C**H), 119.9 (**C**H), 55.1 (**C**), 40.3 (2×**C**H$_2$), 34.0 (2×**C**H$_2$), 32.7 (2×**C**H$_2$), 29.1 (2×**C**H$_2$), 27.8 (2×**C**H$_2$), 23.6 (2×**C**H$_2$) ppm

FT-IR (ν_{max} cm^{-1}, film):
3030 (w), 2928 (m), 2855 (m), 1597 (w), 1452 (m), 1254 (m), 907 (m), 756 (vs), 734 (vs), 700 (vs)

6.3.18 2-([1,1'-Biphenyl]-4-yl)-9,9-*bis*(6-bromohexyl)-9*H*-fluorene

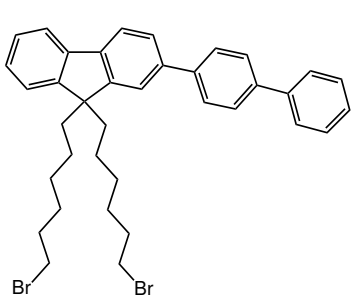

43c
$C_{37}H_{40}Br_2$
Mol Wt: 644.54

Synthesised following the procedure detailed in 6.3.6, with the following reagent amounts, and column conditions:
Dioxaborolane **41**: 1.03 g, 1.67 mmol
4-bromobiphenyl: 387 mg, 1.66 mmol
K_2CO_3: 1.07 g, 7.73 mmol
$Pd(PPh_3)_4$: 66 mg, 0.06 mmol
TBAB: 40 mg, 0.13 mmol
toluene: 8.0 mL
H_2O: 4.0 mL
Reaction time: 15 h
Column chromatography: silica; 10 - 50% $CHCl_3$ in hexane
Yield: 1.03 g, 1.59 mmol, 96% (off-white oil)

HRMS (APPI) Found: 642.1493 $[M]^+$, $C_{37}H_{40}Br_2$, Required: 642.1497

^{1}H NMR (400 MHz, $CDCl_3$, 25 °C):
δ = 7.83 – 7.64 (9H, m, 9×Ar-**H**), 7.62 (1H, dd, J = 1.6, 0.5 Hz, Ar-**H**), 7.53 – 7.47 (2H, m, 2×Ar-**H**), 7.42 – 7.32 (4H, m, 4×Ar-**H**), 3.29 (4H, t, J = 6.8 Hz, 2×C**H**$_2$Br), 2.10 – 2.00 (4H, m, 2×C**H**$_2$), 1.72 – 1.63 (4H, m, 2×C**H**$_2$), 1.27 – 1.18 (4H, m, 2×C**H**$_2$), 1.11 (4H, quin, J = 7.4 Hz, 2×C**H**$_2$), 0.78 – 0.64 (4H, m, 2×C**H**$_2$) ppm

^{13}C NMR (101 MHz, $CDCl_3$, 25 °C):
δ = 151.0 (**C**), 150.6 (**C**), 140.74 (**C**), 140.71 (**C**), 140.51 (**C**), 140.45 (**C**), 140.0 (**C**), 139.6 (**C**), 128.8 (2×**C**H), 127.53 (2×**C**H), 127.50 (2×**C**H), 127.3 (**C**H), 127.2 (**C**H), 127.03 (**C**H), 126.95 (**C**H), 126.0 (**C**H), 122.8 (**C**H), 121.2 (**C**H), 120.0 (2×**C**H), 119.8 (**C**H), 55.0 (**C**), 40.3 (2×**C**H$_2$), 33.9 (2×**C**H$_2$), 32.6 (2×**C**H$_2$), 29.0 (2×**C**H$_2$), 27.8 (2×**C**H$_2$), 23.6 (2×**C**H$_2$) ppm

FT-IR (ν_{max} cm^{-1}, film):
2928 (m), 2854 (m), 1450 (s), 1244 (m), 825 (s), 764 (vs), 740 (vs), 696 (vs), 558 (s)

6.3.19 9,9-*Bis*(6-bromohexyl)-2-phenyl-9*H*-fluorene

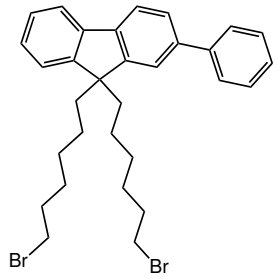

42b
$C_{31}H_{36}Br_2$
Mol Wt: 568.44

Synthesised following the procedure detailed in 6.3.6, with the following reagent amounts, and column conditions:
Dioxaborolane **41**: 3.07 g, 4.97 mmol
bromobenzene: 0.53 mL, 5.03 mmol
$Pd(PPh_3)_4$: 290 mg, 0.25 mmol
TBAB: 340 mg, 1.05 mmol
K_2CO_3: 5.06 g, 36.6 mmol
toluene: 34 mL
H_2O: 16 mL
Reaction time: 20 h
Column chromatography: silica; 10 - 20% DCM in hexane
Yield: 2.38 g, 4.19 mmol, 84% (off-white oil)

HRMS (APPI) Found: 566.1175 $[M]^+$, $C_{31}H_{36}Br_2$, Required: 566.1178

^{1}H NMR (400 MHz, $CDCl_3$, 25 °C):
δ = 7.78 (1H, dd, J = 7.9, 0.4 Hz, Ar-**H**), 7.76 – 7.73 (1H, m, Ar-**H**), 7.72 – 7.68 (2H, m, 2×Ar-**H**), 7.61 (1H, dd, J = 7.8, 1.7 Hz, Ar-**H**), 7.57 (1H, dd, J = 1.7, 0.4 Hz, Ar-**H**), 7.53 – 7.47 (2H, m, 2×Ar-**H**), 7.41 – 7.31 (4H, m, 4×Ar-**H**), 3.28 (4H, t, J = 6.8 Hz, 2×C**H**$_2$Br), 2.09 – 1.99 (4H, m, 2×C**H**$_2$), 1.72 – 1.62 (4H, m, 2×C**H**$_2$), 1.27 – 1.17 (4H, m, 2×C**H**$_2$), 1.10 (4H, quin, J = 7.4 Hz, 2×C**H**$_2$), 0.76 – 0.63 (4H, m, 2×C**H**$_2$) ppm

^{13}C NMR (101 MHz, $CDCl_3$, 25 °C):
δ = 151.0 (**C**), 150.5 (**C**), 141.6 (**C**), 140.7 (**C**), 140.4 (**C**), 140.1 (**C**), 128.8 (2×**C**H), 127.2 (3×**C**H), 127.1 (**C**H), 126.9 (**C**H), 126.1 (**C**H), 122.8 (**C**H), 121.4 (**C**H), 120.0 (**C**H), 119.8 (**C**H), 55.0 (**C**), 40.2 (2×**C**H$_2$), 33.9 (2×**C**H$_2$), 32.6 (2×**C**H$_2$), 29.0 (2×**C**H$_2$), 27.7 (2×**C**H$_2$), 23.5 (2×**C**H$_2$) ppm

FT-IR (ν_{max} cm^{-1}, film):
3029 (vw), 2929 (m), 2855 (w), 1451.7 (m), 907 (m), 758 (s), 731 (vs), 696 (s), 645 (m)

6.3.20 9,9-*Bis*(6-bromohexyl)-2,7-diphenyl-9*H*-fluorene

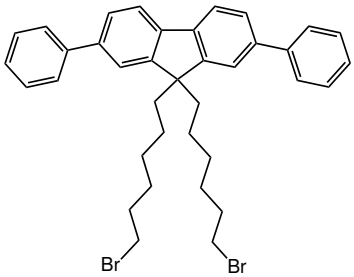

45d
$C_{37}H_{40}Br_2$
Mol Wt: 644.54

Synthesised following the procedure detailed in 6.3.6, with the following reagent amounts, and column conditions:
Dioxaborolane **50**: 2.02 g, 2.71 mmol
bromobenzene: 0.57 mL, 5.43 mmol
$Pd(PPh_3)_4$: 340 mg, 0.27 mmol
TBAB: 550 mg, 1.70 mmol
K_2CO_3: 9.18 g, 66.4 mmol
toluene: 40 mL
H_2O: 20 mL
Reaction time: 20 h
Column chromatography: silica; 5 - 20% DCM in hexane
Yield: 1.23 g, 1.91 mmol, 70% (off-white oil)

HRMS (APPI) Found: 642.1487 $[M]^+$, $C_{37}H_{40}Br_2$, Required: 642.1491

^{1}H NMR (400 MHz, $CDCl_3$, 25 °C):
δ = 7.81 (2H, dd, J = 7.8, 0.5 Hz, 2×Ar-**H**), 7.74 – 7.69 (4H, m, 4×Ar-**H**), 7.63 (2H, dd, J = 7.8, 1.7 Hz, 2×Ar-**H**), 7.59 (2H, dd, J = 1.7, 0.6 Hz, 2×Ar-**H**), 7.54 – 7.48 (4H, m, 4×Ar-**H**), 7.42 – 7.37 (2H, m, 2×Ar-**H**), 3.28 (4H, t, J = 6.8 Hz, 2×C**H**$_2$Br), 2.13 – 2.03 (4H, m, 2×C**H**$_2$), 1.68 (4H, quin, J = 7.2 Hz, 2×C**H**$_2$), 1.28 – 1.18 (4H, m, 2×C**H**$_2$), 1.17 – 1.07 (4H, m, 2×C**H**$_2$), 0.81 – 0.69 (4H, m, 2×C**H**$_2$) ppm

^{13}C NMR (101 MHz, $CDCl_3$, 25 °C):
δ = 151.3 (2×**C**), 141.5 (2×**C**), 140.2 (2×**C**), 140.0 (2×**C**), 128.8 (4×**C**H), 127.2 (6×**C**H), 126.2 (2×**C**H), 121.4 (2×**C**H), 120.1 (2×**C**H), 55.1 (**C**), 40.3 (2×**C**H$_2$), 33.9 (2×**C**H$_2$), 32.6 (2×**C**H$_2$), 29.0 (2×**C**H$_2$), 27.7 (2×**C**H$_2$), 23.6 (2×**C**H$_2$) ppm

FT-IR (ν_{max} cm^{-1}, film):
3028 (vw), 2929 (m), 2855 (w), 1464 (m), 1248 (m), 1053 (m), 756 (vs), 696 (s), 560 (m)

6.3.21 9-(9,9-*Bis*(6-bromohexyl)-9*H*-fluoren-2-yl)phenanthrene

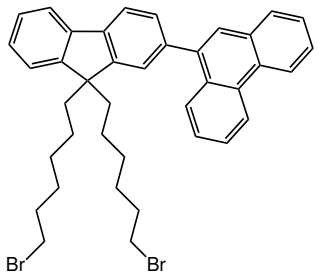

64

$C_{39}H_{40}Br_2$
Mol Wt: 668.56

Synthesised following the procedure detailed in 6.3.6, with the following reagent amounts, and column conditions:
Dioxaborolane **41**: 4.14 g, 6.69 mmol
9-bromophenanthrene: 1.72 g, 6.70 mmol
$Pd(PPh_3)_4$: 281 mg, 0.24 mmol
TBAB: 307 mg, 0.95 mmol
K_2CO_3: 4.64 g, 33.6 mmol
toluene: 70 mL
H_2O: 25 mL
Reaction time: 15 h
Column chromatography: silica; 10 - 30% DCM in petroleum ether
Yield: 4.08 g, 6.10 mmol, 91% (off-white oil)

HRMS (APPI) Found: 666.1948 $[M]^+$, $C_{39}H_{40}Br_2$, Required: 666.1497

^{1}H NMR (400 MHz, $CDCl_3$, 25 °C):
δ = 8.82 (1H, d, J = 8.2 Hz, Ar-**H**), 8.76 (1H, d, J = 8.3 Hz, Ar-**H**), 7.96 (2H, app. dd, J = 8.1, 1.2 Hz, 2×Ar-**H**), 7.86 (1H, dd, J = 7.7, 0.5 Hz, Ar-**H**), 7.82 – 7.77 (2H, m, 2×Ar-**H**), 7.73 – 7.62 (3H, m, 3×Ar-**H**), 7.59 – 7.53 (2H, m, 2×Ar-**H**), 7.52 (1H, dd, J = 1.5, 0.5 Hz, Ar-**H**), 7.43 – 7.34 (3H, m, 3×Ar-**H**), 3.30 (4H, t, J = 6.8 Hz, 2×C**H**$_2$Br), 2.03 (4H, t, J = 8.3 Hz, 2×C**H**$_2$), 1.70 (4H, quin, J = 7.1 Hz, 2×C**H**$_2$), 1.31 – 1.21 (4H, m, 2×C**H**$_2$), 1.18 – 1.08 (4H, m, 2×C**H**$_2$), 0.91 – 0.68 (4H, m, 2×C**H**$_2$) ppm

^{13}C NMR (101 MHz, $CDCl_3$, 25 °C):
δ = 150.6 (**C**), 150.4 (**C**), 140.9 (**C**), 140.4 (**C**), 139.6 (**C**), 139.1 (**C**), 131.6 (**C**), 131.3 (**C**), 130.7 (**C**), 129.9 (**C**), 128.8 (**C**H), 128.6 (**C**H), 127.4 (**C**H), 127.2 (**C**H), 127.0 (**C**H), 126.90 (**C**H), 126.85 (**C**H), 126.6 (**C**H), 126.5 (2×**C**H), 124.6 (**C**H), 123.0 (**C**H), 122.8 (**C**H), 122.6 (**C**H), 119.9 (**C**H), 119.6 (**C**H), 55.0 (**C**), 40.2 (2×**C**H$_2$), 33.9 (2×**C**H$_2$), 32.6 (2×**C**H$_2$), 29.1 (2×**C**H$_2$), 27.8 (2×**C**H$_2$), 23.7 (2×**C**H$_2$) ppm

FT-IR (ν_{max} cm^{-1}, film):
2930 (m), 2856 (w), 1730 (m), 1545 (m), 1437 (s), 1364 (s), 1114 (s), 741 (s)

6.3.22 3,3'-((2,7-*Bis*(4-methoxyphenyl)-9*H*-fluorene-9,9-diyl)*bis*(hexane-6,1-diyl))*bis*(1-methyl-1*H*-imidazol-3-ium) trifluoromethanesulfonate

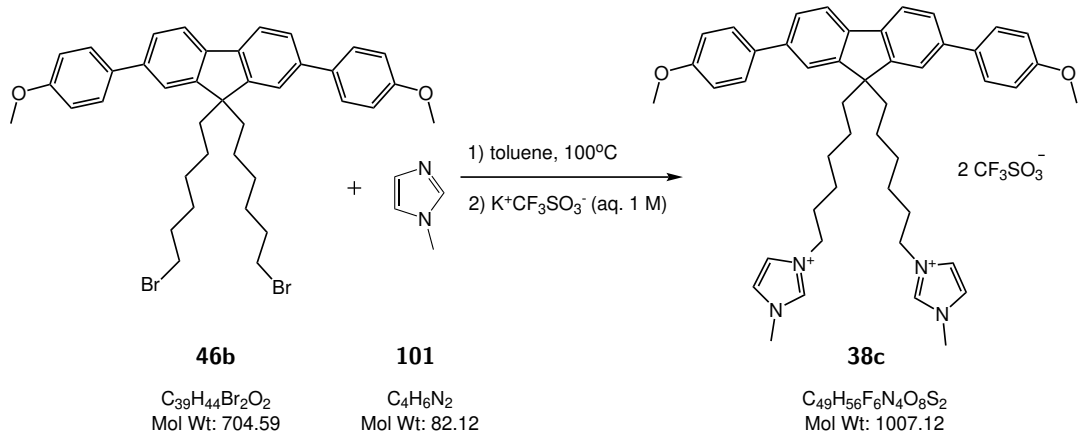

Dibromide **46b** (201.6 mg, 0.29 mmol) and 1-methylimidazole (0.05 mL, 0.64 mmol) in toluene (3.0 mL) were heated at 100°C for 20 hours, then cooled to room temperature, and concentrated *in vacuo*. MeCN and KOTf (aq., 1.0 M, 5.0 mL) were added, and the solvent was removed *in vacuo*. The residue was dissolved in MeCN, filtered through a sinter, and the resulting solution concentrated *in vacuo*. Petroleum ether was added and the resulting suspension was sonicated for 20 minutes. The title compound was collected by filtration as a white oil (96.8 mg, 0.096 mmol 33%).

HRMS (ESI+) Found: 354.2206 $[M]^{2+}$, $C_{47}H_{56}N_4O_2$, Required: 354.2216

^{1}H NMR (400 MHz, DMSO-d6, 25 °C):
δ = 8.93 (2H, br s, 2×Ar-**H**), 7.84 (2H, br d, J = 7.8 Hz, 2×Ar-**H**), 7.74 – 7.51 (12H, m, 12×Ar-**H**), 7.05 (4H, br d, J = 8.3 Hz, 4×Ar-**H**), 3.97 (4H, br t, J = 6.7 Hz, 2×NC**H**$_2$), 3.82 (6H, s, 2×C**H**$_3$), 3.75 (6H, s, 2×C**H**$_3$), 2.13 – 2.09 (4H, m, 2×C**H**$_2$), 1.60 – 1.46 (4H, m, 2×C**H**$_2$), 1.13 – 0.91 (8H, m, 4×C**H**$_2$), 0.67 – 0.48 (4H, m, 2×C**H**$_2$) ppm

^{13}C NMR (101 MHz, DMSO-d6, 25 °C):
δ = 158.9 (2×**C**), 151.0 (2×**C**), 139.1 (2×**C**), 138.7 (2×**C**), 136.3 (2×**C**H), 132.7 (2×**C**), 127.8 (4×**C**H), 123.5 (4×**C**H), 122.3 (2×**C**H), 122.1 (2×**C**H), 119.1 (2×**C**H), 114.4 (4×**C**H), 79.2 (2×**C**H$_3$), 55.2 (**C**), 48.7 (2×**C**H$_3$), 35.7 (2×**C**H$_2$), 30.7 (2×**C**H$_2$), 29.3 (2×**C**H$_2$), 28.8 (2×**C**H$_2$), 25.4 (2×**C**H$_2$), 23.6 (2×**C**H$_2$) ppm

FT-IR (ν_{max} cm^{-1}, film):
2932 (w), 2858 (w), 1466 (w), 1241 (vs), 1228 (vs), 1164 (s), 1025 (vs), 636 (vs)

6.3.23 3,3'-((2,7-*Bis*(3-methoxyphenyl)-9*H*-fluorene-9,9-diyl)*bis*(hexane-6,1-diyl))*bis*(1-octyl-1*H*-imidazol-3-ium) trifluoromethanesulfonate

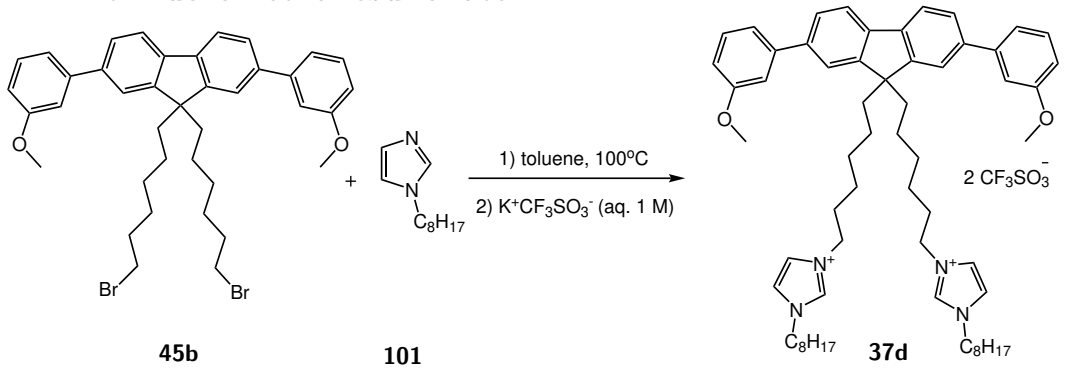

45b $C_{39}H_{44}Br_2O_2$ Mol Wt: 704.59

101 $C_{11}H_{20}N_2$ Mol Wt: 180.30

37d $C_{63}H_{84}F_6N_4O_8S_2$ Mol Wt: 905.37

Dibromide **45b** (753 mg, 1.07 mmol) and 1-octylimidazole (0.85 mL, 4.29 mmol) in toluene (10 mL) were heated at 100°C for 48 hours, then cooled to room temperature. The solvent was removed *in vacuo*, then MeOH (5 mL) and KOTf (aq., 1.0 M, 10 mL) were added. The solvent was removed *in vacuo*, the residue was washed onto a phase separator with H_2O (50 mL), then washed through with acetone (20 mL). The solvent was removed *in vacuo*, then petroleum ether (100 mL) was added. The suspension was sonicated for 30 minutes, then the title compound was collected by filtration as an orange gum (525 mg, 0.44 mmol, 41%).

HRMS (ESI+) Found: 452.3302 $[M]^{2+}$, $C_{61}H_{84}N_4O_2$, Required 452.3292

^{1}H NMR (400 MHz, acetone-d6, 25 °C):

δ = 9.06 (2H, app t, J = 1.5 Hz, 2×Ar-**H**), 7.91 (2H, dd, J = 7.9, 0.4 Hz, 2×Ar-**H**), 7.80 (2H, dd, J = 1.2, 0.4 Hz, 2×Ar-**H**), 7.73 – 7.67 (4H, m, 4×Ar-**H**), 7.63 (2H, t, J = 1.8 Hz, 2×Ar-**H**), 7.45 – 7.38 (2H, m, 2×Ar-**H**), 7.34 (2H, ddd, J = 7.7, 1.6, 1.0 Hz, 2×Ar-**H**), 7.30 – 7.27 (2H, m, 2×Ar-**H**), 6.96 (2H, ddd, J = 8.1, 2.6, 1.0 Hz, 2×Ar-**H**), 4.26 (4H, t, J = 7.3 Hz, 2×NC**H**$_2$), 4.19 (4H, t, J = 7.2 Hz, 2×NC**H**$_2$), 3.89 (6H, s, 2×OC**H**$_3$), 2.24 – 2.15 (4H, m, 2×C**H**$_2$), 1.87 (4H, quin, J = 7.2 Hz, 2×C**H**$_2$), 1.72 (4H, quin, J = 7.2 Hz, 2×C**H**$_2$), 1.29 – 1.10 (28H, m, 14×C**H**$_2$), 0.87 – 0.82 (6H, m, 2×C**H**$_3$), 0.75 – 0.65 (4H, m, 2×C**H**$_2$) ppm

^{13}C NMR (101 MHz, acetone-d6, 25 °C):

δ = 160.6 (2×**C**), 151.9 (2×**C**), 142.9 (2×**C**), 140.6 (2×**C**), 140.2 (2×**C**), 136.3 (2×**C**H), 130.3 (2×**C**H), 126.4 (2×**C**H), 122.9 (2×**C**H), 122.8 (2×**C**H), 121.7 (2×**C**H), 121.6 (q, J = 321.6 Hz, (2×**C**F$_3$), 120.6 (2×**C**H), 119.6 (2×**C**H), 113.0 (2×**C**H), 112.8 (2×**C**H), 55.6 (**C**), 55.1 (2×**C**H$_3$), 49.84 (2×**C**H$_2$), 49.75 (2×**C**H$_2$), 40.0 (2×**C**H$_2$), 31.8 (2×**C**H$_2$), 30.1 (2×**C**H$_2$), 30.1 (2×**C**H$_2$), 29.2 (2×**C**H$_2$), 29.0 (2×**C**H$_2$), 26.2 (2×**C**H$_2$), 25.9 (2×**C**H$_2$), 24.0 (2×**C**H$_2$), 22.7 (2×**C**H$_2$), 13.8 (2×**C**H$_3$) ppm

FT-IR (ν_{max} cm^{-1}, film):

2929 (w), 2857 (w), 1466 (w), 1245 (vs), 1161 (s), 1030 (vs), 638 (s)

UV-Vis (MeCN): λ_{max} = 328 (41500)

6.3.24 3,3'-((2-(*m*-Tolyl)-9*H*-fluorene-9,9-diyl)*bis*(hexane-6,1-diyl))*bis*(1-octyl-1*H*-imidazol-3-ium) trifluoromethanesulfonate

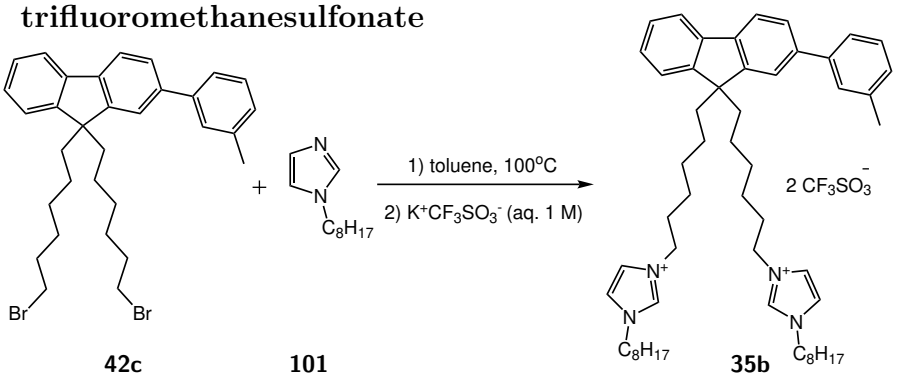

42c **101** **35b**

$C_{32}H_{38}Br_2$ Mol Wt: 582.46 | $C_{11}H_{20}N_2$ Mol Wt: 180.30 | $C_{56}H_{78}F_6N_4O_6S_2$ Mol Wt: 1081.37

Dibromide **42c** (209 mg, 0.36 mmol) and 1-octylimidazole (0.16 mL, 0.81 mmol) in toluene (10.0 mL) were heated at 100 °C for 17 hours, then cooled to room temperature. The solvent was removed *in vacuo*, then MeCN (10 mL) and KOTf (aq., 1.0 M, 5.0 mL) were added. The solvent was removed *in vacuo* and the resulting solids were washed onto a frit with H_2O, then washed through with acetone (30 mL), and the solvent was removed *in vacuo*. The solid thus collected was dissolved in MeCN (10 mL), and filtered through a 0.2 μm filter cartridge, which removed all visible precipitate. After removal of the solvent *in vacuo*, continuous extraction in ethyl acetate/H_2O yielded a yellow gum. Petroleum ether was added and the suspension was sonicated for 10 minutes. The title compound was collected by filtration as a white gum (97 mg, 0.090 mmol 25%).

HRMS (ESI+) Found: 391.3108 $[M]^{2+}$, $C_{54}H_{78}N_4$, Required: 391.3108

^{1}H NMR (400 MHz, acetone-d6, 25 °C):

δ = 9.09 (2H, app. t, J = 1.5 Hz, 2×Ar-**H**), 7.87 (1H, d, J = 7.9 Hz, Ar-**H**), 7.84 – 7.80 (1H, m, Ar-**H**), 7.78 – 7.74 (1H, m, Ar-**H**), 7.74 – 7.63 (5H, m, 5×Ar-**H**), 7.60 – 7.51 (2H, m, 2×Ar-**H**), 7.49 – 7.45 (1H, m, Ar-**H**), 7.41 – 7.31 (3H, m, 3×Ar-**H**), 7.22 – 7.17 (1H, m, Ar-**H**), 4.30 (4H, t, J = 7.3 Hz, 2×C**H**$_2$), 4.22 (4H, t, J = 7.2 Hz, 2×C**H**$_2$), 2.42 (3H, s, C**H**$_3$), 2.15 (4H, br s, 2×C**H**$_2$), 1.97 – 1.84 (4H, m, 2×C**H**$_2$), 1.82 – 1.67 (4H, m, 2×C**H**$_2$), 1.33 – 1.21 (20H, m, 10×C**H**$_2$), 1.16 – 1.05 (8H, m, 4×C**H**$_2$), 0.91 – 0.81 (6H, m, 2×C**H**$_3$), 0.73 – 0.55 (4H, m, 2×C**H**$_2$) ppm

^{13}C NMR (101 MHz, acetone-d6, 25 °C):

δ = 151.5 (**C**), 151.0 (**C**), 141.5 (**C**), 141.2 (**C**), 140.8 (**C**), 140.4 (**C**), 138.7 (**C**), 136.3 (2×**C**H), 129.2 (**C**H), 128.3 (**C**H), 127.9 (**C**H), 127.6 (**C**H), 127.3 (**C**H), 126.2 (**C**H), 124.4 (**C**H), 123.3 (**C**H), 123.0 (2×**C**H), 122.9 (2×**C**H), 121.6 (**C**H), 120.4 (**C**H), 120.1 (**C**H), 55.4 (**C**), 49.9 (2×**C**H$_2$), 49.8 (2×**C**H$_2$), 40.1 (2×**C**H$_2$), 31.9 (4×**C**H$_2$), 30.2 (2×**C**H$_2$), 30.1 (2×**C**H$_2$), 26.2 (4×**C**H$_2$), 25.9 (2×**C**H$_2$), 23.9 (2×**C**H$_2$), 22.7 (4×**C**H$_2$), 21.1 (**C**H$_3$), 13.8 (2×**C**H$_3$) ppm

FT-IR (ν_{max} cm^{-1}, film):

2928 (m), 2857 (w), 1252 (s), 1155 (s), 1029 (vs), 743 (m), 636 (vs)

UV-Vis (MeCN): λ_{max} = 291 (19300)

6.3.25 3,3'-((2-Phenyl-9*H*-fluorene-9,9-diyl)*bis*(hexane-6,1-diyl))*bis*(1-methyl-1*H*-imidazol-3-ium) trifluoromethanesulfonate

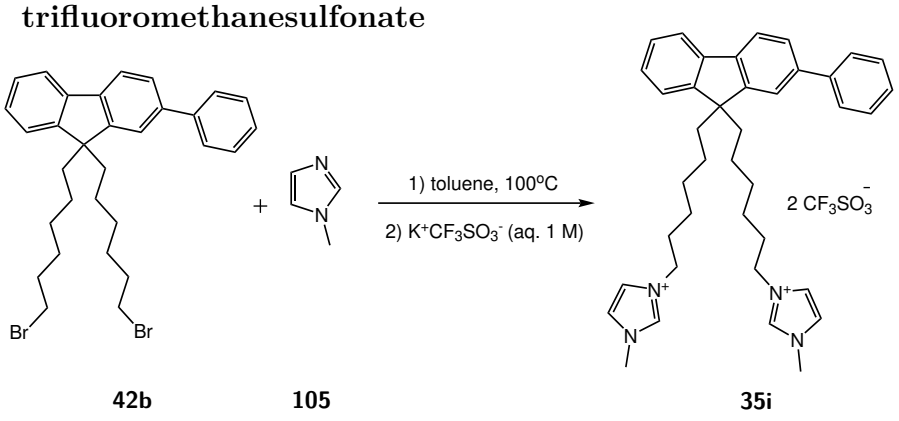

42b **105** **35i**

$C_{31}H_{36}Br_2$ Mol Wt: 568.44 | $C_4H_6N_2$ Mol Wt: 82.12 | $C_{41}H_{48}F_6N_4O_6S_2$ Mol Wt: 870.97

Dibromide **42b** (1.17 g, 2.05 mmol) and 1-methylimidazole (0.65 mL, 8.20 mmol) in toluene (20.0 mL) were heated at 100 °C for 2 days, then cooled to room temperature. The solvent was removed *in vacuo* and the mixture was dissolved in methanol. KOTf (aq., 1 M, 20 mL, 20 mmol) was added, and the solvent removed *in vacuo*. The solids were purified by washing with copious diethyl ether (100 mL), which was then decanted away, followed by sonication in copious water (100 mL) which was then decanted away. The resulting gum was dissolved in acetone (10 mL), transferred to a vial, and the solvent removed *in vacuo*, affording the title compound as a white gum (1.13 g, 1.30 mmol, 63%).

HRMS (ESI+) Found: 286.1932 $[M]^{2+}$, $C_{39}H_{48}N_4$, Required: 286.1934

^{1}H NMR (400 MHz, acetone-d6, 25 °C):

δ = 8.98 (2H, s, 2×Ar-**H**), 7.88 (1H, dd, J = 7.9, 0.6 Hz, Ar-**H**), 7.84-7.81 (1H, m, Ar-**H**), 7.78-7.73 (3H, m, 3×Ar-**H**), 7.67 (1H, dd, J = 7.9, 1.7 Hz, Ar-**H**), 7.63 (4H, d, J = 1.7 Hz, 4×Ar-**H**), 7.51-7.45 (3H, m, 3×Ar-**H**), 7.39-7.33 (3H, m, 3×Ar-**H**), 4.20 (4H, t, J = 7.2 Hz, 2×C**H**$_2$), 3.97 (6H, d, J = 0.5 Hz, 2×C**H**$_3$), 2.20-2.07 (4H, m, 2×C**H**$_2$), 1.71 (4H, quin, J = 7.2 Hz, 2×C**H**$_2$), 1.18-1.05 (8H, m, 4×C**H**$_2$), 0.71-0.56 (4H, m, 2×C**H**$_2$) ppm

^{13}C NMR (101 MHz, acetone-d6, 25 °C):

δ = 151.6 (**C**), 151.0 (**C**), 141.5 (**C**), 141.1 (**C**), 140.9 (**C**), 140.3 (**C**), 137.0 (2×**C**H), 129.2 (2×**C**H), 127.63 (**C**H), 127.57 (**C**H), 127.4 (**C**H), 127.2 (2×**C**H), 126.2 (**C**H), 124.2 (2×**C**H), 123.3 (**C**H), 122.7 (2×**C**H), 121.62 (**C**H), 121.58 (q, J = 321.3 Hz, 2×**C**F$_3$SO$_3$), 120.5 (**C**H), 120.2 (**C**H), 55.4 (**C**), 49.8 (2×**C**H$_2$), 40.1 (2×**C**H$_2$), 36.0 (2×**C**H$_2$), 30.1 (2×**C**H$_2$), 30.1 (2×**C**H$_2$), 25.9 (2×**C**H$_2$), 23.9 (2×**C**H$_3$) ppm

FT-IR (ν_{max} cm^{-1}, film):

3524 (w), 2934 (vw), 1635 (w), 1249 (vs), 1162 (s), 1031 (vs), 763 (m), 639 (s), 577 (m)

UV-Vis (MeCN): λ_{max} = 313 (21000)

6.3.26 3,3'-((2,7-Diphenyl-9*H*-fluorene-9,9-diyl)*bis*(hexane-6,1-diyl))*bis*(1-methyl-1*H*-imidazol-3-ium) trifluoromethanesulfonate

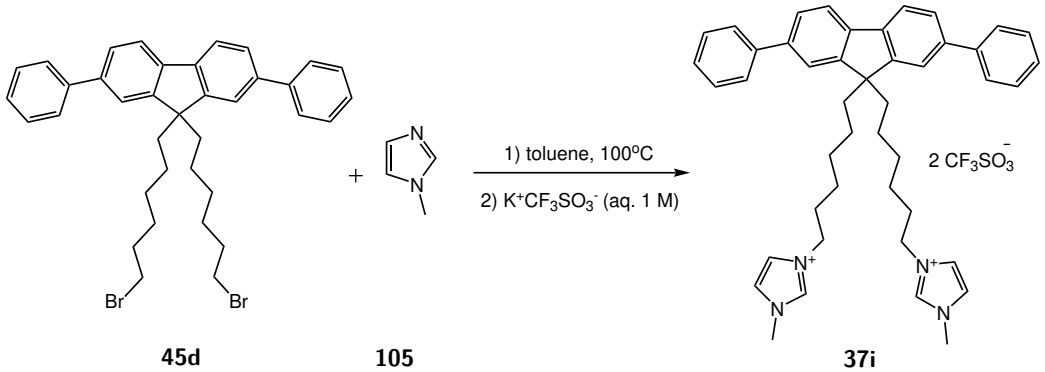

45d $C_{37}H_{40}Br_2$ Mol Wt: 644.54

105 $C_4H_6N_2$ Mol Wt: 82.12

37i $C_{47}H_{52}F_6N_4O_6S_2$ Mol Wt: 947.07

Dibromide **45d** (481 mg, 0.75 mmol), and 1-methylimidazole (0.24 mL, 2.98), in toluene (20 mL) were heated at 100 °C for 3.5 days then cooled to room temperature. The solvent was decanted away from the resulting gum, which was washed with toluene (3×20 mL). The gum was then dissolved in the minimum of methanol and KOTf (aq., 1 M, 20 mL, 20 mmol) was added resulting in the immediate formation of a white precipitate. The solvent was removed *in vacuo*, and the resulting solids were sonicated in water (20 mL) which was decanted away, followed by washing with water (2×20 mL). The resulting gum was dissolved in acetone (10 mL) which was removed*in vacuo*, affording the title compound as an off-white gum (341 mg, 0.37 mmol, 50%).

HRMS (ESI+) Found: 324.2093 $[M]^{2+}$, $C_{45}H_{52}N_4$, Required: 324.2091

^{1}H NMR (400 MHz, acetone-d6, 25 °C):

δ = 8.96 (2H, s, 2×Ar-**H**), 7.92 (2H, dd, J = 7.9, 0.5 Hz, 2×Ar-**H**), 7.80 (2H, dd, J = 1.7, 0.6 Hz, 2×Ar-**H**), 7.79-7.75 (4H, m, 4×Ar-**H**), 7.70 (2H, dd, J = 7.9, 1.7 Hz, 2×Ar-**H**), 7.59 (4H, d, J = 1.6 Hz, 4×Ar-**H**), 7.53-7.47 (4H, m, 4×Ar-**H**), 7.41-7.35 (2H, m, 2×Ar-**H**), 4.19 (4H, t, J = 7.2 Hz, 2×C**H**$_2$), 3.95 (6H, s, 2×C**H**$_3$), 2.25-2.15 (4H, m, 2×C**H**$_2$), 1.71 (4H, quin, J = 7.3 Hz, 2×C**H**$_2$), 1.20-1.05 (8H, m, 4×C**H**$_2$), 0.76-0.64 (4H, m, 2×C**H**$_2$) ppm

^{13}C NMR (101 MHz, acetone-d6, 25 °C):

δ = 151.9 (2×**C**), 141.5 (2×**C**), 140.6 (2×**C**), 140.3 (2×**C**), 137.0 (2×**C**H), 129.3 (4×**C**H), 127.6 (2×**C**H), 127.3 (4×**C**H), 126.3 (2×**C**H), 124.1 (2×**C**H), 122.7 (2×**C**H), 121.71 (2C, q, J = 321.3 Hz, 2×**C**F_3SO_3), 121.66 (2×**C**H), 120.6 (2×**C**H), 55.6 (**C**), 49.8 (2×**C**H_2), 40.1 (2×**C**H_2), 36.0 (2×**C**H_3), 30.1 (2×**C**H_2), 29.4 (2×**C**H_2), 25.9 (2×**C**H_2), 24.0 (2×**C**H_2) ppm

FT-IR (ν_{max} cm^{-1}, film):

3523 (vw), 3114 (vw), 2931 (w), 2858 (w), 1569 (w), 1465 (m), 1252 (vs), 1159 (s), 1030 (vs), 759 (s), 638 (vs), 574 (m)

UV-Vis (MeCN): λ_{max} = 327 (35400)

6.3.27 3,3'-((2,7-*Bis*(3-methoxyphenyl)-9*H*-fluorene-9,9-diyl)*bis*(hexane-6,1-diyl))*bis*(1-methyl-1*H*-imidazol-3-ium) trifluoromethanesulfonate

Synthesised following the procedure detailed in 6.3.22, with the following reagent amounts:
Dibromide **45b**: 170 mg, 0.24 mmol
1-methylimidazole: 0.04 mL, 0.5 mmol
toluene: 4.0 mL
KOTf (aq., 1.0 M): 5.0 mL, 5.0 mmol
Reaction time: 24 h
Yield: 140 mg, 0.14 mmol, 58% (white gum)

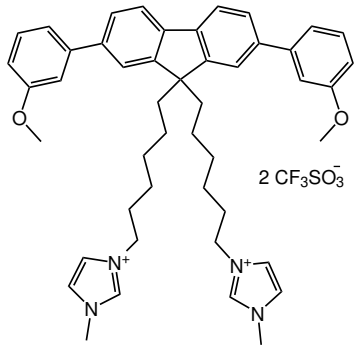

37c
$C_{49}H_{56}F_6N_4O_8S_2$
Mol Wt: 1007.12

HRMS (ESI+) 354.2203 $[M]^{2+}$,
$C_{47}H_{56}N_4O_2$, Required: 354.2196

^{1}H NMR (400 MHz, acetone-d6, 25 °C):
δ = 8.95 (2H, s, 2×Ar-**H**), 7.91 (2H, dd, J = 7.9, 0.5 Hz, 2×Ar-**H**), 7.79 (2H, dd, J = 1.6, 0.5 Hz, 2×Ar-**H**), 7.70 (2H, dd, J = 7.8, 1.7 Hz, 2×Ar-**H**), 7.60 (4H, d, J = 1.7 Hz, 4×Ar-**H**), 7.45 – 7.38 (2H, m, 2×Ar-**H**), 7.33 (2H, ddd, J = 7.7, 1.7, 1.0 Hz, 2×Ar-**H**), 7.29 – 7.26 (2H, m, 2×Ar-**H**), 6.97 (2H, ddd, J = 8.1, 2.6, 1.0 Hz, 2×Ar-**H**), 4.19 (4H, t, J = 7.3 Hz, 2×NC**H**$_2$), 3.96 (6H, s, 2×C**H**$_3$), 3.89 (6H, s, 2×C**H**$_3$), 2.23 – 2.16 (4H, m, 2×C**H**$_2$), 1.71 (4H, quin, J = 7.3 Hz, 2×C**H**$_2$), 1.17 – 1.07 (8H, m, 4×C**H**$_2$), 0.76 – 0.63 (4H, m, 2×C**H**$_2$) ppm

^{13}C NMR (101 MHz, acetone-d6, 25 °C):
δ = 161.5 (2×**C**), 152.7 (2×**C**), 143.8 (2×**C**), 141.5 (2×**C**), 141.0 (2×**C**), 137.8 (2×**C**H), 131.1 (2×**C**H), 127.2 (2×**C**H), 124.9 (2×**C**H), 123.5 (2×**C**H), 122.6 (2×**C**H), 121.4 (2×**C**H), 120.5 (2×**C**H), 113.9 (2×**C**H), 113.6 (2×**C**H), 56.4 (2×**C**H$_3$), 56.0 (**C**), 50.6 (2×**C**H$_2$), 40.9 (2×**C**H$_2$), 36.8 (2×**C**H$_3$), 30.9 (2×**C**H$_2$), 26.7 (2×**C**H$_2$), 24.82 (2×**C**H$_2$), 24.78 (2×**C**H$_2$) ppm

FT-IR (ν^{max} cm^{-1}, film):
2979 (w), 2932 (w), 1245 (vs), 1229 (vs), 1165 (s), 1030 (vs), 637 (vs)

UV-Vis (MeCN): λ_{max} = 328 (26200)

6.3.28 3,3'-((2-(*m*-Tolyl)-9*H*-fluorene-9,9-diyl)*bis*(hexane-6,1-diyl))*bis*(1-methyl-1*H*-imidazol-3-ium) trifluoromethanesulfonate

Synthesised following the procedure detailed in 6.3.22, with the following reagent amounts:
Dibromide **42c**: 356 mg, 0.64 mmol
1-methylimidazole: 0.11 mL, 1.4 mmol
toluene: 10.0 mL
KOTf (aq., 1.0 M): 10.0 mL, 10.0 mmol
Reaction time: 17 h
Yield: 366 mg, 0.41 mmol, 65% (off-white gum)

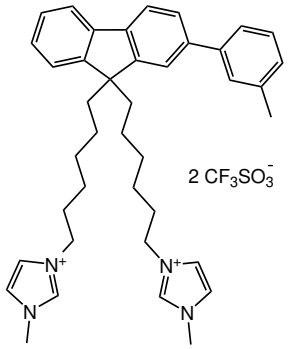

35a
$C_{42}H_{50}F_6N_4O_6S_2$
Mol Wt: 884.99

HRMS (APPI) Found: 293.2010 $[M]^{2+}$, $C_{40}H_{50}N_4$, Required: 293.2012

^{1}H NMR (400 MHz, acetone-d6, 25 °C):
δ = 8.98 (2H, s, 2×Ar-**H**), 7.87 (1H, dd, J = 7.9, 0.5 Hz, Ar-**H**), 7.84 – 7.81 (1H, m, Ar-**H**), 7.76 (1H, dd, J = 1.7, 0.6 Hz, Ar-**H**), 7.66 (1H, dd, J = 7.9, 1.7 Hz, Ar-**H**), 7.64 – 7.62 (4H, m, 4×Ar-**H**), 7.59 – 7.56 (1H, m, Ar-**H**), 7.56 – 7.51 (1H, m, Ar-**H**), 7.48 – 7.45 (1H, m, Ar-**H**), 7.40 – 7.31 (3H, m, 3×Ar-**H**), 7.22 – 7.17 (1H, m, Ar-**H**), 4.20 (4H, t, J = 7.2 Hz, 2×C**H**$_2$), 3.97 (6H, s, 2×C**H**$_3$), 2.41 (3H, s, C**H**$_3$), 2.19 – 2.09 (4H, m, 2×C**H**$_2$), 1.71 (4H, quin, J = 7.2 Hz, 2×C**H**$_2$), 1.18 – 1.04 (8H, m, 4×C**H**$_2$), 0.71 – 0.54 (4H, m, 2×C**H**$_2$) ppm

^{13}C NMR (101 MHz, acetone-d6, 25 °C):
δ = 151.5 (**C**), 151.0 (**C**), 141.5 (**C**), 141.2 (**C**), 140.8 (**C**), 140.4 (**C**), 138.7 (**C**), 137.0 (2×**C**H), 129.1 (**C**H), 128.3 (**C**H), 127.9 (**C**H), 127.6 (**C**H), 127.3 (**C**H), 126.2 (**C**H), 124.4 (**C**H), 124.1 (2×**C**H), 123.3 (**C**H), 122.7 (2×**C**H), 121.6 (**C**H), 120.4 (**C**H), 120.1 (**C**H), 55.4 (**C**), 49.7 (2×**C**H$_3$), 40.1 (2×**C**H$_2$), 36.0 (2×**C**H$_2$), 30.1 (2×**C**H$_2$), 30.1 (2×**C**H$_2$), 25.9 (2×**C**H$_2$), 23.9 (2×**C**H$_2$), 21.0 (**C**H$_3$) ppm

FT-IR ($\nu_{\max}$ cm^{-1}, film):
3110 (w), 2929 (w), 2857 (w), 1465 (m), 1253 (vs), 1155 (s), 1029 (vs), 757 (m), 636 (vs)

UV-Vis (MeCN): λ_{max} = 292 (20200)

6.3.29 3,3'-((2,7-*Bis*(4-methoxyphenyl)-9*H*-fluorene-9,9-diyl)*bis*(hexane-6,1-diyl))*bis*(1-octyl-1*H*-imidazol-3-ium) trifluoromethanesulfonate

Synthesised following the procedure detailed in 6.3.23, with the following reagent amounts:
Dibromide **46b**: 206 mg, 0.29 mmol
1-octylimidazole: 124 mg, 0.68 mmol
toluene: 3.0 mL
KOTf (aq., 1.0 M): 5.0 mL, 5.0 mmol
Reaction time: 20 h
Yield: 390 mg, 0.32 mmol, 58% (white oil)

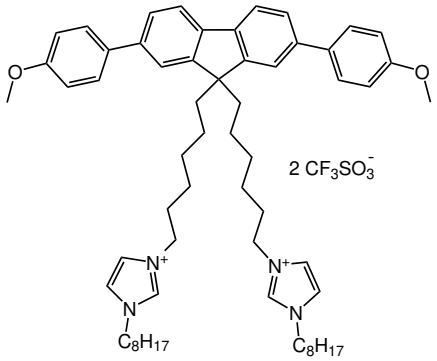

38d
$C_{63}H_{84}F_6N_4O_8S_2$
Mol Wt: 1203.50

HRMS (ESI+) Found: 452.3306 $[M]^{2+}$, $C_{61}H_{84}N_4O_2$, Required: 452.3292

^{1}H NMR (400 MHz, DMSO-d6, 25 °C):
δ = 9.07 (2H, t, J = 1.4 Hz, 2×Ar-**H**), 7.85 (2H, dd, J = 7.9, 0.2 Hz, 2×Ar-**H**), 7.76 – 7.67 (8H, m, 8×Ar-**H**), 7.66 – 7.61 (4H, m, 4×Ar-**H**), 7.09 – 7.02 (4H, m, 4×Ar-**H**), 4.26 (4H, t, J = 7.3 Hz, 2×C**H**$_2$), 4.20 (4H, t, J = 7.2 Hz, 2×C**H**$_2$), 3.86 (6H, s, 2×C**H**$_3$), 2.21 – 2.12 (4H, m, 2×C**H**$_2$), 1.93 – 1.81 (4H, m, 2×C**H**$_2$), 1.72 (4H, quin, J = 7.2 Hz, 2×C**H**$_2$), 1.30 – 1.09 (28H, m, 14×C**H**$_2$), 0.88 – 0.81 (6H, m, 2×C**H**$_3$), 0.76 – 0.63 (4H, m, 2×C**H**$_2$) ppm

^{13}C NMR (101 MHz, DMSO-d6, 25 °C):
δ = 159.8 (2×**C**), 151.8 (2×**C**), 140.0 (2×**C**), 139.8 (2×**C**), 136.3 (2×**C**H), 133.9 (2×**C**), 128.3 (4×**C**H), 125.7 (2×**C**H), 122.90 (2×**C**H), 122.85 (2×**C**H), 121.1 (2×**C**H), 120.4 (2×**C**H), 114.7 (4×**C**H), 55.5 (**C**), 55.2 (2×**C**H$_3$), 49.9 (2×**C**H$_2$), 49.8 (2×**C**H$_2$), 40.1 (2×**C**H$_2$), 31.9 (4×**C**H$_2$), 30.1 (2×**C**H$_2$), 30.0 (2×**C**H$_2$), 26.2 (4×**C**H$_2$), 25.9 (2×**C**H$_2$), 24.0 (2×**C**H$_2$), 22.7 (4×**C**H$_2$), 13.8 (2×**C**H$_3$) ppm

FT-IR (ν_{max} cm^{-1}, film):
2930 (w), 2858 (w), 1517 (w), 1466 (w), 1243 (vs), 1161 (s), 1026 (vs), 636 (vs)

UV-Vis (MeCN): λ_{max} = 334 (46500)

6.3.30 3,3'-((2,7-Di-*m*-tolyl-9*H*-fluorene-9,9-diyl)*bis*(hexane-6,1-diyl))*bis*(1-methyl-1*H*-imidazol-3-ium) trifluoromethanesulfonate

Synthesised following the procedure detailed in 6.3.23, with the following reagent amounts:
Dibromide **45a**: 115 mg, 0.17 mmol
1-methylimidazole: 0.03 mL, 04 mmol
toluene: 2.5 mL
KOTf (aq., 1.0 M): 5.0 mL
Reaction time: 18 h
Yield: 87 mg, 0.089 mmol, 52% (white gum)

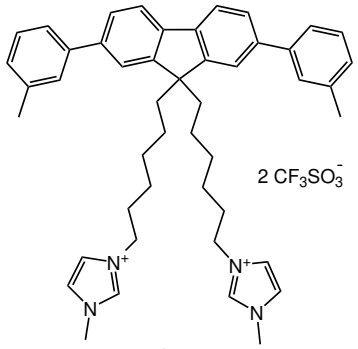

37a
$C_{49}H_{56}F_6N_4O_6S_2$
Mol Wt: 975.12

HRMS (ESI+) Found: 338.2254 $[M]^{2+}$, $C_{47}H_{56}N_4$, Required: 338.2247

^{1}H NMR (400 MHz, acetone-d6, 25 °C):
δ = 8.96 (2H, s, Ar-**H**), 7.91 (2H, dd, J = 7.9, 0.4 Hz, 2×Ar-**H**), 7.81 – 7.77 (2H, m, 2×Ar-**H**), 7.69 (2H, dd, J = 7.8, 1.7 Hz, 2×Ar-**H**), 7.64 – 7.57 (6H, m, 6×Ar-**H**), 7.55 (2H, dd, J = 7.7, 0.6 Hz, 2×Ar-**H**), 7.38 (2H, t, J = 7.6 Hz, 2×Ar-**H**), 7.23 – 7.17 (2H, m, 2×Ar-**H**), 4.19 (4H, t, J = 7.3 Hz, 2×C**H**$_2$), 3.99 – 3.94 (6H, m, 2×C**H**$_3$), 2.42 (6H, s, 2×C**H**$_3$), 2.24 – 2.15 (4H, m, 2×C**H**$_2$), 1.71 (4H, quin, J = 7.3 Hz, 2×C**H**$_2$), 1.18 – 1.06 (8H, m, 4×C**H**$_2$), 0.74 – 0.63 (4H, m, 2×C**H**$_2$) ppm

^{13}C NMR (101 MHz, acetone-d6, 25 °C):
δ = 151.9 (2×**C**), 141.5 (2×**C**), 140.5 (2×**C**), 140.4 (2×**C**), 138.7 (2×**C**), 137.0 (2×**C**H), 129.2 (2×**C**H), 128.3 (2×**C**H), 127.9 (2×**C**H), 126.3 (2×**C**H), 124.4 (2×**C**H), 124.1 (2×**C**H), 122.7 (2×**C**H), 121.6 (2×**C**H), 120.5 (2×**C**H), 55.6 (**C**), 49.8 (2×**C**H$_2$), 40.1 (2×**C**H$_2$), 36.0 (2×**C**H$_3$), 30.1 (2×**C**H$_2$), 29.4 (2×**C**H$_2$), 25.9 (2×**C**H$_2$), 24.0 (2×**C**H$_2$), 21.0 (2×**C**H$_3$) ppm

FT-IR (ν_{max} cm^{-1}, film):
2929 (w), 2857 (w), 2348 (w), 1465 (m), 1255 (vs), 1158 (s), 1030 (vs), 783 (s), 638 (vs)

UV-Vis (MeCN): λ_{max} = 326 (36000)

6.3.31 3,3'-((2,7-Di-*m*-tolyl-9*H*-fluorene-9,9-diyl)*bis*(hexane-6,1-diyl))*bis*(1-octyl-1*H*-imidazol-3-ium) trifluoromethanesulfonate

Synthesised following the procedure detailed in 6.3.23, with the following reagent amounts:
Dibromide **45a**: 89 mg, 0.13 mmol
1-octylimidazole: 100 mg, 0.55 mmol
toluene: 2.5 mL
KOTf (aq., 1.0 M): 5.0 mL, 5.0 mmol
Reaction time: 18 h
Yield: 281 mg, 0.24 mmol, 70% (orange gum)

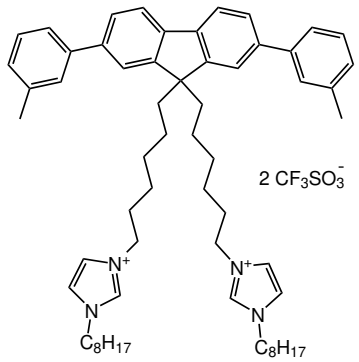

37b
$C_{63}H_{84}F_6N_4O_6S_2$
Mol Wt: 1171.50

HRMS (ESI+) Found: 436.3353 $[M]^{2+}$, $C_{61}H_{84}N_4$, Required: 436.3343

^{1}H NMR (400 MHz, acetone-d6, 25 °C):
δ = 9.11 – 9.01 (2H, m, 2×Ar-**H**), 7.90 (2H, d, J = 7.8 Hz, 2×Ar-**H**), 7.79 (2H, d, J = 1.2 Hz, 2×Ar-**H**), 7.72 – 7.52 (10H, m, 10×Ar-**H**), 7.41 – 7.34 (2H, m, 2×Ar-**H**), 7.23 – 7.16 (2H, m, 2×Ar-**H**), 4.26 (4H, t, J = 7.3 Hz, 2×C**H**$_2$), 4.20 (4H, t, J = 7.2 Hz, 2×C**H**$_2$), 2.42 (6H, s, 2×C**H**$_3$), 2.24 – 2.15 (4H, m, 2×C**H**$_2$), 1.93 – 1.83 (4H, m, 2×C**H**$_2$), 1.77 – 1.67 (4H, m, 2×C**H**$_2$), 1.29 – 1.09 (28H, m, 14×C**H**$_2$), 0.87 – 0.82 (6H, m, 2×C**H**$_3$), 0.75 – 0.64 (4H, m, 2×C**H**$_2$) ppm

^{13}C NMR (101 MHz, acetone-d6, 25 °C):
δ = 151.8 (2×**C**), 141.5 (2×**C**), 140.5 (2×**C**), 140.4 (2×**C**), 138.7 (2×**C**), 136.3 (2×**C**H), 129.2 (2×**C**H), 128.3 (2×**C**H), 127.9 (2×**C**H), 126.2 (2×**C**H), 124.4 (2×**C**H), 122.9 (2×**C**H), 122.8 (2×**C**H), 121.6 (2×**C**H), 120.5 (2×**C**H), 55.6 (**C**), 49.9 (2×**C**H$_2$), 49.8 (2×**C**H$_2$), 40.1 (2×**C**H$_2$), 31.8 (4×**C**H$_2$), 30.1 (2×**C**H$_2$), 30.0 (2×**C**H$_2$), 30.1 (2×**C**H$_2$), 26.2 (2×**C**H$_2$), 25.9 (2×**C**H$_2$), 24.0 (2×**C**H$_2$), 22.7 (4×**C**H$_2$), 21.1 (2×**C**H$_3$), 13.8 (2×**C**H$_3$) ppm

FT-IR (ν_{max} cm^{-1}, film):
2928 (w), 2857 (w), 2359 (w), 1246 (vs), 1159 (s), 1029 (vs), 637 (vs)

UV-Vis (MeCN): λ_{max} = 326 (33200)

6.3.32 3,3'-((2,7-Di-*p*-tolyl-9*H*-fluorene-9,9-diyl)*bis*(hexane-6,1-diyl))*bis*(1-methyl-1*H*-imidazol-3-ium) trifluoromethanesulfonate

Synthesised following the procedure detailed in 6.3.23, with the following reagent amounts:
Dibromide **46a**: 450 mg, 0.67 mmol
1-octylimidazole: 0.30 mL, 3.8 mmol
toluene: 10.0 mL
KOTf (aq., 1.0 M): 10 mL, 10 mmol
Reaction time: 3 days
Yield: 592 mg, 0.61 mmol, 91% (off-white solid)

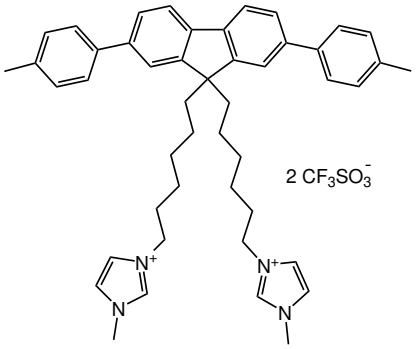

38a
$C_{49}H_{56}F_6N_4O_6S_2$
Mol Wt: 975.12

MP 68.8 - 70.1 °C

HRMS (ESI+) Found: 338.2254 $[M]^{2+}$, $C_{47}H_{56}N_4$, Required: 338.2247

^{1}H NMR (400 MHz, acetone-d6, 25 °C):
δ = 8.96 (2H, s, 2×Ar-**H**), 7.88 (2H, d, J = 7.8 Hz, 2×Ar-**H**), 7.79 – 7.74 (2H, m, 2×Ar-**H**), 7.71 – 7.62 (6H, m, 6×Ar-**H**), 7.61 – 7.57 (4H, m, 4×Ar-**H**), 7.31 (4H, dd, J = 8.4, 0.6 Hz, 2×Ar-**H**), 4.18 (4H, t, J = 7.2 Hz, 2×C**H**$_2$), 3.95 (6H, s, 2×C**H**$_3$), 2.38 (6H, s, 2×C**H**$_3$), 2.24 – 2.14 (4H, m, 2×C**H**$_2$), 1.70 (4H, quin, J = 7.3 Hz, 2×C**H**$_2$), 1.21 – 1.04 (8H, m, 4×C**H**$_2$), 0.77 – 0.62 (4H, m, 2×C**H**$_2$) ppm

^{13}C NMR (101 MHz, acetone-d6, 25 °C):
δ = 151.8 (2×**C**), 140.3 (2×**C**), 140.2 (2×**C**), 138.6 (2×**C**), 137.2 (2×**C**), 137.0 (2×**C**H), 129.9 (4×**C**H), 127.1 (4×**C**H), 126.0 (2×**C**H), 124.1 (2×**C**H), 122.7 (2×**C**H), 121.4 (2×**C**H), 120.5 (2×**C**H), 55.6 (**C**), 49.7 (2×**C**H$_2$), 40.1 (2×**C**H$_2$), 36.0 (2×**C**H$_3$), 30.1 (2×**C**H$_2$), 29.4 (2×**C**H$_2$), 25.9 (2×**C**H$_2$), 24.0 (2×**C**H$_2$), 20.6 (2×**C**H$_3$) ppm

FT-IR (ν_{max} cm^{-1}, solid):
3112 (w), 2929 (w), 2857 (w), 1466 (m), 1253 (vs), 1156 (s), 1029 (vs), 809 (s), 756 (m), 636 (vs)

UV-Vis (MeCN): λ_{max} = 330 (37700)

6.3.33 3,3'-((2,7-Di-*p*-tolyl-9*H*-fluorene-9,9-diyl)*bis*(hexane-6,1-diyl))*bis*(1-octyl-1*H*-imidazol-3-ium) trifluoromethanesulfonate

Synthesised following the procedure detailed in 6.3.23, with the following reagent amounts:
Dibromide **46a**: 366 mg, 0.54 mmol
1-octylimidazole: 0.60 mL, 3.0 mmol
toluene: 10 mL
KOTf (aq., 1.0 M): 10 mL, 10 mmol
Reaction time: 3 days
Yield: 523 mg, 0.43 mmol, 83% (white gum)

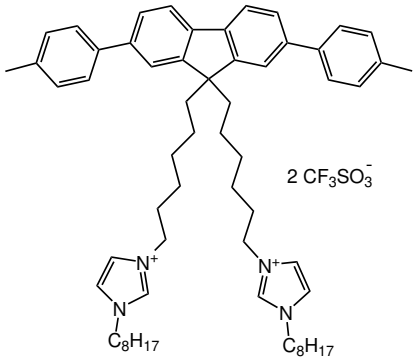

38b
$C_{63}H_{84}F_6N_4O_6S_2$
Mol Wt: 1171.50

HRMS (ESI+) Found: 436.3346 $[M]^{2+}$, $C_{61}H_{84}N_4$, Required: 436.3343

^{1}H NMR (400 MHz, acetone-d6, 25 °C):
δ = 9.06 (2H, s, 2×Ar-**H**), 7.88 (2H, d, J = 7.9 Hz, 2×Ar-**H**), 7.79 – 7.75 (2H, m, 2×Ar-**H**), 7.71 – 7.64 (8H, m, 8×Ar-**H**), 7.62 (2H, t, J = 1.8 Hz, 2×Ar-**H**), 7.35 – 7.26 (4H, m, 4×Ar-**H**), 4.26 (4H, t, J = 7.3 Hz, 2×C**H**$_2$), 4.20 (4H, t, J = 7.2 Hz, 2×C**H**$_2$), 2.39 (6H, s, 2×C**H**$_3$), 2.23 – 2.14 (4H, m, 2×C**H**$_2$), 1.87 (4H, quin, J = 7.2 Hz, 2×C**H**$_2$), 1.72 (4H, quin, J = 7.2 Hz, 2×C**H**$_2$), 1.30 – 1.22 (20H, m, 10×C**H**$_2$), 1.17 – 1.07 (8H, m, 4×C**H**$_2$), 0.87 – 0.82 (6H, m, 2×C**H**$_3$), 0.75 – 0.64 (4H, m, 2×C**H**$_2$) ppm

^{13}C NMR (101 MHz, acetone-d6, 25 °C):
δ = 151.8 (2×**C**), 140.3 (2×**C**), 140.2 (2×**C**), 138.6 (2×**C**), 137.2 (2×**C**), 136.3 (2×**C**H), 129.9 (4×**C**H), 127.1 (4×**C**H), 126.0 (2×**C**H), 122.91 (2×**C**H), 122.85 (2×**C**H), 121.4 (2×**C**H), 120.5 (2×**C**H), 55.6 (**C**), 49.9 (2×**C**H$_2$), 49.8 (2×**C**H$_2$), 40.1 (2×**C**H$_2$), 31.9 (4×**C**H$_2$), 30.1 (2×**C**H$_2$), 30.1 (2×**C**H$_2$), 26.2 (4×**C**H$_2$), 25.9 (2×**C**H$_2$), 24.0 (2×**C**H$_2$), 22.7 (4×**C**H$_2$), 20.6 (2×**C**H$_3$), 13.8 (2×**C**H$_3$) ppm

FT-IR (ν_{max} cm^{-1}, film):
3141 (vw), 2926 (m), 2856 (w), 1466 (m), 1254 (s), 1156 (s), 1029 (vs), 810 (s), 637 (vs)

UV-Vis (MeCN): λ_{max} = 329 (35100)

6.3.34 3,3'-((2,7-Di([1,1'-biphenyl]-3-yl)-9*H*-fluorene-9,9-diyl)*bis*(hexane-6,1-diyl))*bis*(1-methyl-1*H*-imidazol-3-ium) trifluoromethanesulfonate

Synthesised following the procedure detailed in 6.3.23, with the following reagent amounts:
Dibromide **45c**: 360 g, 0.45 mmol
1-methylimidazole: 0.10 mL, 1.3 mmol
toluene: 10.0 mL
KOTf (aq., 1.0 M): 5.0 mL, 5.0 mmol
Reaction time: 17 h
Yield: 162 mg, 0.15 mmol, 33% (off-white solid)

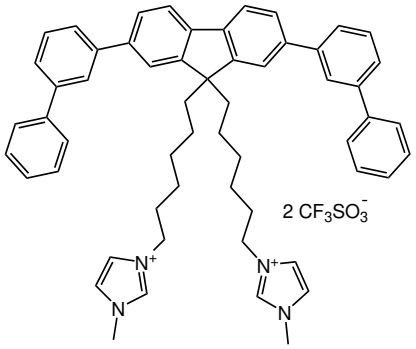

37e

$C_{59}H_{60}F_6N_4O_6S_2$
Mol Wt: 1099.26

MP 94.6 - 98.0 °C

HRMS (ESI+) Found: 400.2414 $[M]^{2+}$, $C_{57}H_{60}N_4$, Required: 400.2404

^{1}H NMR (400 MHz, DMSO-d6, 25 °C):
δ = 9.06 – 8.89 (2H, m, 2×Ar-**H**), 8.04 – 7.88 (6H, m, 6×Ar-**H**), 7.87 – 7.73 (8H, m, 8×Ar-**H**), 7.71 – 7.65 (2H, m, 2×Ar-**H**), 7.64 – 7.55 (6H, m, 6×Ar-**H**), 7.55 – 7.46 (4H, m, 4×Ar-**H**), 7.42 (2H, d, J = 7.5 Hz, 2×Ar-**H**), 4.18 (4H, t, J = 7.2 Hz, 2×C**H**$_2$), 3.94 (6H, s, 2×C**H**$_3$), 2.29 – 2.18 (4H, m, 2×C**H**$_2$), 1.72 (4H, quin, J = 7.3 Hz, 2×C**H**$_2$), 1.19 – 1.06 (8H, m, 4×C**H**$_2$), 0.79 – 0.64 (4H, m, 2×C**H**$_2$) ppm

^{13}C NMR (101 MHz, DMSO-d6, 25 °C):
δ = 153.0 (2×**C**), 143.2 (2×**C**), 143.1 (2×**C**), 142.4 (2×**C**), 141.7 (2×**C**), 141.3 (2×**C**), 137.9 (2×**C**H), 130.9 (2×**C**H), 130.3 (4×**C**H), 128.9 (2×**C**H), 128.5 (4×**C**H), 127.5 (2×**C**H), 127.4 (2×**C**H), 127.3 (2×**C**H), 126.9 (2×**C**H), 125.1 (2×**C**H), 123.7 (2×**C**H), 122.9 (2×**C**H), 121.7 (2×**C**H), 56.8 (**C**), 50.8 (2×**C**H$_2$), 41.1 (2×**C**H$_2$), 37.0 (2×**C**H$_3$), 31.12 (2×**C**H$_2$), 31.06 (2×**C**H$_2$), 26.9 (2×**C**H$_2$), 25.1 (2×**C**H$_2$) ppm

FT-IR (ν_{max} cm^{-1}, solid):
3111 (vw), 2930 (w), 2857 (w), 1569 (w), 1464 (w), 1253 (s), 1153 (s), 1029 (vs), 758 (s), 636 (vs)

UV-Vis (MeCN): λ_{max} = 327 (41300)

6.3.35 3,3'-((2,7-Di([1,1'-biphenyl]-3-yl)-9*H*-fluorene-9,9-diyl)*bis*(hexane-6,1-diyl))*bis*(1-octyl-1*H*-imidazol-3-ium) trifluoromethanesulfonate

Synthesised following the procedure detailed in 6.3.23, with the following reagent amounts:
Dibromide **45c**: 285 mg, 0.36 mmol
1-octylimidazole: 0.14 mL, 0.71 mmol
toluene: 10.0 mL
KOTf (aq., 1.0 M): 5.0 mL, 5.0 mmol
Reaction time: 17 h
Yield: 264 mg, 0.20 mmol, 57% (yellow oil)

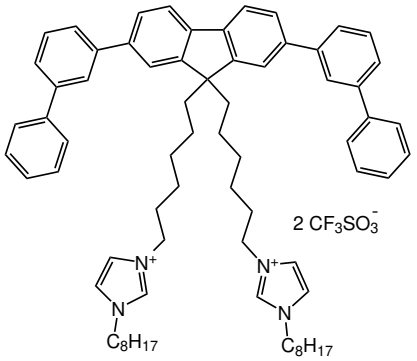

37f

$C_{73}H_{88}F_6N_4O_6S_2$
Mol Wt: 1295.64

HRMS (ESI+) Found:
498.3529 $[M]^{2+}$, $C_{71}H_{88}N_4$, Required: 498.3499

^{1}H NMR (400 MHz, acetone-d6, 25 °C):
δ = 9.97 (2H, s, 2×Ar-**H**), 8.08 – 8.00 (4H, m, 4×Ar-**H**), 7.94 (2H, d, J = 7.8 Hz, 2×Ar-**H**), 7.85 – 7.75 (10H, m, 10×Ar-**H**), 7.70 (2H, t, J = 1.8 Hz, 2×Ar-**H**), 7.67 – 7.62 (2H, m, 2×Ar-**H**), 7.62 – 7.56 (2H, m, 2×Ar-**H**), 7.54 – 7.46 (4H, m, 4×Ar-**H**), 7.42 – 7.35 (2H, m, 2×Ar-**H**), 4.31 – 4.20 (8H, m, 4×C**H**$_2$), 2.34 – 2.19 (4H, m, 2×C**H**$_2$), 1.89 – 1.76 (4H, m, 2×C**H**$_2$), 1.75 – 1.64 (4H, m, 2×C**H**$_2$), 1.28 – 1.10 (28H, m, 14×C**H**$_2$), 0.84 – 0.78 (6H, m, 2×C**H**$_3$), 0.77 – 0.67 (4H, m, 2×C**H**$_2$) ppm

^{13}C NMR (101 MHz, acetone-d6, 25 °C):
δ = 153.3 (2×**C**), 143.1 (2×**C**), 143.0 (2×**C**), 142.3 (2×**C**), 141.6 (2×**C**), 141.1 (2×**C**), 138.0 (2×**C**H), 130.9 (2×**C**H), 130.3 (4×**C**H), 128.8 (2×**C**H), 128.6 (4×**C**H), 127.6 (2×**C**H), 127.4 (2×**C**H), 127.2 (2×**C**H), 126.9 (2×**C**H), 123.8 (2×**C**H), 123.6 (2×**C**H), 123.1 (2×**C**H), 121.7 (2×**C**H), 56.8 (**C**), 50.6 (2×**C**H$_2$), 50.5 (2×**C**H$_2$), 40.8 (2×**C**H$_2$), 32.9 (4×**C**H$_2$), 31.3 (2×**C**H$_2$), 31.0 (2×**C**H$_2$), 27.2 (4×**C**H$_2$), 26.6 (2×**C**H$_2$), 24.8 (2×**C**H$_2$), 23.7 (4×**C**H$_2$), 14.8 (2×**C**H$_3$) ppm

FT-IR (ν_{max} cm^{-1}, film):
2925 (m), 2855 (m), 1559 (m), 1464 (s), 1257 (s), 1157 (s), 1030 (s), 757 (vs), 702 (s), 637 (vs)

UV-Vis (MeCN): λ_{max} = 328 (46800)

6.3.36 3,3'-((2,7-Di([1,1'-biphenyl]-4-yl)-9*H*-fluorene-9,9-diyl)*bis*(hexane-6,1-diyl))*bis*(1-methyl-1*H*-imidazol-3-ium) trifluoromethanesulfonate

Synthesised following the procedure detailed in 6.3.23, with the following reagent amounts:
Dibromide **46c**: 423 mg, 0.53 mmol
1-methylimidazole: 0.10 mL, 1.3 mmol
toluene: 10.0 mL
KOTf (aq., 1.0 M): 5.0 mL, 5.0 mmol
Reaction time: 17 h
Yield: 81 mg, 0.074 mmol, 14%
(orange solid)

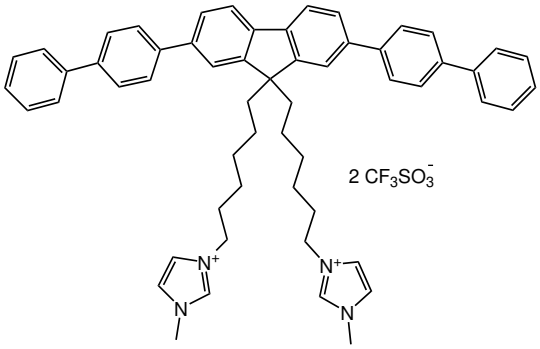

38e

$C_{59}H_{60}F_6N_4O_6S_2$
Mol Wt: 1099.26

MP 167.5 - 169.0 °C

HRMS (ESI+) Found: 400.2411 $[M]^{2+}$, $C_{57}H_{60}N_4$, Required: 400.2404

^{1}H NMR (400 MHz, DMSO-d6, 25 °C):
δ = 8.96 (2H, s, 2×Ar-**H**), 7.95 (2H, d, J = 7.9 Hz, 2×Ar-**H**), 7.92 – 7.86 (6H, m, 6×Ar-**H**), 7.82 – 7.72 (10H, m, 10×Ar-**H**), 7.59 (4H, t, J = 1.9 Hz, 4×Ar-**H**), 7.53 – 7.46 (4H, m, 4×Ar-**H**), 7.43 – 7.36 (2H, m, 2×Ar-**H**), 4.18 (4H, t, J = 7.2 Hz, 2×C**H**$_2$), 3.93 (6H, s, 2×C**H**$_3$), 2.29 – 2.18 (4H, m, 2×C**H**$_2$), 1.77 – 1.66 (4H, m, 2×C**H**$_2$), 1.18 – 1.05 (8H, m, 4×C**H**$_2$), 0.80 – 0.66 (4H, m, 2×C**H**$_2$) ppm

^{13}C NMR (101 MHz, DMSO-d6, 25 °C):
δ = 152.1 (2×**C**), 140.7 (4×**C**), 140.4 (2×**C**), 140.2 (2×**C**), 139.7 (2×**C**), 137.0 (2×**C**H), 129.3 (4×**C**H), 127.8 (2×**C**H), 127.74 (4×**C**H), 127.71 (4×**C**H), 127.1 (4×**C**H), 126.2 (2×**C**H), 124.1 (2×**C**H), 122.7 (2×**C**H), 121.6 (2×**C**H), 120.7 (2×**C**H), 55.7 (**C**), 49.8 (2×**C**H$_2$), 40.1 (2×**C**H$_2$), 36.0 (2×**C**H$_3$), 30.1 (2×**C**H$_2$), 30.1 (2×**C**H$_2$), 25.9 (2×**C**H$_2$), 24.0 (2×**C**H$_2$) ppm

FT-IR (ν_{max} cm^{-1}, solid):
2962 (w), 2857 (w), 1466 (m), 1254 (s), 1152 (s), 1029 (vs), 820 (m), 763 (s), 636 (vs)

UV-Vis (MeCN): λ_{max} = 339 (48400)

6.3.37 3,3'-((2,7-Di([1,1'-biphenyl]-4-yl)-9*H*-fluorene-9,9-diyl)*bis*(hexane-6,1-diyl))*bis*(1-octyl-1*H*-imidazol-3-ium) trifluoromethanesulfonate

Synthesised following the procedure detailed in 6.3.23, with the following reagent amounts:
Dibromide **46c**: 312 mg, 0.39 mmol
1-octylimidazole: 0.15 mL, 0.76 mmol
toluene: 10.0 mL
KOTf (aq., 1.0 M): 5.0 mL, 5.0 mmol
Reaction time: 17 h
Yield: 290 mg, 0.22 mmol, 57%
(yellow gum)

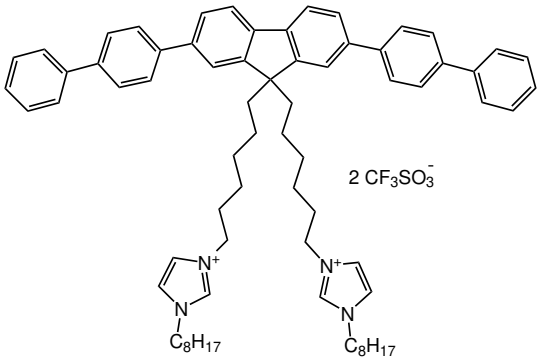

38f
$C_{73}H_{88}F_6N_4O_6S_2$
Mol Wt: 1295.64

HRMS (ESI+) Found: 498.3509 $[M]^{2+}$, $C_{71}H_{88}N_4$, Required: 498.3499

^{1}H NMR (400 MHz, acetone-d6, 25 °C):
δ = 9.06 (2H, t, J = 1.5 Hz, 2×Ar-**H**), 7.95 (2H, d, J = 7.9 Hz, 2×Ar-**H**), 7.93 – 7.86 (6H, m, 6×Ar-**H**), 7.84 – 7.70 (10H, m, 10×Ar-**H**), 7.67 (2H, app. t, J = 1.8 Hz, 2×Ar-**H**), 7.63 (2H, app. t, J = 1.8 Hz, 2×Ar-**H**), 7.54 – 7.46 (4H, m, 4×Ar-**H**), 7.43 – 7.36 (2H, m, 2×Ar-**H**), 4.31 – 4.15 (8H, m, 4×C**H**$_2$), 2.31 – 2.17 (4H, m, 2×C**H**$_2$), 1.93 – 1.79 (4H, m, 2×C**H**$_2$), 1.72 (4H, quin, J = 7.2 Hz, 2×C**H**$_2$), 1.29 – 1.09 (28H, m, 14×C**H**$_2$), 0.90 – 0.80 (6H, m, 2×C**H**$_3$), 0.79 – 0.65 (4H, m, 2×C**H**$_2$) ppm

^{13}C NMR (101 MHz, acetone-d6, 25 °C):
δ = 152.1 (2×**C**), 140.69 (2×**C**), 140.67 (2×**C**), 140.4 (2×**C**), 140.1 (2×**C**), 139.7 (2×**C**), 136.3 (2×**C**H), 129.3 (4×**C**H), 127.8 (2×**C**H), 127.74 (4×**C**H), 127.70 (4×**C**H), 127.1 (4×**C**H), 126.2 (2×**C**H), 122.9 (2×**C**H), 122.9 (2×**C**H), 121.6 (2×**C**H), 120.7 (2×**C**H), 55.7 (**C**), 49.9 (2×**C**H$_2$), 49.8 (2×**C**H$_2$), 40.1 (2×**C**H$_2$), 31.9 (2×**C**H$_2$), 30.1 (2×**C**H$_2$), 30.0 (2×**C**H$_2$), 29.2 (2×**C**H$_2$), 29.0 (2×**C**H$_2$), 26.2 (2×**C**H$_2$), 25.8 (2x**C**H$_2$), 24.0 (2×**C**H$_2$), 22.7 (2×**C**H$_2$), 13.8 (2×**C**H$_3$) ppm (2×**C**H$_2$ coincident with another unidentifiable signal)

FT-IR (ν_{max} cm^{-1}, film):
2927 (m), 2856 (w), 1466 (m), 1253 (vs), 1154 (s), 1029 (vs), 821 (m), 766 (s), 636 (vs)

UV-Vis (MeCN): λ_{max} = 339 (54200)

6.3.38 3,3'-((2-(3-Methoxyphenyl)-9*H*-fluorene-9,9-diyl)*bis*(hexane-6,1-diyl))*bis*(1-methyl-1*H*-imidazol-3-ium) trifluoromethanesulfonate

Synthesised following the procedure detailed in 6.3.23, with the following reagent amounts:
Dibromide **42a**: 575 mg, 0.96 mmol
1-methylimidazole: 0.31 mL, 3.9 mmol
toluene: 10.0 mL
KOTf (aq., 1.0 M): 5.0 mL, 5.0 mmol
Reaction time: 16 h
Yield: 813 mg, 0.90 mmol, 94% (yellow oil)

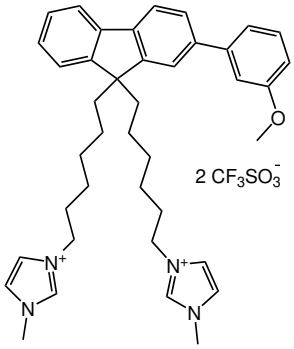

35c
$C_{42}H_{50}F_6N_4O_7S_2$
Mol Wt: 900.99

HRMS (ESI+) Found: 301.1994 $[M]^{2+}$, $C_{40}H_{50}N_4O$, Required: 301.1987

^{1}H NMR (400 MHz, acetone-d6, 25 °C):
δ = 8.98 (2H, s, 2×Ar-**H**), 7.87 (1H, dd, J = 7.9, 0.5 Hz, Ar-**H**), 7.84 – 7.81 (1H, m, Ar-**H**), 7.77 (1H, dd, J = 1.7, 0.5 Hz, Ar-**H**), 7.68 (1H, dd, J = 7.8, 1.7 Hz, Ar-**H**), 7.62 (4H, app. d, J = 1.7 Hz, 4×Ar-**H**), 7.49 – 7.45 (1H, m, Ar-**H**), 7.43 – 7.38 (1H, m, Ar-**H**), 7.38 – 7.30 (3H, m, 3×Ar-**H**), 7.28 – 7.25 (1H, m, Ar-**H**), 6.95 (1H, ddd, J = 8.1, 2.5, 1.0 Hz, Ar-**H**), 4.19 (4H, t, J = 7.3 Hz, 2×C**H**$_2$), 3.97 (6H, s, 2×C**H**$_3$), 3.88 (3H, s, C**H**$_3$), 2.20 – 2.06 (4H, m, 2×C**H**$_2$), 1.71 (4H, quin, J = 7.2 Hz, 2×C**H**$_2$), 1.17 – 1.02 (8H, m, 4×C**H**$_2$), 0.72 – 0.54 (4H, m, 2×C**H**$_2$) ppm

^{13}C NMR (101 MHz, acetone-d6, 25 °C):
δ = 160.6 (**C**), 151.5 (**C**), 151.0 (**C**), 142.9 (**C**), 141.1 (**C**), 141.0 (**C**), 140.1 (**C**), 136.9 (2×**C**H), 130.3 (**C**H), 127.6 (**C**H), 127.3 (**C**H), 126.2 (**C**H), 124.1 (2×**C**H), 123.3 (**C**H), 122.6 (2×**C**H), 121.6 (**C**H), 120.4 (**C**H), 120.1 (**C**H), 119.6 (**C**H), 113.0 (**C**H), 112.8 (**C**H), 55.3 (**C**), 55.1 (**C**H$_3$), 49.7 (2×**C**H$_2$), 40.0 (2×**C**H$_2$), 35.9 (2×**C**H$_3$), 30.1 (2×**C**H$_2$), 25.8 (2×**C**H$_2$), 23.9 (2×**C**H$_2$) ppm (2×**C**H$_2$ coincident with another unidentifiable signal)

FT-IR ($\nu_{\max}$ cm^{-1}, film):
3153 (w), 3114 (w), 2939 (w), 2861 (w), 1570 (m), 1252 (vs), 1157 (s), 1028 (vs), 744 (m), 637 (vs)

UV-Vis (MeCN): λ_{max} = 314 (24500)

6.3.39 3,3'-((2-(3-Methoxyphenyl)-9*H*-fluorene-9,9-diyl)*bis*(hexane-6,1-diyl))*bis*(1-octyl-1*H*-imidazol-3-ium) trifluoromethanesulfonate

Synthesised following the procedure detailed in 6.3.23, with the following reagent amounts:
Dibromide **42a**: 175 mg, 0.29 mmol
1-octylimidazole: 0.30 mL, 1.8 mmol
toluene: 10.0 mL
KOTf (aq., 1.0 M): 10.0 mL, 10.0 mmol
Reaction time: 19 h
Yield: 230 mg, 21 mmol, 72% (orange oil)

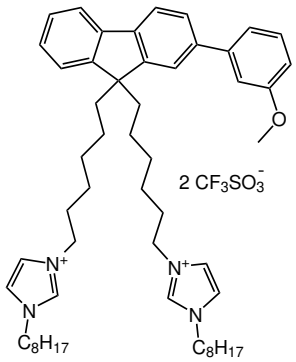

35d
$C_{56}H_{78}F_6N_4O_6S_2$
Mol Wt: 1097.37

HRMS (ESI+) Found: 399.3086 $[M]^{2+}$, $C_{54}H_{78}N_4O$, Required: 399.3082

^{1}H NMR (400 MHz, acetone-d6, 25 °C):
δ = 9.08 (2H, t, J = 1.4 Hz, 2×Ar-**H**), 7.87 (1H, d, J = 7.9 Hz, Ar-**H**), 7.84 – 7.81 (1H. m, Ar-**H**), 7.76 (1H, d, J = 1.2 Hz, Ar-**H**), 7.72 (2H, app. t, J = 1.8 Hz, 2×Ar-**H**), 7.69-7.64 (3H, m, 3×Ar-**H**), 7.49 – 7.45 (1H, m, Ar-**H**), 7.38 – 7.30 (4H, m, 4×Ar-**H**), 7.28 – 7.24 (1H, m, Ar-**H**), 6.95 (1H, ddd, J = 8.1, 2.5, 1.0 Hz, Ar-**H**), 4.29 (4H, t, J = 7.3 Hz, 2×C**H**$_2$), 4.21 (4H, t, J = 7.2 Hz, 2×C**H**$_2$), 3.88 (3H, s, OC**H**$_3$), 2.20 – 2.09 (4H, m, 2×C**H**$_2$), 1.89 (4H, quin,J = 6.8, 2xC**H**$_2$), 1.72 (4H, quin, J = 7.1 Hz, 2×C**H**$_2$), 1.32 – 1.23 (20H, m, 10×C**H**$_2$), 1.16 – 1.06 (8H, m, 4×C**H**$_2$), 0.88 – 0.82 (6H, m, 2×C**H**$_3$), 0.72 – 0.56 (4H, m, 2×C**H**$_2$) ppm

^{13}C NMR (101 MHz, acetone-d6, 25 °C):
δ = 160.7 (**C**), 151.5 (**C**), 151.0 (**C**), 143.0 (**C**), 141.1 (**C**), 141.0 (**C**), 140.1 (**C**), 136.3 (2×**C**H), 130.3 (**C**H), 127.6 (**C**H), 127.3 (**C**H), 126.2 (**C**H), 123.3 (**C**H), 122.93 (2×**C**H), 122.87 (2×**C**H), 121.7 (**C**H), 120.4 (**C**H), 120.2 (**C**H), 119.6 (**C**H), 113.0 (**C**H), 112.8 (**C**H), 55.4 (**C**H$_3$), 55.1 (**C**), 49.9 (2×**C**H$_2$), 49.8 (2×**C**H$_2$), 40.0 (2×**C**H$_2$), 31.9 (4×**C**H$_2$), 30.1 (2×**C**H$_2$), 30.07 (2×**C**H$_2$), 30.05 (2×**C**H$_2$), 29.2 (2×**C**H$_2$), 29.0 (2×**C**H$_2$), 26.2 (4×**C**H$_2$), 25.9 (2×**C**H$_2$), 23.9 (2×**C**H$_2$), 22.7 (4×**C**H$_2$), 13.8 (2×**C**H$_3$) ppm

FT-IR (ν_{max} cm^{-1}, film):
3113 (w), 2936 (m), 2860 (w), 1570 (m), 1254 (vs), 1158 (s), 1029 (vs), 743 (s), 637 (vs)

UV-Vis (MeCN): λ_{max} = 314 (28800)

6.3.40 3,3'-((2-(4-Methoxyphenyl)-9*H*-fluorene-9,9-diyl)*bis*(hexane-6,1-diyl))*bis*(1-methyl-1*H*-imidazol-3-ium) trifluoromethanesulfonate

Synthesised following the procedure detailed in 6.3.23, with the following reagent amounts:
Dibromide **43a**: 128 mg, 0.21 mmol
1-methylimidazole: 0.10 mL, 1.3 mmol
toluene: 10.0 mL
KOTf (aq., 1.0 M): 10.0 mL, 10.0 mmol
Reaction time: 16 h
Yield: 122 mg, 0.14 mmol, 64% (white oil)

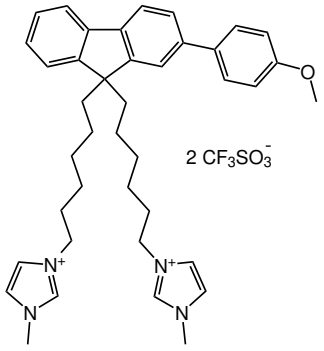

36c

$C_{42}H_{50}F_6N_4O_6S_2$
Mol Wt: 900.99

HRMS (ESI+) Found: 301.1994 $[M]^{2+}$, $C_{40}H_{50}N_4O$, Required: 301.1987

^{1}H NMR (400 MHz, acetone-d6, 25 °C):
δ = 8.99 (2H, s, 2×Ar-**H**), 7.88 – 7.78 (2H, m, 2×Ar-**H**), 7.74 – 7.60 (8H, m, 8×Ar-**H**), 7.48 – 7.43 (1H, m, Ar-**H**), 7.39 – 7.30 (2H, m, 2×Ar-**H**), 7.10 – 7.02 (2H, m, 2×Ar-**H**), 4.20 (4H, t, J = 7.3 Hz, 2×C**H**$_2$), 3.98 (6H, s, 2×C**H**$_3$), 3.85 (3H, s, C**H**$_3$), 2.19 – 2.09 (4H, m, 2×C**H**$_2$), 1.71 (4H, quin, J = 7.2 Hz, 2×C**H**$_2$), 1.16 – 1.05 (8H, m, 4×C**H**$_2$), 0.71 – 0.55 (4H, m, 2×C**H**$_2$) ppm

^{13}C NMR (101 MHz, acetone-d6, 25 °C):
δ = 159.8 (**C**), 151.5 (**C**), 150.9 (**C**), 141.3 (**C**), 140.2 (**C**), 140.0 (**C**), 137.0 (**C**H), 133.9 (**C**), 128.3 (2×**C**H), 127.4 (**C**H), 127.3 (**C**H), 125.7 (**C**H), 124.2 (2×**C**H), 123.3 (**C**H), 122.7 (2×**C**H), 121.1 (**C**H), 120.4 (**C**H), 120.2 (**C**H), 120.0 (**C**H), 114.7 (2×**C**H), 55.4 (**C**H$_3$), 55.2 (**C**), 49.8 (2×**C**H$_3$), 40.1 (2×**C**H$_2$), 36.0 (2×**C**H$_2$), 30.1 (4×**C**H$_2$), 25.9 (2×**C**H$_2$), 23.9 (2×**C**H$_2$) ppm

FT-IR (ν_{max} cm^{-1}, film):
2928 (w), 2856 (w), 1739 (w), 1452 (m), 1253 (vs), 1146 (vs), 1029 (vs), 826 (m), 744 (m), 637 (vs)

UV-Vis (MeCN): λ_{max} = 313 (26000)

6.3.41 3,3'-((2-(4-Methoxyphenyl)-9*H*-fluorene-9,9-diyl)*bis*(hexane-6,1-diyl))*bis*(1-octyl-1*H*-imidazol-3-ium) trifluoromethanesulfonate

Synthesised following the procedure detailed in 6.3.23, with the following reagent amounts:
Dibromide **43a**: 101 mg, 0.17 mmol
1-octylimidazole: 0.20 mL, 1.0 mmol
toluene: 10.0 mL
KOTf (aq., 1.0 M): 10 mL, 10 mmol
Reaction time: 16 h
Yield: 125 mg, 0.11 mmol, 67% (off-white gum)

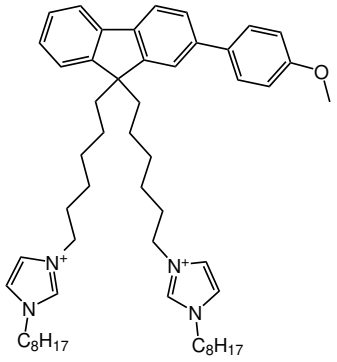

36d
$C_{56}H_{78}F_6N_4O_6S_2$
Mol Wt: 1097.37

HRMS (ESI+) Found: 399.3089 $[M]^{2+}$, $C_{54}H_{78}N_4O$, Required: 399.3082

^{1}H NMR (400 MHz, acetone-d6, 25 °C):
δ = 9.07 (2H, t, J = 1.5 Hz, 2×Ar-**H**), 7.83 (1H, d, J = 7.8 Hz, Ar-**H**), 7.80 (1H, s, Ar-**H**), 7.74 - 7.58 (8H, m, 8×Ar-**H**), 7.48 - 7.43 (1H, m, Ar-**H**), 7.38 - 7.29 (2H, m, 2×Ar-**H**), 7.09 - 7.02 (2H, m, 2×Ar-**H**), 4.28 (4H, t, J = 7.3 Hz, 2×C**H**$_2$), 4.21 (4H, t, J = 7.2 Hz, 2×C**H**$_2$), 3.85 (3H, s, C**H**$_3$), 2.18 - 2.09 (4H, m, 2×C**H**$_2$), 1.94 - 1.83 (4H, m, 2×C**H**$_2$), 1.78 - 1.65 (4H, m, 2×C**H**$_2$), 1.31 - 1.08 (28H, m, 14×C**H**$_2$), 0.88 - 0.82 (6H, m, 2×C**H**$_3$), 0.71 - 0.54 (4H, m, 2×C**H**$_2$) ppm

^{13}C NMR (101 MHz, acetone-d6, 25 °C):
δ = 159.7 (**C**), 151.5 (**C**), 150.9 (**C**), 141.2 (**C**), 140.2 (**C**), 140.0 (**C**), 136.3 (**C**H), 133.8 (**C**), 128.3 (2×**C**H), 127.4 (**C**H), 127.3 (**C**H), 125.6 (**C**H), 123.2 (**C**H), 122.93 (2×**C**H), 122.86 (2×**C**H), 121.5 (q, J = 321.1, 2×**C**F$_3$), 121.1 (**C**H), 120.4 (**C**H), 120.0 (**C**H), 114.6 (2×**C**H), 55.3 (**C**), 55.1 (2×**C**H$_3$), 49.9 (2×**C**H$_2$), 49.8 (2×**C**H$_2$), 40.1 (2×**C**H$_2$), 31.8 (2×**C**H$_2$), 30.11 (2×**C**H$_2$), 30.06 (2×**C**H$_2$), 30.0 (2×**C**H$_2$), 29.2 (2×**C**H$_2$), 29.0 (2×**C**H$_2$), 26.2 (2×**C**H$_2$), 25.8 (2×**C**H$_2$), 23.9 (2×**C**H$_2$), 22.7 (2×**C**H$_2$), 13.8 (2×**C**H$_3$) ppm

FT-IR (ν_{max} cm^{-1}, film):
2935 (w), 2560 (w), 1622 (m), 1245 (vs), 1159 (s), 1030 (vs), 637 (vs), 577 (s)

UV-Vis (MeCN): λ_{max} = 313 (11200)

6.3.42 3,3'-((2-(*p*-Tolyl)-9*H*-fluorene-9,9-diyl)*bis*(hexane-6,1-diyl))*bis*(1-methyl-1*H*-imidazol-3-ium) trifluoromethanesulfonate

Synthesised following the procedure detailed in 6.3.23, with the following reagent amounts:
Dibromide **43b**: 851 mg, 1.42 mmol
1-methylimidazole: 0.23 mL, 2.8 mmol
toluene: 10.0 mL
KOTf (aq., 1.0 M): 20 mL, 20 mmol
Reaction time: 20 h
Yield: 880 mg, 0.99 mmol, 70% (off-white gum)

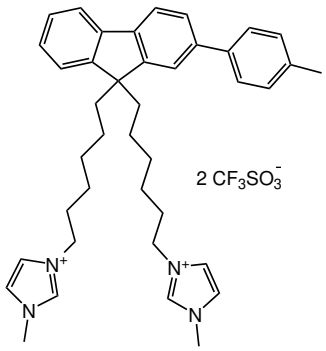

36a

$C_{42}H_{50}F_6N_4O_6S_2$
Mol Wt: 884.99

HRMS (ESI+) Found: 293.2018 $[M]^{2+}$, $C_{40}H_{50}N_4$, Required: 293.2012

^{1}H NMR (400 MHz, acetone-d6, 25 °C):
δ = 8.99 (2H, s, 2×Ar-**H**), 7.86 (1H, d, J = 7.9 Hz, Ar-**H**), 7.84 - 7.80 (1H, m, Ar-**H**), 7.75 (1H, d, J = 1.1 Hz, Ar-**H**), 7.68 - 7.61 (7H, m, 7×Ar-**H**), 7.49 - 7.45 (1H, m, Ar-**H**), 7.37 - 7.28 (4H, m, 4×Ar-**H**), 4.20 (4H, t, J = 7.2 Hz, 2×C**H**$_2$), 3.98 (6H, s, 2×C**H**$_3$), 2.38 (3H, s, C**H**$_3$), 2.19 - 2.09 (4H, m, 2×C**H**$_2$), 1.71 (4H, quin, J = 7.1 Hz, 2×C**H**$_2$), 1.15 - 1.04 (8H, m, 4×C**H**$_2$), 0.70 - 0.55 (4H, m, 2×C**H**$_2$) ppm

^{13}C NMR (101 MHz, acetone-d6, 25 °C):
δ = 151.5 (**C**), 151.0 (**C**), 141.2 (**C**), 140.6 (**C**), 140.2 (**C**), 138.6 (**C**), 137.2 (**C**), 137.0 (2×**C**H), 129.9 (2×**C**H), 127.5 (**C**H), 127.3 (**C**H), 127.1 (2×**C**H), 125.9 (**C**H), 124.1 (2×**C**H), 123.3 (**C**H), 122.7 (2×**C**H), 121.4 (**C**H), 120.4 (**C**H), 120.1 (**C**H), 55.4 (**C**), 49.8 (2×**C**H$_2$), 40.1 (2×**C**H$_2$), 36.0 (2×**C**H$_3$), 30.1 (2×**C**H$_2$), 29.4 (2×**C**H$_2$), 25.9 (2×**C**H$_2$), 23.9 (2×**C**H$_2$), 20.5 (**C**H$_3$) ppm

FT-IR (ν_{max} cm^{-1}, film):
3113 (w), 2930 (w), 2858 (w), 1570 (w), 1451 (w), 1253 (vs), 1154 (s), 1028 (vs), 816 (m), 743 (m), 636 (vs)

UV-Vis (MeCN): λ_{max} = 294 (27300)

6.3.43 3,3'-((2-(*p*-Tolyl)-9*H*-fluorene-9,9-diyl)*bis*(hexane-6,1-diyl))*bis*(1-octyl-1*H*-imidazol-3-ium) trifluoromethanesulfonate

Synthesised following the procedure detailed in 6.3.23, with the following reagent amounts:
Dibromide **43b**: 707 mg, 1.18 mmol
1-octylimidazole: 0.47 mL, 2.36 mmol
toluene: 10.0 mL
KOTf (aq., 1.0 M): 10 mL, 10 mmol
Reaction time: 20 h
Yield: 1.27 g, 1.17 mmol, 99% (off-white gum)

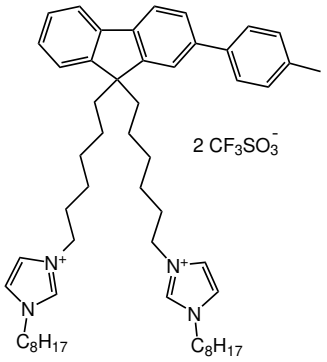

36b

$C_{56}H_{78}F_6N_4O_6S_2$
Mol Wt: 1081.37

HRMS (ESI+) Found: 391.3117 $[M]^{2+}$, $C_{54}H_{78}N_4$, Required: 391.3108

^{1}H NMR (400 MHz, acetone-d6, 25 °C):
δ = 9.09 (2H, t, J = 1.5 Hz, 2×Ar-**H**), 7.85 (1H, dd, J = 7.9, 0.4 Hz, Ar-**H**), 7.83 - 7.79 (1H, m, Ar-**H**), 7.75 (1H, dd, J = 1.8, 0.5 Hz, Ar-**H**), 7.72 (2H, t, J = 1.8 Hz, 2×Ar-**H**), 7.68 - 7.62 (5H, m, 5×Ar-**H**), 7.49 - 7.44 (1H, m, Ar-**H**), 7.36 - 7.27 (4H, m, 4×Ar-**H**), 4.29 (4H, t, J = 7.3 Hz, 2×C**H**$_2$), 4.21 (4H, t, J = 7.2 Hz, 2×C**H**$_2$), 2.38 (3H, s, C**H**$_3$), 2.21 - 2.09 (4H, m, 2×C**H**$_2$), 1.96 - 1.83 (4H, m, 2×C**H**$_2$), 1.78 - 1.66 (4H, m, 2×C**H**$_2$), 1.31 - 1.08 (28H, m, 14×C**H**$_2$), 0.87 - 0.83 (6H, m, 2×C**H**$_3$), 0.73 - 0.53 (4H, m, 2×C**H**$_2$) ppm

^{13}C NMR (101 MHz, acetone-d6, 25 °C):
δ = 151.5 (**C**), 151.0 (**C**), 141.2 (**C**), 140.6 (**C**), 140.2 (**C**), 138.6 (**C**), 137.2 (**C**), 136.3 (2×**C**H), 129.9 (2×**C**H), 127.5 (**C**H), 127.3 (**C**H), 127.1 (2×**C**H), 125.9 (**C**H), 123.3 (**C**H), 122.93 (2×**C**H), 122.87 (2×**C**H), 121.4 (**C**H), 120.4 (**C**H), 120.1 (**C**H), 55.3 (**C**), 49.9 (2×**C**H$_2$), 49.8 (2×**C**H$_2$), 40.1 (2×**C**H$_2$), 31.9 (4×**C**H$_2$), 30.14 (2×**C**H$_2$), 30.06 (2×**C**H$_2$), 26.2 (4×**C**H$_2$), 25.8 (2×**C**H$_2$), 23.9 (2×**C**H$_2$), 22.7 (4×**C**H$_2$), 20.5 (**C**H$_3$), 13.8 (2×**C**H$_3$) ppm

FT-IR (ν_{max} cm^{-1}, film):
3142 (w), 3107 (w), 2928 (m), 2857 (w), 1560 (w), 1465 (m), 1253 (s), 1156 (s), 1029 (vs), 636 (vs)

UV-Vis (MeCN): λ_{max} = 294 (21300)

6.3.44 3,3'-((2-([1,1'-Biphenyl]-3-yl)-9*H*-fluorene-9,9-diyl)*bis*(hexane-6,1-diyl))*bis*(1-methyl-1*H*-imidazol-3-ium) trifluoromethanesulfonate

Synthesised following the procedure detailed in 6.3.23, with the following reagent amounts:
Dibromide **42d**: 619 mg, 0.96 mmol
1-methylimidazole: 0.23 mL, 2.87 mmol
toluene: 10.0 mL
KOTf (aq., 1.0 M): 10 mL, 10 mmol
Reaction time: 16 h
Yield: 315 mg, 0.33 mmol, 35% (off-white gum)

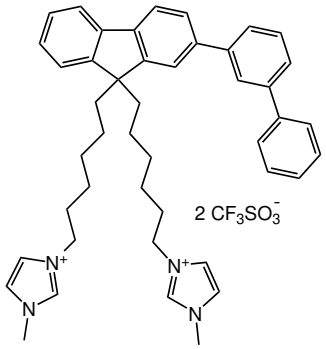

35e
$C_{47}H_{52}F_6N_4O_6S_2$
Mol Wt: 947.07

HRMS (ESI+) Found: 324.2092 $[M]^{2+}$, $C_{45}H_{52}N_4$, Required: 324.2091

^{1}H NMR (400 MHz, acetone-d6, 25 °C):
δ = 8.97 (2H, s, 2×Ar-**H**), 7.99 (1H, td, J = 1.8, 0.5 Hz, Ar-**H**), 7.94 – 7.88 (2H, m, 2×Ar-**H**), 7.87 – 7.83 (1H, m, Ar-**H**), 7.81 – 7.73 (4H, m, 4×Ar-**H**), 7.69 – 7.56 (6H, m, 6×Ar-**H**), 7.54 – 7.46 (3H, m, 3×Ar-**H**), 7.43 – 7.31 (3H, m, 3×Ar-**H**), 4.19 (4H, t, J = 7.2 Hz, 2× C**H**$_2$), 3.96 (6H, s, 2× C**H**$_3$), 2.23 – 2.07 (4H, m, 2× C**H**$_2$), 1.77 – 1.66 (4H, m, 2×C**H**$_2$), 1.19 – 1.01 (8H, m, 4× C**H**$_2$), 0.74 – 0.54 (4H, m, 2×C**H**$_2$) ppm

^{13}C NMR (101 MHz, acetone-d6, 25 °C):
δ = 151.6 (**C**), 151.0 (**C**), 142.2 (**C**), 142.1 (**C**), 141.3 (**C**), 141.13 (**C**), 141.07 (**C**), 140.2 (**C**), 137.0 (2×**C**H), 129.9 (**C**H), 129.3 (2×**C**H), 127.8 (**C**H), 127.7 (**C**H), 127.44 (2×**C**H), 127.36 (**C**H), 126.4 (2×**C**H), 126.2 (**C**H), 125.8 (**C**H), 124.1 (2×**C**H), 123.3 (**C**H), 122.7 (2×**C**H), 121.8 (**C**H), 120.5 (**C**H), 120.2 (**C**H), 55.4 (**C**), 49.8 (2×**C**H$_2$), 40.1 (2×**C**H$_2$), 36.0 (2×**C**H$_3$), 30.1 (2×**C**H$_2$), 29.4 (2×**C**H$_2$), 25.9 (2×**C**H$_2$), 23.9 (2×**C**H$_2$) ppm

FT-IR ($\nu_{\max}$ cm^{-1}, film):
3115 (w), 2938 (w), 1575 (m), 1251 (vs), 1157 (s), 1049 (w), 758 (s), 636 (vs)

UV-Vis (MeCN): λ_{max} = 290 (25800)

6.3.45 3,3'-((2-([1,1'-Biphenyl]-3-yl)-9*H*-fluorene-9,9-diyl)*bis*(hexane-6,1-diyl))*bis*(1-octyl-1*H*-imidazol-3-ium) trifluoromethanesulfonate

Synthesised following the procedure detailed in 6.3.23, with the following reagent amounts:
Dibromide **42d**: 579 mg, 0.90 mmol
1-octylimidazole: 0.54 mL, 2.73 mmol
toluene: 10.0 mL
KOTf (aq., 1.0 M): 10 mL, 10 mmol
Reaction time: 16 h
Yield: 144 mg, 0.13 mmol, 14% (off-white oil)

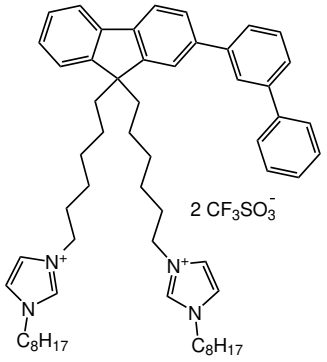

35f

$C_{61}H_{80}F_6N_4O_6S_2$
Mol Wt: 1143.44

HRMS (ESI+) Found: 422.3197 $[M]^{2+}$, $C_{59}H_{80}N_4$, Required: 422.3186

^{1}H NMR (400 MHz, acetone-d6, 25 °C):
δ = 9.07 (2H, t, J = 1.6 Hz, 2×Ar-**H**), 7.99 (1H, t, J = 1.6 Hz, Ar-**H**), 7.93 – 7.88 (2H, m, 2×Ar-**H**), 7.87 – 7.83 (1H, m, Ar-**H**), 7.80 – 7.74 (4H, m, 4×Ar-**H**), 7.72 – 7.63 (5H, m, 5×Ar-**H**), 7.62 – 7.57 (1H, m, Ar-**H**), 7.54 – 7.45 (3H, m, 3×Ar-**H**), 7.43 – 7.34 (3H, m, 3×Ar-**H**), 4.28 (4H, t, J = 7.3 Hz, 2×C**H**$_2$), 4.21 (4H, t, J = 7.2 Hz, 2×C**H**$_2$), 2.23 – 2.07 (4H, m, 2×C**H**$_2$), 1.93 – 1.84 (4H, m, 2×C**H**$_2$), 1.72 (4H, quin, J = 7.2 Hz, 2×C**H**$_2$), 1.30 – 1.10 (28H, m, 14×C**H**$_2$), 0.87 – 0.81 (6H, m, 2×C**H**$_3$), 0.74 – 0.56 (4H, m, 2×C**H**$_2$) ppm

^{13}C NMR (101 MHz, acetone-d6, 25 °C):
δ = 151.6 (**C**), 151.0 (**C**), 142.2 (**C**), 142.1 (**C**), 141.4 (**C**), 141.2 (**C**), 141.1 (**C**), 140.2 (**C**), 136.3 (2×**C**H), 129.9 (**C**H), 129.3 (2×**C**H), 127.8 (**C**H), 127.7 (**C**H), 127.45 (2×**C**H), 127.36 (**C**H), 126.4 (**C**H), 126.2 (**C**H), 125.8 (**C**H), 123.3 (**C**H), 122.94 (2×**C**H), 122.88 (2×**C**H), 121.8 (**C**H), 120.5 (**C**H), 120.2 (**C**H), 120.1 (**C**H), 55.5 (**C**), 49.9 (2×**C**H$_2$), 49.8 (2×**C**H$_2$), 40.1 (2×**C**H$_2$), 31.9 (4×**C**H$_2$), 30.14 (2×**C**H$_2$), 30.06 (2×**C**H$_2$), 26.2 (4×**C**H$_2$), 25.9 (2×**C**H$_2$), 23.9 (2×**C**H$_2$), 22.7 (4×**C**H$_2$), 13.8 (2×**C**H$_3$) ppm

FT-IR (ν_{max} cm^{-1}, film):
3106 (w), 2930 (m), 2858 (m), 1560 (m), 1456 (m), 1253 (vs), 1155 (s), 1029 (vs), 757 (s), 636 (vs)

UV-Vis (MeCN): λ_{max} = 291 (27600)

6.3.46 3,3'-((2-([1,1'-Biphenyl]-4-yl)-9*H*-fluorene-9,9-diyl)*bis*(hexane-6,1-diyl))*bis*(1-methyl-1*H*-imidazol-3-ium) trifluoromethanesulfonate

Synthesised following the procedure detailed in 6.3.23, with the following reagent amounts:
Dibromide **43c**: 269 mg, 0.42 mmol
1-methylimidazole: 0.10 mL, 1.3 mmol
toluene: 10 mL
KOTf (aq., 1.0 M): 10 mL, 10 mmol
Reaction time: 16 h
Yield: 135 mg, 0.14 mmol, 34% (orange oil)

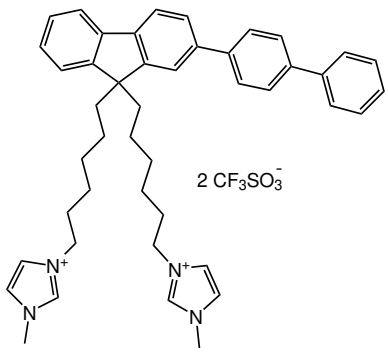

36e

$C_{47}H_{52}F_6N_4O_6S_2$
Mol Wt: 947.07

HRMS (ESI+) Found: 324.2098 $[M]^{2+}$, $C_{45}H_{52}N_4$, Required: 324.2091

^{1}H NMR (400 MHz, acetone-d6, 25 °C):
δ = 8.98 (2H, s, 2×Ar-**H**), 7.94 – 7.71 (10H, m, 10×Ar-**H**), 7.65 – 7.61 (4H, m, 4×Ar-**H**), 7.53 – 7.45 (3H, m, 3×Ar-**H**), 7.42 – 7.32 (3H, m, 3×Ar-**H**), 4.20 (4H, t, J = 7.2 Hz, 2×C**H**$_2$), 4.02 – 3.93 (6H, m, 2×C**H**$_3$), 2.28 – 2.09 (4H, m, 2×C**H**$_2$), 1.78 – 1.66 (4H, m, 2×C**H**$_2$), 1.20 – 1.04 (8H. m, 4×C**H**$_2$), 0.75 – 0.55 (4H, m, 2×C**H**$_2$) ppm

^{13}C NMR (101 MHz, acetone-d6, 25 °C):
δ = 151.6 (**C**), 151.0 (**C**), 141.1 (**C**), 141.0 (**C**), 140.7 (**C**), 140.4 (**C**), 140.1 (**C**), 139.6 (**C**), 137.0 (2×**C**H), 129.3 (2×**C**H), 127.8 (**C**H), 127.72 (2×**C**H), 127.69 (3×**C**H), 127.4 (**C**H), 127.1 (2×**C**H), 126.1 (**C**H), 124.2 (2×**C**H), 123.3 (**C**H), 122.7 (2×**C**H), 121.5 (**C**H), 120.5 (**C**H), 120.2 (**C**H), 55.4 (**C**), 49.8 (2×**C**H$_2$), 40.1 (2×**C**H$_2$), 36.0 (2×**C**H$_3$), 30.1 (2×**C**H$_2$), 29.40 (2×**C**H$_2$), 25.9 (2×**C**H$_2$), 23.9 (2×**C**H$_2$) ppm

FT-IR (ν_{max} cm^{-1}, film):
3567 (w), 3115 (w), 2938 (w), 1572 (m), 1250 (vs), 1158 (s), 1029 (vs), 744 (m), 636 (vs)

UV-Vis (MeCN): λ_{max} = 319 (33200)

6.3.47 3,3'-((2-([1,1'-Biphenyl]-4-yl)-9*H*-fluorene-9,9-diyl)*bis*(hexane-6,1-diyl))*bis*(1-octyl-1*H*-imidazol-3-ium) trifluoromethanesulfonate

Synthesised following the procedure detailed in 6.3.23, with the following reagent amounts:
Dibromide **43c**: 226 mg, 0.35 mmol
1-octylimidazole: 0.21 mL, 1.1 mmol
toluene: 10 mL
KOTf (aq., 1.0 M): 10 mL, 10 mmol
Reaction time: 16 h
Yield: 322 mg, 0.28 mmol, 80% (off-white gum)

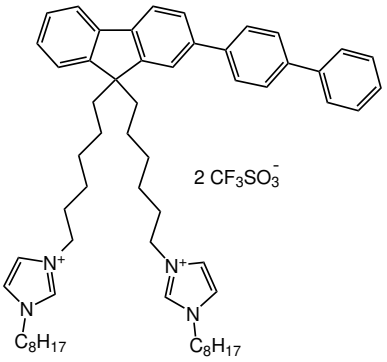

36f

$C_{61}H_{80}F_6N_4O_6S_2$
Mol Wt: 1143.44

HRMS (ESI+) Found: 422.3197 $[M]^{2+}$, $C_{59}H_{80}N_4$, Required: 422.3186

^{1}H NMR (400 MHz, acetone-d6, 25 °C):
δ = 9.08 (2H, t, J = 1.5 Hz, 2×Ar-**H**), 7.92 – 7.65 (14H, m, 14×Ar-**H**), 7.53 – 7.46 (3H, m, 3×Ar-**H**), 7.42 – 7.33 (3H, m, 3×Ar-**H**), 4.27 (4H, t, J = 7.3 Hz, 2×C**H**$_2$), 4.21 (4H, t, J = 7.2 Hz, 2×C**H**$_2$), 2.22 – 2.09 (4H, m, 2×C**H**$_2$), 1.93 – 1.83 (4H, m, 2×C**H**$_2$), 1.72 (4H, quin, J = 7.2 Hz, 2×C**H**$_2$), 1.31 – 1.09 (28H, m, 14×C**H**$_2$), 0.89 – 0.79 (6H, m, 2×C**H**$_3$), 0.74 – 0.58 (4H, m, 2×C**H**$_2$) ppm

^{13}C NMR (101 MHz, acetone-d6, 25 °C):
δ = 151.6 (**C**), 151.0 (**C**), 141.1 (**C**), 141.0 (**C**), 140.7 (**C**), 140.4 (**C**), 140.1 (**C**), 139.6 (**C**), 136.3 (2×**C**H), 129.3 (2×**C**H), 127.8 (**C**H), 127.72 (2×**C**H), 127.69 (2×**C**H), 127.4 (**C**H), 127.0 (2×**C**H), 126.0 (**C**H), 123.33 (**C**H), 123.30 (**C**H), 122.93 (2×**C**H), 122.87 (2×**C**H), 121.5 (**C**H), 120.5 (**C**H), 120.2 (**C**H), 55.4 (**C**), 49.9 (2×**C**H$_2$), 49.8 (2×**C**H$_2$), 40.1 (2×**C**H$_2$), 31.9 (2×**C**H$_2$), 30.1 (2×**C**H$_2$), 30.0 (2×**C**H$_2$), 29.2 (2×**C**H$_2$), 29.0 (2×**C**H$_2$) 26.2 (2×**C**H$_2$), 25.8 (2×**C**H$_2$), 23.9 (2×**C**H$_2$), 22.7 (2×**C**H$_2$), 13.8 (2×**C**H$_3$) ppm

FT-IR (ν_{max} cm^{-1}, film):
3106 (w), 2930 (m), 2858 (m), 1560 (m), 1456 (m), 1251 (s), 1156 (s), 1029 (vs), 636 (vs)

UV-Vis (MeCN): λ_{max} = 318 (37800)

6.3.48 3,3'-((2-Phenyl-9*H*-fluorene-9,9-diyl)*bis*(hexane-6,1-diyl))*bis*(1-octyl-1*H*-imidazol-3-ium) trifluoromethanesulfonate

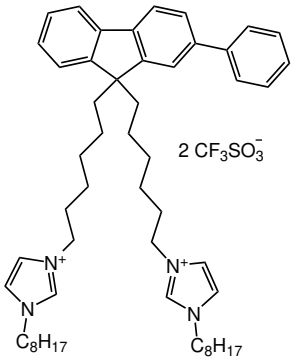

35j

$C_{55}H_{76}F_6N_4O_6S_2$
Mol Wt: 1067.35

Synthesised following the procedure detailed in 6.3.25, with the following reagent amounts:
Dibromide **42b**: 1.06 g, 1.87 mmol
1-octylimidazole: 1.48 mL, 7.38 mmol
toluene: 20 mL
KOTf (aq., 1.0 M): 20 mL, 20 mmol
Reaction time: 2 days
Yield: 1.55 g, 1.45 mmol, 77% (off-white gum)

HRMS (ESI+) Found: 384.3039 $[M]^{2+}$, $C_{53}H_{76}N_4$, Required: 384.3030

^{1}H NMR (400 MHz, acetone-d6, 25 °C):
δ = 9.07 (2H, t, J = 1.6 Hz, 2×Ar-**H**), 7.87 (1H, dd, J = 7.9, 0.6 Hz, Ar-**H**), 7.84-7.80 (1H, m, Ar-**H**), 7.77-7.73 (3H, m, 3×Ar-**H**), 7.72-7.64 (5H, m, 5×Ar-**H**), 7.51-7.45 (3H, m, 3×Ar-**H**), 7.39-7.31 (3H, m, 3×Ar-**H**), 4.28 (4H, t, J = 7.3 Hz, 2×C**H**$_2$), 4.21 (4H, t, J = 7.2 Hz, 2×C**H**$_2$), 2.12 (4H, m, 2×C**H**$_2$), 1.94-1.84 (4H, m, 2×C**H**$_2$), 1.72 (4H, quin, J = 7.3 Hz, 2×C**H**$_2$), 1.31-1.06 (28H, m, 14×C**H**$_2$), 0.88-0.82 (6H, m, 2×C**H**$_3$), 0.70-0.55 (4H, m, 2×C**H**$_2$) ppm

^{13}C NMR (101 MHz, acetone-d6, 25 °C):
δ = 151.5 (**C**), 151.0 (**C**), 141.5 (**C**), 141.1 (**C**), 140.9 (**C**), 140.2 (**C**), 136.3 (2×**C**H), 129.2 (2×**C**H), 127.6 (**C**H), 127.5 (**C**H), 127.3 (**C**H), 127.2 (2×**C**H), 126.1 (**C**H), 123.3 (**C**H), 122.93 (2×**C**H), 122.87 (2×**C**H), 121.6 (**C**H), 121.5 (2C, q, J = 320.6 Hz, 2×**C**F_3SO_3), 120.4 (**C**H), 120.1 (**C**H), 55.4 (**C**), 49.9 (2×**C**H_2), 49.8 (2×**C**H_2), 40.1 (2×**C**H_2), 31.8 (4×**C**H_2), 30.1 (2×**C**H_2), 30.1 (2×**C**H_2), 30.0 (2×**C**H_2), 26.2 (2×**C**H_2), 25.8 (2×**C**H_2), 23.9 (2×**C**H_2), 22.7 (4×**C**H_2), 13.8 (2×**C**H_3) ppm

FT-IR (ν_{max} cm^{-1}, film):
3523 (w), 2929 (w), 2858 (w), 1455 (w), 1252 (vs), 1159 (s), 1030 (vs), 764 (m), 638 (vs), 576 (m)

UV-Vis (MeCN): λ_{max} = 313 (17700)

6.3.49 3,3'-((2,7-Diphenyl-9*H*-fluorene-9,9-diyl)*bis*(hexane-6,1-diyl))*bis*(1-octyl-1*H*-imidazol-3-ium) trifluoromethanesulfonate

Synthesised following the procedure detailed in 6.3.26, with the following reagent amounts:
Dibromide **45d**: 418 mg, 0.65 mmol
1-octylimidazole: 0.51 mL, 2.6 mmol
toluene: 20 mL
KOTf (aq., 1.0 M): 20 mL, 20 mmol
Reaction time: 3.5 days
Yield: 644 mg, 0.56 mmol, 87% (off-white gum)

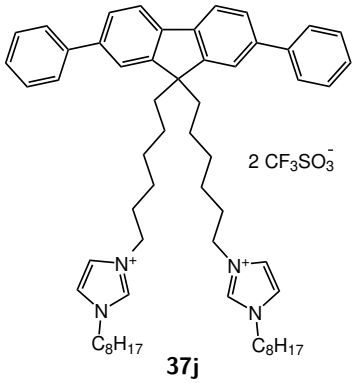

37j

$C_{61}H_{80}F_6N_4O_6S_2$
Mol Wt: 1143.44

HRMS (ESI+) Found: 422.3191 $[M]^{2+}$, $C_{59}H_{80}N_4$, Required: 422.3186

^{1}H NMR (400 MHz, acetone-d6, 25 °C):
δ = 9.07 (2H, t, J = 1.5 Hz, 2×Ar-**H**), 7.92 (2H, dd, J = 7.8, 0.5 Hz, 2×Ar-**H**), 7.81 (2H, dd, J = 1.7, 0.6 Hz, 2×Ar-**H**), 7.79-7.76 (4H, m, 4×Ar-**H**), 7.72-7.67 (4H, m, 4×Ar-**H**), 7.63 (2H, t, J = 1.8 Hz, 2×Ar-**H**), 7.53-7.46 (4H, m, 4×Ar-**H**), 7.41-7.35 (2H, m, 2×Ar-**H**), 4.27 (4H, t, J = 7.3 Hz, 2×C**H**$_2$), 4.20 (4H, t, J = 7.3 Hz, 2×C**H**$_2$), 2.26-2.16 (4H, m, 2×C**H**$_2$), 1.93-1.82 (4H, m, 2×C**H**$_2$), 1.72 (4H, quin, J = 7.2 Hz, 2×C**H**$_2$), 1.31-1.09 (28H, m, 14×C**H**$_2$), 0.88-0.82 (6H, m, 2×C**H**$_3$), 0.75-0.65 (4H, m, 2×C**H**$_2$) ppm

^{13}C NMR (101 MHz, acetone-d6, 25 °C):
δ = 151.9 (2×**C**), 141.5 (2×**C**), 140.6 (2×**C**), 140.3 (2×**C**), 136.3 (2×**C**H), 129.3 (4×**C**H), 127.6 (2×**C**H), 127.3 (4×**C**H), 126.3 (2×**C**H), 122.93 (2×**C**H), 122.86 (2×**C**H), 121.7 (2×**C**H), 120.6 (2×**C**H), 55.6 (**C**), 49.9 (2×**C**H$_2$), 49.8 (2×**C**H$_2$), 40.1 (2×**C**H$_2$), 31.9 (2×**C**H$_2$), 30.13 (2×**C**H$_2$), 30.06 (2×**C**H$_2$), 29.4 (2×**C**H$_2$), 29.2 (2×**C**H$_2$), 29.0 (2×**C**H$_2$), 26.2 (2×**C**H$_2$), 25.9 (2×**C**H$_2$), 24.0 (2×**C**H$_2$), 22.7 (2×**C**H$_2$), 13.8 (2×**C**H$_3$) ppm

FT-IR (ν_{max} cm^{-1}, film):
3108 (vw), 2928 (m), 2857 (w), 1465 (m), 1254 (vs), 1156 (s), 1030 (vs), 762 (s), 637 (vs), 573 (m)

UV-Vis (MeCN): λ_{max} = 327 (40400)

6.3.50 3,3'-((2-(Phenanthren-9-yl)-9*H*-fluorene-9,9-diyl)*bis*(hexane-6,1-diyl))*bis*(1-methyl-1*H*-imidazol-3-ium) trifluoromethanesulfonate

Synthesised following the procedure detailed in 6.3.26, with the following reagent amounts:
Dibromide **64**: 817 mg, 1.22 mmol
1-methylimidazole: 0.24 mL, 3.01 mmol
toluene: 10.0 mL
KOTf (aq., 0.1 M): 30 mL, 3.0 mmol
Reaction time: 20 h
Yield: 745 mg, 0.77 mmol, 63% (off-white gum)

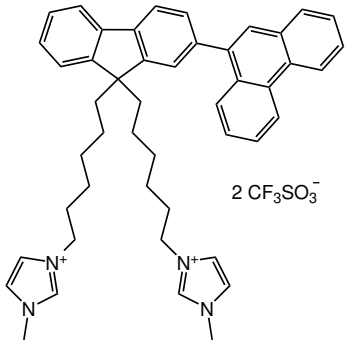

62a
$C_{49}H_{52}F_6N_4O_6S_2$
Mol Wt: 971.09

HRMS (ESI+) Found: 336.2091 $[M]^{2+}$, $C_{47}H_{52}N_4$, Required: 336.2091

^{1}H NMR (400 MHz, acetone-d6, 25 °C):
δ = 8.86-9.00 (4H, m, 4×Ar-**H**), 8.06 (1H, dd, J = 7.8, 1.3 Hz, Ar-**H**), 7.99 (1H, d, J = 7.7 Hz, Ar-**H**), 7.91-7.87 (1H, m, Ar-**H**), 7.85-7.80 (2H, m, 2×Ar-**H**), 7.77-7.67 (3H, m, 3×Ar-**H**), 7.64 (4H, app. t, J = 1.8 Hz, 2×Ar-**H**), 7.61 (4H, app. t, J = 1.8 Hz, 2×Ar-**H**), 7.57 (1H, d, J = 1.1 Hz, Ar-**H**), 7.55-7.46 (3H, m, 3×Ar-**H**), 7.41-7.33 (2H, m, 2×Ar-**H**), 4.02 (4H, t, J = 7.1 Hz, 2×C**H**$_2$), 3.78 (6H, s, 2×C**H**$_3$), 2.06-1.95 (4H, m, 2×C**H**$_2$), 1.59 (4H, quin, J = 7.3 Hz, 2×C**H**$_2$), 1.13-0.96 (8H, m, 4×C**H**$_2$), 0.73-0.53 (4H, m, 2×C**H**$_2$) ppm

^{13}C NMR (101 MHz, acetone-d6, 25 °C):
δ = 150.3 (**C**), 150.1 (**C**), 140.3 (**C**), 140.0 (**C**), 138.8 (**C**), 138.4 (**C**), 136.4 (2×**C**H), 131.1 (**C**), 130.6 (**C**), 130.3 (**C**), 129.4 (**C**), 128.7 (2×**C**H), 127.4 (**C**H), 127.2 (**C**H), 127.1 (2×**C**H), 127.0 (**C**H), 126.8 (**C**H), 126.7 (**C**H), 126.1 (**C**H), 124.5 (**C**H), 123.5 (4×**C**H), 122.9 (**C**H), 122.8 (**C**H), 122.2 (2×**C**H), 120.7 (2C, q, J = 322.1 Hz, 2×**C**F$_3$SO$_3$), 120.1 (**C**H), 54.7 (**C**), 48.7 (2×**C**H$_2$), 35.7 (2×**C**H$_3$), 30.7 (2×**C**H$_2$), 29.4 (2×**C**H$_2$), 28.9 (2×**C**H$_2$), 25.4 (2×**C**H$_2$), 23.6 (2×**C**H$_2$) ppm

FT-IR (ν_{max} cm^{-1}, film):
3525 (w), 2931 (w), 1723 (w), 1244 (vs), 1162 (s), 1027 (vs), 766 (w), 636 (vs), 577 (m)

6.3.51 3,3'-((2-(Phenanthren-9-yl)-9*H*-fluorene-9,9-diyl)*bis*(hexane-6,1-diyl))*bis*(1-octyl-1*H*-imidazol-3-ium) trifluoromethanesulfonate

Synthesised following the procedure detailed in 6.3.26, with the following reagent amounts:
Dibromide **64**: 434 mg, 0.65 mmol
1-octylimidazole: 0.27 mL, 1.34 mmol
toluene: 5.0 mL
KOTf (aq., 1.0 M): 10.0 mL, 10.0 mmol
Reaction time: 24 h
Yield: 590 mg, 0.51 mmol, 78% (off-white gum)

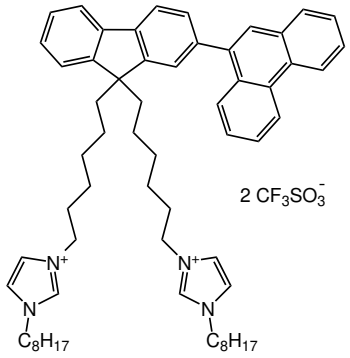

62b
$C_{63}H_{80}F_6N_4O_6S_2$
Mol Wt: 1167.47

HRMS (ESI+) Found: 434.3197 $[M]^{2+}$, $C_{61}H_{80}N_4$, Required: 434.3186

^{1}H NMR (400 MHz, acetone-d6, 25 °C):
δ = 9.09 (2H, t, J = 1.5 Hz, 2×Ar-**H**), 8.97-8.92 (1H, m, Ar-**H**), 8.91-8.86 (1H, m, Ar-**H**), 8.02 (1H, dd, J = 7.7, 1.6 Hz, Ar-**H**), 7.99 (1H, dd, J = 7.7, 0.5 Hz, Ar-**H**), 7.94-7.88 (2H, m, 2×Ar-**H**), 7.81 (1H, s, Ar-**H**), 7.77-7.66 (7H, m, 7×Ar-**H**), 7.60 (1H, dd, J = 1.6, 0.5 Hz, Ar-**H**), 7.58-7.49 (3H, m, 3×Ar-**H**), 7.43-7.35 (2H, m, 2×Ar-**H**), 4.31-4.21 (8H, m, 4×C**H**$_2$), 2.14-2.07 (4H, m, 2×C**H**$_2$), 1.93-1.83 (4H, m, 2×C**H**$_2$), 1.77 (4H, quin, J = 7.2 Hz, 2×C**H**$_2$), 1.31-1.13 (28H, m, 14×C**H**$_2$), 0.89-0.81 (6H, m, 2×C**H**$_3$), 0.81-0.65 (4H, m, 2×C**H**$_2$) ppm

^{13}C NMR (101 MHz, acetone-d6, 25 °C):
δ = 151.0 (**C**), 150.8 (**C**), 141.2 (**C**), 140.9 (**C**), 139.8 (**C**), 139.3 (**C**), 136.3 (2×**C**H), 132.0 (**C**), 131.5 (**C**), 131.2 (**C**), 130.3 (**C**), 129.14 (**C**H), 129.06 (**C**H), 127.7 (**C**H), 127.6 (**C**H), 127.4 (**C**H), 127.2 (**C**H), 127.1 (**C**H), 127.0 (**C**H), 126.9 (**C**H), 125.0 (**C**H), 123.6 (**C**H), 123.4 (**C**H), 123.0 (**C**H), 122.95 (2×**C**H), 122.90 (2×**C**H), 121.6 (2C, q, J = 322.0, 2×**C**F$_3$SO$_3$), 120.24 (**C**H), 120.17 (**C**H), 121.6 (**C**H), 55.4 (**C**), 49.9 (2×**C**H$_2$), 49.8 (2×**C**H$_2$), 40.1 (2×**C**H$_2$), 31.9 (2×**C**H$_2$), 30.14 (2×**C**H$_2$), 30.11 (2×**C**H$_2$), 29.4 (2×**C**H$_2$), 29.2 (2×**C**H$_2$), 29.0 (2×**C**H$_2$), 26.2 (2×**C**H$_2$), 26.0 (2×**C**H$_2$), 24.0 (2×**C**H$_2$), 22.7 (2×**C**H$_2$), 13.8 (2×**C**H$_3$) ppm

FT-IR (ν_{max} cm^{-1}, film):
2930 (w), 1242 (vs), 1170 (s), 1025 (vs), 769 (w), 636 (vs), 577 (m)

6.4 Substituted fluorenes

6.4.1 2,4,6-*Tris*(2-fluorophenyl)-1,3,5,2,4,6-trioxatriborinane

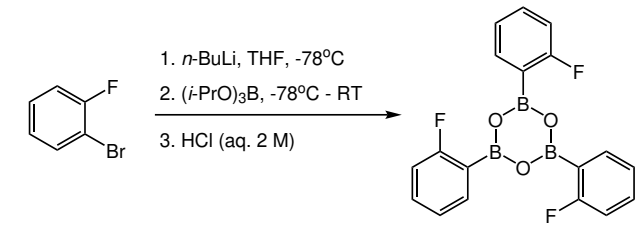

106
C_6H_4BrF
Mol Wt: 175.00

107
$C_{18}H_{12}B_3F_3O_3$
Mol Wt: 365.72

To a solution of 2-bromo-1-fluorobenzene (7.65 mL, 70.0 mmol) in THF (200 mL) at -78 °C, was added *n*-butyllithium (30.0 mL, 75.0 mmol), dropwise over 20 min. Triisopropyl borate (24.0 mL, 105 mmol) was added and the resulting mixture was warmed to room temperature over 1 hour. HCl (aq. 2 M, 100 mL) was added, then the solution was concentrated *in vacuo*. The resulting suspension was dissolved in water (200 mL) and extracted with ethyl acetate (2×50 mL). The combined organic phases were washed with water (50 mL), dried over $MgSO_4$, and concentrated *in vacuo* to yield the title compound as an off-white solid (7.61 g, 54.4 mmol, 78%). The crude mixture was used without further purification. Analytical data are consistent with literature values.[93]

MP 97.5 - 101.0 °C

LRMS (EI) m/z: 366 $[M]^+$, $C_{18}H_{12}B_3F_3O_3$, Relative intensity: 100%

^{1}H NMR (400 MHz, acetone-d6, 25 °C):
δ = 7.75 (1H, ddd, J = 7.4, 6.4, 1.9 Hz, Ar-**H**), 7.46 (1H, dddd, J = 8.3, 7.4, 5.4, 1.9 Hz, Ar-**H**), 7.18 (1H, app. tt, J = 7.4, 0.9 Hz, Ar-**H**), 7.15 (2H, d, J = 1.8 Hz, OH), 7.06 (1H, ddd, J = 9.9, 8.3, 0.9 Hz, Ar-**H**) ppm
(Dissolution in moisture-containing acetone-d6 causes hydrolysis to the boronic acid)

^{13}C NMR (101 MHz, acetone-d6, 25 °C):
δ = 167.3 (d, J_{CF} = 244.3, **C**F), 136.5 (d, J_{CF} = 8.8, **C**H), 132.8 (d, J_{CF} = 8.8, **C**H), 124.2 (d, J_{CF} = 2.9, **C**H), 115.1 (d, J_{CF} = 24.9, **C**H) ppm.
1×(**C**) not observed due to splitting by boron nucleus.

^{19}F NMR (376 MHz, acetone-d6, 25 °C):
δ = -107.3 (1F, s, Ar-**F**) ppm

6.4.2 2'-Fluoro-[1,1'-biphenyl]-2-amine

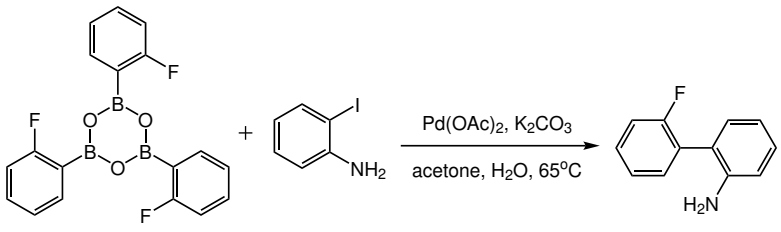

107 $C_{18}H_{12}B_3F_3O_3$ Mol Wt: 365.72

108 C_6H_6IN Mol Wt: 219.03

109 $C_{12}H_{10}FN$ Mol Wt: 187.22

The trimeric anhydride of 2-fluorophenylboronic acid **107** (2.02 g, 14.4 mmol), 2-iodoaniline (2.24 g, 10.2 mmol), and K_2CO_3 (3.50 g, 25.3 mmol) were dissolved in a mixture of acetone (18 mL) and water (24 mL), and heated at 65 °C under an argon atmosphere. $Pd(OAc)_2$ (10 mg, 0.045 mmol) was dissolved in acetone (4 mL) and added using a syringe. After 20 hours, the reaction mixture was cooled to room temperature, filtered through celite, concentrated *in vacuo* and extracted with ethyl acetate (4×40 mL). The combined organic phases were washed with water (50 mL), dried over $MgSO_4$ and concentrated *in vacuo*. Purification by column chromatography (silica; 4% to 20% ethyl acetate in hexane) gave the title compound as a brown solid (1.21 g, 6.45 mmol, 63%). Analytical data are consistent with literature values.[94]

MP 89.0 - 91.0 °C

LRMS (ESI+) m/z: 188 $[M+H]^+$, $C_{12}H_{10}FN$, Relative intensity: 100%

^{1}H NMR (400 MHz, acetone-d6, 25 °C):
δ = 7.41 (1H, dddd, J = 8.2, 7.2, 5.4, 2.1 Hz, Ar-**H**), 7.38 (1H, tdd, J = 7.6, 2.1, 0.4, Ar-**H**), 7.27 (1H, ddd, J = 7.6, 7.3, 1.2 Hz, Ar-**H**), 7.22 (1H, dddd, J = 10.3, 8.3, 1.2, 0.4 Hz, Ar-**H**), 7.12 (1H, ddd, J = 8.1, 7.3, 1.5 Hz, Ar-**H**), 7.02 (1H, dddd, J = 7.8, 1.5, 0.7, 0.4 Hz, Ar-**H**), 6.83 (1H, ddd, J = 8.1, 1.3, 0.5 Hz, Ar-**H**), 6.70 (1H, ddd, J = 7.7, 7.3, 1.2 Hz, Ar-**H**), 4.35 (2H, br s, 2×N**H**$_2$) ppm

^{13}C NMR (101 MHz, acetone-d6, 25 °C):
δ = 160.3 (d, J_{CF} = 245.0, **C**), 146.0 (**C**), 132.3 (d, J_{CF} = 3.7, **C**H), 131.0 (**C**H), 129.7 (d, J_{CF} = 8.1, **C**H), 129.2 (**C**H), 127.5 (d, J_{CF} = 16.9, **C**), 124.9 (d, J_{CF} = 3.7, **C**H), 120.9 (**C**), 117.2 (**C**H), 116.2 (d, J_{CF} = 22.7, **C**H), 115.6 (**C**H) ppm

^{19}F NMR (376 MHz, acetone-d6, 25 °C):
δ = -109.7 (1F, s, Ar-**F**) ppm

6.4.3 3'-Fluoro-[1,1'-biphenyl]-2-amine

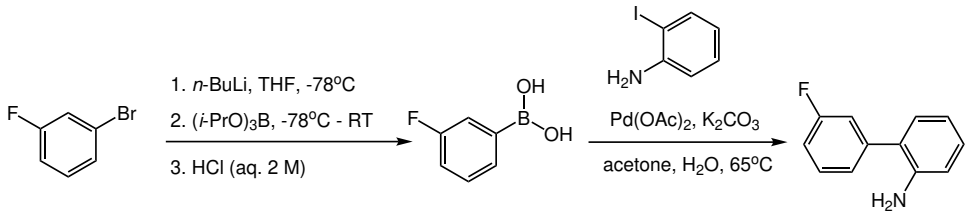

110
C_6H_4BrF
Mol Wt: 175.00

111
$C_6H_6BFO_2$
Mol Wt: 139.92

112
$C_{12}H_{10}FN$
Mol Wt: 187.22

Synthesised following the procedures detailed in 6.4.1 and 6.4.2. Boronic acid intermediate **111** (m/z: 366, $C_{18}H_{12}B_3O_3F_3$, Relative intensity: 100%) was used without purification. The following reagents, conditions and column conditions were used:
3-fluorobromobenzene: 25.0 g, 143 mmol
n-butyllithium (2.5 M in hexanes): 60 mL, 150 mL
triisopropylborate: 44 mL, 191 mmol
HCl (2.0 M, aq.): 200 mL, 400 mmol
THF: 400 mL
3-fluorophenylboronic acid: 3.80 g, 27 mmol
2-iodoaniline: 6.56 g, 30 mmol
Pd(OAc): 70 mg, 0.30 mmol
K_2CO_3: 9.00 g, 65 mmol
H_2O: 65 mL
acetone: 60 mL
Column chromatography: silica, 0 - 10% ethyl acetate in hexane
Yield: 4.44 g, 23.7 mmol, 88%, colourless oil
Analytical data are consistent with literature values.[94]

LRMS (EI) m/z: 188 $[M+H]^+$, $C_{12}H_{10}FN$, Relative intensity: 55%

^{1}H NMR (400 MHz, acetone-d6, 25 °C):
δ = 7.47 (1H, dddd, J = 8.2, 8.0, 6.2, 0.4 Hz, Ar-**H**), 7.28 (1H, ddd, J = 7.6, 1.5, 1.4 Hz, Ar-**H**), 7.20 (1H, dddd, J = 10.3, 2.7, 1.6, 0.4 Hz, Ar-**H**), 7.13-7.07 (2H, m, 2×Ar-**H**), 7.05 (1H, ddd, J = 7.7, 1.7, 0.2 Hz, Ar-**H**), 6.83 (1H, ddd, J = 8.1, 1.2, 0.4 Hz, Ar-**H**), 6.71 (1H, ddd, J = 7.6, 7.4, 1.2 Hz, Ar-**H**), 4.51 (2H, br s, N**H**$_2$) ppm

^{13}C NMR (101 MHz, acetone-d6, 25 °C):
δ = 163.3 (d, J_{CF} = 244.3 Hz, **C**), 145.2 (**C**), 143.0 (d, J_{CF} = 8.1 Hz, **C**), 130.9 (d, J_{CF} = 8.8 Hz, **C**H), 130.4 (**C**H), 129.1 (**C**H), 125.6 (d, J_{CF} = 2.2 Hz, **C**), 125.2 (d, J_{CF} = 2.9 Hz, **C**H), 117.8 (**C**H), 115.94 (**C**H), 115.87 (d, J_{CF} = 21.3 Hz, **C**H), 113.8 (d, J_{CF} = 21.3 Hz, **C**H) ppm

^{19}F NMR (376 MHz, acetone-d6, 25 °C):
δ = -113.6 (1F, s, Ar-**F**) ppm

6.4.4 2-Fluoro-2'-iodo-1,1'-biphenyl

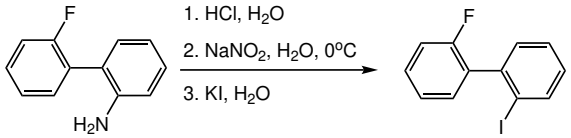

109
$C_{12}H_{10}FN$
Mol Wt: 187.22

113
$C_{12}H_8FI$
Mol Wt: 298.10

A solution of HCl (conc., 0.23 mL, 2.80 mmol) in water (0.85 mL) was added slowly to 2-fluoro-2'-amino-1,1'-biphenyl **109** (95 mg, 0.51 mmol). The mixture was cooled to 0-5 °C, then $NaNO_2$ (260 mg, 3.77 mmol) in water (1.0 mL) was added. After 1 h and 40 min at 0-5 °C, KI (0.17 g, 1.02 mmol) in water (1.0 mL) was added resulting in immediate precipitation of a dark red solid. Water (2.0 mL) was added to facilitate stirring and after 22 h, ethyl acetate (20 mL), water (10 mL), and sodium metabisulfite (500 mg) were added. The aqueous phase was washed with ethyl acetate (3×10 mL) and the combined organic phases were dried over $MgSO_4$ and concentrated *in vacuo*. Purification by column chromatography (silica; 2% to 30% ethyl acetate in hexane) gave the title compound as a colourless oil (102 mg, 0.34 mmol, 67%). Analytical data are consistent with literature values.[(94)]

GCMS (EI) m/z: 298 $[M]^+$, $C_{12}H_8FI$, Relative intensity: 100%

^{1}H NMR (400 MHz, acetone-d6, 25 °C):
δ = 8.01 (1H, ddd, J = 8.0, 1.2, 0.5 Hz, Ar-**H**), 7.51 (1H, ddd, J = 7.6, 7.4, 1.2 Hz, Ar-**H**), 7.52-7.46 (1H, m, Ar-**H**), 7.35 (1H, ddd, J = 7.6, 1.7, 0.5 Hz, Ar-**H**), 7.30 (1H, tdd, J = 7.7, 1.0, 0.4 Hz, Ar-**H**), 7.27 (1H, tdd, J = 7.3, 2.3, 0.5 Hz, 2×Ar-**H**), 7.23 (1H, dddd, J = 9.5, 8.4, 1.0, 0.4 Hz, Ar-**H**), 7.18 (1H, ddd, J = 8.0, 7.3, 1.7 Hz, Ar-**H**) ppm

^{13}C NMR (101 MHz, acetone-d6, 25 °C):
δ = 159.4 (d, J_{CF} = 245.0, **C**), 141.7 (**C**), 139.5 (**C**H), 132.3 (d, J_{CF} = 16.1, **C**), 131.8 (d, J_{CF} = 2.9, **C**H), 130.9 (**C**H), 130.5 (d, J_{CF} = 8.1, **C**H), 130.0 (**C**H), 128.6 (**C**H), 124.5 (d, J_{CF} = 3.7, **C**H), 115.9 (**C**H), 99.4 (**C**) ppm

^{19}F NMR (376 MHz, acetone-d6, 25 °C):
δ = -114.7 (1F, s, Ar-**F**) ppm

6.4.5 3'-Fluoro-2-iodo-1,1'-biphenyl

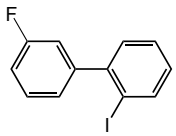

114

$C_{12}H_8FI$
Mol Wt: 298.10

Synthesised following the procedure detailed in 6.4.4 with the following reagent amounts and column conditions:
2-(3'-fluorophenyl)aniline: 2.48 g, 13.2 mmol
HCl (37%): 5.50 mL, 67.0 mmol
$NaNO_2$: 6.50 g, 94.2 mmol
KI: 4.40 g, 26.5
H_2O: 45 mL
Column chromatography: silica, hexane
Yield: 2.10 g, 7.04 mmol, 53%, colourless oil
Analytical data are consistent with literature values.[94]

GCMS (EI) m/z: 298 $[M]^+$, $C_{12}H_8FI$, Relative intensity: 100%

^{1}H NMR (400 MHz, acetone-d6, 25 °C):
δ = 8.01 (1H, ddd, J = 7.9, 1.3, 0.4 Hz, Ar-**H**), 7.53-7.46 (2H, m, 2×Ar-**H**), 7.36 (1H, ddd, J = 7.6, 1.7, 0.4 Hz, Ar-**H**), 7.22-7.13 (3H, m, 3×Ar-**H**), 7.10 (1H, dddd, J = 9.9, 2.6, 1.6, 0.5 Hz, Ar-**H**) ppm

^{13}C NMR (101 MHz, acetone-d6, 25 °C):
δ = 162.6 (d, J_{CF} = 244.3 Hz, **C**), 146.7 (d, J_{CF} = 8.1 Hz, **C**), 145.6 (d, J_{CF} = 2.2 Hz, **C**), 140.0 (**C**H), 130.4 (**C**H), 130.3 (d, J_{CF} = 8.8 Hz, **C**H), 129.8 (**C**H), 128.8 (**C**H), 125.7 (d, J_{CF} = 2.9 Hz, **C**H), 116.4 (d, J_{CF} = 22.0 Hz, **C**H), 114.7 (d, J_{CF} = 20.5 Hz, **C**H), 97.8 (**C**I) ppm

^{19}F NMR (376 MHz, acetone-d6, 25 °C):
δ = -114.0 (1F, s, Ar-**F**) ppm

6.4.6 4-Fluorofluorene

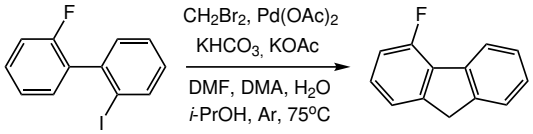

113
$C_{12}H_8FI$
Mol Wt: 298.10

66a
$C_{13}H_9F$
Mol Wt: 184.21

A mixture of 2-fluoro-2-iodobiphenyl **113** (1.00 g, 3.35 mmol), CH_2Br_2 (1.0 mL, 14.3 mmol), $Pd(OAc)_2$ (336 mg, 1.5 mmol), KOAc (3.00 g, 30.0 mmol), $NaHCO_3$ (2.30 g, 32.0 mmol), DMF (20 mL), DMA (6.7 mL), H_2O (8.3 mL), and IPA (0.5 mL, 65 mmol) was sonicated under a flow of Ar for 15 min, then heated at 75 °C for 18 h. The mixture was cooled to r.t., further $Pd(OAc)_2$ (336 mg, 1.5 mmol) was added, and the stirrer bar was replaced due to palladium deposition. The mixture was heated at 75 °C under Ar for 22 h, then cooled to room temperature and extracted with ethyl acetate (3×50 mL). The combined organic phases were washed with water (50 mL), dried over $MgSO_4$, and concentrated *in vacuo*. Purification by column chromatography (silica, hexane) gave the title compound as a colourless oil (334 mg, 1.81 mmol, 54%). Analytical data are consistent with literature values.[(94)]

GCMS (EI) m/z: 184 $[M]^+$, $C_{13}H_9F$, Relative intensity: 86%

^{1}H NMR (400 MHz, $CDCl_3$, 25 °C):
δ = 8.02 (1H, d, J = 7.6 Hz, Ar-**H**), 7.56 (1H, app. dquin, J = 7.5, 1.0 Hz, Ar-**H**), 7.43 (1H, t, J = 7.6 Hz, Ar-**H**), 7.38-7.32 (2H, m, 2×Ar-**H**), 7.27 (1H, ddd, J = 8.1, 7.5, 5.0 Hz, Ar-**H**), 7.08 (1H, ddd, J = 10.0, 8.2, 0.6 Hz, Ar-**H**), 3.97 (2H, s, C**H**$_2$) ppm

^{13}C NMR (101 MHz, $CDCl_3$, 25 °C):
δ = 158.5 (d, J_{CF} = 250.2 Hz, **C**), 146.1 (d, J_{CF} = 5.9 Hz, **C**), 142.5 (**C**), 138.8 (d, J_{CF} = 2.9 Hz, **C**), 128.9 (d, J_{CF} = 14.7 Hz, **C**), 127.8 (d, J_{CF} = 7.3 Hz, **C**H), 127.0 (**C**H), 126.8 (**C**H), 124.7 (**C**H), 123.4 (d, J_{CF} = 5.1 Hz, **C**H), 120.6 (d, J_{CF} = 2.9 Hz, **C**H), 113.7 (d, J_{CF} = 19.8 Hz, **C**H), 37.4 (**C**H$_2$) ppm

^{19}F NMR (376 MHz, $CDCl_3$, 25 °C):
δ = -120.7 (1F, s, Ar-**F**) ppm

UV-Vis (MeCN): λ_{max} = 260 (39200)

6.4.7 3-Fluorofluorene

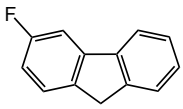

66b

$C_{13}H_9F$
Mol Wt: 184.21

Synthesised following the procedure detailed in 6.4.6 with the following reagent amounts and column conditions:
2-(3'fluorophenyl)iodobenzene:
245 mg, 0.82 mmol
CH_2Br_2: 0.23 mL, 3.3 mmol
$Pd(OAc)_2$: 90 mg, 0.40 mmol
KOAc: 726 mg, 7.40 mmol
$NaHCO_3$: 656 mg, 7.81 mmol
DMF: 5.0 mL
DMA: 1.7 mL
H_2O: 2.1 mL
IPA: 120 μL, 16 mmol
Column chromatography: silica, hexane
Yield: 66.3 mg, 0.360 mmol, 44%
Analytical data are consistent with literature values.[94]

GCMS (EI) m/z: 184 $[M]^+$, $C_{13}H_9F$, Relative intensity: 96%

^{1}H NMR (400 MHz, $CDCl_3$, 25 °C):
δ = 7.75 (1H, d, J = 7.3 Hz, Ar-**H**), 7.56 (1H, ddt, J = 7.4, 2.0, 0.9 Hz, Ar-**H**), 7.50-7.43 (2H, m, 2×Ar-**H**), 7.40 (1H, app. tdt, J = 7.5, 1.3, 0.6 Hz, Ar-**H**), 7.37-7.32 (1H, m, Ar-**H**), 7.01 (1H, ddd, J = 9.3, 8.3, 2.5 Hz, Ar-**H**), 3.87 (2H, s, C**H**$_2$) ppm

^{13}C NMR (101 MHz, $CDCl_3$, 25 °C):
δ = 162.6 (d, J_{CF} = 242.8 Hz, **C**), 144.2 (**C**), 143.6 (d, J_{CF} = 8.8 Hz, **C**), 141.0 (d, J_{CF} = 2.9 Hz, **C**), 138.4 (d, J_{CF} = 2.2 Hz, **C**), 127.3 (**C**H), 126.8 (**C**H), 125.9 (d, J_{CF} = 8.8 Hz, **C**H), 125.1 (**C**H), 120.1 (**C**H), 113.5 (d, J_{CF} = 22.7 Hz, **C**H), 106.8 (d, J_{CF} = 22.7 Hz, **C**H), 36.3 (**C**H$_2$) ppm

^{19}F NMR (376 MHz, $CDCl_3$, 25 °C):
δ = -116.7 (1F, s, Ar-**F**) ppm

UV-Vis (MeCN): λ_{max} = 258 (25100)

6.5 Phenanthrenes

6.5.1 2-(6-Bromohexyl)isoindoline-1,3-dione

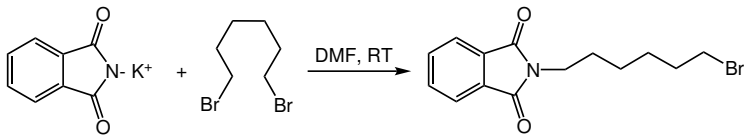

115 $C_8H_4NO_2K$ Mol Wt: 146.13

116 $C_6H_{12}Br_2$ Mol Wt: 243.97

117 $C_{14}H_{16}BrNO_2$ Mol Wt: 310.19

A suspension of potassium phthalimide (70.0 g, 380 mmol) and 1,6-dibromohexane (112 mL, 730 mmol) in dimethyl formamide (140.0 mL) was stirred under argon for 18 h. The mixture was partitioned between ethyl acetate (140 mL) and water (140 mL), then the aqueous phase was separated, and washed with ethyl acetate (100 mL). The combined organic phases were washed with water (5×1 L), dried with $MgSO_4$, then the solvent was removed *in vacuo*. Purification by column chromatography (silica; 30% DCM in petroleum ether) yielded the title compound as a white solid, (64.0 g, 206 mmol, 55%). Analytical data are consistent with literature values.[95]

MP 55.0 - 57.0 °C (lit. 57 - 58 °C)[96]

LRMS (ESI+) m/z: 310 $[M+H]^+$, $C_{14}H_{16}BrNO_2$, Relative intensity: 100%

^{1}H NMR (400 MHz, $CDCl_3$, 25 °C):
δ = 7.88-7.80 (2H, m, 2×Ar-**H**), 7.75-7.68 (2H, m, 2×Ar-**H**), 3.72-3.65 (2H, t, J = 7.2 Hz, C**H**$_2$), 3.39 (2H, t, J = 6.8 Hz, C**H**$_2$), 1.90-1.80 (2H, m, C**H**$_2$), 1.74-1.65 (2H, m, C**H**$_2$), 1.54-1.43 (2H, m, C**H**$_2$), 1.42-1.32 (2H, m, C**H**$_2$) ppm

^{13}C NMR (101 MHz, $CDCl_3$, 25 °C):
δ = 168.4 (2×**C**), 133.9 (2×**C**), 132.1 (2×**C**H), 123.2 (2×**C**H), 37.8 (**C**H$_2$), 33.7 (**C**H$_2$), 32.6 (**C**H$_2$), 28.4 (**C**H$_2$), 27.7 (**C**H$_2$), 26.0 (**C**H$_2$) ppm

6.5.2 2-(6-(1*H*-Imidazol-1-yl)hexyl)isoindoline-1,3-dione

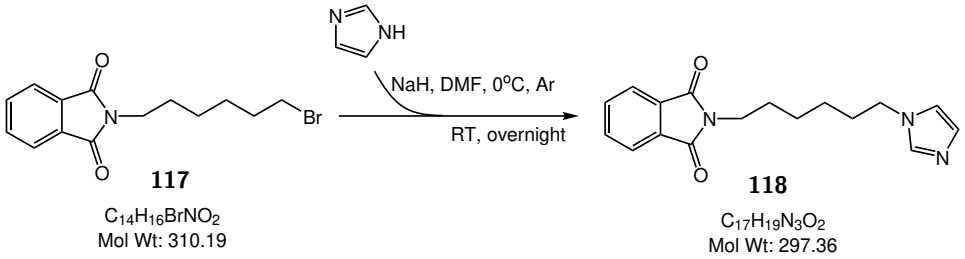

Imidazole (3.00 g, 44.1 mmol) was dissolved in dimethylformamide (30 mL), and cooled to 0 °C under argon. The mixture was cannulated onto cold NaH (60% suspension in mineral oil, 1.91 g, 47.8 mmol), then the resulting mixture was warmed to room temperature. After 2 h, the mixture was cooled to 0 °C, cannulated onto phthalimide **117** (13.6 g, 43.8 mmol) at 0 °C then warmed to room temperature. After 3 days, The mixture was partitioned between water (50 mL) and ethyl acetate (50 mL), then the aqueous phase was separated and extracted with ethyl acetate (3×50 mL). The combined organic phases were washed with water (6×100 mL), dried over $MgSO_4$, and concentrated *in vacuo* yielding a yellow/brown oil to which a small amount of petroleum ether was added causing a white solid to precipitate from the mixture. The solids were washed with petroleum ether yielding the title compound as a white solid. (9.62 g, 32.3 mmol, 74%). Analytical data are consistent with literature values.[95]

MP 82.0 - 85.0 °C

LRMS (ESI+) m/z: 298 $[M+H]^+$, $C_{17}H_{19}N_3O_2$, Relative intensity: 100%

^{1}H NMR (400 MHz, $CDCl_3$, 25 °C):
δ = 7.85-7.78 (2H, m, 2×Ar-**H**), 7.73-7.64 (2H, m, 2×Ar-**H**), 7.43 (1H, br s, Ar-**H**), 7.02 (1H, br s, Ar-**H**), 6.88 (1H, br s, Ar-**H**), 3.90 (2H, t, J = 7.2 Hz, C**H**$_2$), 3.65 (2H, t, J = 7.2 Hz, C**H**$_2$), 1.75 (2H, quin, J = 7.2 Hz, C**H**$_2$), 1.65 (2H, quin, J = 7.2 Hz, C**H**$_2$), 1.42-1.28 (4H, m, 2×C**H**$_2$) ppm

^{13}C NMR (101 MHz, $CDCl_3$, 25 °C):
δ = 168.4 (2×**C**), 136.9 (**C**H), 133.9 (2×**C**H), 132.0 (2×**C**), 129.1 (**C**H), 123.1 (2×**C**H), 118.7 (**C**H), 46.9 (**C**H$_2$), 37.6 (**C**H$_2$), 30.8 (**C**H$_2$), 28.3 (**C**H$_2$), 26.2 (**C**H$_2$), 26.0 (**C**H$_2$) ppm

6.5.3 6-(1*H*-Imidazol-1-yl)hexan-1-amine

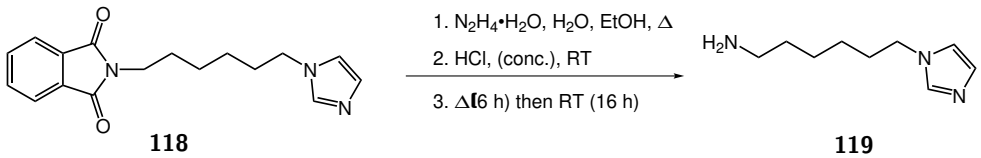

118
$C_{17}H_{19}N_3O_2$
Mol Wt: 297.36

119
$C_9H_{17}N_3$
Mol Wt: 167.26

Phthalimide **118** (2.85 g, 9.58 mmol) was dissolved in a 3:1 mixture of ethanol and water (600 mL), then hydrazine monohydrate (1.02 mL, 21.0 mmol) was added. The mixture was heated at reflux for 18 hours, then cooled to room temperature. HCl (conc. 7.0 mL, 83 mmol) was added dropwise, then the mixture was heated at reflux for 6 hours, then cooled to room temperature for a further 16 hours. The solvent was removed*in vacuo* and the resulting mixture was partitioned between water (150 mL) and DCM (150 mL). The aqueous phase was washed with DCM (2×50 mL), then basified to pH 11 with NaOH (aq., 2 M). The basified aqueous solution was extracted with DCM (3×100 mL), then the combined organic phases were dried over $MgSO_4$. The solvent was then removed *in vacuo* yielding the title compound as a yellow oil, (1.22 g, 7.31 mmol, 76%). Analytical data are consistent with literature values.[95]

LRMS (ESI+) m/z: 168 $[M+H]^+$, $C_9H_{17}N_3$, Relative intensity: 100%

^{1}H NMR (400 MHz, $CDCl_3$, 25 °C):
δ = 7.37 (1H, s, Ar-**H**), 6.95 (1H, s, Ar-**H**), 6.82 (1H, s, Ar-**H**), 3.84 (2H, t, J = 7.1 Hz, NC**H**$_2$), 2.59 (2H, t, J = 6.8 Hz, NC**H**$_2$), 1.76-1.64 (4H, m, C**H**$_2$ and N**H**$_2$), 1.41-1.17 (6H, m, 3×C**H**$_2$) ppm

^{13}C NMR (101 MHz, $CDCl_3$, 25 °C):
δ = 136.8 (**C**H), 129.1 (**C**H), 118.5 (**C**H), 46.7 (**C**H$_2$), 41.6 (**C**H$_2$), 33.0 (**C**H$_2$), 30.8 (**C**H$_2$), 26.14 (**C**H$_2$), 26.09 (**C**H$_2$) ppm

6.5.4 3,4-Dimethoxycyclobut-3-ene-1,2-dione

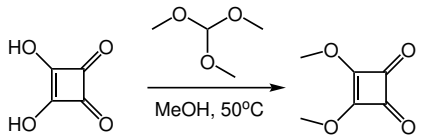

71

$C_4H_2O_4$
Mol Wt: 114.06

120

$C_6H_6O_4$
Mol Wt: 142.11

3,4-Dihydroxycyclobut-3-ene-1,2-dione (39.0 g, 342 mmol), and trimethyl orthoformate (76.0 mL, 695 mmol) were dissolved in methanol (250 mL) and the mixture was heated at 50 °C for 20 hours. The solvent was removed *in vacuo*, and the residue was partitioned between DCM (200 mL) and saturated aqueous $NaHCO_3$ (100 mL). The aqueous phase was separated and extracted with DCM (3×50 mL), then the combined organic phases were washed with H_2O (3×100 mL), dried over $MgSO_4$, and concentrated *in vacuo*. Recrystallisation from ethyl acetate gave the title compound as a white solid (16.0 g, 113 mmol, 33%). Analytical data are consistent with literature values.[97]

MP 53.5 - 55.5 °C (lit. 52 - 54 °C)

LRMS (ESI+) m/z: 143 $[M+H]^+$, $C_6H_6O_4$, Relative intensity: 100%

^{1}H NMR (400 MHz, $CDCl_3$, 25 °C):
δ = 4.35 (6H, s, 2×C**H**$_3$) ppm

^{13}C NMR (101 MHz, $CDCl_3$, 25 °C):
δ = 189.1 (2×**C**), 184.4 (2×**C**), 60.9 (2×**C**H$_3$) ppm

6.5.5 4-Hydroxy-2,3-dimethoxy-4-phenylcyclobut-2-en-1-one

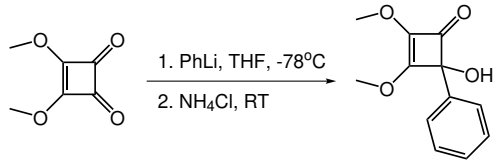

120
$C_6H_6O_4$
Mol Wt: 142.11

73a
$C_{12}H_{12}O_4$
Mol Wt: 220.22

Dimethoxycyclobutenedione **120** (1.01 g, 7.09 mmol) was dissolved in THF (60 mL) and cooled to -78 °C under argon flow. Phenyllithium (1.9 M in dibutyl ether, 4.75 mL, 9.03 mmol) was added dropwise and the mixture was stirred for 90 min at -78 °C. After warming to room temperature, sat. NH_4Cl (30.0 mL) was added, and the mixture was extracted with CH_2Cl_2 (3×50 mL). The combined organic phases were dried over $MgSO_4$ and the solvent was removed *in vacuo*, giving the title compound as a yellow solid (752 mg, 3.41 mmol, 48%). Analytical data are consistent with literature values.[98]

MP 200.0 - 204.0 °C

LRMS (ESI+) m/z: 189 $[M\text{-}OMe]^+$, $C_{12}H_{12}O_4$, Relative intensity: 100%

^{1}H NMR (400 MHz, $CDCl_3$, 25 °C):
δ = 7.50-7.55 (2H, m, 2×Ar-**H**), 7.29-7.42 (3H, m, 3×Ar-**H**), 4.05 (3H, s, C**H**$_3$), 4.00 (3H, s, C**H**$_3$), 3.73 (1H, br s, O**H**) ppm

^{13}C NMR (101 MHz, $CDCl_3$, 25 °C):
δ = 194.8 (**C**), 192.8 (**C**), 192.3 (**C**), 173.7 (**C**), 132.8 (**C**H), 129.1 (2×**C**H), 127.8 (2×**C**H), 127.6 (**C**), 61.7 (2×**C**H$_3$) ppm

6.5.6 3,4,4-Trimethoxy-2-phenylcyclobut-2-en-1-one

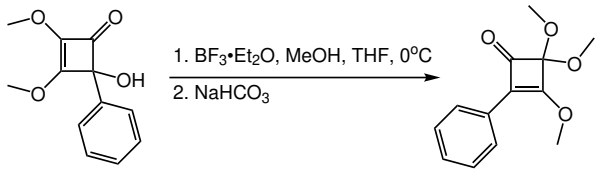

73a
$C_{12}H_{12}O_4$
Mol Wt: 220.22

74a
$C_{13}H_{14}O_4$
Mol Wt: 234.25

Alcohol **73a** was dissolved in THF (50 mL) at 0 °C. MeOH (0.25 mL, 6.27 mmol) and $BF_3{\cdot}Et_2O$ were added and the mixture was stirred at 0 °C for 3 hours. After warming to room temperature, sat. $NaHCO_3$ (20 mL) was added, and the mixture was extracted with Et_2O (3×30 mL). The combined organic phases were washed with water (50 mL) and dried over $MgSO_4$, then the solvent was removed *in vacuo*. Purification by column chromatography (silica; 10% ethyl acetate in hexane) gave **74**, slightly impure, as a yellow oil (505 mg, 2.15 mmol, 69%) which was used without further purification. Analytical data are consistent with literature values.[99]

LRMS (EI) m/z: 234 $[M]^+$, $C_{13}H_{14}O_4$, Relative intensity: 234%

^{1}H NMR (400 MHz, $CDCl_3$, 25 °C):
δ = 7.78-7.83 (2H, m, 2×Ar-**H**), 7.36-7.41 (2H, m, 2×Ar-**H**), 7.29-7.34 (1H, m, Ar-**H**), 4.26 (3H, s, C**H**$_3$), 3.60 (6H, s, 2×C**H**$_3$) ppm

^{13}C NMR (101 MHz, $CDCl_3$, 25 °C):
δ = 189.6 (**C**), 180.7 (**C**), 129.2 (**C**), 128.6 (**C**H), 128.5 (2×**C**H), 128.1 (**C**), 127.1 (2×**C**H), 115.2 (**C**), 60.2 (**C**H$_3$), 53.9 (2×**C**H$_3$) ppm. A cyclobutenedione is produced by hydrolysis of the acetal. Peaks corresponding to this impurity have been omitted.

6.5.7 3,4-Diphenylcyclobut-3-ene-1,2-dione

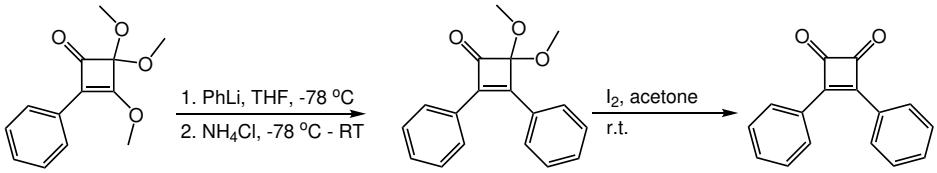

74a
$C_{13}H_{14}O_4$
Mol Wt: 234.25

121
$C_{18}H_{16}O_3$
Mol Wt: 280.32

75a
$C_{16}H_{10}O_2$
Mol Wt: 234.25

To a solution of cyclobutenone **74a** (840 mg, 3.59 mmol) in THF (60 mL), at -78 °C, was added, dropwise, phenyllithium (1.9 M in dibutyl ether, 2.0 mL, 3.80 mmol). The mixture was stirred at -78 °C for 90 min, then NH_4Cl (sat. aq., 45 mL) was added. After warming to room temperature, the mixture was extracted with CH_2Cl_2 (3×50 mL) and the combined organic phases were dried over $MgSO_4$. The solvent was removed *in vacuo* giving cyclobutenone **121**, as a yellow oil, which was dissolved in acetone (25 mL). Iodine (104 mg, 0.410 mmol) was added and the mixture was stirred at room temperature for 30 min, then the solvent was removed *in vacuo*. The mixture was dissolved in Et_2O (50 mL) and washed with $Na_2S_2O_3$ (sat. aq., 25 mL) and water (2×50 mL). The aqueous phase was washed with Et_2O (2×50 mL) and the combined organic phases were dried over $MgSO_4$. The solvent was removed *in vacuo* then purification by column chromatography (silica; 5 - 100% Et_2O in hexane) gave the title compound as a yellow solid (816 mg, 3.48 mmol, 97%). Analytical data are consistent with literature values.[100]

MP 91.5 - 93.5 °C (lit. 95 - 96 °C)

LRMS (ESI+) m/z: 235 $[M+H]^+$, $C_{16}H_{10}O_2$, Relative intensity: 100%

^{1}H NMR (400 MHz, $CDCl_3$, 25 °C):
δ = 8.04-8.13 (4H, m, 4×Ar-**H**), 7.50-7.66 (6H, m, 6×Ar-**H**) ppm

^{13}C NMR (101 MHz, $CDCl_3$, 25 °C):
δ = 196.1 (2×**C**), 187.5 (2×**C**), 133.4 (2×**C**H), 129.3 (4×**C**H), 128.2 (4×**C**H), 128.1 (2×**C**) ppm

6.5.8 Phenanthro[9,10-*c*]furan-1,3-dione

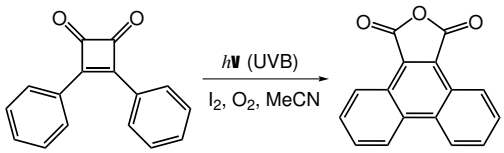

75a
$C_{16}H_{10}O_2$
Mol Wt: 234.25

122a
$C_{16}H_8O_3$
Mol Wt: 248.24

A solution of cyclobutenedione **75a** (535 mg, 2.28 mmol) and iodine (100 mg, 0.39 mmol) in acetonitrile (120 mL) was irradiated with UV-B light, under circulating flow conditions described in Chapter 3 (flow set up 3), at a flow rate of 20 mL min^{-1}, for 3 hours. The resulting precipitate was filtered from the mother liquor giving an orange solid (270 mg, 1.09 mmol, 48%) that was used without further purification. Analytical data are consistent with literature values.[101]

MP 317.5 - 319.0 °C

LRMS (EI) Found: 248.2 $[M]^+$, $C_{16}H_8O_3$, Required: 248.2

^{1}H NMR (400 MHz, $CDCl_3$, 25 °C):
δ = 9.04 (2H, ddd, J = 8.1, 0.9, 0.5 Hz, 2×Ar-**H**), 8.82 (2H, d, J = 8.4 Hz, 2×Ar-**H**), 7.95 (2H, ddd, J = 8.4, 7.0, 1.4 Hz, 2×Ar-**H**), 7.87 (2H, ddd, J = 8.2, 7.1, 1.0 Hz, 2×Ar-**H**) ppm

^{13}C NMR (101 MHz, $CDCl_3$, 25 °C):
δ = 131.0 (2×**C**H), 129.1 (2×**C**H), 126.4 (2×**C**H), 123.5 (2×**C**H) ppm.
8×**C** not observed/coincident.

UV-Vis (MeCN): λ_{max} = 356 (8760)

6.5.9 4-Hydroxy-2,3-dimethoxy-4-(4-methoxyphenyl)cyclobut-2-en-1-one

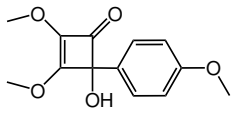

73b

Synthesised
following the procedure detailed in 6.5.5, with the following reagent amounts and column conditions:
dimethylsquarate **120**: 2.30 g, 16.2 mmol
4-bromoanisole: 2.05 mL, 16.3 mmol
n-butyllithium: 6.50 mL, 16.3 mmol
THF: 160 mL
Column chromatography: silica, 0 - 40% ethyl acetate in hexane
Yield: 2.85 g, 11.4 mmol, 70%
Analytical data are consistent with literature values.[97]

LRMS (ESI+) m/z: 251 $[M+H]^+$, $C_{13}H_{14}O_5$, Relative intensity: 100%

^{1}H NMR (400 MHz, $CDCl_3$, 25 °C):
δ = 7.47-7.40 (2H, m, 2×Ar-**H**), 6.91-6.87 (2H, m, 2×Ar-**H**), 4.06 (3H, s, C**H**$_3$), 4.00 (3H, s, C**H**$_3$), 3.80 (3H, s, C**H**$_3$), 3.54 (1H, s, O**H**) ppm

^{13}C NMR (101 MHz, $CDCl_3$, 25 °C):
δ = 184.5 (**C**), 166.4 (**C**), 159.6 (**C**), 135.0 (**C**), 129.3 (**C**), 127.1 (2×**C**H), 113.9 (2×**C**H), 87.2 (**C**), 60.1 (**C**H$_3$), 58.6 (**C**H$_3$), 55.2 (**C**H$_3$) ppm. Many other peaks observed. Used without further purification.

6.5.10 3-(4-Methoxyphenyl)-4-phenylcyclobut-3-ene-1,2-dione

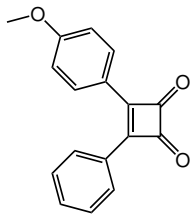

75b

$C_{17}H_{12}O_3$
Mol Wt: 264.28

Synthesised following the procedures detailed in 6.5.6 and 6.5.7, without purification of the trimethoxycyclobuteneone intermediate, with the following reagent amounts and column conditions:
alcohol 6.5.9: 2.85 g, 11.4 mmol
MeOH: 0.90 mL, 22.8 mmol
$BF_3{\cdot}Et_2O$: 1.70 mL, 13.8 mmol
THF: 2×80 mL
PhLi (1.9 M in DBE): 4.3 mL, 7.98 mmol
I_2: 300 mg, 1.20 mmol
acetone: 50 mL
Column chromatography: silica, 0 - 20% ethyl acetate in hexane
Yield: 590 mg, 2.23 mmol, 20%
Analytical data are consistent with literature values.[102]

MP 131.5 - 134.0 °C

LRMS (ESI+) m/z: 265 $[M+H]^+$, $C_{17}H_{12}O_3$, Relative intensity: 100%

^{1}H NMR (400 MHz, $CDCl_3$, 25 °C):
δ = 8.19-8.11 (2H, m, 2×Ar-**H**), 8.07-8.00 (2H, m, 2×Ar-**H**), 7.62-7.50 (3H, m, 3×Ar-**H**), 7.08-7.01 (2H, m, 2×Ar-**H**), 3.92 (3H, s, C**H**$_3$) ppm

^{13}C NMR (101 MHz, $CDCl_3$, 25 °C):
δ = 196.7 (**C**), 195.7 (**C**), 186.3 (**C**), 185.2 (**C**), 164.0 (**C**), 132.7 (**C**H), 130.7 (2×**C**H), 129.2 (2×**C**H), 128.5 (**C**), 127.9 (2×**C**H), 120.9 (**C**), 114.8 (2×**C**H), 55.6 (**C**H$_3$) ppm

6.5.11 6-Methoxyphenanthro[9,10-*c*]furan-1,3-dione

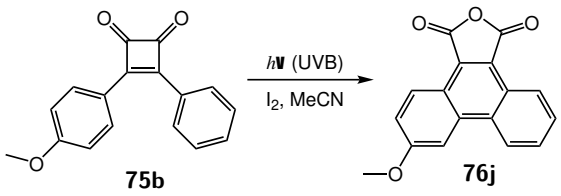

75b
$C_{17}H_{12}O_3$
Mol Wt: 264.28

76j
$C_{17}H_{10}O_4$
Mol Wt: 278.26

A solution of cyclobutenedione **75b** (250 mg, 0.946 mmol) and iodine (200 mg, 0.946 mmol) in acetonitrile (50 mL) was irradiated with UV-B light, under circulating flow conditions described in Chapter 3 (flow set up 2), at a flow rate of 15 mL min^{-1}, for a total of 23 hours across 3 sessions. The reaction was monitored by UV/Visible spectroscopy, and terminated when there was negligible cyclobutenedione **75b** remaining in the reaction mixture. The solvent was removed *in vacuo*. DCM (50 mL) was added and the resulting precipitate was filtered through a glass frit, then concentrated *in vacuo*. Purification by column chromatography (silica; 0 - 100% DCM in hexane) gave the title compound as a yellow solid (67 mg, 0.241 mmol, 25%)

MP 219.5 - 221.5 °C

LRMS (ESI+) m/z: 279 $[M+H]^+$, $C_{17}H_{10}O_4$, Relative intensity: 100%

^{1}H NMR (400 MHz, CD_2Cl_2, 25 °C):
δ = 8.91 (1H, ddd, J = 8.1, 1.7, 0.6 Hz, Ar-**H**), 8.86 (1H, d, J = 9.0 Hz, Ar-**H**), 8.70 (1H, dddd, J = 8.6, 1.7, 0.6 Hz, Ar-**H**), 8.09 (1H, br d, J = 2.4 Hz, Ar-**H**), 7.90 (1H, ddd, J = 8.7, 7.0, 1.7 Hz, Ar-**H**), 7.85 (1H, ddd, J = 8.1, 7.0, 1.7 Hz, Ar-**H**), 7.46 (1H, dd, J = 9.0, 2.4 Hz, Ar-**H**), 4.08 (3H, s, C**H**$_3$) ppm

^{13}C NMR (101 MHz, CD_2Cl_2, 25 °C):
δ = 164.5 (**C**), 164.3 (**C**), 162.5 (**C**), 137.1 (**C**), 133.7 (**C**), 130.9 (**C**H), 129.8 (**C**H), 128.4 (**C**H), 126.6 (**C**H), 125.8 (**C**), 124.2 (**C**H), 119.8 (**C**H), 105.7 (**C**H), 56.3 (**C**H$_3$) ppm. 3×**C** not observed/coincident.

6.5.12 3-(Benzo[*d*][1,3]dioxol-5-yl)-4-phenylcyclobut-3-ene-1,2-dione

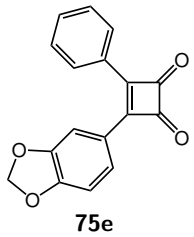

75e

$C_{17}H_{10}O_4$
Mol Wt: 278.26

Synthesized following the methods detailed in 6.5.5, 6.5.6, and 6.5.7, without purification of the intermediates, and with the following reagents and column conditions:

Step 1

dimethylsquarate: 2.00 g, 14.1 mmol

3,4-methylenedioxybromobenzene: 1.86 mL, 15.4

n-butyllithium: 6.00 mL, 15.0 mmol

THF: 150 mL

Step 2

methanol: 0.93 mL, 23.0 mmol

$BF_3{\cdot}Et_2O$: 1.70 mL, 13.8 mmol

THF: 160 mL

Step 3

PhLi (1.9 M in dibutyl ether): 6.0 mL, 11.4 mmol

I_2: 300 mg, 1.18 mmol

acetone: 15 mL

Column chromatography: silica gel; 13% ethyl acetate in hexane

Yield: 943 mg, 3.39 mmol, 30%

MP 55.1 - 55.8 °C

LRMS (ESI+) m/z: 279 $[M+H]^+$, $C_{17}H_{10}O_4$, Relative intensity: 100%

^{1}H NMR (400 MHz, $CDCl_3$, 25 °C):
δ = 8.05-8.01 (2H, m, 2×Ar-**H**), 7.86 (1H, dd, J = 8.2, 1.7 Hz, Ar-**H**), 7.61-7.54 (4H, m, 4×Ar-**H**), 6.99 (1H, dd, J = 8.2, 0.2 Hz, Ar-**H**), 6.11 (2H, s, C**H**$_2$) ppm

^{13}C NMR (101 MHz, $CDCl_3$, 25 °C):
δ = 196.4 (**C**), 195.6 (**C**), 186.2 (**C**), 185.5 (**C**), 152.3 (**C**), 148.4 (**C**), 132.9 (**C**H), 129.3 (2×**C**H), 128.3 (**C**), 128.0 (2×**C**H), 125.2 (**C**H), 122.2 (**C**), 109.3 (**C**H), 107.7 (**C**H), 102.1 (**C**H$_2$) ppm

6.5.13 2-(6-(1*H*-Imidazol-1-yl)hexyl)-1*H*-dibenzo[*e*,*g*]isoindole-1,3(2*H*)-dione

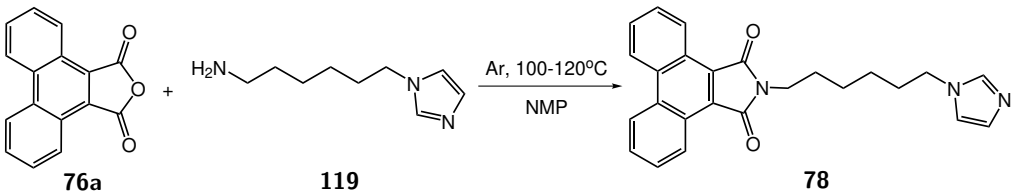

76a
$C_{16}H_8O_3$
Mol Wt: 248.24

119
$C_9H_{17}N_3$
Mol Wt: 167.26

78
$C_{25}H_{23}N_3O_2$
Mol Wt: 397.48

Acid anhydride **76a** (270 mg, 1.09 mmol) and amine **119** (187 mg, 1.12 mmol) were dissolved in *N*-methyl-2-pyrrolidone (20 mL) and heated at 100 °C, under an argon blanket, for 20 hours, after which time the title compound and the singly-condensed carboxylic acid intermediate were visible by mass spectrometry. The reaction mixture was heated at 120 °C under an argon blanket for a further 24 hours, after which the aforementioned intermediate had been consumed. The mixture was cooled to room temperature, and partitioned in water (50 mL) and CH_2Cl_2 (50 mL). The aqueous phase was washed with DCM (4×50 mL) until no further colour-change was observed, and the combined organic phases were dried over $MgSO_4$. Concentration *in vacuo*, and purification by column chromatography (silica; 0 - 100% ethyl acetate in hexane) gave the title compound as an orange solid (270 mg, 0.68 mmol, 62%).

MP 149.5 - 150.0 °C

HRMS (ESI) Found: 398.1863 $[M+H]^+$, $C_{25}H_{24}N_3O_2$, Required: 398.1864

^{1}H NMR (400 MHz, $CDCl_3$, 25 °C):
δ = 9.05-9.11 (2H, m, 2×Ar-**H**), 8.64-8.70 (2H, m, 2×Ar-**H**), 7.79 (2H, ddd, J = 8.4, 7.0, 1.6 Hz, 2×Ar-**H**), 7.74 (2H, ddd, J = 8.1, 7.0, 1.4 Hz, 2×Ar-**H**), 7.48 (1H, s, Ar-**H**), 7.05 (1H, s, Ar-**H**), 6.90 (1H, s, Ar-**H**), 3.93 (2H, t, J = 7.2 Hz, C**H**$_2$), 3.73 (2H, t, J = 7.2 Hz, C**H**$_2$), 1.70-1.85 (4H, m, 2×C**H**$_2$), 1.34-1.49 (4H, m, 2×C**H**$_2$) ppm

^{13}C NMR (101 MHz, $CDCl_3$, 25 °C):
δ = 169.9 (2×**C**), 137.0 (**C**H), 133.2 (2×**C**), 129.3 (3×**C**H), 128.3 (2×**C**H), 127.3 (2×**C**), 126.1 (2×**C**H), 125.4 (2×**C**), 123.1 (2×**C**H), 118.7 (**C**H), 46.9 (**C**H$_2$), 37.5 (**C**H$_2$), 30.9 (**C**H$_2$), 28.5 (**C**H$_2$), 26.3 (**C**H$_2$), 26.1 (**C**H$_2$) ppm

FT-IR (ν_{max} cm^{-1}, film):
2920 (w), 1839 (m), 1766 (s), 1704 (m), 1446 (m), 1187 (s), 1158 (s), 906 (s), 767 (vs), 717 (s), 632 (s)

6.5.14 1-(6-(1,3-Dioxo-1,3-dihydro-2*H*-dibenzo[*e*,*g*]isoindol-2-yl)hexyl)-3-methyl-1*H*-imidazol-3-ium trifluoromethanesulfonate

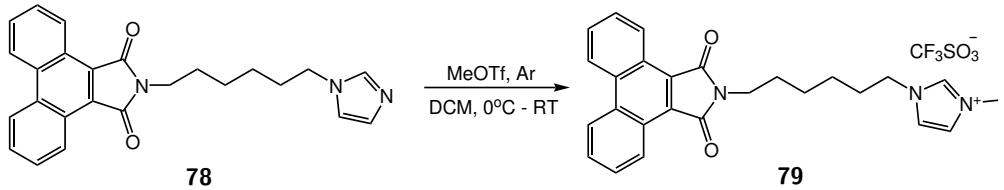

78
$C_{25}H_{23}N_3O_2$
Mol Wt: 397.48

79
$C_{27}H_{26}F_3N_3O_5S$
Mol Wt: 561.57

Imidazole **78** (240 mg, 0.604 mmol) was dissolved in anhydrous CH_2Cl_2 (15 mL) and cooled to 0 °C under argon flow. MeOTf (0.12 mL, 1.08 mmol) was added dropwise and the mixture was warmed to room temperature, with immediate formation of a precipitate. After 2 h, the solvent was removed *in vacuo*, giving the title compound as an orange solid (332 mg, 0.591 mmol, 99%).

MP 194.0 - 198.0 °C

HRMS (ESI) Found: 412.2025 $[M]^+$, $C_{26}H_{26}N_3O_2$, Required: 412.2020

^{1}H NMR (400 MHz, acetonitrile-d3, 25 °C):
δ = 8.97 (2H, ddd, J = 8.1, 1.5, 0.5 Hz, 2×Ar-**H**), 8.72-8.76 (2H, m, 2×Ar-**H**), 8.42 (1H, br s, Ar-**H**), 7.82 (2H, ddd, J = 8.4, 6.6, 1.6 Hz, 2×Ar-**H**), 7.77 (2H, ddd, J = 8.4, 6.6, 1.4 Hz, 2×Ar-**H**), 7.35 (1H, t, J = 1.8 Hz, Ar-**H**), 7.31 (1H, t, J = 1.8 Hz, Ar-**H**), 4.11 (2H, t, J = 7.2 Hz, C**H**$_2$), 3.80 (3H, s, C**H**$_3$), 3.65 (2H, t, J = 7.0 Hz, C**H**$_2$), 1.83 (2H, quin, J = 7.3 Hz, C**H**$_2$), 1.71 (2H, quin, J = 7.2 Hz, C**H**$_2$), 1.32-1.47 (4H, m, 2×C**H**$_2$) ppm

^{13}C NMR (101 MHz, acetonitrile-d3, 25 °C):
δ = 170.9 (2×**C**), 137.0 (**C**H), 134.1 (2×**C**), 130.5 (2×**C**H), 129.6 (2×**C**H), 128.5 (2×**C**), 126.6 (2×**C**H), 126.4 (2×**C**), 124.7 (**C**H), 124.6 (2×**C**H), 123.4 (**C**H), 50.5 (**C**H$_2$), 38.4 (**C**H$_2$), 36.9 (**C**H$_3$), 30.5 (**C**H$_2$), 29.2 (**C**H$_2$), 26.9 (**C**H$_2$), 26.3 (**C**H$_2$) ppm

^{19}F NMR (376 MHz, acetonitrile-d3, 25 °C):
δ = -78.7 (1F, s, C**F**$_3$SO$_3^-$) ppm

FT-IR (ν_{max} cm^{-1}, solid):
3000 (w), 2945 (w), 1841 (m), 1762 (vs), 1614 (s), 1522 (m), 1456 (s), 1411 (s), 1322 (s), 1222 (s), 1157 (vs), 1018 (s), 907 (vs), 780 (vs), 719 (s), 600 (s)

UV-Vis (MeCN): λ_{max} = 382 (5300)

6.6 Pyridine systems

6.6.1 4-(4-Methoxyphenyl)pyridine

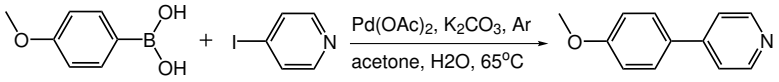

95 $C_7H_9BO_3$ Mol Wt: 151.96

96 C_5H_4IN Mol Wt: 205.10

93k $C_{12}H_{11}NO$ Mol Wt: 185.23

Synthesised following the method detailed in 6.4.2 with the following reagent amounts and column conditions:
4-methoxyphenylboronic acid: 1.26 g, 8.29 mmol
4-iodopyridine: 1.70 g, 8.29 mmol
$Pd(OAc)_2$: 19.1 mg, 0.085 mmol
K_2CO_3: 2.94 g, 21.3 mmol
H_2O: 20 mL
acetone: 20 mL
Column chromatography: silica gel; 0 - 65% ethyl acetate in hexane
Yield: 1.08 g, 5.84 mmol, 70%
Analytical data are consistent with literature values.[103]

MP 97.4 - 98.0 °C

LRMS (ESI+) m/z: 186 $[M+H]^+$, $C_{12}H_{11}NO$, Relative intensity: 100%

^{1}H NMR (400 MHz, $CDCl_3$, 25 °C):
δ = 8.61 (2H, app. d, J = 4.5 Hz, 2×Ar-**H**), 7.59 (2H, app. d, J = 8.0 Hz, 2×Ar-**H**), 7.47 (2H, app. dd, J = 4.5, 1.6 Hz, 2×Ar-**H**), 7.01 (2H, app. d, J = 8.0 Hz, 2×Ar-**H**), 3.86 (3H, s, C**H**$_3$) ppm

^{13}C NMR (101 MHz, $CDCl_3$, 25 °C):
δ = 160.5 (**C**), 150.0 (2×**C**H), 147.8 (**C**), 130.2 (**C**), 128.1 (2×**C**H), 121.0 (2×**C**H), 114.5 (2×**C**H), 55.3 (**C**H$_3$) ppm

UV-Vis (MeCN): λ_{max} = 274 (23300)

6.6.2 4-(4-Methoxyphenyl)-1-methylpyridin-1-ium trifluoromethanesulfonate

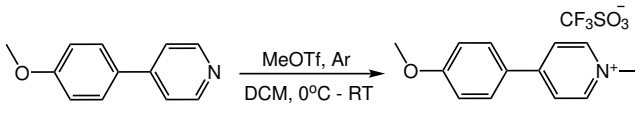

93k
$C_{12}H_{11}NO$
Mol Wt: 185.23

97
$C_{14}H_{14}F_3NO_4S$
Mol Wt: 349.32

Synthesised following the method detailed in 6.5.14 with the following reagent amounts:
4-methoxyphenylpyridine **93k**: 500 mg, 2.70 mmol
MeOTf: 0.36 mL, 3.20 mmol
DCM: 15 mL
Yield: 0.941 g, 2.69 mmol, 100%

MP 147.5 - 149.0 °C

HRMS (ESI+) Found: 200.1073 $[M]^+$, $C_{13}H_{14}NO$, Required: 200.1070

^{1}H NMR (400 MHz, acetonitrile-d3, 25 °C):
δ = 8.57-8.51 (2H, m, 2×Ar-**H**), 8.20-8.14 (2H, m, 2×Ar-**H**), 7.95-7.90 (2H, m, 2×Ar-**H**), 7.17-7.11 (2H, m, 2×Ar-**H**), 4.23 (3H, s, C**H**$_3$), 3.89 (3H, s, C**H**$_3$) ppm

^{13}C NMR (101 MHz, acetonitrile-d3, 25 °C):
δ = 164.4 (**C**), 156.3 (**C**), 145.9 (2×**C**H), 131.0 (2×**C**H), 126.6 (**C**), 124.5 (2×**C**H), 116.3 (2×**C**H), 56.6 (**C**H$_3$), 48.2 (**C**H$_3$) ppm

FT-IR ($\nu_{\max}$ cm^{-1}, solid):
3049 (w), 2842 (w), 1640 (m), 1603 (s), 1502 (m), 1255 (vs), 1148 (vs), 1028 (s), 826 (s), 635 (s)

UV-Vis (MeCN): λ_{max} = 334 (69700)

Appendix A

Absorbance spectra

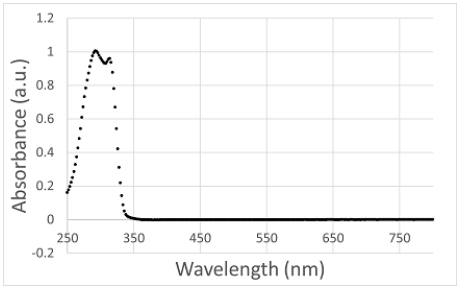

35a

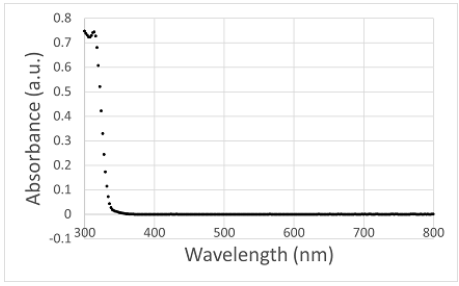

35b

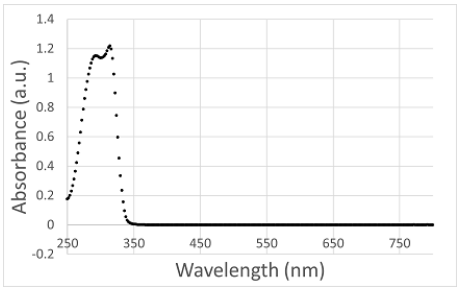

35c

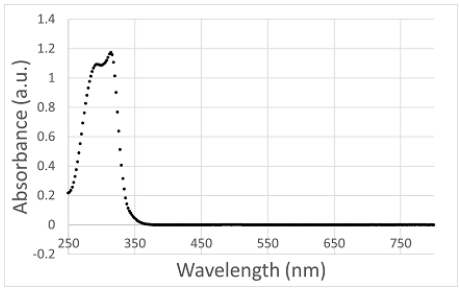

35d

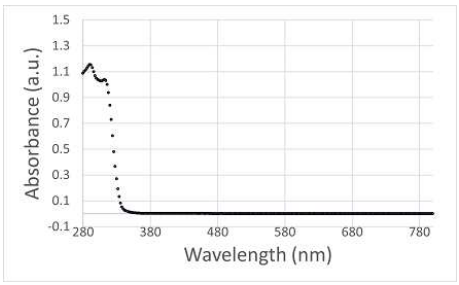

35e

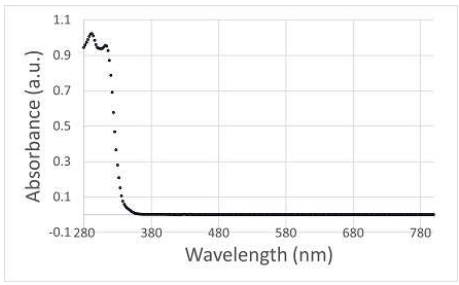

35f

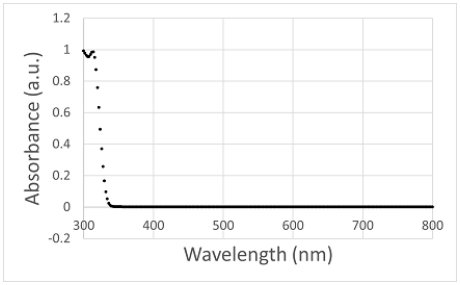

35i

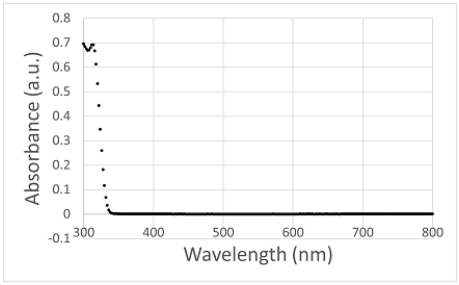

35j

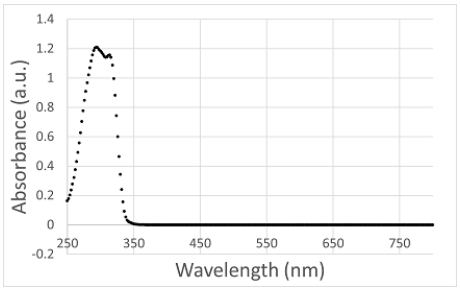

36a

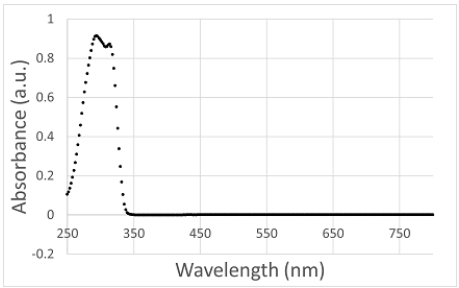

36b

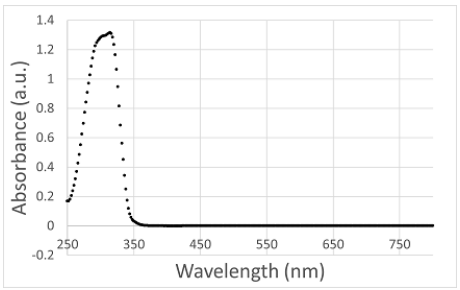

36c

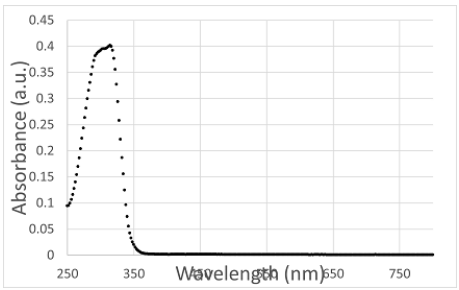

36d

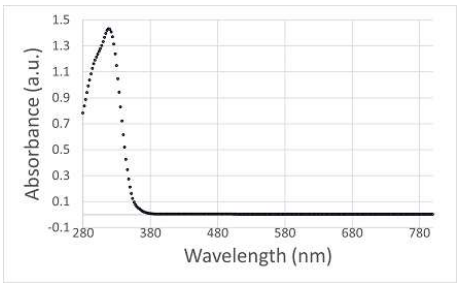

36e

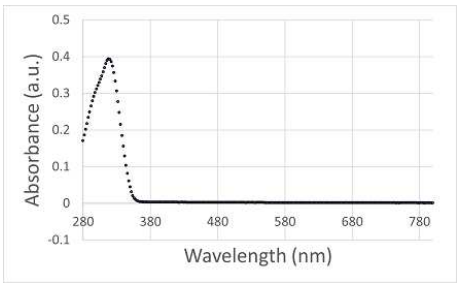

36f

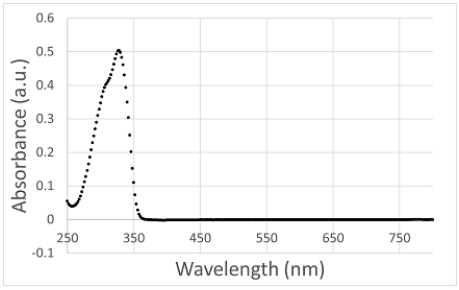

37a

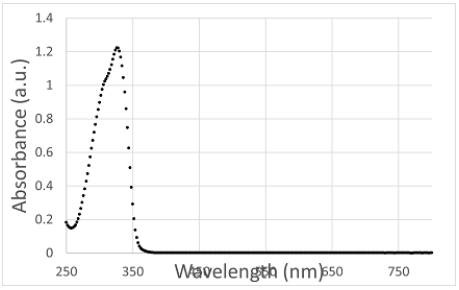

37b

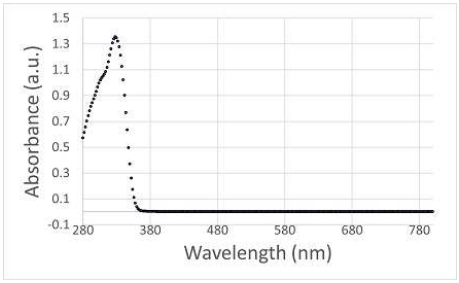

37c

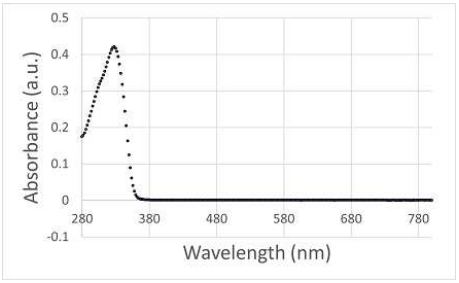

37e

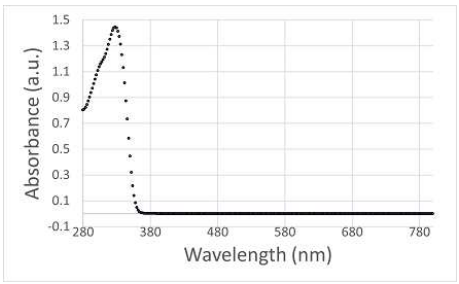

37f

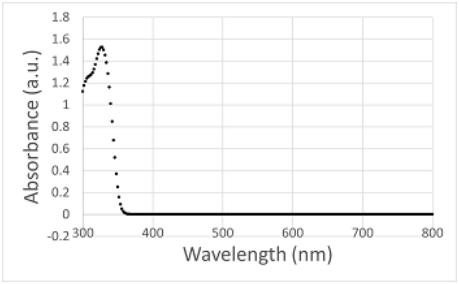

37i

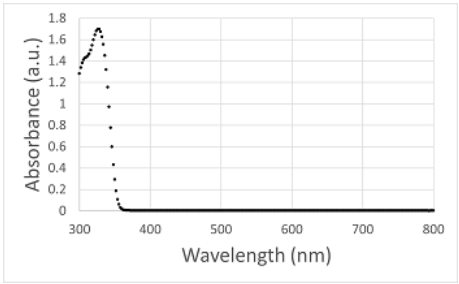

37j

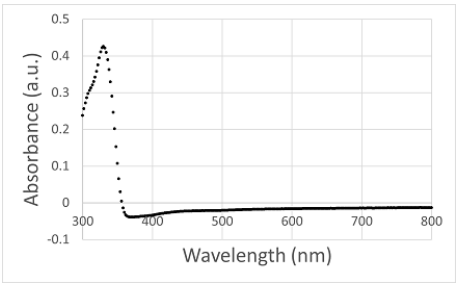

38a

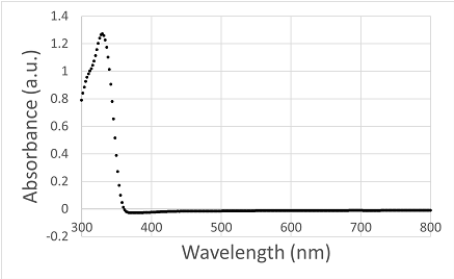

38b

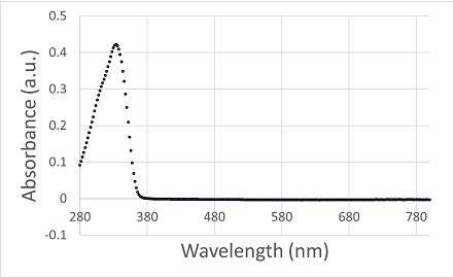

38c

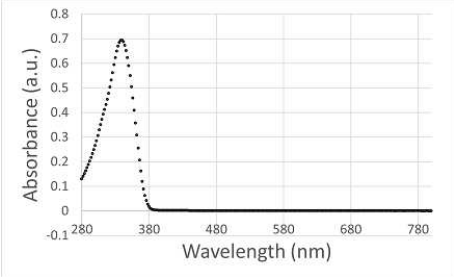

38e

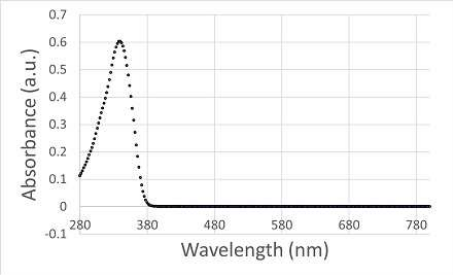

38f

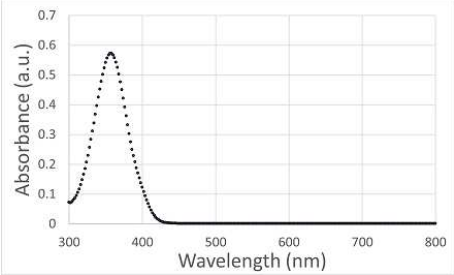

76a

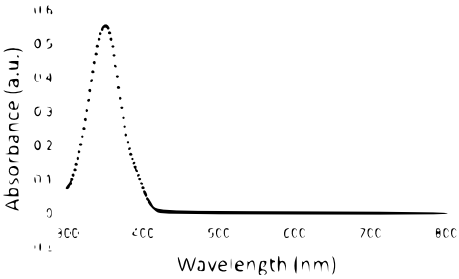

76c

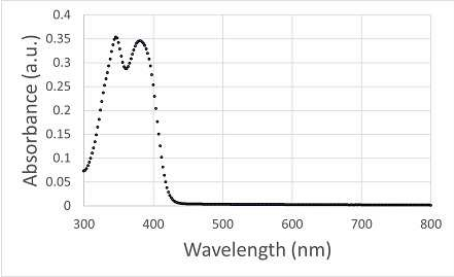

76f

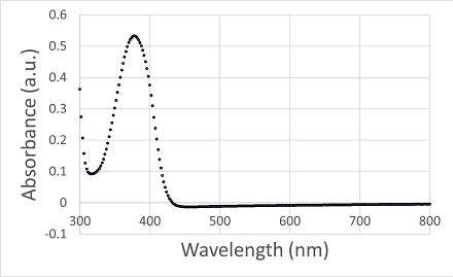

76d

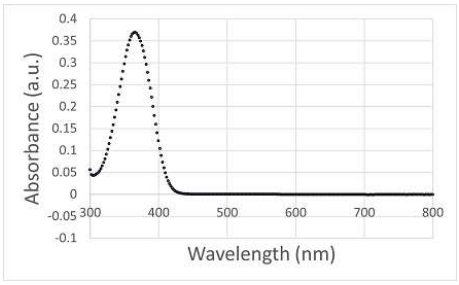

76b

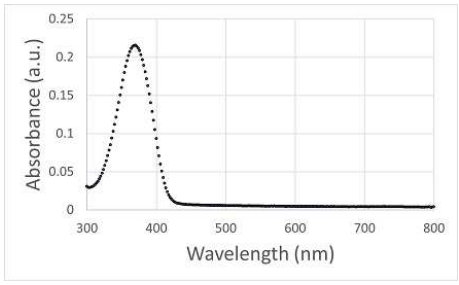

76g

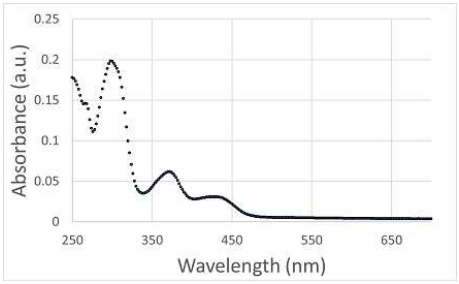

77a

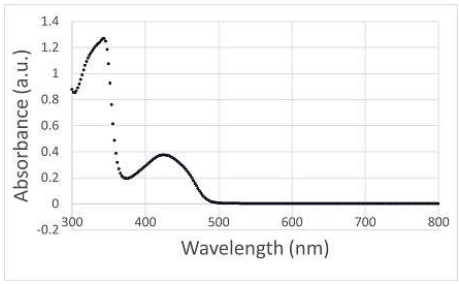

77c

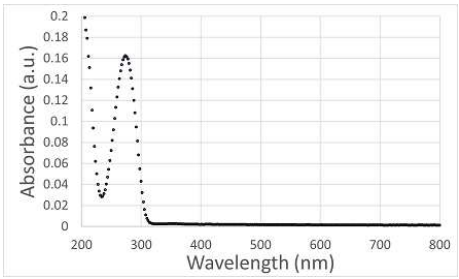

93k

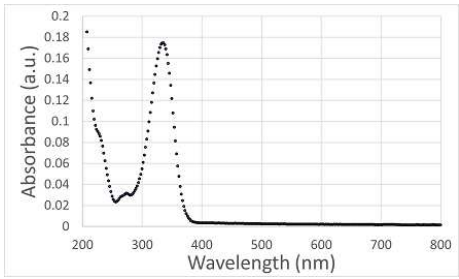

97

Appendix B

Photoluminescence spectra

B.1 Film state

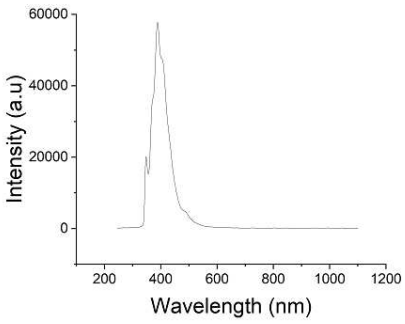

35a

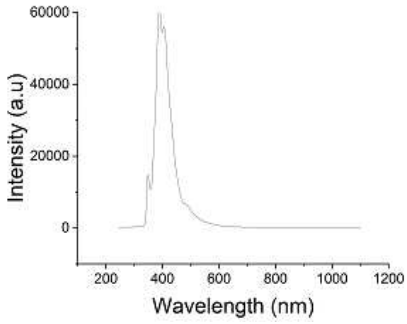

35b

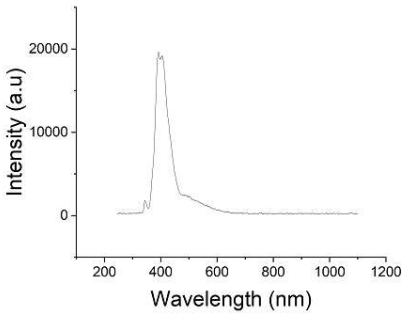

35c

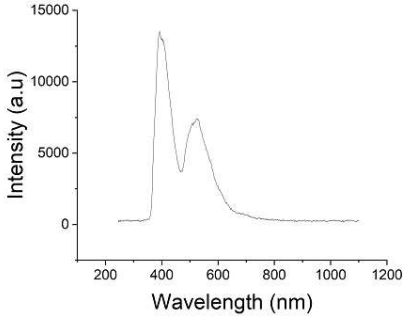

35d

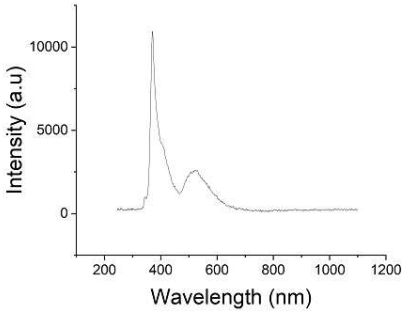

35e

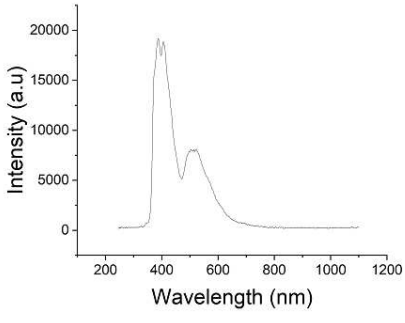

35f

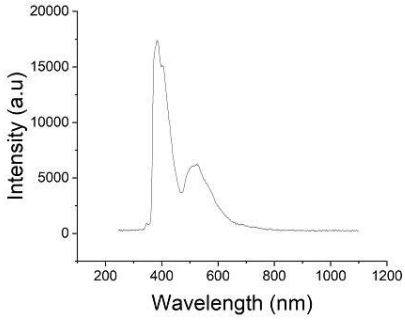

36a

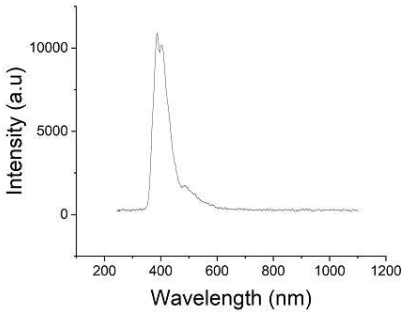

36b

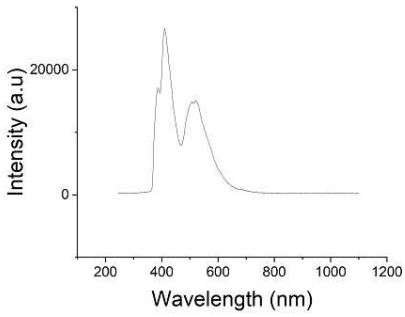

36c

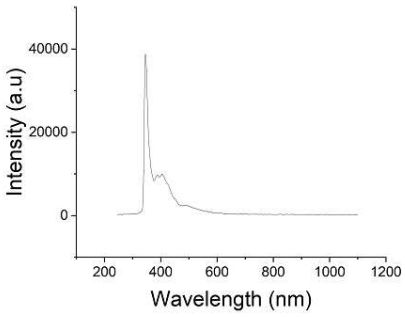

36d

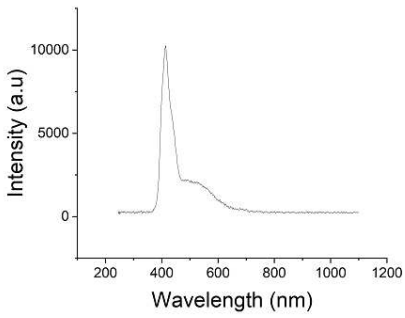

36e

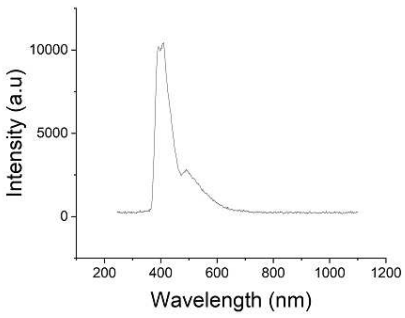

36f

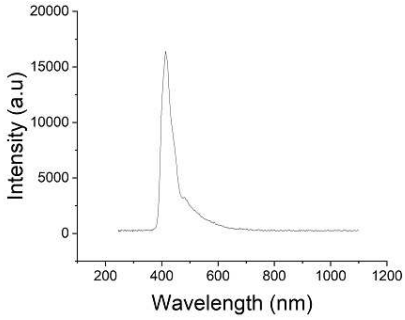

37a

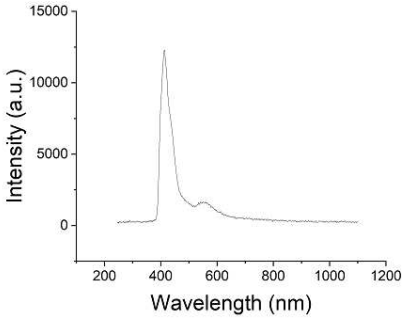

37b

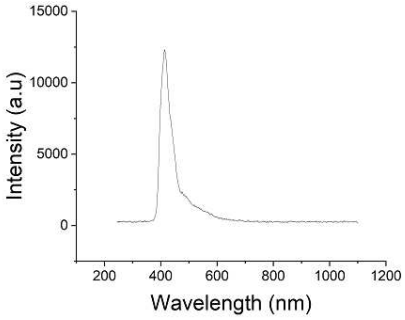

37d

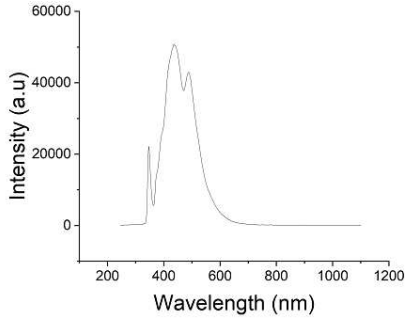

38a

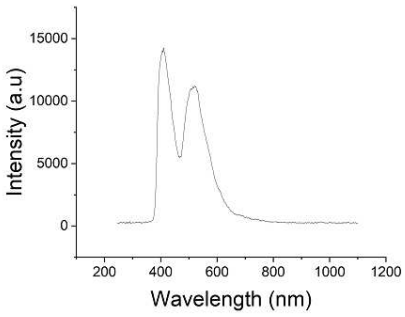

38b

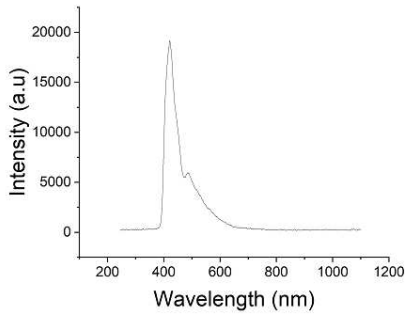

38d

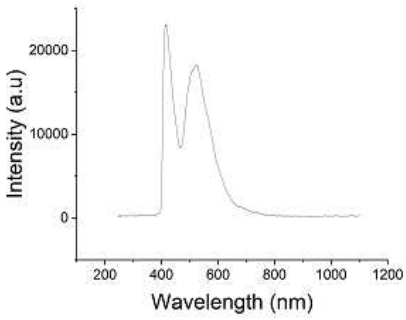

38e

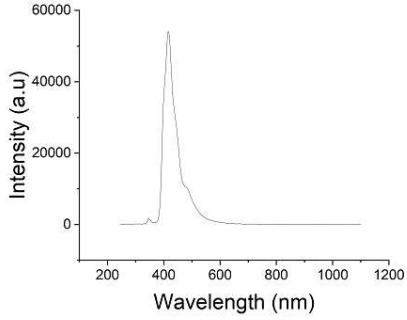

38f

B.2 Solution state

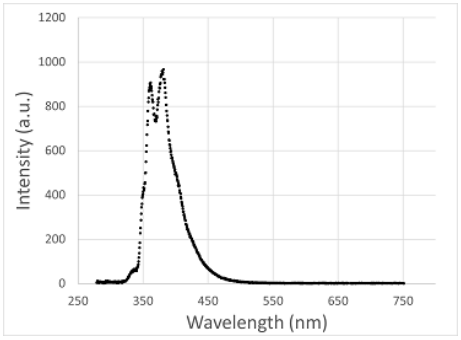

35a

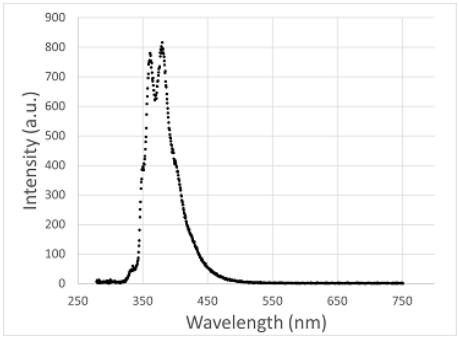

35b

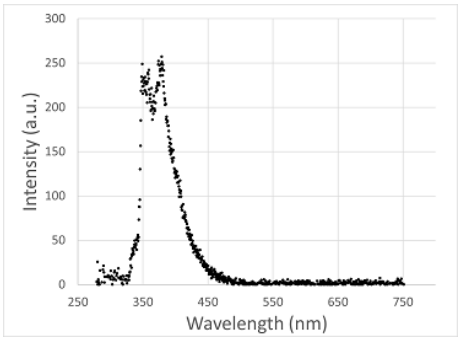

35c

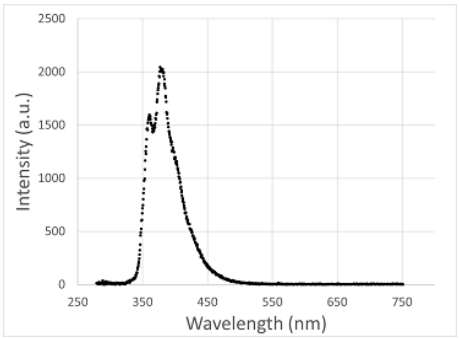

35d

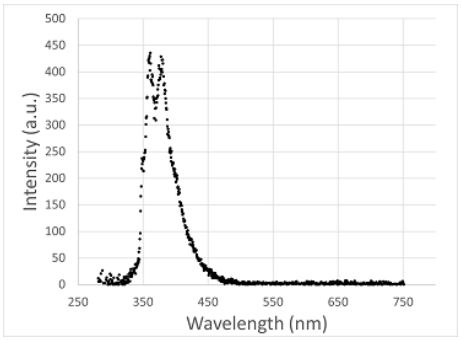

35e

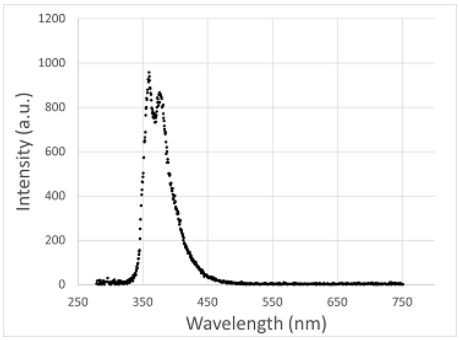

35f

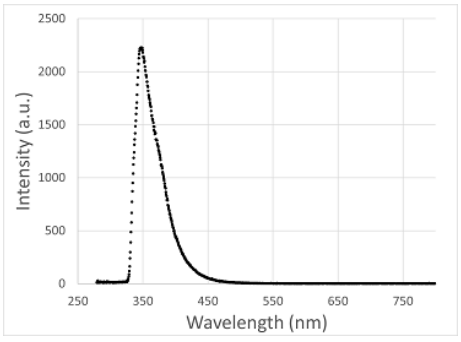

35i

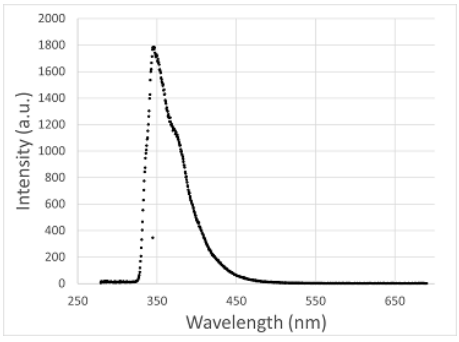

35j

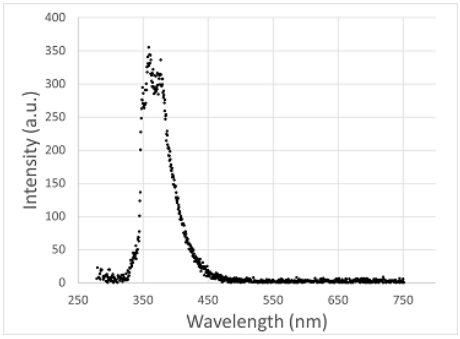

36a

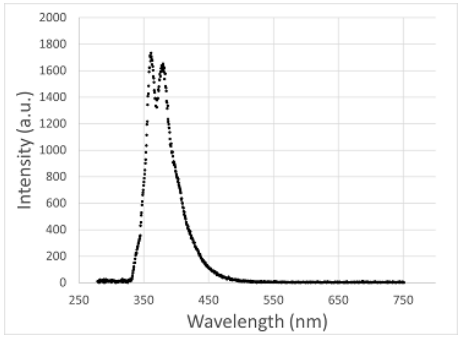

36b

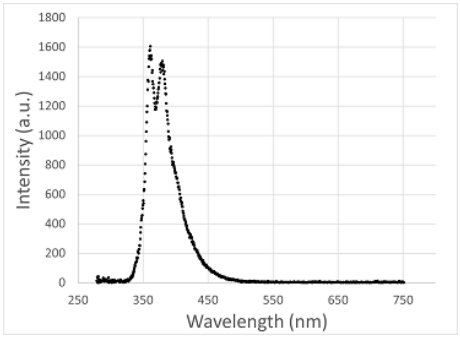

36c

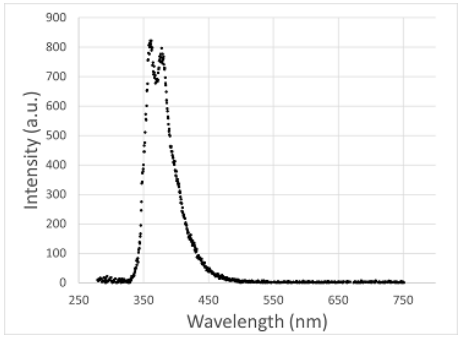

36d

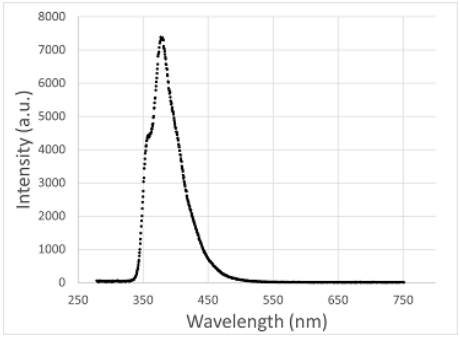

36e

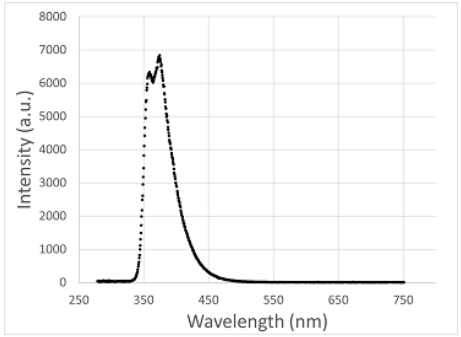

36f

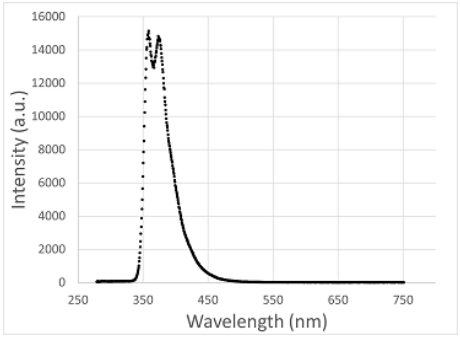

37a

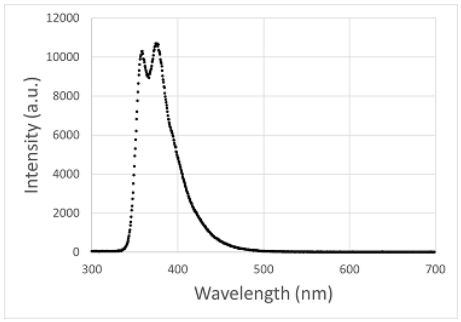

37b

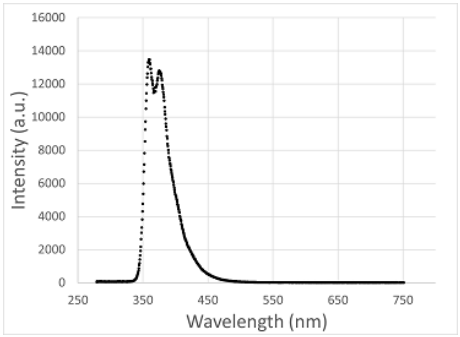

37c

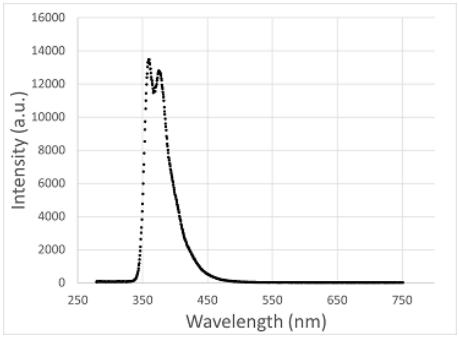

37d

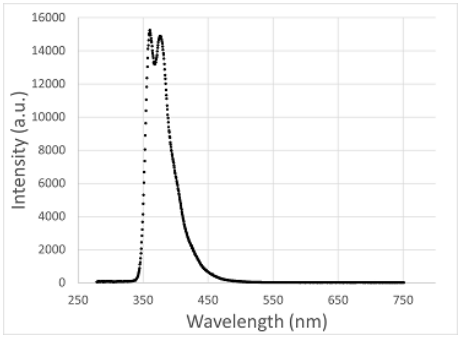

37e

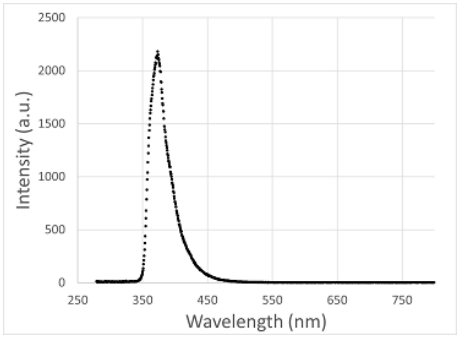

37i

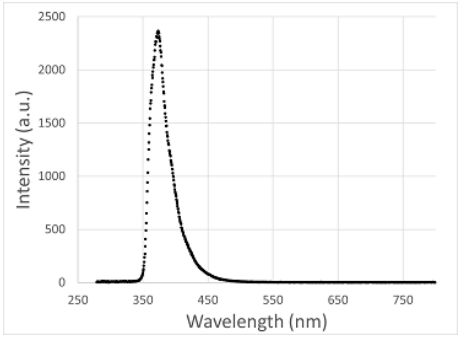

37j

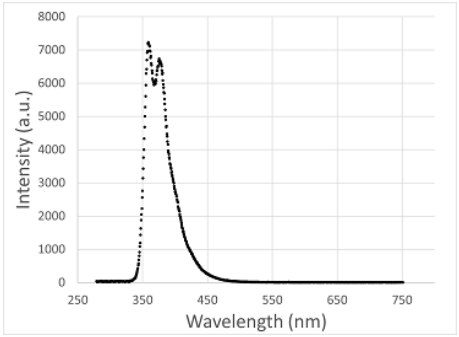

38a

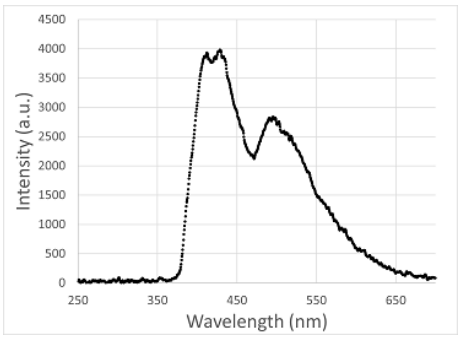

38b

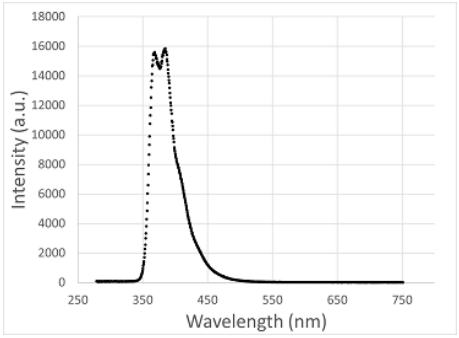

38c

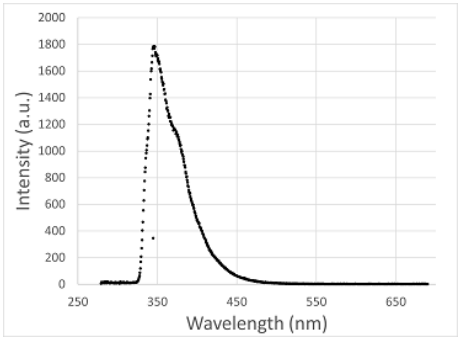

38d

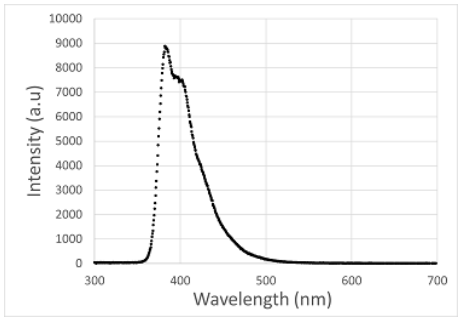

38e

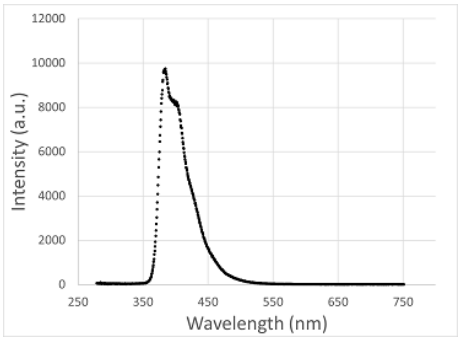

38f

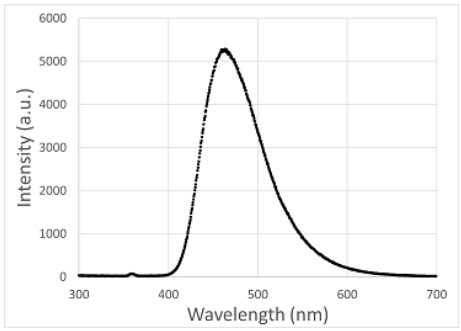

76a

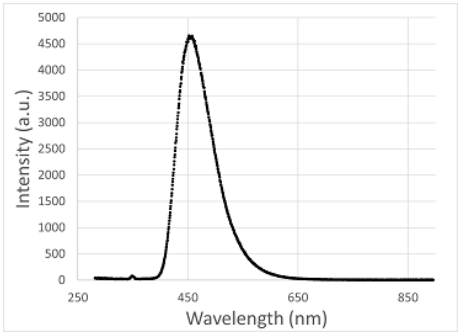

76c

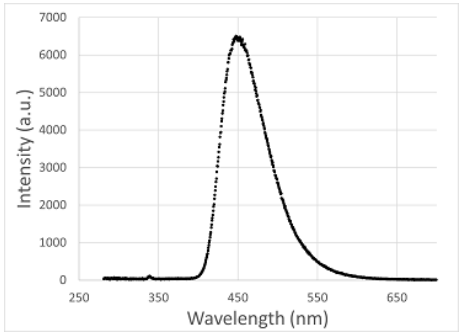

76f

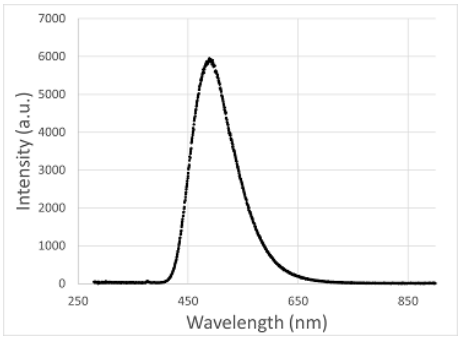

76d

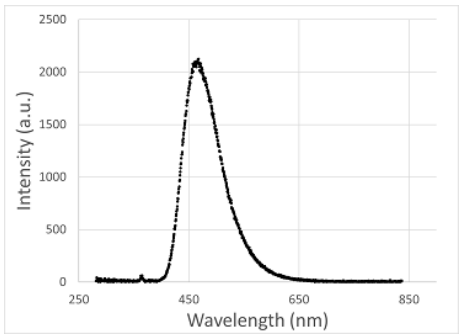

76b

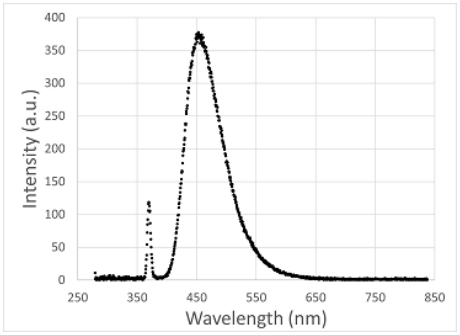

76g

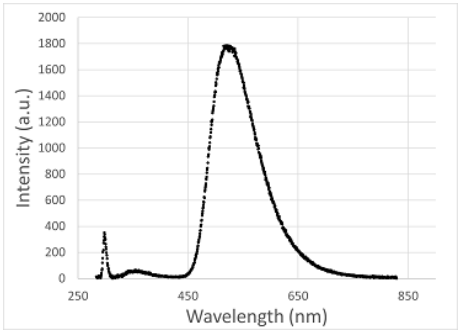

77a

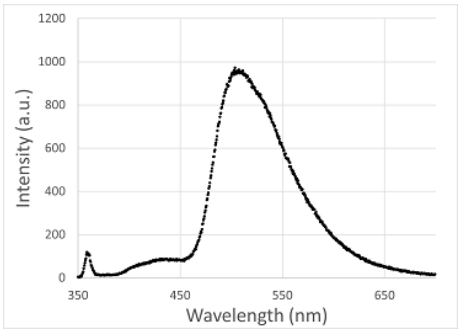

77c

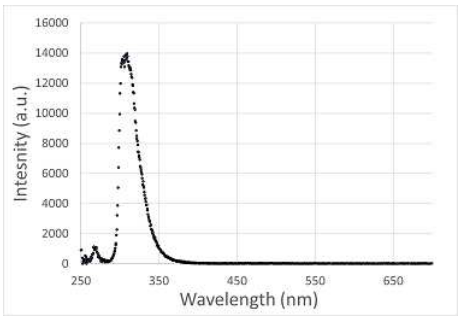

66b

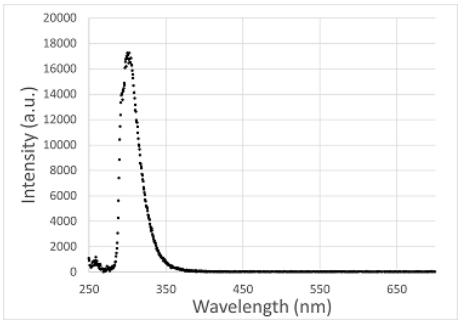

66a

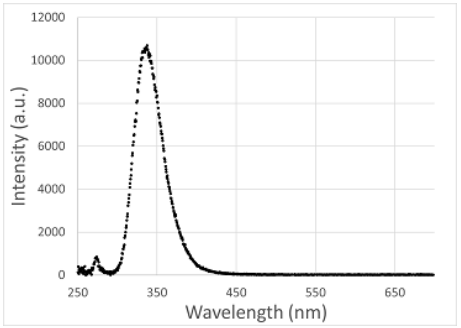

93k

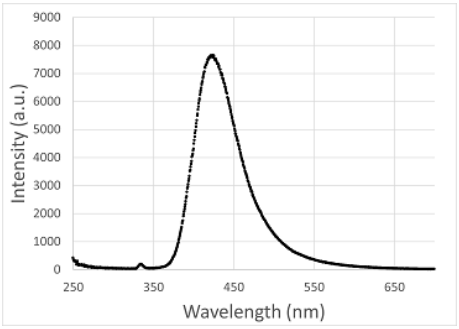

97

Appendix C

Electroluminescence spectra

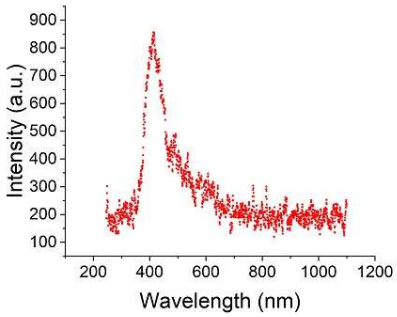

35a

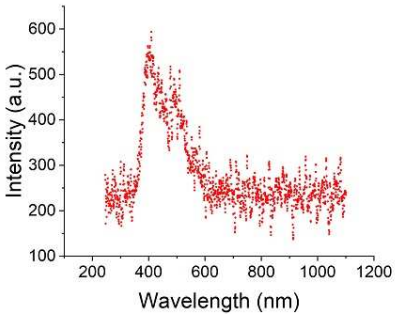

35c

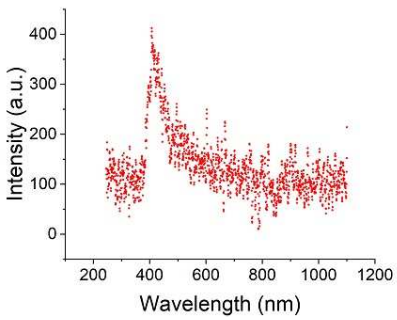

35e

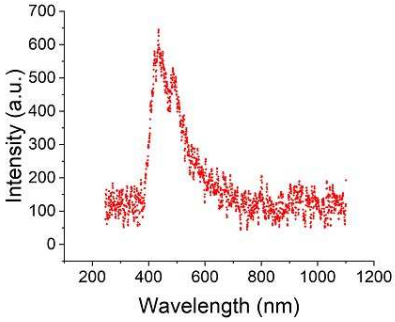

35f

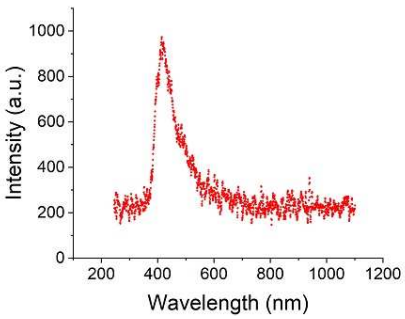

35i

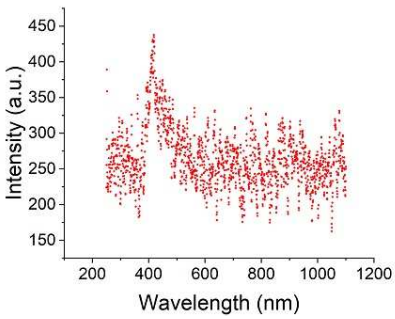

35j

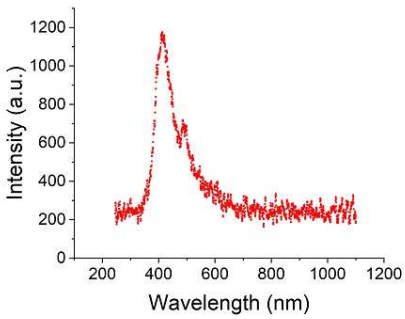

36a

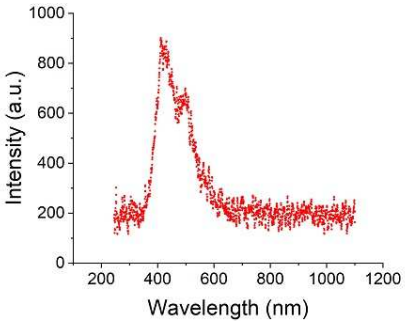

36c

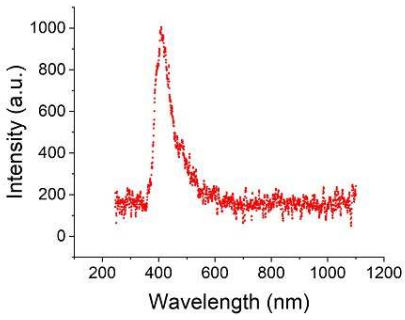

36e

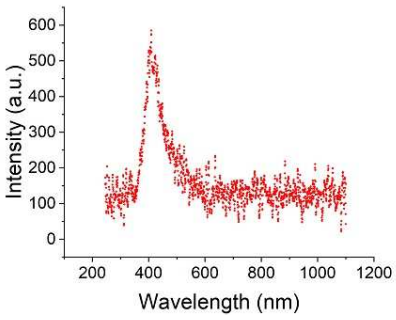

36f

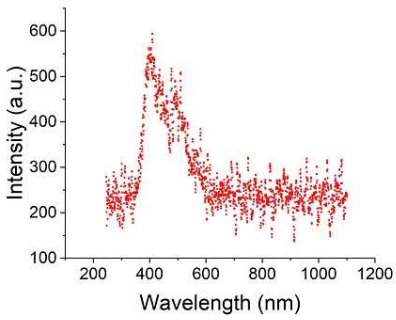

37a

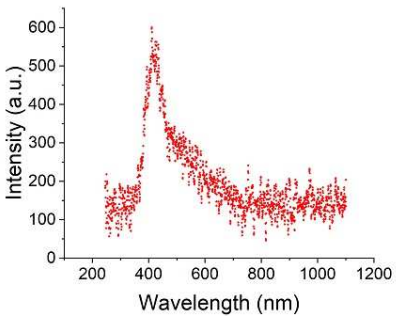

37b

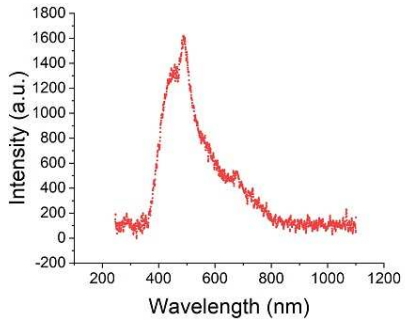

37c

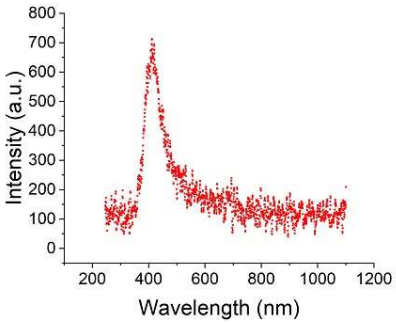

37d

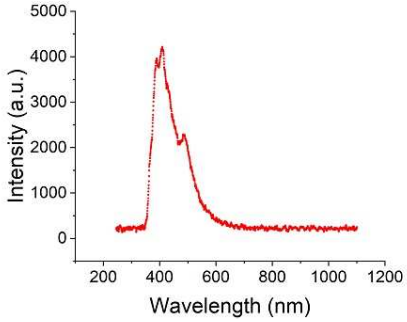

37i

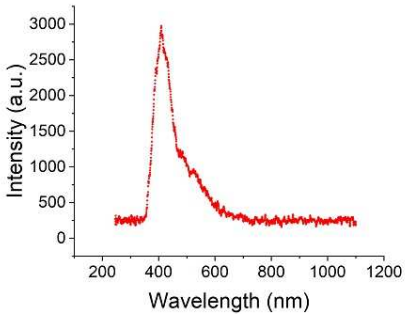

37j

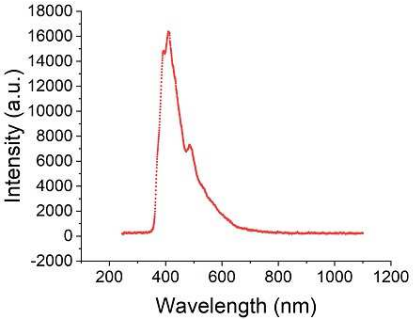

38a

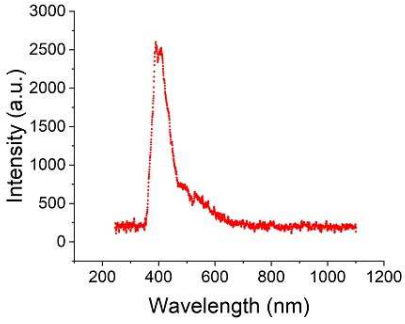

38b

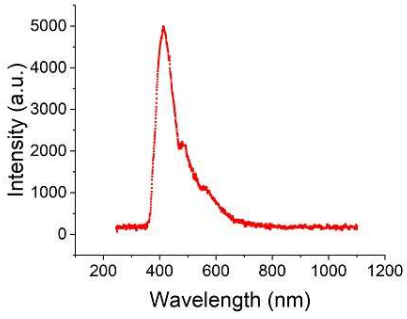

38d

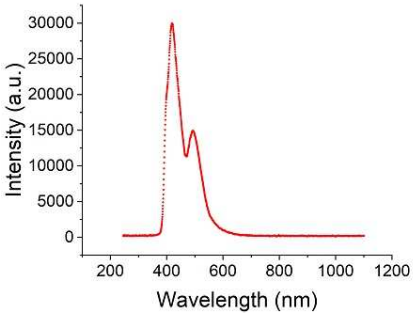

38e

Appendix D

Cyclic voltammograms

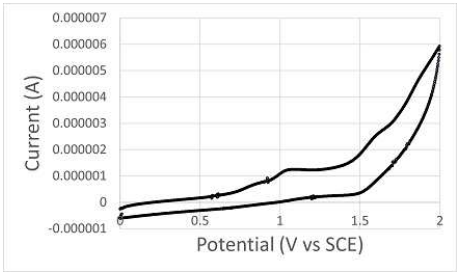

35a

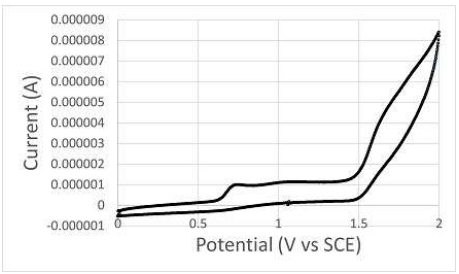

35b

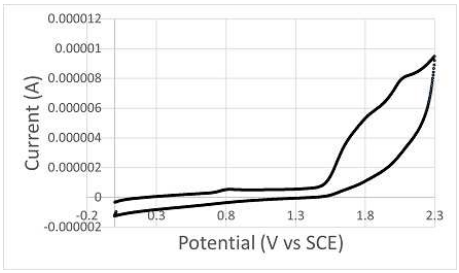

35c

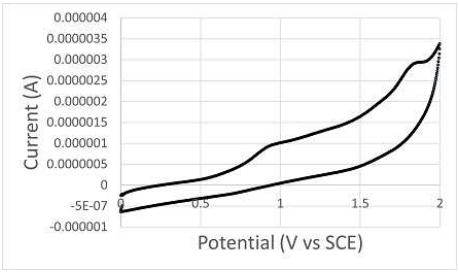

35d

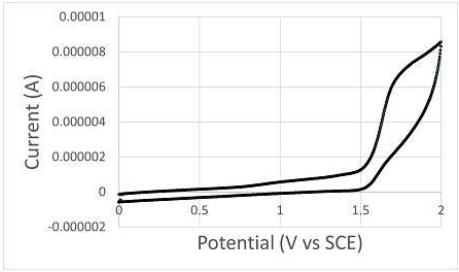

35e

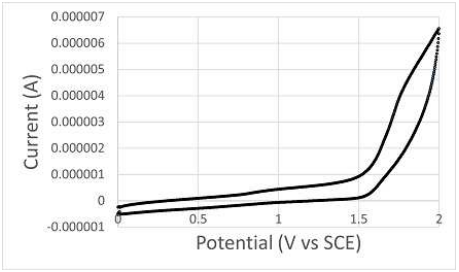

35f

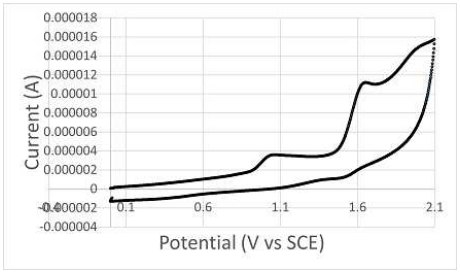

35i

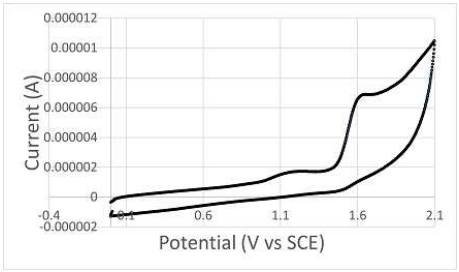

35j

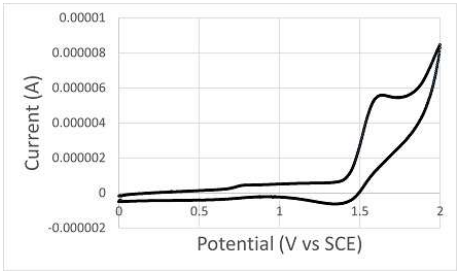

36a

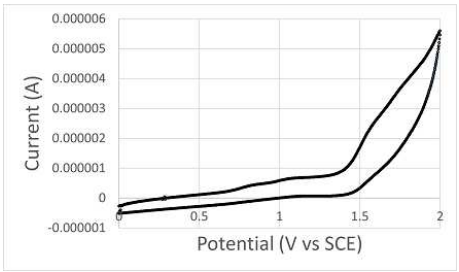

36b

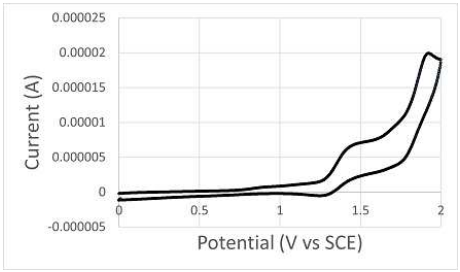

36c

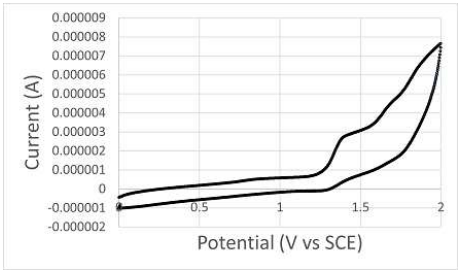

36d

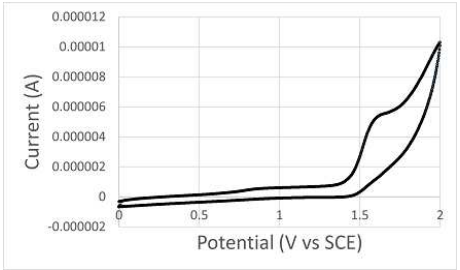

36e

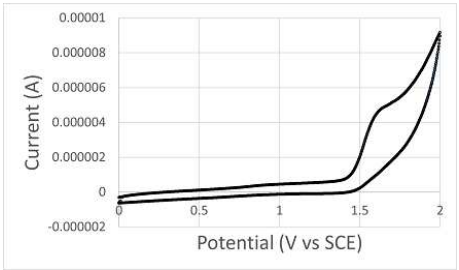

36f

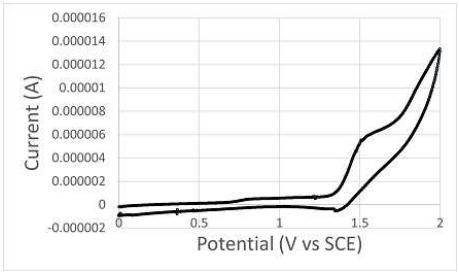

37a

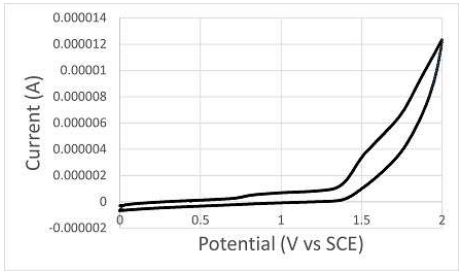

37b

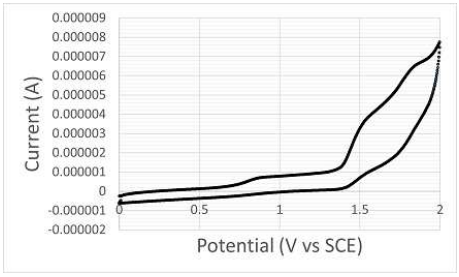

37c

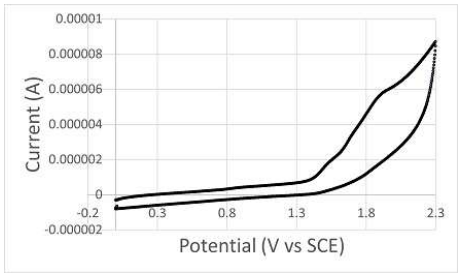

37d

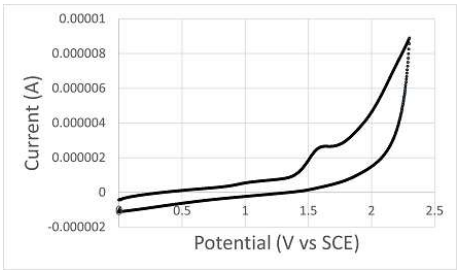

37e

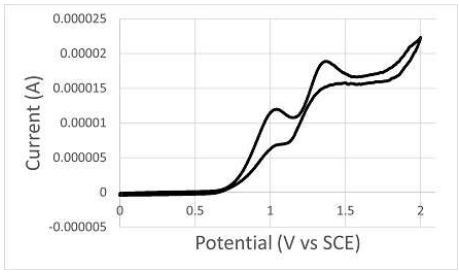

37f

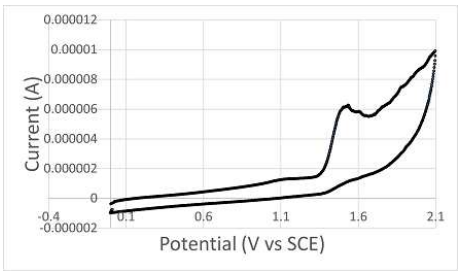

37i

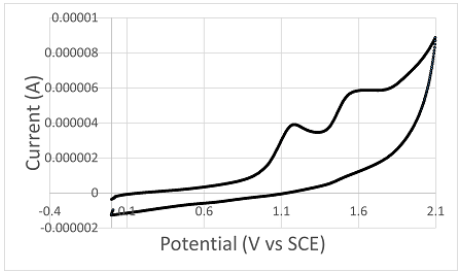

37j

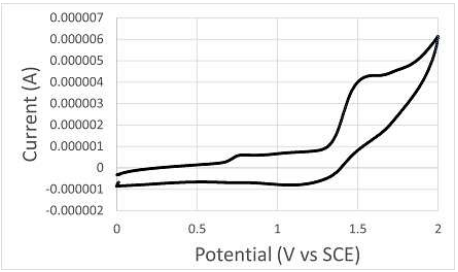

38a

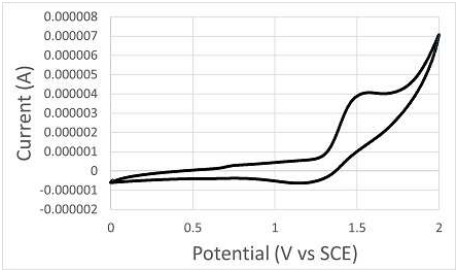

38b

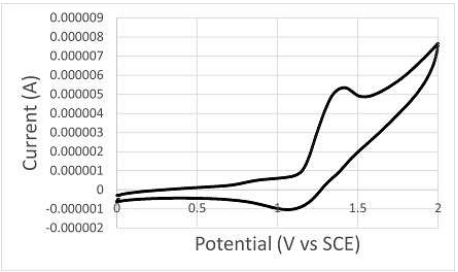

38d

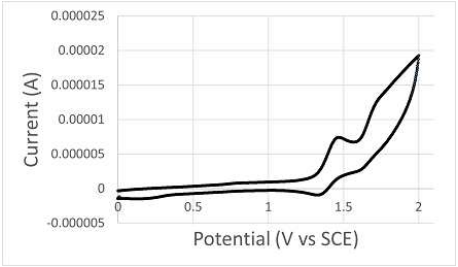

38e

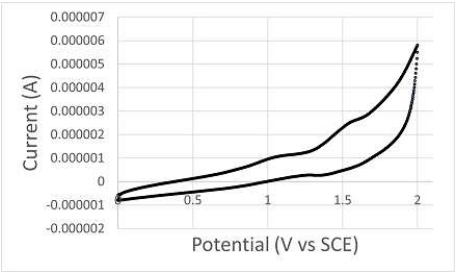

38f

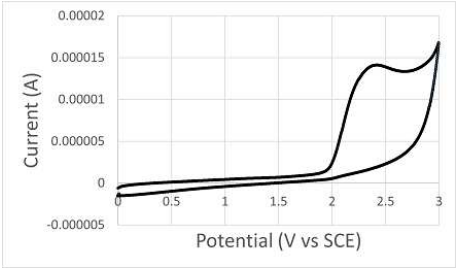

78

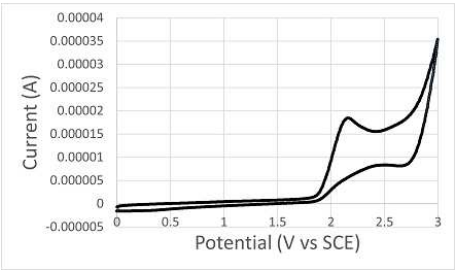

97

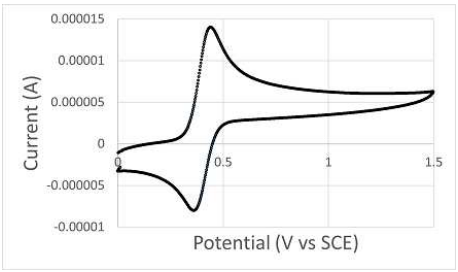

Ferrocene

Appendix E

Scanning electron microscope images

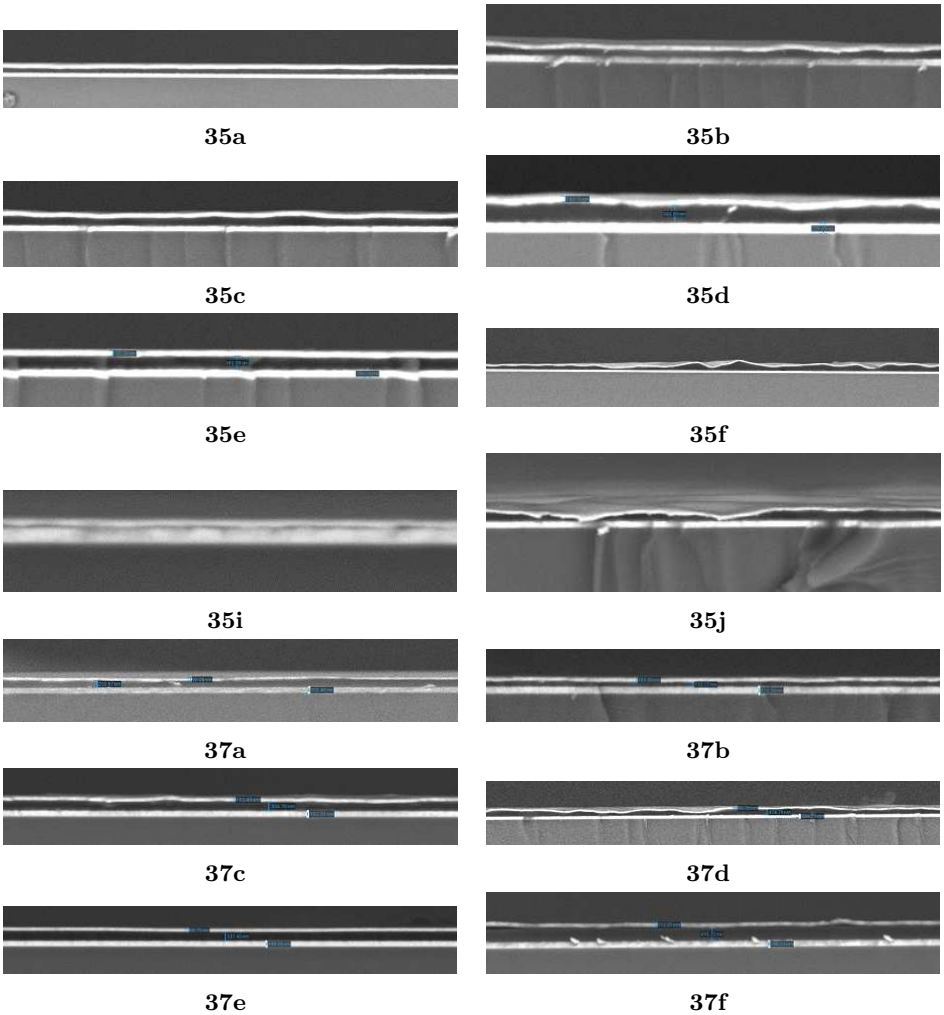

35a

35b

35c

35d

35e

35f

35i

35j

37a

37b

37c

37d

37e

37f

37i

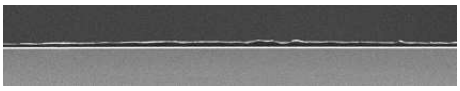

37j

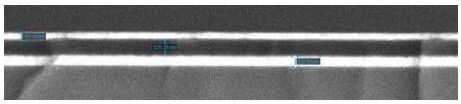

38a

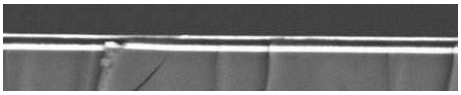

38b

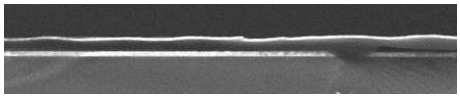

38d

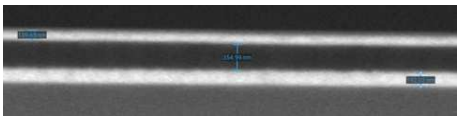

38e

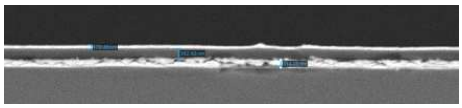

38f

Appendix F

Computational data

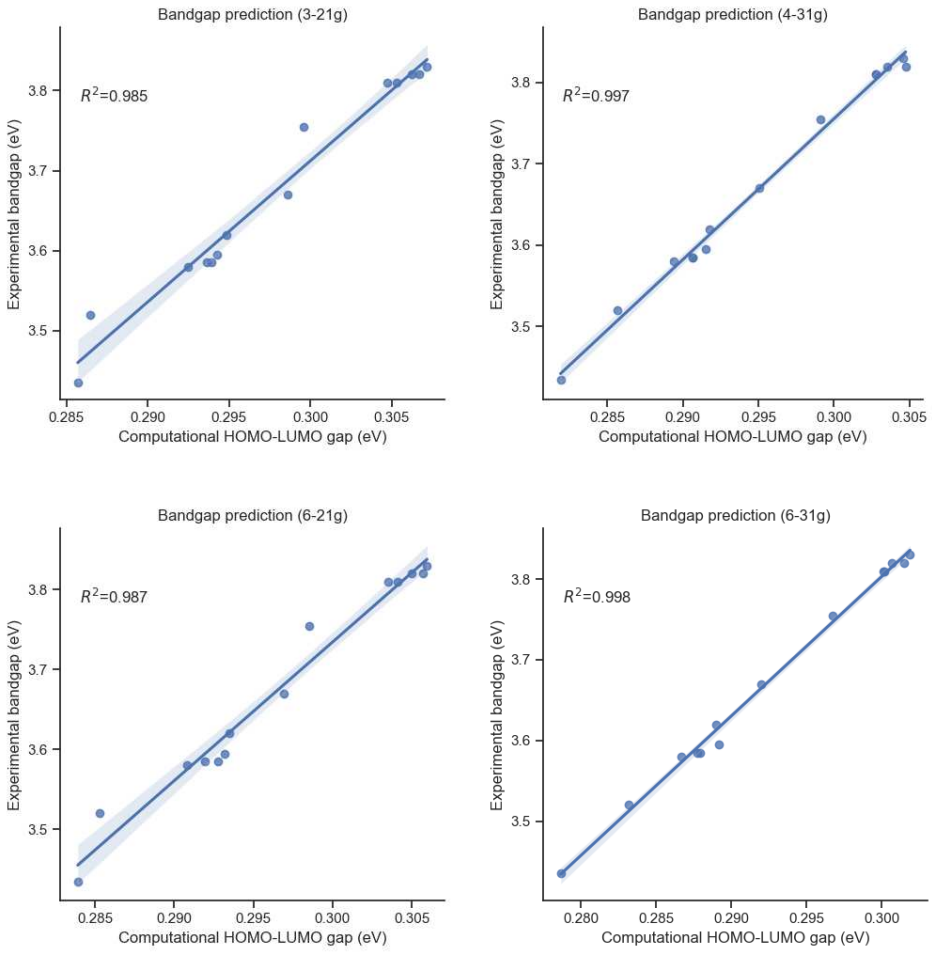

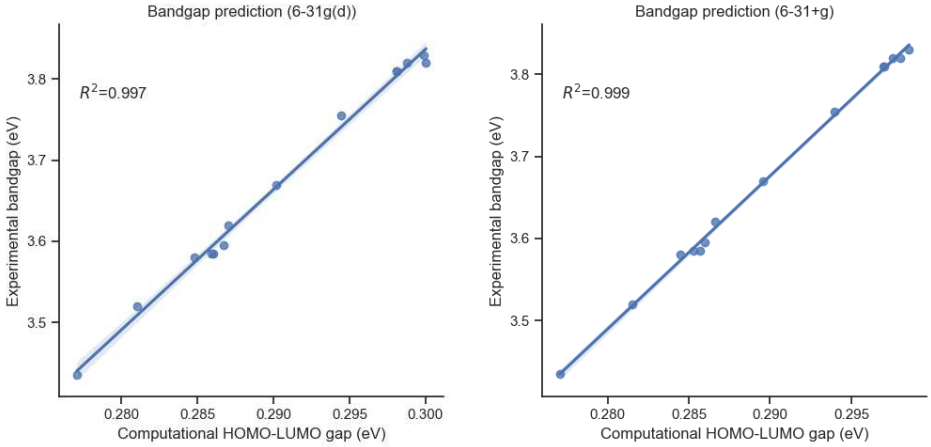
Bandgap prediction (6-31g(d))
R^2=0.997
Experimental bandgap (eV)
Computational HOMO-LUMO gap (eV)
Bandgap prediction (6-31+g)
R^2=0.999
Experimental bandgap (eV)
Computational HOMO-LUMO gap (eV)

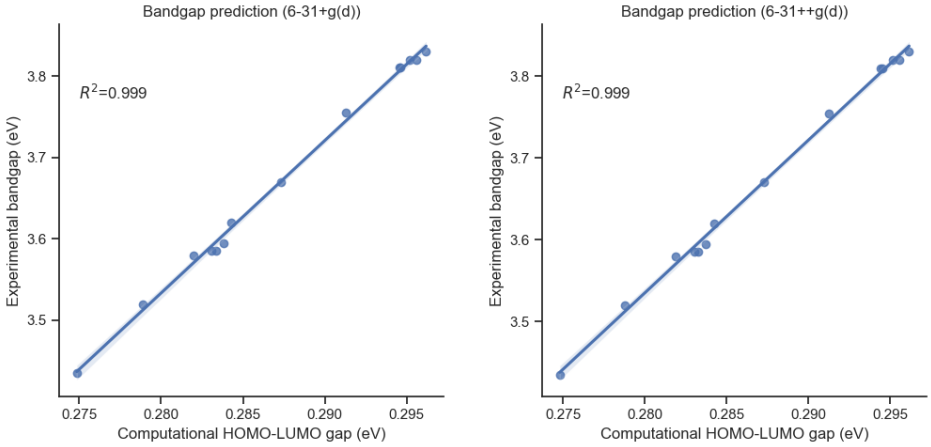
Bandgap prediction (6-31+g(d))
R^2=0.999
Experimental bandgap (eV)
Computational HOMO-LUMO gap (eV)
Bandgap prediction (6-31++g(d))
R^2=0.999
Experimental bandgap (eV)
Computational HOMO-LUMO gap (eV)

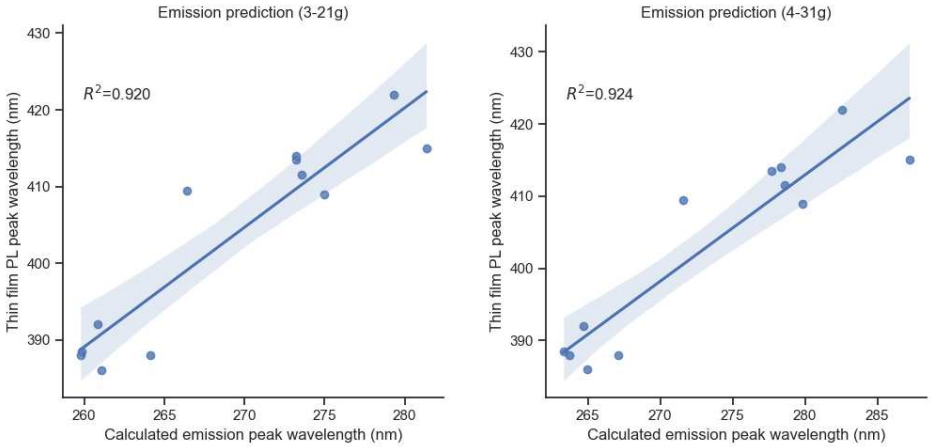
Emission prediction (3-21g)
R^2=0.920
Thin film PL peak wavelength (nm)
Calculated emission peak wavelength (nm)
Emission prediction (4-31g)
R^2=0.924
Thin film PL peak wavelength (nm)
Calculated emission peak wavelength (nm)

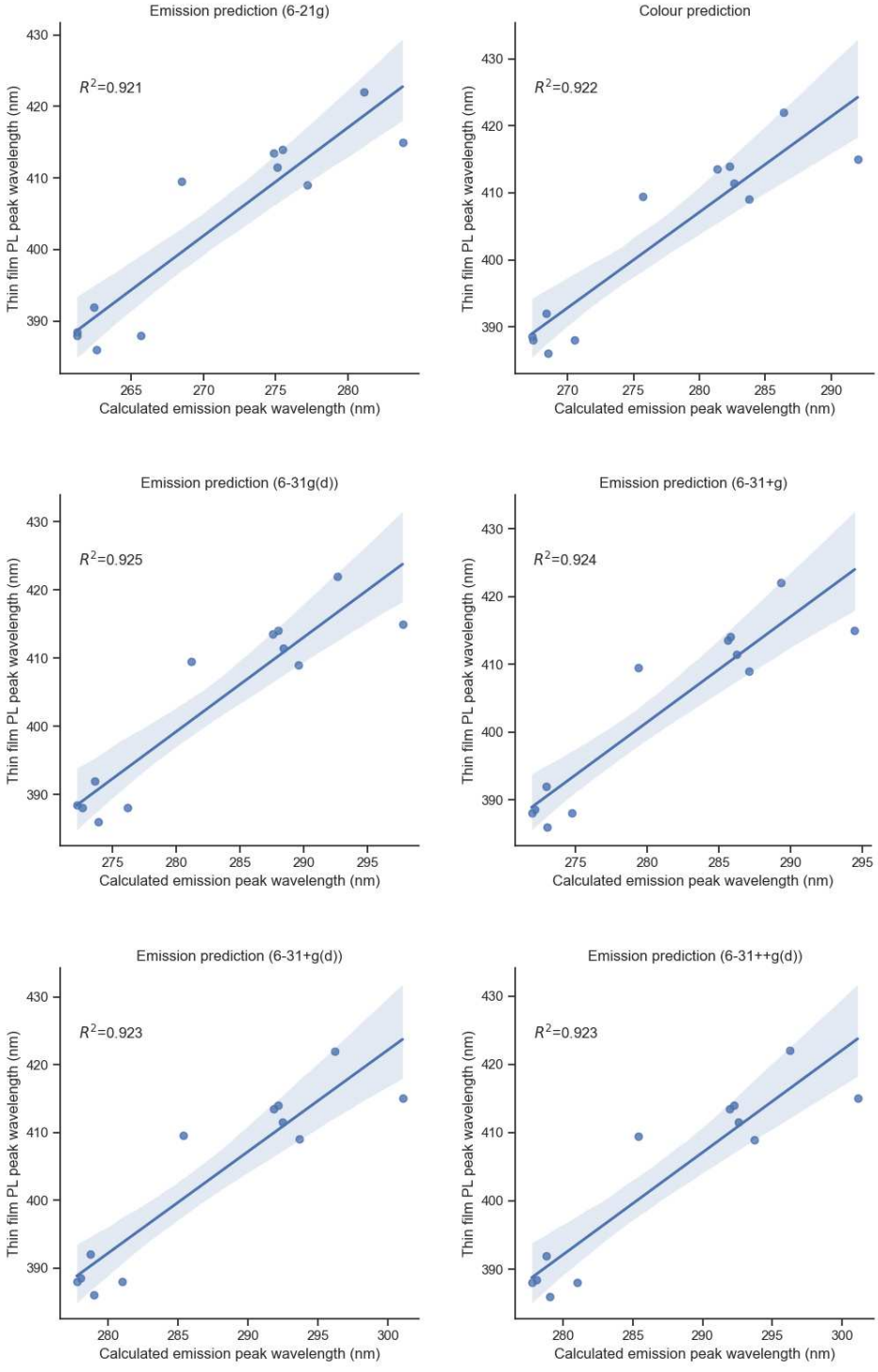
Emission prediction (6-21g)
R^2=0.921
Colour prediction
R^2=0.922
Emission prediction (6-31g(d))
R^2=0.925
Emission prediction (6-31+g)
R^2=0.924
Emission prediction (6-31+g(d))
R^2=0.923
Emission prediction (6-31++g(d))
R^2=0.923
Thin film PL peak wavelength (nm)
Calculated emission peak wavelength (nm)

Appendix G

Tabulated data

Table G.1: Emission and absorption of arylfluorene smart inks

	EL λ_{max} (nm)	Film PL λ_{max} (nm)	Solution PL λ_{max} (nm)	Abs λ_{max} (nm)
35a	412.5	388.5	382	292
35b	-	389	381	291
35c	417.5	392	378	314
35d	-	392	378	314
35e	407.5	371	380	290
35f	435	388	381	291
35i	415	414	347	313
35j	418.5	414	346	313
36a	413	385.5	361	294
36b	-	387	362	294
36c	411.5	410.5	363	313
36d	-	405	362	313
36e	409.5	414	378	319
36f	409.5	414	375	318

Table G.2: Emission and absorption of diarylfluorene smart inks

	EL λ_{max} (nm)	Film PL λ_{max} (nm)	Solution PL λ_{max} (nm)	Abs λ_{max} (nm)
37a	411	414	359	326
37b	411.5	413	375	326
37c	487.5	414	360	328
37d	412	414.5	360	328
37e	410	392.5	360	327
37f	-	391	361	328
37i	409	410	373	327
37j	409.5	409	374	327
38a	410	434.5	359	330
38b	409	409	349	329
38c	-	416.5	-	-
38d	412.5	422	385	334
38e	419.5	414	382	339
38f	-	416.5	385	339

References

[1] R. Haitz and J. Y. Tsao, *Phys. Status Solidi A*, 2011, **208**, 17–29.

[2] G. G. Malliaras, J. D. Slinker, J. A. Defranco, M. J. Jaquith, W. R. Silveira, Y. W. Zhong, J. M. Moran-Mirabal, H. G. Craighead, H. D. Abrũa and J. A. Marohn, *Nat. Mater.*, 2008, **7**, 167–168.

[3] S. B. Meier, D. Tordera, A. Pertegás, C. Roldán-Carmona, E. Ortí and H. J. Bolink, *Mater Today*, 2014, **17**, 217–223.

[4] S. Tang and L. Edman, *Top. Curr. Chem.*, 2016, **374**, 1–21.

[5] S. B. Meier, S. Van Reenen, B. Lefevre, D. Hartmann, H. J. Bolink, A. Winnacker, W. Sarfert and M. Kemerink, *Adv. Funct. Mater.*, 2013, **23**, 3531–3538.

[6] S. Kanagaraj, A. Puthanveedu and Y. Choe, *Adv. Funct. Mater.*, 2020, **30**, 1–22.

[7] S. Arumugam, Y. Li, J. Pearce, M. D. B. Charlton, J. Tudor, D. Harrowven and S. Beeby, *IEEE Trans. Electron Devices*, 2021, **68**, 1717–1722.

[8] Z. Shu, O. Pabst, E. Beckert, R. Eberhardt and A. Tunnermann, Organic Photonic Materials and Devices Xviii, 2016.

[9] Z. Chen, F. Li, Q. Zeng, K. Yang, Y. Liu, Z. Su and G. Shan, *Org. Electron.*, 2019, **69**, 336–342.

[10] K. P. S. Zanoni, M. S. Sanematsu and N. Y. Murakami Iha, *Inorg. Chem. Commun.*, 2014, **43**, 162–164.

[11] A. Sandström, H. F. Dam, F. C. Krebs and L. Edman, *Nat. Commun.*, 2012, **3**, 1–5.

[12] J. Katsumata, F. Osawa, G. Sato, A. Sato, K. Miwa, S. Ono and K. Marumoto, *Commun. Mater.*, 2023, **4**, 4.

[13] K. Yasuji, T. Sakanoue, F. Yonekawa and K. Kanemoto, *Nat. Commun.*, 2023, **14**, 14.

[14] P. Matyba, H. Yamaguchi, G. Eda, M. Chhowalla, L. Edman and N. D. Robinson, *ACS Nano*, 2010, **4**, 637–642.

[15] P. Matyba, H. Yamaguchi, M. Chhowalla, N. D. Robinson and L. Edman, *ACS Nano*, 2011, **5**, 574–580.

[16] Z. Yu, L. Hu, Z. Liu, M. Sun, M. Wang, G. Grüner and Q. Pei, *Appl. Phys. Lett.*, 2009, **95**, 203304.

[17] G. Qian, Y. Lin, G. Wantz, A. R. Davis, K. R. Carter and J. J. Watkins, *Adv. Funct. Mater.*, 2014, **24**, 4484–4490.

[18] H. Zhang, H. Lin, C. Liang, H. Liu, J. Liang, Y. Zhao, W. Zhang, M. Sun, W. Xiao, H. Li, S. Polizzi, D. Li, F. Zhang, Z. He and W. C. H. Choy, *Adv. Funct. Mater.*, 2015, **25**, 7226–7232.

[19] Z. B. Hill, D. B. Rodovsky, J. M. Leger and G. P. Bartholomew, *Chem. Commun.*, 2008, 6594–6596.

[20] S. Tang, W.-Y. Tan, X.-H. Zhu and L. Edman, *Chem. Commun.*, 2013, **49**, 4926–4928.

[21] P. Matyba, M. R. Andersson and L. Edman, *Org. Electron.*, 2008, **9**, 699–710.

[22] S. Y. Hu and J. Gao, in *Materials and physics of light-emitting electrochemical cells (LECs)*, Elsevier Ltd., 2019, book section 22, pp. 727–757.

[23] C. E. Housecroft and E. C. Constable, *Coord. Chem. Rev.*, 2017, **350**, 155–177.

[24] Y. Shen, D. D. Kuddes, C. A. Naquin, T. W. Hesterberg, C. Kusmierz, B. J. Holliday and J. D. Slinker, *Appl. Phys. Lett.*, 2013, **102**, 203305.

[25] C. D. Sunesh and Y. Choe, *Mater. Chem. Phys.*, 2015, **156**, 206–213.

[26] C. D. Sunesh, G. Mathai and Y. Choe, *ACS Appl. Mater. Interfaces*, 2014, **6**, 17416–17425.

[27] C. D. Sunesh, M. Chandran, G. Mathai and Y. Choe, *Opt.*, 2013, **35**, 407–413.

[28] H. J. Bolink, E. Coronado, R. D. Costa, E. Ortí, M. Sessolo, S. Graber, K. Doyle, M. Neuburger, C. E. Housecroft and E. C. Constable, *Adv. Mater.*, 2008, **20**, 3910–3913.

[29] G. E. Schneider, A. Pertegás, E. C. Constable, C. E. Housecroft, N. Hostettler, C. D. Morris, J. A. Zampese, H. J. Bolink, J. M. Junquera-Hernández, E. Ortí and M. Sessolo, *J. Mater. Chem. C*, 2014, **2**, 7047–7055.

[30] A. M. Bünzli, E. C. Constable, C. E. Housecroft, A. Prescimone, J. A. Zampese, G. Longo, L. Gil-Escrig, A. Pertegás, E. Ortí and H. J. Bolink, *Chem. Sci.*, 2015, **6**, 2843–2852.

[31] G. Kalyuzhny, M. Buda, J. McNeill, P. Barbara and A. J. Bard, *J. Am. Chem. Soc.*, 2003, **125**, 6272–6283.

[32] M. D. Weber, E. Fresta, M. Elie, M. E. Miehlich, J.-L. Renaud, K. Meyer, S. Gaillard and R. D. Costa, *Adv. Funct. Mater.*, 2018, **28**, 1707423.

[33] Q. Pei, G. Yu, C. Zhang, Y. Yang and A. J. Heeger, *Science*, 1995, **269**, 1086–1088.

[34] S. Tang, J. Pan, H. A. Buchholz and L. Edman, *J. Am. Chem. Soc.*, 2013, **135**, 3647–3652.

[35] Z. Yu, M. Wang, G. Lei, J. Liu, L. Li and Q. Pei, *J. Phys. Chem. Lett.*, 2011, **2**, 367–372.

[36] A. Asadpoordarvish, A. Sandström, S. Tang, J. Granström and L. Edman, *Appl. Phys. Lett.*, 2012, **100**, 193508.

[37] S. Biswas, B. Das, P. Alam, A. Ghatak, U. K. Ghorai, A. Ghosh, B. B. Das, I. R. Laskar and S. Acharya, *J. Phys. Chem. C*, 2021, **125**, 4730–4742.

[38] D. Xiang, Q. Shen, S. Zhang and X. Jiang, *J. Appl. Polym. Sci.*, 2003, **88**, 1350–1356.

[39] H.-F. Chen, C.-T. Liao, T.-C. Chen, H.-C. Su, K.-T. Wong and T.-F. Guo, *J. Mater. Chem.*, 2011, **21**, 4175.

[40] A. Pertegás, D. Tordera, J. J. Serrano-Pérez, E. Ortí and H. J. Bolink, *J. Am. Chem. Soc.*, 2013, **135**, 18008–18011.

[41] K. Shanmugasundaram, M. S. Subeesh, C. D. Sunesh, R. K. Chitumalla, J. Jang and Y. Choe, *J. Phys. Chem. C*, 2016, **120**, 20247–20253.

[42] X. J. Chen, Y. T. Huang, D. Luo, C. H. Chang, C. W. Lu and H. C. Su, *Chem. Eur. J.*, 2023, **29**, 29.

[43] D. Volz, *J. Photonics Energy*, 2016, **6**, 6.

[44] T. T. Bui, F. Goubard, M. Ibrahim-Ouali, D. Gigmes and F. Dumur, *Appl. Sci.*, 2018, **8**, 8.

[45] B. Adranno, S. Tang, V. Paterlini, V. Smetana, O. Renier, G. Bousrez, L. Edman and A. V. Mudring, *Adv. Photonics*, 2023, **4**, 4.

[46] J. Luo, Z. Xie, J. W. Y. Lam, L. Cheng, B. Z. Tang, H. Chen, C. Qiu, H. S. Kwok, X. Zhan, Y. Liu and D. Zhu, *Chem, Commun.*, 2001, 1740–1741.

[47] Z. Chen, J. Liang, X. Han, J. Yin, G. A. Yu and S. H. Liu, *Dyes Pigm.*, 2015, **112**, 59–66.

[48] Z. J. Gong and J. B. Lagowski, *Int. J. Quantum Chem.*, 2007, **107**, 159–171.

[49] S. Fleming, A. Mills and T. Tuttle, *Beilstein J. Org. Chem.*, 2011, **7**, 432–441.

[50] A. G. Martynov, J. Mack, A. K. May, T. Nyokong, Y. G. Gorbunova and A. Y. Tsivadze, *ACS Omega*, 2019, **4**, 7265–7284.

[51] A. D. Laurent, C. Adamo and D. Jacquemin, *Phys. Chem. Chem. Phys.*, 2014, **16**, 14334–14356.

[52] R. Sanchez-De-Armas, M. A. San Miguel, J. Oviedo and J. F. Sanz, *Phys. Chem. Chem. Phys.*, 2012, **14**, 225–233.

[53] E. R. Triboni, M. R. Fernandes, J. R. Garcia, M. C. Carreira, R. G. S. Berlinck, P. Berci, L. S. Roman, I. A. Hümmelgen, R. Reyes and M. Cremona, *J. Taibah Univ. Sci.*, 2015, **9**, 579–585.

[54] B. Chan and K. Hirao, *J. Phys. Chem. Lett.*, 2020, **11**, 7882–7885.

[55] S. Zein, F. Delbecq and D. Simon, *Phys. Chem. Chem. Phys.*, 2009, **11**, 694–702.

[56] A. Ali, M. I. Rafiq, Z. Zhang, J. Cao, R. Geng, B. Zhou and W. Tang, *Phys. Chem. Chem. Phys.*, 2020, **22**, 7864–7874.

[57] C. A. Barboza, P. A. M. Vazquez, D. M. Carey and R. Arratia-Perez, *Int. J. Quantum Chem.*, 2012, **112**, 3434–3438.

[58] A. Adegoke, J. Wang and J. Leszczynski, *Chem. Phys. Lett.*, 2012, **532**, 63–67.

[59] H. Roohi and N. Abdollahinezhad, *Org. Electron.*, 2015, **25**, 121–130.

[60] I. Yamaguchi and K. Miyawaki, *React. Funct. Polym.*, 2017, **120**, 14–19.

[61] B. Liu and S. K. Dishari, *Chem. Eur. J.*, 2008, **14**, 7366–7375.

[62] J. P. Huo, W. Y. Zou, Y. B. Zhang, W. L. Chen, X. H. Hu, Q. J. Deng and D. C. Chen, *RSC Adv.*, 2019, **9**, 6163–6168.

[63] L. Scalon, A. L. Neto, L. O. Araujo, S. Zaioncz, J. B. Floriano, A. G. Macedo, C. M. Araujo, C. F. N. Marchiori and P. C. Rodrigues, *ACS Appl. Polym. Mater.*, 2021, **3**, 4223–4233.

[64] S. Yao, H. Y. Ahn, X. H. Wang, J. Fu, E. W. Van Stryland, D. J. Hagan and K. D. Belfield, *J. Org. Chem.*, 2010, **75**, 3965–3974.

[65] J. Mahar, G. Shabir, P. A. Channar, A. Saeed, K. D. Belfield, M. Irfan and A. Ul-Hamid, *J. Fluoresc.*, 2020, **30**, 419–426.

[66] C. Chakraborty, M. K. Bera, U. Rana and S. Malik, *Chem. Commun.*, 2015, **51**, 13123–13126.

[67] H. F. Chen, C. T. Liao, M. C. Kuo, Y. S. Yeh, H. C. Su and K. T. Wong, *Org. Electron.*, 2012, **13**, 1765–1773.

[68] S. Arumugam, Y. Li, J. E. Pearce, K. L. Court, G. Piana, E. H. Jackman, O. J. Ward, M. D. Charlton, J. Tudor, D. C. Harrowven and S. P. Beeby, *Org. Electron.*, 2022, **105**, 105.

[69] K. Shanmugasundaram, M. S. Subeesh, C. D. Sunesh and Y. Choe, *RSC Adv.*, 2016, **6**, 28912–28918.

[70] E. H. Jackman, unpublished work, Harrowven group, University of Southampton, 2021.

[71] C. M. Cardona, W. Li, A. E. Kaifer, D. Stockdale and G. C. Bazan, *Adv. Mater.*, 2011, **23**, 2367–2371.

[72] G. Zhang, Y. Fu, Z. Xie and Q. Zhang, *Polymer*, 2011, **52**, 415–421.

[73] M. Schwarting, S. Siol, K. Talley, A. Zakutayev and C. Phillips, *Mater. Discov.*, 2017, **10**, 43–52.

[74] Y. Li, unpublished work, Beeby group, University of Southampton, 2022.

[75] K. Court, unpublished work, Beeby group, University of Southampton, 2022.

[76] M. Hedouin, unpublished work, Chataigner group, Université de Rouen Normandie, 2022.

[77] L. V. Langenhove, T. Rijavec and S. Bračko, *Smart Textiles for Medicine and Healthcare*, Wodhead Publishing, 2007.

[78] Z. M. Essam, G. E. Ozmen, D. Setiawan, R. R. Hamid, R. M. Abd El-Aal, R. Aneja, D. Hamelberg and M. Henary, *Org. Biomol. Chem.*, 2021, **19**, 1835–1846.

[79] N. S. Babu, *ChemistryOpen*, 2022, **11**, 11.

[80] M. Hédouin, E. Luppi, O. Ward, D. Harrowven, C. Fressigné and I. Chataigner, *ChemistrySelect*, 2023, **8**, 29.

[81] L. Wilding-Steele, *Ph.D. thesis*, University of Southampton, 2022.

[82] R. M. Bennett, *Ph.D. thesis*, University of Southampton, 2021.

[83] Y. J. Deng, M. Z. Wang, Y. L. Zhuang, S. J. Liu, W. Huang and Q. Zhao, *Light Sci. Appl.*, 2021, **10**, 10.

[84] M. Kitahara, K. Hara, S. Suzuki, H. Iwasaki, S. Yagi and Y. Imai, *Org. Electron.*, 2023, **119**, 119.

[85] T. Ishida, A. Isawa, S. Kuroki, Y. Kameoka and T. Tatsuma, *Appl. Phys. Lett.*, 2023, **123**, 123.

[86] C. L. He and Y. Li, *Chin. Chem. Lett.*, 2023, **34**, 34.

[87] J. Johal, unpublished work, Day group, University of Southampton, 2023.

[88] C. Y. Cheng, J. E. Campbell and G. M. Day, *Chem. Sci.*, 2020, **11**, 4922–4933.

[89] M. Skoulikas, unpublished work, Whitby group, University of Southampton, 2022.

[90] A. Shiels, unpublished work, Brown group, University of Southampton, 2022.

[91] O. F. Doria, R. Castro, M. Gutierrez, D. G. Valenzuela, L. Santos, D. Ramirez and L. Guzman, *Mol.*, 2018, **23**, 2354.

[92] B. Liu, B. S. Gaylord, S. Wang and G. C. Bazan, *J. Am. Chem. Soc.*, 2003, **125**, 6705–6714.

[93] B. Gierczyk, M. Kaźmierczak, Łukasz Popenda, A. Sporzyński, G. Schroeder and S. Jurga, *Magn. Reson. Chem.*, 2014, **52**, 202–213.

[94] G. Shi, D. Chen, H. Jiang, Y. Zhang and Y. Zhang, *Org. Lett.*, 2016, **18**, 2958–2961.

[95] V. Gauchot, M. Branca and A. Schmitzer, *Chem. Eur. J.*, 2014, **20**, 1530–1538.

[96] X. F. Kong, Z. Q. He, Y. N. Zhang, L. P. Mu, C. J. Liang, B. Chen, X. P. Jing and A. N. Cammidge, *Organic Letters*, 2011, **13**, 764–767.

[97] M. Mohamed, T. P. Gonåalves, R. J. Whitby, H. F. Sneddon and D. C. Harrowven, *Chem. Eur. J.*, 2011, **17**, 13698–13705.

[98] M. Mohamed, T. P. Gonçalves, R. J. Whitby, H. F. Sneddon and D. C. Harrowven, *Chem. Eur. J.*, 2011, **17**, 13698–13705.

[99] L. M. Gayo, M. P. Winters, H. W. Moore, H. W. J. A. C. Soc, K. J. O and H. W. J. Org, *Tetrahedron Lett.*, 1992, **57**, 27.

[100] M. Periasamy, C. Rameshkumar, U. Radhakrishnan and J.-J. Brunet, *J. Org. Chem.*, 1998, **63**, 4930–4935.

[101] E. K. Fields, S. J. Behrend, S. Meyerson, M. L. Winzenburg, B. R. Ortega and H. K. H. Jr, *J. Org. Chem.*, 1990, **55**, 5165–5170.

[102] W. Ried and D. P. Schaefer, *Chem. Ber.*, 1969, **102**, 4193–4198.

[103] Y. Zhang, T.-Y. Zhou, K.-D. Zhang, J.-L. Dai, Y.-Y. Zhu and X. Zhao, *Chem. Asian J.*, 2014, **9**, 1530–1534.